PARTICLE IMAGE VELOCIMETRY STUDIES OF SUSPENSION TRANSPORT IN BIFURCATING CHANNELS

A Thesis Submitted in the Partial Fulfillment of the Requirements for the

Award of the Degree of

Doctor of Philosophy

By

Bhaskar Jyoti Medhi

Roll no. : 126107023

Department of Chemical Engineering

Indian Institute of Technology Guwahati

Guwahati - 781039, India

November 2018

Dedicated to

My beloved parents and wife Sikha

CERTIFICATE

*It is certified that the work contained in the thesis entitled "***Particle Image Velocimetry Studies of Suspension Transport in Bifurcating Channels,***" by* ***Bhaskar Jyoti Medhi****, has been carried out under my supervision and that this work has not been submitted elsewhere for a degree.*

Date:

Dr. ANUGRAH SINGH
Professor
Department of Chemical Engineering
IIT Guwahati, Guwahati 781039 India

STATEMENT

I do hereby declare that the matter embedded in this thesis and the result of investigations has been carried out by me under the supervision of Dr. Anugrah Singh at the Department of Chemical Engineering, IIT Guwahati. Assam, India.

In keeping with general practice of reporting scientific observations, due acknowledgements have been made wherever the work described and is based on the findings of other investigations.

Date: _____

BHASKAR JYOTI MEDHI

Acknowledgments

I have spent in IIT Guwahati the best time of my life. This fantastic experience would not have been the same without all the people I have met and who have helped me and supported me during my PhD.

First of all I wish to express my deepest gratitude to my supervisor, Dr. Anugrah Singh for giving me the opportunity to work in Flow Visualization laboratory. He has constantly encouraged me and trusted me in times of both joy and despair, which empowered me to put the best effort I could in my work. There is nothing more I could have expected from my advisor.

I would like to thank my Doctoral committee members: Dr. Anoop K. Dass, Dr. G. Pugazhenthi and Dr. R. K. Upadhyay for taking interest in my research and supporting me to reach the conclusion of my work.

I would like to extend my gratitude to Mr. Minesh Ch. Medhi from central workshop IIT Guwahati for fabrication of my experimental setups. I would also like to thank the Chemical Engineering Department staffs for always being prompt for all help in official works, which makes my research life so much easier.

I would like to express my heartiest thanks to past and present lab members (Dr. Ashish Kumar Thokchom, Dr.S.Yadav, M.Mallikarjuna Reddy, Sudarshan, Najrul, Vipin, Gaurav, Ajeeth ,Vikas, Preetisagar, Imran, Aslam, Niloy, Nasaba, Jyoti Krishana, Shadab, Delli Ganesh and Manjunath) for their all-time support and encouragement. I particularly enjoyed going to tea with them and the discussion we had on wide-ranging topics.

My friends at IIT Guwahati made my life joyful and were constant source of encouragement. I appreciate their help and friendship. Thanks to all my friends for their support.

I saved the last but the biggest thanks to my parents (Mr. Mahesh Chandra Medhi and Mrs. Binapani Medhi), wife Sikha, sister Pompi, brother-in-law Monoj and nephew Swapnanil who always put my happiness ahead of their aspirations. It would have been impossible for me to complete this work without their unconditional love, support and encouragement.

Bhaskar Jyoti Medhi

Abstract

The suspension flow at low Reynolds number in vivo or in vitro bifurcation channels has many relevant applications in biological and industrial systems. Although studies have been conducted for solid-liquid two phase flows in micro bifurcations network in the past, many aspects of it not completely understood. Till now it is not clear why the redistribution of particles near the bifurcation junctions yield nearly equal particle partitioning but unequal flow partitioning even though the channel is asymmetric. Many interesting phenomena often observed in the suspension flow such as shear-induced migration, blunting velocity profile, wall slip, etc. are not encountered in simple Newtonian homogenous liquid. Some recent studies on suspension flow in bifurcation channel shown that distribution of fluid and particles near the bifurcation depends upon dispersed particle size, branching angle, type of flow.

We have performed the micro-PIV/PTV experiments for single-phase Newtonian fluid and dilute suspension of two different size particles, in bifurcation channels for a range of branching angle for diverging and converging flow condition. The daughter branches have the same channel width as that of the parent branch. We have also conducted experiments on diverging-converging channels of varying width. We observed that for diverging flow crests in velocity profiles in daughter branches shifted towards the outer wall in contrast to converging flow where profiles are shifted towards inner side. Shifting of velocity profile was more for suspension flow compared to the Newtonian fluid. For converging flow we observed reversibility in results for velocity profiles at the end of inlet branches for symmetric bifurcation channels but for the asymmetric channels the profiles at the same locations were not same due to irreversible nature of shear-induce particle migration.

From the velocity vector map of particle phase generated from μ-PTV analysis, it is clearly observed that more number of vectors located at the center of the channel in the inlet branch. This can be directly related to shear- induce migration phenomena for which particles migrate from the wall to the center of the channel. In daughter branches more numbers of vectors located near the inner wall. To verify the above findings we have qualitatively studied the concentration profile at different locations of all the channels using Particle counting

MATLAB programme. From the comparison of concentration profiles in the inlet section, we observed an inverted V-shape of the profile which can be related to shear-induced migration phenomena. As we move from initial location to near the bifurcation, peak of the concentration profile also rises. At the outlet section for converging flow, we have observed the peak-valley-peak concentration profile and this is due to combining of two streams in the outlet section. As we move downstream locations in the outlet section, the peak-valley peak pattern in the concentration profile gradually decreases and only a single peak in the concentration profile emerges.

The comparison of the streamlines for the bulk flow and the particles showed significant deviation near the bifurcation region. Streamline comparison near the bifurcation shows that dispersed solid particles do not follow the fluid path near the bifurcation which leads to unequal flow and particle distribution at this region. Due to irreversible nature of shear-induced particle migration, the profiles were not the same near the bifurcation locations for converging and diverging flow conditions.

Contents

2. Experimental details and methodology

3. Suspension flow in diverging channel

Nomenclature

Notation

Re	Reynolds number
Re_p	Particle Reynolds number
Re_c	Channel Reynolds number
Pe	Peclet number
C_{tr}	Tracer particle concentration
M	Magnification number
NA	Numerical aperture of the objective lens
a	Particle radius
T	Temperature (K)
D	Diffusivity (m^2/s)
D_ϕ	Diffusion coefficient
w	Width of channel (m)
N_I	Particle density
z_0	Light-sheet thickness
M_0	Image magnification
D_I	Interrogation spot diameter
$I>$	Mean Intensity
I'	Intensity of fluctuation
R_C	Correlation between mean intensity and intensity fluctuations
R_F	Mean background correlation

R_D	Correlation of image fluctuations
L_f	Measured flow thickness,
s_0	Focal plane distance of the objective
n_0	Refractive index of the lens immersion liquid
V_z	Particle visibility

Greek Symbol

η	Effective viscosity of the suspension
η_0	Viscosity of the suspending fluid
ϕ	Particle volume fraction
ϕ_m	Maximum volume fraction or maximum packing fraction of particles
θ	Bifurcation angle
γ	Shear rate of the flow field
k	Boltzmann constant
ε	Relative threshold
ρ_p	Density of the particle
λ	Wavelength of laser,
τ_p	Response time

Abbreviations

CCD	Charge Coupled Device
CFD	Computational Fluid dynamics
CSLM	Confocal Scanning Laser Microscopy
DFM	Diffusive Flux Model
FFT	Fast Fourier Transform
LDV	Laser Doppler Velocimetry
LDA	Laser Doppler Anemometry
LED	Light Emitting Diode
MRI	Magnetic resonance imaging
Nd:YAG	Neodymium : yttrium aluminum garnet
NMR	Nuclear magnetic resonance
PDMS	Polymerized Poly dimethyl siloxane
PIV	Particle Image Velocimetry
PSD	Power spectral density
PTV	Particle Tracking Velocimetry
RBC	Red blood cell
SBM	Suspension Balance Model

List of Figures

List of Tables

Chapter 1

Introduction and literature Survey

1.1 Fluid-particle Suspensions

A suspension comprises of dispersions of solid particles in a continuous fluid medium. In order to ensure the continuity of the suspension and the liquid phase around particles, it is (necessary but not sufficient) that the order of magnitude of the suspended particle diameter should be (intermediate mesoscopic) between that of typical interstitial fluid element (microscopic) and a characteristic length (macroscopic) of the suspension sample as a whole.

Figure 1.1. Example of suspensions (Image source: Google image).

A suspension is common in natural setting such as flood wave carrying very fine sediments as well as in several material processing operations. Moreover, a suspension is also an integral part of our modern day to day life in the form of chocolate, milk, ice cream, tea, soup, curd, ink, paper, paint, and toothpaste etc. Some examples of suspension is shown in

Figure 1.1. The study of suspension rheology has vast applications in biological processes like blood cell separation, DNA analysis, proteomics, drug delivery etc. An important issue of suspension is the definition and classification in a scientific manner.

1.1.1 Classification of suspensions

1.1.1.1 Classification based on particle volume fraction (ϕ)

Suspensions are generally classified based on particle volume fraction (ϕ), as the rheological property of suspension varies with the increase of particle concentration.

$$\phi = \tfrac{4}{3}\pi a^3 n \qquad (1.1)$$

where "n" is the particle number density, and "a" is particle radius.

Viscosity is one of the significant rheological properties of suspension flow. The viscosity of a suspension depends on the structural packing and interaction potential of particles. The viscosity of suspension increase with the increase in of particle volume fraction. Relating to viscosity, suspensions are generally classified into three categories:-

(a) **Dilute Suspension:-** A suspension is said to be dilute usually if particle volume fraction (ϕ)<5%. Dilute suspensions are often treated as suspending fluid without significant difference in viscosity. For creeping flow in a neutrally buoyant dilute suspensions of Brownian hard spheres (i.e. Pe < 1) with no particle-particle or particle-boundary interactions and no slip at particle surface, Einstein (1906) determined analytically the equation relating bulk fluid viscosity with volume fraction to a first order approximation.

$$\eta = (1+2.5\,\phi)\,\eta_0 \qquad (1.2)$$

In the equation η is the effective viscosity of the suspension , η_0 is the viscosity of the suspending fluid and ϕ is particle volume fraction.

(b) **Semi-dilute suspension: -** For semi-dilute suspension particle volume fraction is in the range of $5\% \le \phi \ge 30\%$. Here particle-particle interactions alter the flow characteristics. Batchelor (1977) give the expression for viscosity as a function of

higher order particle volume fraction considering particle-particle interactions and assuming suspension still behaved in a Newtonian manner.

$$\eta = (1+2.5\,\phi + 6.2\,\phi^2)\eta_0 \qquad (1.3)$$

(c) **Concentrated Suspension: -** When particle volume fraction $\phi \geq 30\%$,suspension become dense or concentrated. The term "dense" can be interpreted in a number of ways, i.e. in terms of the average separation between particles, in terms of proximity to the jamming transition, or simply in terms of significant observed deviation from Newtonian flow behavior [Stickel and Powell (2005)].In concentrated suspensions, the hydrodynamic interactions and particle-particle contacts considerably change the flow features and we typically notice several interesting phenomena such as shear-induced migration, particle segregation, blunted velocity profile, wall slip, surface corrugation etc. which are not seen in the flow of a Newtonian homogeneous fluid under similar boundary conditions. The relationships between suspension viscosity and volume fraction stated above have been further extended by many rheologists to calculate the viscosity of suspensions with volume fractions up to the maximum packing.

1.1.1.2 Classification based upon forces on particles

Different forces act on the particles inside a suspension. For moving, suspension three major forces develop in a suspension.

(a) **Hydrodynamic force: -** When there is a relative motion between the particle and a viscous, incompressible fluid at low Reynolds number flow, it experiences hydrodynamic forces.

(b) **Brownian force: -** For a dispersed particle size of less than 1 μm in solid-liquid flows, the collisions of molecules of the fluid with the surrounding particles give rise to an unbalanced forces, called Brownian forces. Brownian force causes a rapid change of the particle velocity both in magnitude and direction.

(c) **Colloidal forces:-** Colloidal forces depends on the particle size and the distance between particles. It includes forces like electrostatic interaction, van der Waals force etc. [Brader, (2010)].

To define the force inside a suspension, the non-dimensional number such as Reynold number (Re) and the Peclet number (Pe) mostly uses.

Reynolds number (Re)

It is the ratio of inertial to viscous forces and can be expressed as -

$$\mathrm{Re}_p = \frac{\gamma \rho_p a^2}{\eta_o} \tag{1.4}$$

In the above equation, $\mathrm{Re_p}$ is particle Reynolds number ρ_p is the density of the particle, a is the particle radius, γ is the shear rate of the flow field, and η_o is the viscosity of the suspending fluid. If, $\mathrm{Re_p}<1$ then the motion of freely suspended particles is regulated by viscous and pressure forces. In this case inertial driven migration across streamlines is unimportant causing only shear-induced particle migration.

Péclet number (Pe)

The ratio between hydrodynamic forces and Brownian diffusion is known as Péclet number (Pe). It specifies whether hydrodynamic migration or Brownian diffusion is dominant and relates this to dimensions of the device. When Pe=1, the transition from Brownian to hydrodynamic migration take place. Peclet number can be expressed as-

$$Pe = \frac{\gamma a^2}{D} = \frac{6\gamma a^3 \eta_o \pi}{kT} \tag{1.5}$$

Where k is the Boltzmann constant and T is the temperature (K) and D can be estimated from Stokes-Einstein diffusivity (m^2/s) equation.

$$D = \frac{kT}{6\pi\eta_0 a} \tag{1.6}$$

Generally, dispersed particles cross other particles in a slow moving fluid and interact with each other. When these interactions involve three or more particles at certain point of time

they displaced from fluid streamline imitating random distribution of particles. Generally in suspension three types of interactions that may occur that are particle-fluid, particle-particle and particle-boundary interactions. Particle size is important to determine the different type of interactions and finally decide which will dominate to determine the behavior of the system. For particle size $d_p < 1nm$, Brownian force and colloidal forces dominate. Hydrodynamic force dominate to determine system behavior for $d_p < 10\mu m$. For $1nm < d_p < 10\mu m$ hydrodynamic, Brownian and inter-particle forces effect the system behavior.

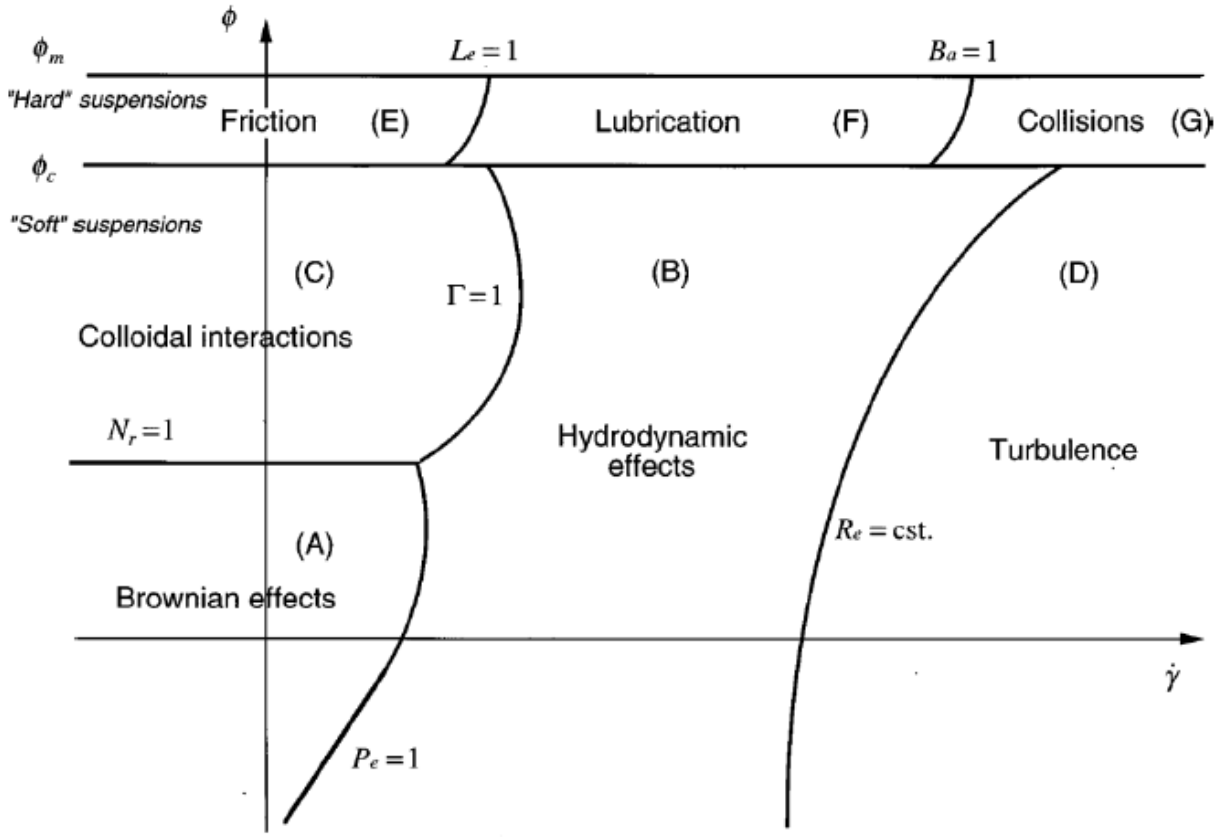

Figure 1.2. Different rheophysical regimes of a suspension as a function of shear rate (γ) and particle volume fraction (ϕ) on a logarithmic scale (From Coussot and Ancey, 1999, *Physical Review E*, **59 (4)**, 4445–57. Copyright 1999 by American Physical Society).

Figure 1.2 shows the variation of particle volume fraction, shear rate and dominant force act on the suspension [Coussot and Ancey (1999)]. In small shear rates and low concentrations, the Brownian effect mainly dominant (zone A). With the increase in shear rate, hydrodynamic force starts dominating (zone B). As the volume fraction of particles increases, the colloidal forces are the most significant (zone C). At very high shear rates, the inertial forces dominant (zone D). Inter-particles forces dominant for very high concentrated suspension, (zone E, F, G).

1.1.1.3 Classification based on types and size of the particles

Based on dispersed particles types and size, suspension can be categorized as -

(a) Mono-dispersed: - In monodispersed suspension dispersed particles are of uniform size or density. In this work, we have considered mono dispersed noncolloidal suspension. Artificial suspension ubiquitously encountered in our daily life such as ink, paper, paint, tea, soup, plaster, cement, curd, rubber, and skincare products are generally mono-dispersed.

(b) Poly-dispersed: - Polydispersed suspensions consist of particles differing in size or density that are dispersed in a continuous fluid. Most of the geological suspensions like rivers, mud slides and volcanic lavas are poly-dispersed.

More specifically, based on the size of the particle dispersed in the continuous phase suspensions can be further categorised as-.

I. **Homogenous solution:-** Homogenous solution as the name signifies it is a homogenous mixture of a solute in a solvent, which is commonly termed as a true solution. Here mixture is in a liquid phase and it is optically transparent. In homogenous dispersion, solute particles cannot separate through filtration and observe under microscope. The dispersed phase (solute) size is less than 1 nm. The examples of molecular dispersions: Sugar in water and salt in water.

II. **Colloidal suspension:-** Colloids are heterogeneous dispersed systems, in which the size of the particles of dispersed phase in the range of $1nm < a < 1\mu m$. In colloids, solute particles can be separate through microfiltration and also can be observed with a necked eye or under a microscope. Dispersed phase of colloids may be separated from the dispersion medium by micro-filtration. The examples of colloids are milk, fog etc.

III. **Non-colloidal suspension: -** It is a heterogeneous dispersed system, where particles of the dispersed phase are larger than $1\mu m$. Non-colloidal dispersions are characterized by comparatively fast sedimentation of the dispersed phase caused by gravity or other forces. Here solute particles can be separate from solution through filtration.

Particle size and shape is a significant parameter as it determines the interaction between the particles and the suspending fluid. Although various shapes of particles are available in practical applications, but our study is limited to spherical particles suspended in Newtonian fluid. This type of suspensions is of great practical applications in industry, medicine, and research. The suspensions of interest in this work are inertia less, neutrally buoyant, monodispersed, non-Brownian and non-colloidal spheres suspended in a Newtonian fluid. Neutrally buoyant means that the densities of the particles and fluid are equal and thus settling of the particles due to gravity does not occur. In industrial applications, an in-depth knowledge of complex rheological behavior of suspensions is required for the optimum manufacturing, processing and design of the materials. Hence, the suspension flow problems are quite challenging and become an attractive area of research among fluid mechanic researchers.

1.1.1.4 Classification based on particle transport mechanism

In suspension generally, three types of transport mechanism occur Brownian diffusion, Shear-induced diffusion and Inertial lift. Their relative importance depends upon particle size and shape, channel width, particle concentration, shear rate, viscosity of suspension etc.

Summary of conditions at which different migration phenomena dominant is shown in the Table 1.

Table 1:- Summary of conditions at which different migration phenomena dominate.

Transport mechanism	Pe	Re	Re_p	ϕ
Brownian diffusion	<1	<10	<1	Increase of ϕ decreases Brownian diffusion
Shear-induced diffusion	>1	<10	<1	Increase of ϕ increases Shear induce migration
Inertial lift.	>1	10-100	1-100	Increase of ϕ decrease Inertial lift

(a) Brownian diffusion: - Brownian motion is the random motion of dispersed particles in solid-liquid flows. It is due to collision of molecules of the fluid with the surrounding particles. Peclet number (Pe) is one of the important parameter which gives the comparative importance of hydrodynamic force to Brownian forces. For Pe < 1, the hydrodynamic forces dominate over Brownian force. In this work, we have considered laminar flow regime and the dispersed particle size is larger than 1μm, where Brownian diffusion of suspension particles is insignificant.

(b) Shear-induced migration: - The shear-induced migration phenomenon at low Reynolds number is one of the most significant non-linear behaviors of flow with particulate suspensions. Shear-induced migration is defined as a phenomenon in which initially well mixed non-colloidal, neutrally buoyant particles in a viscous Newtonian fluid subjected to in-homogeneous shear flow, particles migrate from regions of high to low shear rate. Shear-induced migration occurs when particles disturb the flow field around another particle; either by their rotation in shear flow, or by their movement since they move in a slower or faster-moving streamline. For shear-induced migration, the diffusion coefficient is proportional to γa^2 can be described in Equation [Leighton and Acrivos (1987)].

$$D_{shear} = \gamma a^2 D_\phi \tag{1.7}$$

Here γ shear rate(s^{-1}), a is particle radius (m), ϕ solid volume fraction, D_ϕ is the diffusion coefficient and can be expressed as-

$$D_\phi = \frac{1}{3}\phi^2(1+0.5e^{8.8\phi}) \tag{1.8}$$

From equation 1.7 we observed that larger particles are much more influenced by shear-induced diffusion. For the system where concentration gradient exists along with shear rate and viscosity, the equation alone 1.8 cannot directly describe migration. In this case, Diffusive flux model proposed by Phillips et al. (1992) should be taken in to account. The equation for migration is-

$$J_{mig} = -\rho K_c a^2(\phi^2\nabla\dot{\gamma} + \phi\dot{\gamma}\nabla\phi) - \rho K_\eta \dot{\gamma}\phi^2\left(\frac{a^2}{\eta}\right)\frac{d\eta}{d\phi}\nabla\phi \tag{1.9}$$

Here η is the viscosity of a suspension. Diffusion coefficients K_c and K_η are empirical constants having value 0.41 and 0.62 respectively as suggested by Philips et al. (1992).

(c) Inertial lift: - It is exerted on a particle by the fluid, due to the flow profile and if the particle moves close to the wall. It is dependent on the particle Reynolds number which is a ratio between inertial and viscous forces. Inertial lift is relevant for particle Reynolds numbers (Re_p) > 1. In our experiments the particle Reynolds numbers were below 1, signifying that inertial lift did not play a role. In the equation Re_c is the channel Reynolds number, w is the width of channel (m) and $\eta(\phi)$ is the viscosity as a function of the solid volume fraction of the suspension (Pa.s).

$$\mathrm{Re}_p = \mathrm{Re}_c\left(\frac{2a(w+2H)}{4wH}\right)^2 = \frac{\gamma a^2\rho(w+2H)}{3\eta(\phi)w} \tag{1.10}$$

$$\mathrm{Re}_c = \frac{4wH}{(w+2H)}\frac{\bar{v}\rho}{\eta(\phi)} \tag{1.11}$$

In our case particle-particle interaction caused the shear induce migration. Although particle volume fraction is 5 % in our case, suspended particles can occupy significant part of the channel to interact with each other and the bounding walls and are expected to perturb the surrounding flow which causes migration of particle. As particle moves into the channel, due

to shear-induced migration, more and more particle moves to the centre of channel increasing local particle volume fraction. As a result, probability of particle-particle interaction increases, which further accelerate shear induce migration of particle. As the Reynolds number is small, and the fluid motion is so slow that the inertial forces are negligible in comparison to viscous forces.

1.2 Viscosity

According to the recent literature, a majority of research in suspension flow can be divided into two groups. One group emphases on the viscosity of suspensions, to determine the relationship between relative viscosity with particle concentration, shear rate or other factors. The other group measured the velocity profiles and the particle concentration distributions of suspension flow in different geometries (Couette, capillaries and microchannels) to study the flow dynamics of suspensions.

Viscosity is one of the significant rheological properties of suspension flow. The viscosity of a suspension depends on the structural packing and interaction potential of particles. The viscosity of suspension increase with the increase in of particle volume fraction. Considerable progress has been made in predicting the viscosity from volume fraction for dilute, semi-dilute and concentrated suspension.

1.2.1 Particle volume fraction effect

Generally dilute suspension behaves in a Newtonian manner, with the shear stress being proportional to a rate independent viscosity. This provides ground for a first approximation of the variation of viscosity η with volume fraction ϕ. The expressions for viscosity can be express in the following form-

$$\tau = \mu(\phi)\gamma \qquad (1.12)$$

Einstein's in 1907 showed that in absence of particle-particle interaction viscosity is a function of particle volume fraction according to the equation-

$$\eta = (1+2.5\phi)\,\eta_0 \qquad (1.13)$$

Here η is the effective viscosity of the suspension η_0 is suspending fluid viscosity and ϕ is particle volume fraction.

For semi dilute suspension Batchelor (1977) considered particle-particle interactions and extended Einstein's equation to a second order approximation

$\eta = (1+2.5\ \phi\ +6.2\ \phi^{2})\ \eta_0$ (1.14)

Predicting the viscosity of increasingly dense suspensions becomes difficult due to many body hydrodynamic interactions. In dense systems, the viscosity is therefore, dependent on the microstructure of the particle network along with hydrodynamic interactions.

For volume fraction greater than 0.3, a model developed by Maron and Pierce (1956) and popularised by Quemada (1977) commonly known as MPQ model considering multi-body particle interactions.

$$\eta_s = \left(1-\frac{\phi}{\phi_m}\right)^{-2} \quad (1.15)$$

Where ϕ_m is the maximum volume fraction or maximum packing fraction of particles. For monodispersed suspensions of hard spheres its value found to be between 0.58 (for cubical packing) and 0.72 (tetrahedral packing). When suspension concentration reaches ϕ_m, jamming of flow occur as there is no enough fluid to lubricate the relative motion of particles and viscosity increases to infinity consequently.

Then Krieger-Dougherty gives an equation based on the concept that, once shear is applied to Brownian particles in close vicinity, certain particles will rotate as singlets and others as doublets. Krieger-Dougherty derived a model for extensive variety of suspensions, from hard spheres to polymer suspensions in contrast to the MPQ model which is simply valid for spheres.

$$\eta_s = \left(1-\frac{\phi}{\phi_m}\right)^{-2.5\phi_m} \quad (1.16)$$

These models are further modified by many rheologists. Some of the important models are-

Leighton and Acrivos (1986): $$\eta_s = \left(1+\frac{1.5\phi}{1-\frac{\phi}{\phi_m}}\right)^{2} \quad (1.17)$$

Morris and Boulay (1999): $$\eta_s = 1+2.5\varphi(1-\frac{\phi}{\phi_m})^{-1}+0.1(\frac{\phi}{\phi_m})^{2}(1-\frac{\phi}{\phi_m})^{-2} \quad (1.18)$$

Krieger (1972) have given relationships to calculate the viscosity of suspensions with volume fractions up to the maximum packing fraction.

$$\eta(\phi) = \eta_o \left(1 - \frac{\phi}{\phi_{\max}}\right)^{-1.82} \tag{1.19}$$

1.2.2 Effect of Shear rate

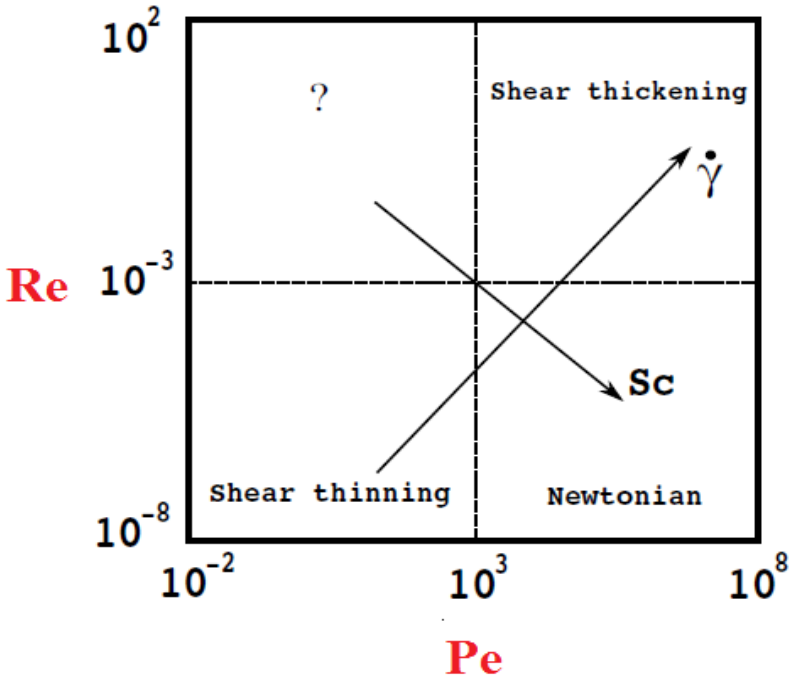

Figure 1.3. Suspension rheology phase diagram based on dimensionless numbers (From Stickel and Powell 2005, *Annual Review of Fluid Mechanics,* **37 (1)**, 129–49. Copyright 2005 by Annual Reviews group).

The viscosity of rigid particle suspensions is independent of shear rate at low particle concentrations. Mainly shear rate effect is noticeable at high concentration. Stickel and Powell (2005) describe suspension viscosity based on shear rate and dimensionless Re and Pe numbers. They classified suspension into four regimes: Shear-thinning, Newtonian, shear-thickening and an unknown region (Figure1.3). They reported that with the increase of shear rate, the nature of suspension changes from shear-thinning to Newtonian, and finally to shear-thickening.

1.3 Shear-Induced Particle Migration

The shear-induced migration phenomenon at low Reynolds number is one of the most significant non-linear behaviors of flow with particulate suspensions. Shear-induced migration is defined as a phenomenon in which initially well mixed non-colloidal, neutrally buoyant particles in a viscous Newtonian fluid when subjected to in-homogeneous shear flow, particles migrates from regions of high to low shear rate. It is observed that although the suspending fluid is Newtonian, the flowing suspension shows non-Newtonian behavior. Shear-induced migration phenomena have drawn the attention of researchers in recent years due to its widespread application in biomedical and material process industries.

For better understanding, shear induce migration phenomena can be shown in the following schematic.

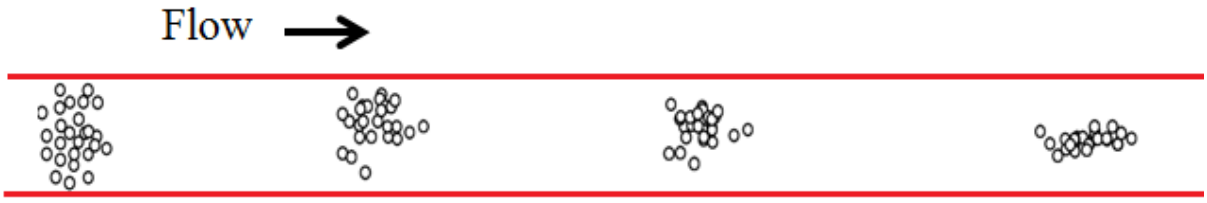

Figure 1.4. Schematic of shear induce migration phenomena.

Here in Figure 1.4 we can see that as the flow progresses uniformly distributed particles slowly move towards the center of the channel. The first experimental evidence of particle migration at low Reynolds number was provided by the work of Gadala-Maria and Acrivos (1980), when they detected shear-thinning of suspension of neutrally buoyant particles in cylindrical Couette geometry over prolonged shearing. After that Leighton and Acrivos (1987) showed from their experiments in a Couette reservoir flow that particles migrate from a region of high shear stress to low shear stress and proposed a model popularly known as shear-induced migration.

At low Reynolds number (based on particle size) flow, the inertia driven migration across streamlines is insignificant. Moreover, it is also well known that the trajectories of two isolated, interacting smooth spheres undergoing Stokes flow are symmetric and reversible and no net migration should occur. Simultaneous interactions between three or more particles can lead to asymmetric net displacements that are irreversible resulting in a diffusivity of the particles. In reality the particles are not smooth and any roughness can also result into the irreversible migration. Due to this reason the irreversible migration of particles have been observed for suspensions at low Reynolds number. The diffusivity of the particles in the

velocity gradient direction scales linearly with shear rate. In micro channels the mean velocity gradient can be appreciable due to small channel width and the distance over which migration has to take place is considerably less. Therefore, as reported by Dinther et al. (2012) the shear induced particle migration would be prominent in micro channels as compared to the conventional channels with larger dimensions. For the conditions of very low Reynolds number, Frank et.al (2003), Gao and Gilchrist (2008) reported significant shear induced migration in micro-channels for dilute suspension of particle volume fractions having 0.05 and 0.1 respectively in micro channel having entrance length less than half of our reported work. Although particle volume fraction of rigid spherical particle is much less, but in micro channels particle-particle interaction plays an important role for migration to occur. In a micro-channel the suspended particles can occupy significant part of the channel, interact with each other and the bounding walls and are expected to perturb the surrounding flow.

Medhi et al. (2010) conducted experiments using Particle Image Velocimetry technique in open channel flow of concentrated suspension under slip and no-slip conditions of the channel wall and reported blunting of the velocity profile, apparent wall slip. Even if its origin is not absolutely clear, it is well known that wall slip is present when suspensions are sheared. The wall slip phenomenon is basically the occurrence of apparent relative velocity between the wall and the fluid at the wall which is primarily apparent slip velocity. However, since the fluid is continuum, even in suspensions there is no 'true slip'. It is in reality an 'apparent slip' created by a region of high velocity gradient close to the wall compared to the bulk. This appears as an apparent slippage of the suspension through a thin liquid-rich layer (slip layer) at the wall. The slip layer is depleted of suspended particles compared to the adjacent regions of bulk suspension. Near the smooth, solid boundary, the local microstructure is depleted because the suspended particles cannot penetrate the solid walls. Shear induced migration can also cause depletion of particles near the wall and enhance the wall slip. Under the conditions of inhomogeneous shear flow, there can be migration near the wall which can increase the depletion of particles resulting into enhanced slip. In our case also, the migration of particles away from the channel walls gives rise to a thin layer of fluid there which could be the reason for apparent slip. As we have carried out experiment with dilute suspension having low viscosity, it is well known that smaller viscosity also gives rise to a greater wall slip velocity. In our experiments the particles were rigid therefore, we do not believe the deformability to induce wall slip.

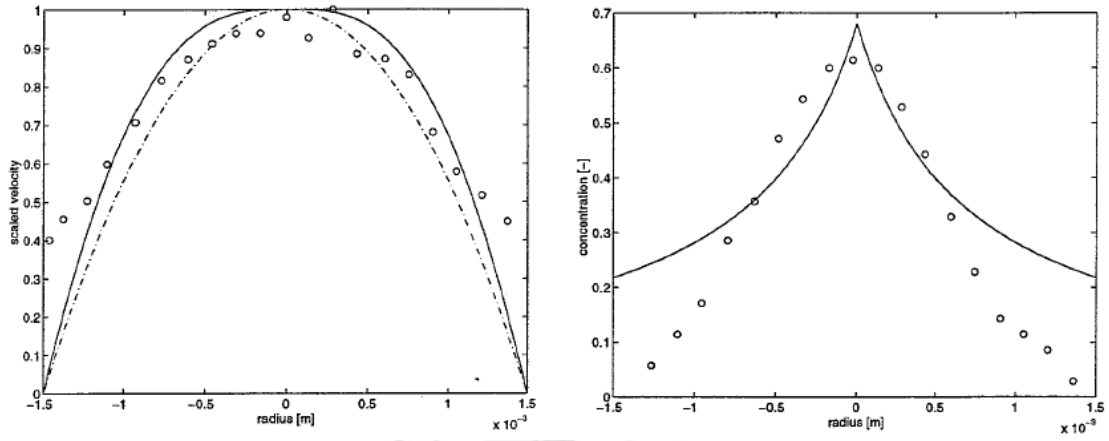

Figure 1.5. Velocity and concentration profiles of suspension of rigid particles (o) predicted profiles by the transport equation (-) and a parabolic velocity distribution (-.).(From Koh *et al*. 1994, *Journal of Fluid Mechanics,* ***266,*** 1-32. Copyright 1994 by Cambridge University Press).

Koh et al. (1994) and Lyon and Leal (1998) observed substantial particle migration accompanied by blunting of the velocity profile in rectangular channel flow using Laser Doppler Velocimetry method. In Figure 1.5 we have presented the results for velocity and concentration profile from Koh et al. (1994). Hampton et al. (1997) reported that for pressure-driven pipe flow the particles migrate from the regions of high shear (near the walls) to regions of low shear (the centreline). In addition, a number of curvilinear flows have been studied including wide-gap circular Couette flow, parallel-plate torsional flow, and small angle cone-and-plate torsional flow. Abbott et al. (1991) studied particle migration in wide-gap Couette using NMRI technique. They found that the particles migrate from high shear rate region near inner rotating cylinder to low shear rate region at the outer wall. Chapman (1990) observed little to no particle migration in a parallel-plate torsional flow while Chow et al. (1995) reported migration that is radially outward from the cone apex in the torsional cone-and-plate flow. Frank et al. (2003), Gao and Gilchrist (2008) reported about the shear-induced migration of particles in a dilute suspension flowing through a rectangular microchannel of shorter entrance length. Recently Kim and Yoo, (2008, 2010) using the Micro-Particle Image Velocimetry technique studied the lateral migration of the particles in a dilute suspension flowing through a circular microchannel. Semwogerere et.al (2007) carried out an experimental study to measure concentration profiles from the entrance to the downstream of a microchannel. They reported the effect of Brownian motion on shear-induced particle migration for monodisperse suspension. Semwogerere and Weeks (2008) carried out a similar experiment for bi-disperse suspension and their results are presented in Figure 1.6. They

concluded that shorter entrance length can be attained by increasing the volume fraction ϕ and increasing the particle radius a. If the size of two particles fixed then by increasing ϕ for one of the species, that species is encouraged to migrate towards center. For fixed-volume fractions of each species, by increasing the size of one particle species, that species will have a shorter entrance length and thus have its concentration higher in the center.

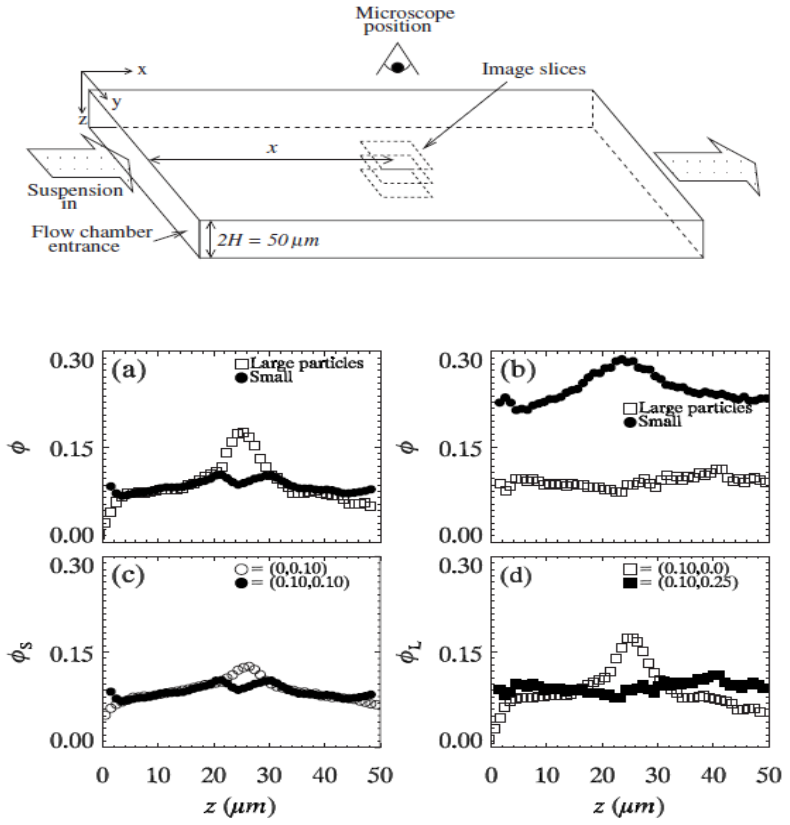

Figure 1.6. Top image - Glass rectangular chamber showing the relative position of the microscope and the corresponding image slices.

Bottom image – Concentration profiles showing (a) Higher migration of large particles for binary suspension, $\left(\phi_{large},\phi_{small}\right)$= (0.10, 0.10) at x/H=1600 (b) Higher migration of small particles at x/H=1850 for $\left(\phi_{large},\phi_{small}\right)$=(0.10, 0.25) (c) Comparison of the small particles in binary suspension (0.10,0.10)with monodisperse suspension (0.0,0.10) at x/H=1600. (d)Comparison of the large particles in binary suspension (0.10, 0.25) with monodisperse suspension (0.10, 0.0) at x/H=1850. (From Semwogerere and Weeks, 2008, *Physics of Fluids*, **23 (20),** 043306. Copyright 2008 by AIP Publishing).

The mathematical models to understand shear-induced particle migration in concentrated suspension basically fall into two categories. The first model, named as "Diffusive flux model (DFM)" was proposed by Phillips et al. (1992) for predicting particle concentration and velocity field in concentrated suspensions depending upon the scaling arguments of Leighton and Acrivos (1987) and on particle concentration dependent viscosity. The second model, named as "Suspension balance model (SBM)" was proposed by Nott and Brady (1994) and their results are presented in Figure 1.7.

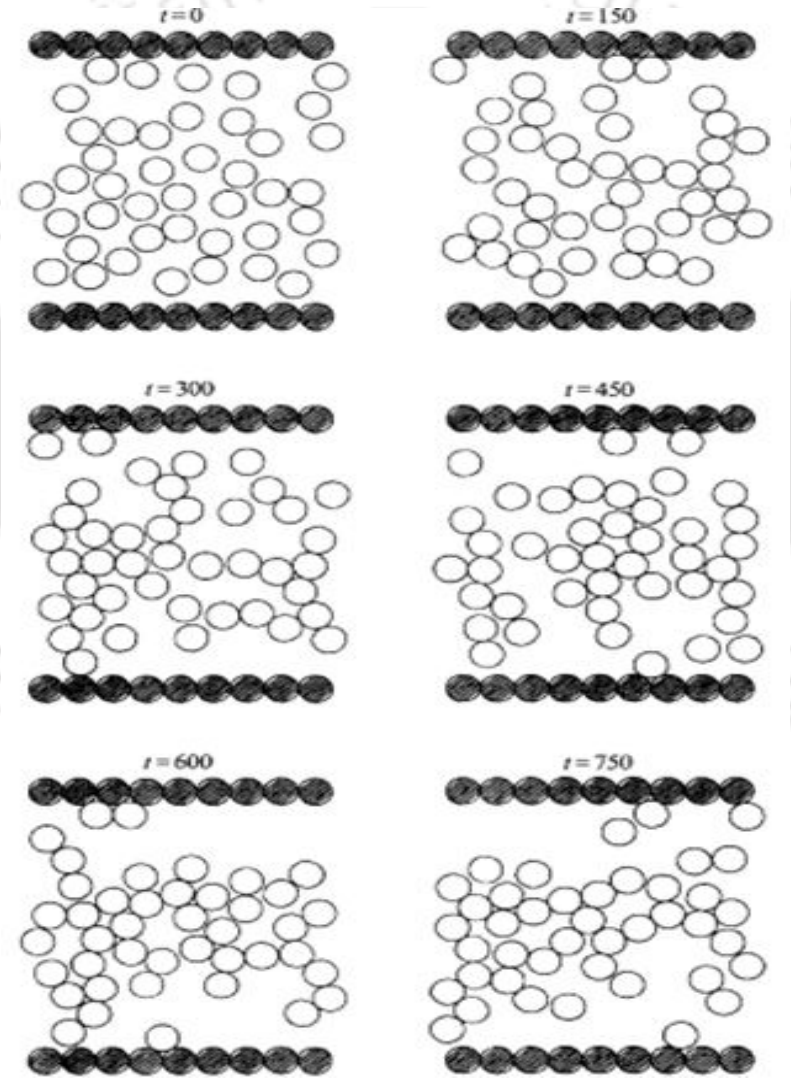

Figure 1.7. Particle configuration snapshot showing migration of particles towards the center of channel. Black circles represent wall and open circles are dispersed particles. (From Nott & Brady, 1994, *Journal of Fluid Mechanics,* ***275***, 157-199. Copyright 1994 by Cambridge University Press).

This model is based on the conservation of mass and momentum for the suspension phase as well as particle phase. The particle velocity fluctuations are introduced with a non-local description of suspension temperature. Stokesian Dynamics simulations were conducted for pressure-driven flow in a channel of a non-Brownian suspension at zero Reynolds number. It was observed that disperse particles gradually migrate towards the center of the channel, resulting in an inhomogeneous concentration profile and a blunting of the particle velocity profile.

1.4 Background and Motivation

Microfluidics has attracted considerable attention in the past few decades because of its wide scientific and engineering applications in medical, pharmaceutical, specialty chemical and food industries. Their advantages are the small volume and large surface area, leading to better mass and heat transfer. The ability to make microfluidic devices optically transparent has made them a natural fit for suspension flow measurement along with the microscopic visualization of change in structure and dynamics of complex fluids, soft particles etc. Flow behavior in these small devices or system is called lab-on-a-chip (LOC), or micro total analysis systems (μTAS). Stone and Kim (2001) and Gravesen et al. (1993) gave some excellent and instructive overviews on microfluidics. When the dimensions of a device or system reach a certain size so that particles of fluid or particles suspended in the fluid, become comparable in size with the apparatus itself, it significantly alters system behavior. For suspension flow in small scale we often observe some interesting phenomenon like shear-induced migration, blunted velocity profile, wall slip etc. Shear-induced particle migration which causes the particles to migrate from the region of high shear rate to low shear rate was explained by Leighton and Acrivos (1987). Dinther et al. (2012) reported that shear-induced particle migration is much more expected to occur in microchannels than in conventional channels with larger dimensions as in microchannels the gradients will be more and the distance over which migration has to take place is considerably less.

To track micron-sized particles in micochannels is not easy as at these small scales, process conditions also effect migration intensely, which further creates difficulty in measuring velocity and concentration profiles. So researchers have used various optical measuring methods. The main experimental methods that Dinther et al. (2012) reported to study the suspension flow in microchannels are electrical impedance tomography, NMR/MRI,

radioactive particle tracking, ultrasound imaging, and optical methods. The important optical methods are laser Doppler velocimetry (LDV), Particle image velocimetry (PIV), Particle tracking velocimetry (PTV), Fluorescence spectral microscopy and Confocal Scanning Laser Microscopy (CSLM). Each of these methods has advantages and disadvantages. NMR and MRI are quite useful in studying concentrated suspensions and do not require refractive index matched suspension. However, due to limited spatial resolution and high cost of equipment's their use in microfluidics research is limited. CSLM method is good but very expensive. The PIV and PTV methods are comparatively low cost and robust to study velocity profile in micro as well as macro sized channels. We aim to employ the combination of PIV and PTV techniques for simultaneous measurement velocity and concentration profile in microfluidic devices. This will help us to understand the effect of channel geometry, size of the particles (relative to the channel width) and particle concentrations on the distribution of flow as well as particles in the test geometry.

1.5 Definition of the problem

So far several fundamental questions have to be answered related to suspension flow in a microfluidic channel under varying geometrical parameters. Till now it is not clear why the redistribution of particles near the bifurcation junctions yield nearly equal particle partitioning but unequal flow partitioning even though the channel is asymmetric. Many interesting phenomena often observed in the suspension flow such as shear-induced migration, particle segregation, blunted velocity profile, wall slip, surface corrugation etc. which are not encountered in simple Newtonian homogenous liquid.

The shear-induced migration phenomenon at low Reynolds number in vivo or in vitro bifurcation channels (Figure 1.8) has many relevant applications in biological and industrial systems. In biomedical application, the artificial heart valves can be designed by a proper understanding of the distribution of the particles in bifurcation channels. Where as in industrial processes it is desired to improve the processing quality of particulate materials and suspensions, which often involve flow in bifurcation channels. Therefore, the effect of bifurcation angle, bulk concentration and flow rate on flow and particle partitioning in symmetric and asymmetric bifurcation channels need to be ascertained to control the shear induce migration of particles.

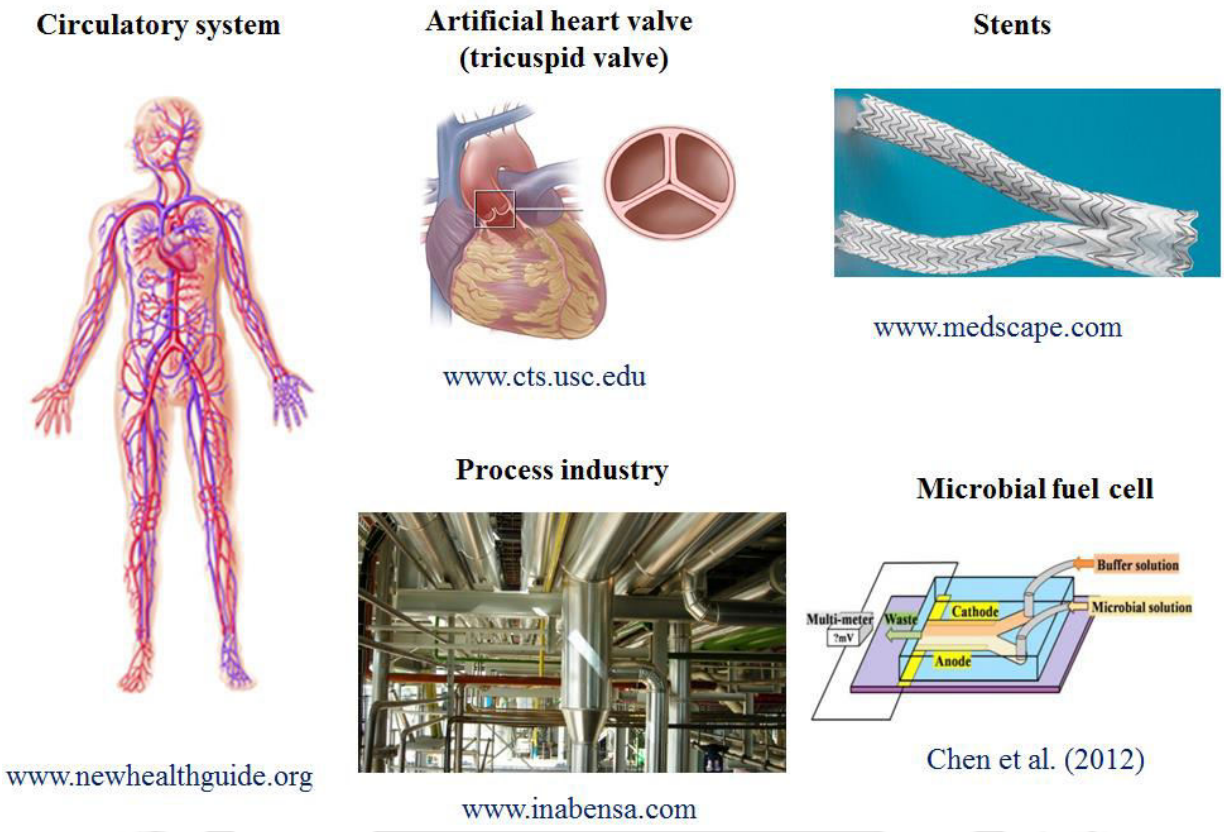

Figure 1.8. Examples of different bifurcation networks.

The objectives for the proposed work can be summarized as follows: -

1. Experimental study of velocity and concentration profile in both symmetric and asymmetric bifurcation channels using the combination of micro PIV and PTV technique.

2. Study the effect of bifurcation geometry (angle, channel width), bulk particle concentration and particle size on particle partitioning and flow partitioning in bifurcation channels.

3. Study the velocity and concentration profile in a diverging-converging channel.

1.6 Literature Review

Majority of the experimental and numerical studies on shear-induced particle migration have been conducted in straight channels or tubes [Min and Kim (2010), Arola et al. (2008), Claesson et.al (2012)].Some recent studies have investigated the dynamics of suspension transport in channels with bifurcations [Leble et al. (2011), Wang et al. (2016)]. Velocity field near the bifurcations is characterized by high deformation rates even at small Reynolds numbers. Shear-induced migration of particles in bifurcating channels can significantly alter the flow field which may have important consequences in physiological flows. A microvascular system in the human body has a number of bifurcation networks, especially in the lung, aorta, and brain. In a blood circulatory system the bifurcation region has been detected as the region prone to aneurysm, Reynaud, coronary artery, carotid disease etc. (Figure 1.9).

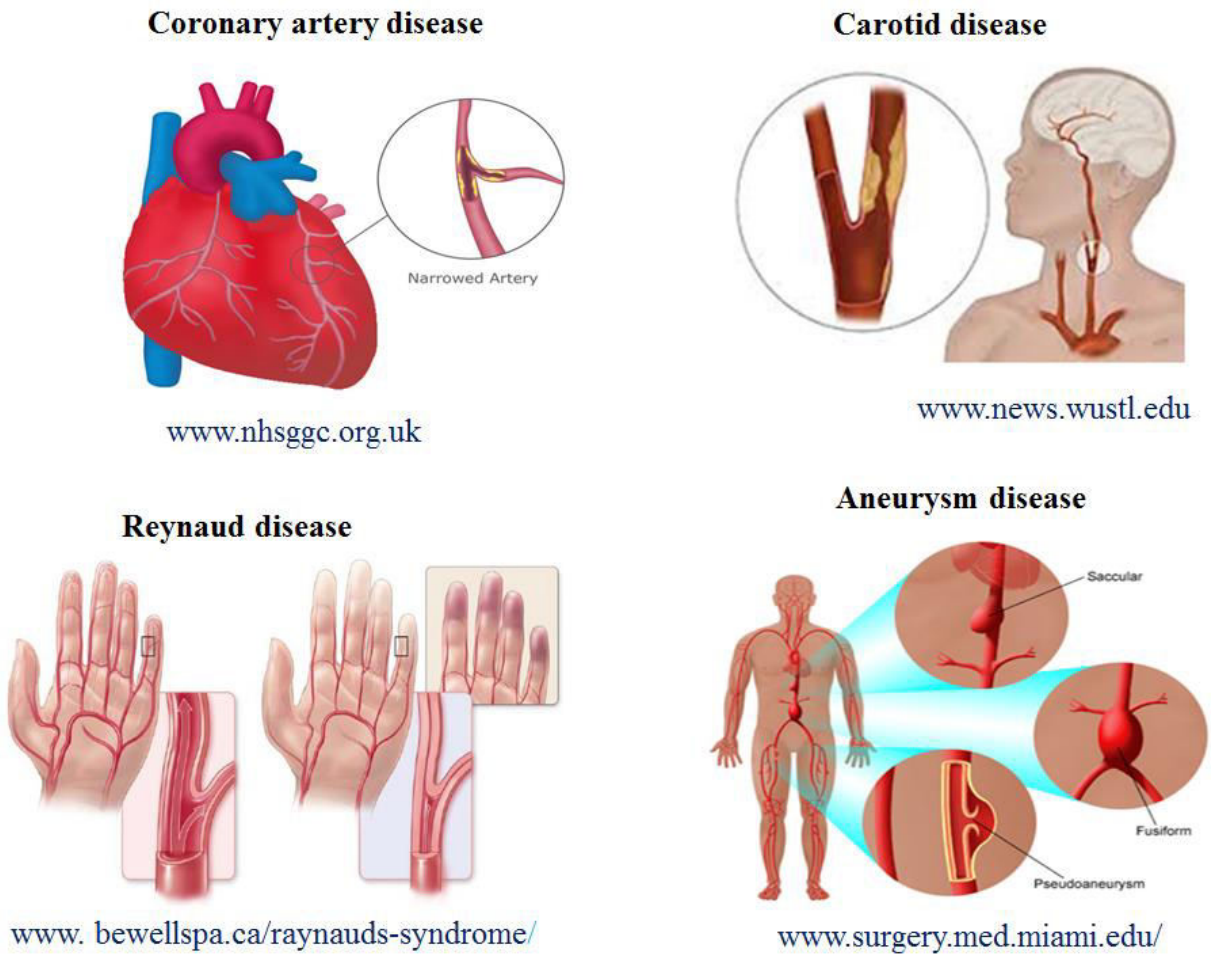

Figure 1.9. Different diseases occur in the bifurcation of blood circulatory system.

It has been broadly acknowledged that the studies of suspension flow in bifurcating network are more significant because the microvascular system consists of various bifurcations which form a closed network. Moreover blood is also a suspension consisting of a continuous Newtonian phase, the plasma, and a solid phase composed of blood cells such as red blood cells (RBC, 6-8 µm diameter), white blood cells (WBC, 10-12µm diameter) and platelets (2-3 µm diameter).Many experimental evidence shows shear-induced migration of RBC in micro and small vessels. Leble et al. (2011) investigated the velocity profiles of RBC through divergent and convergent bifurcation channels using Micro-Particle Tracking Velocimetry (µ-PTV) technique and their geometry is shown in Figure 1.10. They reported that in both bifurcations the velocities of RBCs are asymmetric in nature.

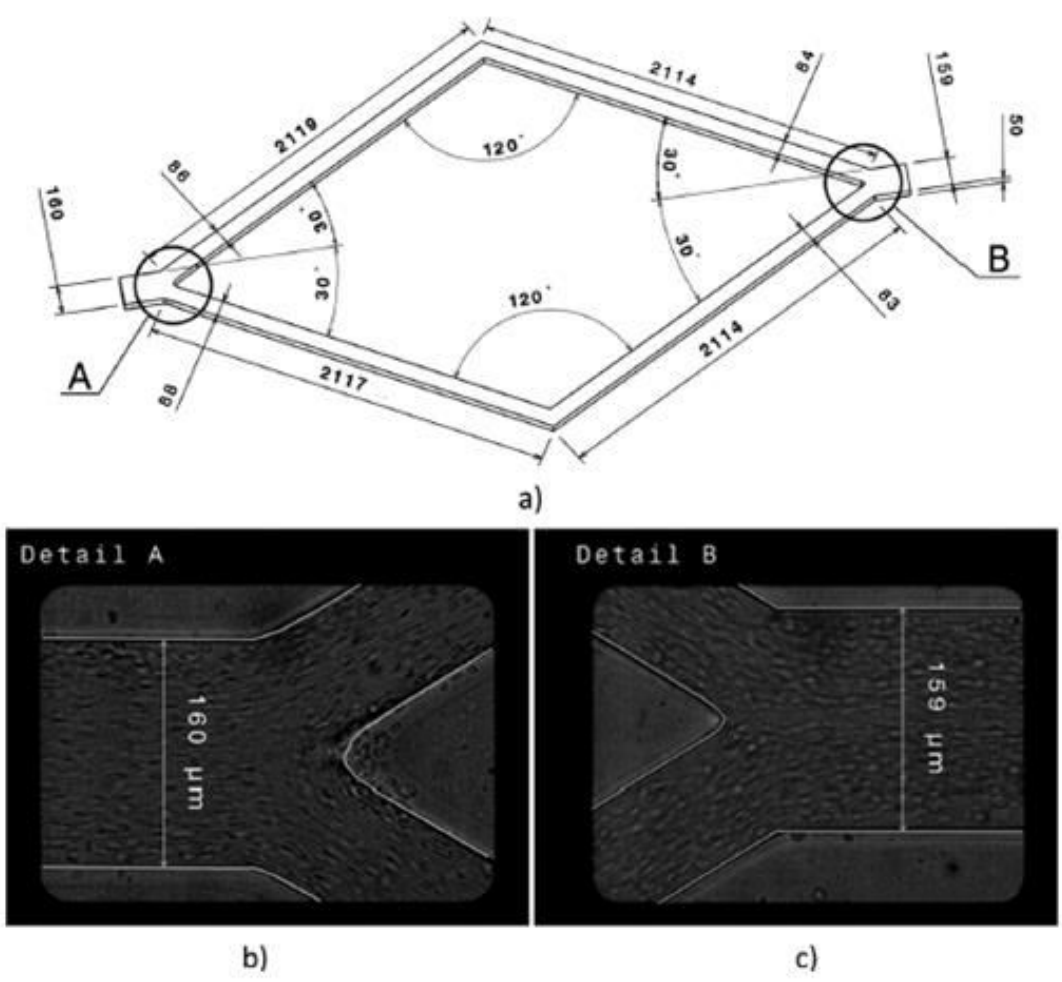

Figure 1.10. Top image: - (a) Full geometry of diverging-converging microchannel. **Bottom image**:- (b, c) zoom image and width of diverging and converging channel respectively. (From Leble *et al*.2011, Biomicrofluidics, **5**, 044120. Copyright 2011 by AIP Publishing).

Ye et al. (2018) carried out dissipative particle dynamics simulation for three-dimensional motion and deformation of a red blood cell (RBC) in a bifurcated microvessel with diverging and converging bifurcations. Sherwood et al. (2014) proposed an approach to infer hematocrit profiles of human blood flowing through bifurcating micro-channel and predicted how the non-uniform distribution of viscosity influences the velocity profiles. They observed blunts in velocity profiles in the inlet section and skewing in the downstream branches. Ha et al. (2012) used a hybrid μ-PIV-PTV technique to measure the centreline velocity of blood flow in rat mesenteric vessels. Lima et al. (2009) studied the shear-induced migration of RBC using a confocal μ-PTV system for different concentration of RBC and channel diameter. Aarts et al. (1988) proposed a method known as "plasma skimming" which is used to separate red blood cells from whole blood by flowing blood through a network of well-designed bifurcations. Enden and Popel (1994) observed that the distribution of red blood cells into branches of bifurcation (Y and T type bifurcation) differs from the distribution of bulk flow. Barber et al. (2008) observed that RBC are significantly deviated from streamlines at bifurcation because of cell migration effects. Anastasiou et al. (2012) used μ-PIV technique to measure the velocity profile, wall shear stress in a circular Y-bifurcation channel for blood analog fluid. Aragall et al. (2015) carried out PIV/PTV measurement and numerical analysis of mono and bi-disperse semi-dilute suspensions in a vertical axisymmetric sudden expansion. They have reported velocity and concentration profile up to 4 % particle volume concentration. Han et. al (2016) carried out numerical simulation in bifurcated vascular networks and results are compared with experimental findings to link local hydrodynamic effect with the bifurcation angle .Their results for velocity profile are presented in Figure.1.11. Gijsen et al. (1999) studied the effect of non-Newtonian properties of blood on the velocity distribution in carotid bifurcation experimentally and numerically. They found that the axial velocity profile of the non-Newtonian fluid was blunted. The non- Newtonian fluid had low velocity gradients at divider wall and high velocity gradients at non-divider wall. Audet and Olbricht (1987) observed that in small vessels, spherical particles having the diameters comparable to the vessel diameter could experience significant drift across background fluid streamlines. Schmid-Schonbein et al. (1980), Perkkio and Keskinen (1983) have proposed mathematical models to understand the flow and particle partitioning and computed the cell distribution at bifurcations. Doutel et al. (2013) measured velocity profiles in a bifurcated channel with stenosis using μ-PIV technique and numerical simulation.

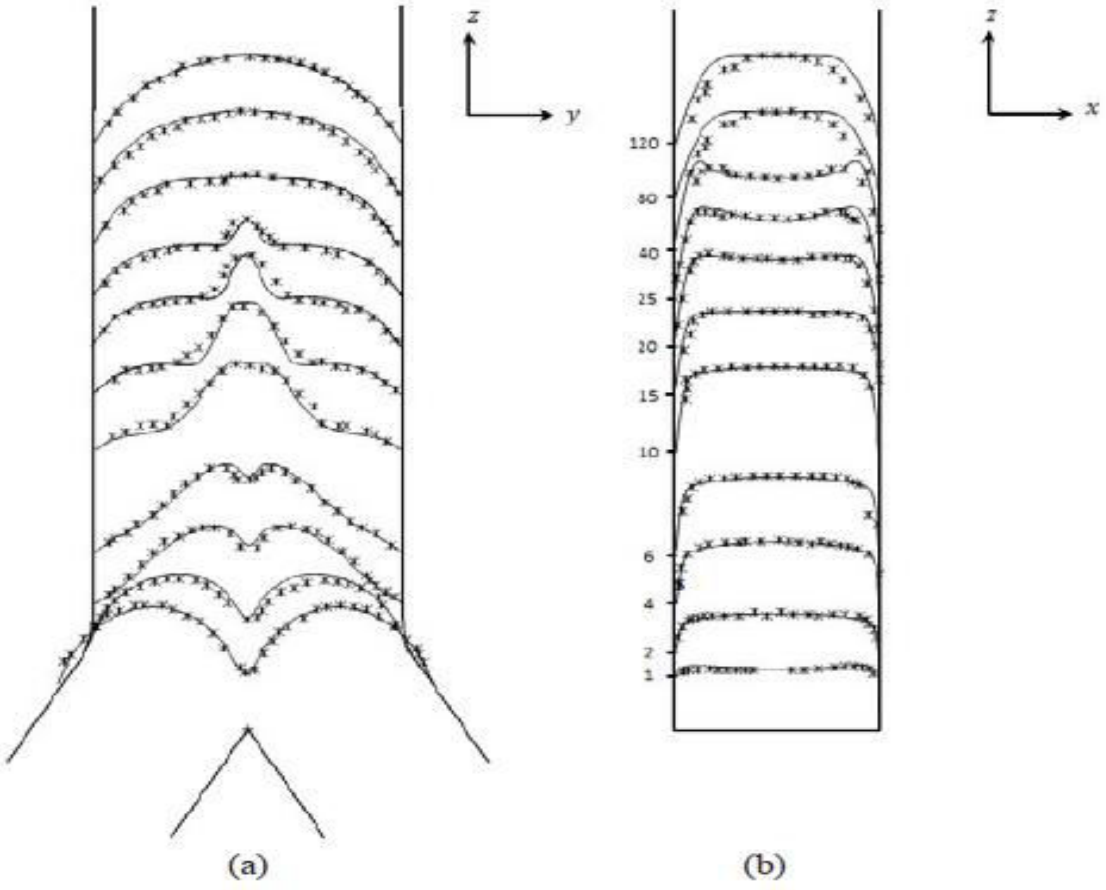

Figure 1.11. Comparison of simulation (-) and experimental (x) velocity profile for bifurcation angle $\theta = 63^0$ in (a) zy plane and (b) zx plane. (From Han *et al.*2016, *Procedia CIRP,* **49**, 14 - 18. Copyright 2016 by Elsevier).

Although studies have been conducted for solid-liquid two phase flows in micro bifurcations network in the past, many aspects of it not completely understood. Ditchfield and Olbricht (1996), Roberts and Olbricht (2003, 2006), Bushi et al. (2005) carried out experiments for low Reynolds number flow of a dilute suspension of monodispersed particles in a Newtonian fluid to study the partitioning of particles in daughter branches of bifurcation channel. Schematic diagram of bifurcation geometry and experimental results of Roberts and Olbricht (2003) are presented in Figure.1.12. Koh and Kim (2007) carried out similar experiments for suspension of bi-dispersed particles in Newtonian as well as non-Newtonian fluids. Davis and Pozrikidis (2012) computed the hydrodynamic instability of spherical mono-dispersed suspension in a circular branching network.

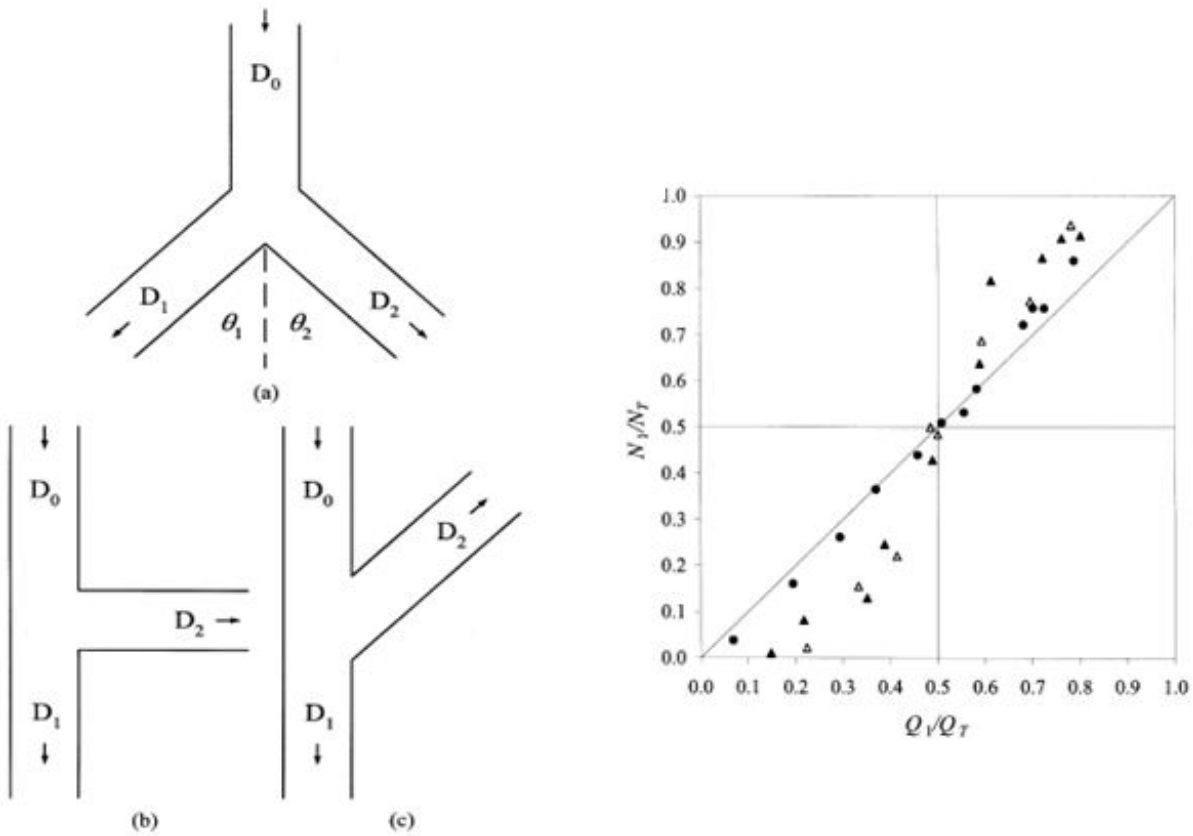

Figure 1.12. Schematic representation of different bifurcation geometry used in the experiment (a) Y shape (b) T shape and (c) oblique. Right side plot showing fraction of particles entering in daughter branch (D_1) as a function of the fraction of total volume entering in the inlet branch of Y-shaped bifurcation. (From Roberts and Olbricht, 2003, *AIChE J*, ***49*** **(11)**, 2842-2849. Copyright 2003 by Wiley publishing group).

Balan and Balan (2012) using μ-PIV and numerical methods studied the velocity profile and vortex formation in bifurcating microchannels with one closed daughter branch for shear-thinning fluids. Their experimental set-up is shown in Figure.1.13. Fridjonsson et al. (2011) using dynamic NMR microscopy studied the flow and distribution of Newtonian, polymeric and colloid suspension fluids in Y-shape bifurcation having dissimilar opening. They reported that secondary flows generated near the bifurcation influences the partitioning of fluid in the daughter branches. For two phases flow where the interest is to know the velocity profiles of both the phases hybrid μ-PIV-PTV method is widely used [Aragall et.al (2015), Korevaar et al. (2015)].

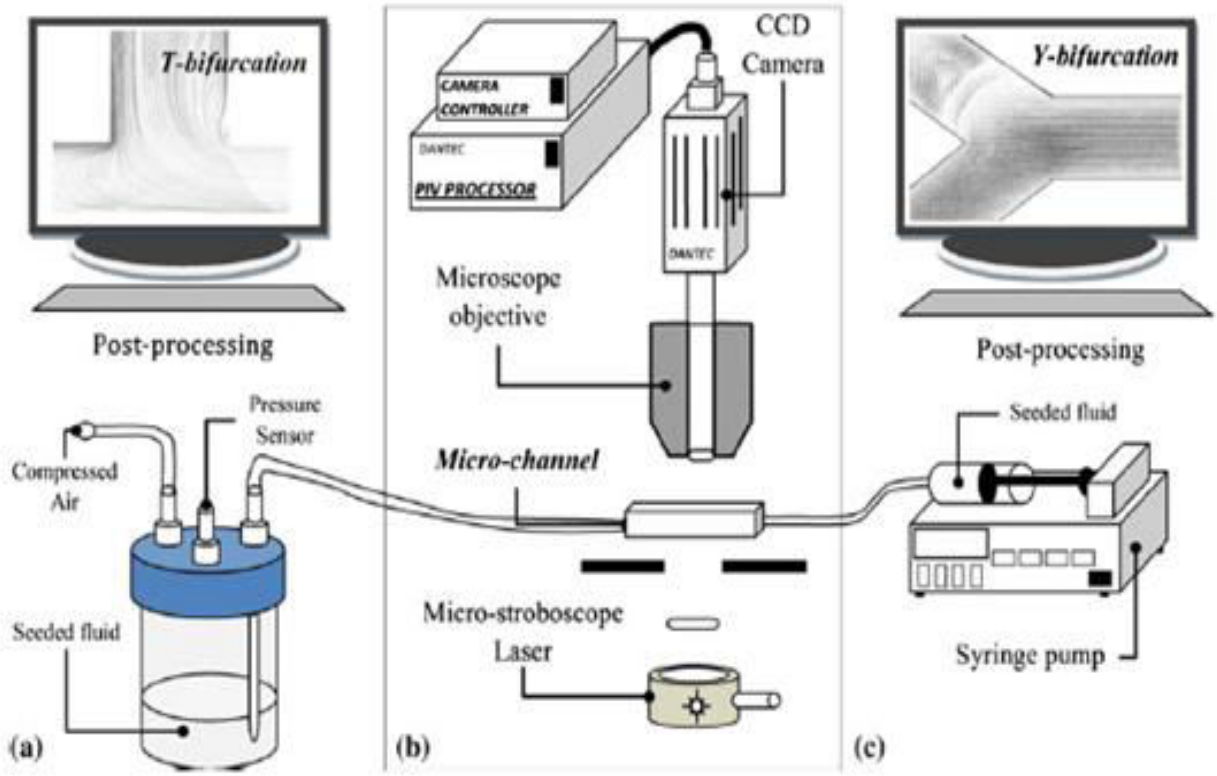

Figure 1.13. (a,c) T and Y shape geometry used in the experimental (b) Schematic representation of the micro-PIV measurement system. (From Balan and Balan, 2012, *Microfluidics and Nanofluidics,* **13**,819–833. Copyright 2012 by Springer).

Xi and Shapley (2008) carried out experimental measurements using nuclear magnetic resonance (NMR) technique to study velocity and concentration profile of concentrated suspension flowing through an asymmetric bifurcation channel and their results are presented in Figure.1.14. Later Ahmed and Singh (2009) performed numerical simulations of concentrated suspension flow in the same channel that was used in the experiments of Xi and Shapley (2009) using the Diffusive flux model, Phillips et al.(1992) and observed good agreement of their simulation results with the experimental data.

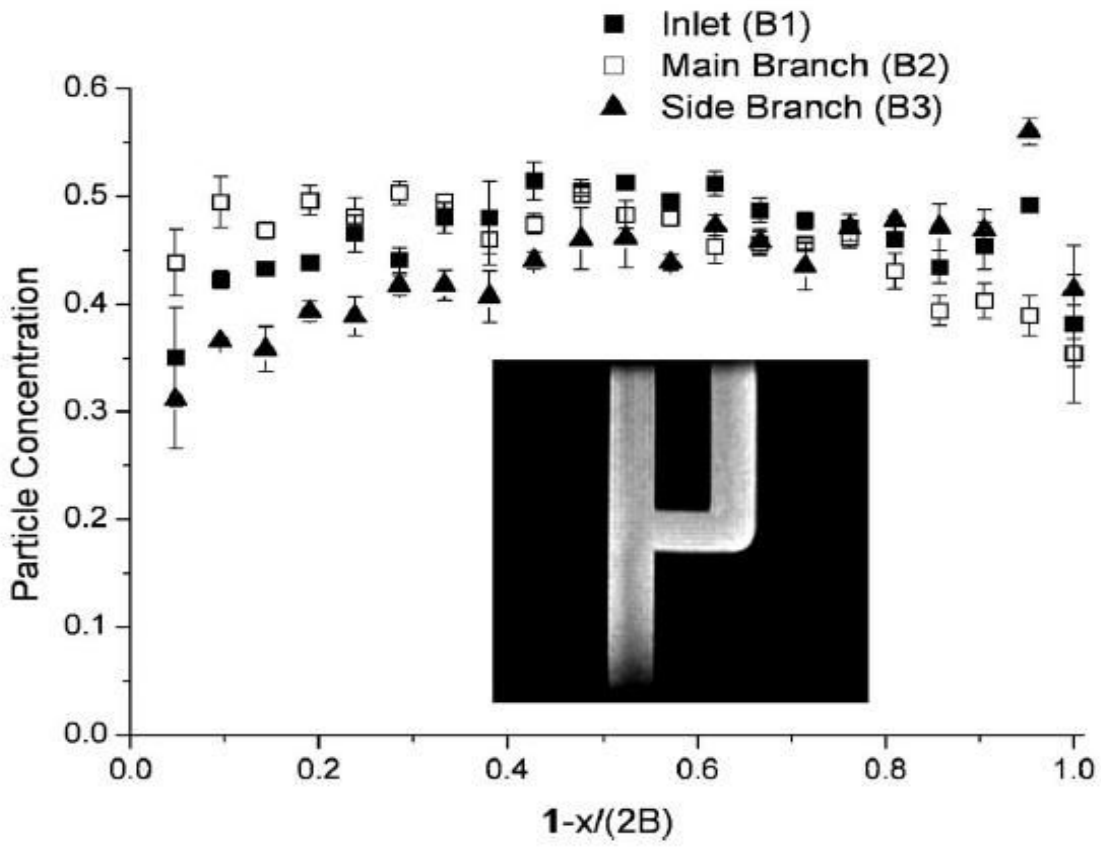

Figure 1.14. Particle concentration profiles along the centre lines (B1, B2, B3), where ϕ=0.4, Q=16.1 ml/min and Re=0.046. (From Xi and Shapley, 2009, *Journal of Rheology*, **52(2)**, 625-647. Copyright 2009 by Society of Rheology).

Subsequent to these studies there has been several other works where numerical simulations using the 'Diffusive flux model' was used to study velocity and particle concentration profiles in bifurcating channels [Siqueira et al. (2017), Reddy and Singh(2014), Yadav et al.(2015,2016)]. These studies have reported that the particle partitioning in the daughter branches does not follow the flow partitioning due to shear-induced particle migration. The velocity and concentration profile for suspension flow were observed to be symmetric in the inlet branch but asymmetric in the daughter branches. Simulation results of Reddy and Singh (2014) are presented in Figure 1.15. Recently Medhi et al. (2018) reported from μ-PIV/PTV experiments on different bifurcation geometry that migration of particles occurs across the streamline and symmetric velocity and concentration profile in the inlet branch becomes asymmetric in the daughter branches. Further migration of particles towards the center of the channel in the daughter branches makes the profiles again symmetric. D'Avino et al. (2015) investigated numerically the effect of fluid rheology in partitioning of particles suspended in

non-Newtonian fluids flowing in a T-junction. All these experimental and numerical studies have demonstrated that the partitioning of particles between the two downstream branches is different from the partitioning of the total suspension between these branches. The magnitudes of fluid-particle partitioning in bifurcation channel depends upon particle size, the particle volume fraction, volumetric flow rate, angles between the branches. Although in these experiments particles loading seem small but they observed that interactions between particles inside the bifurcation were considerably more common which causes unequal distribution of particles in bifurcation network. Observations shows that as the particles near the apex of a bifurcation its transitional velocity decreases and the next particles in the upstream has time to enter the bifurcation and interact with the earlier particles. These interactions perturb the trajectory of particles near the bifurcations resulting unequal fluid and particle partitioning in the downstream branches.

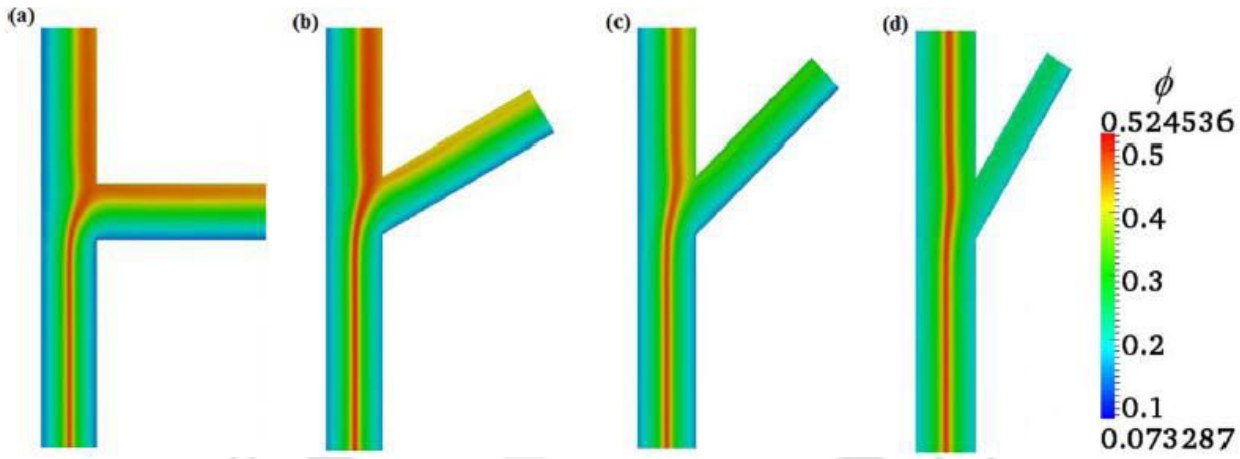

Figure 1.15. Contours of particle volume fraction of suspension for different bifurcation angles: (a) $\theta = 0^0$ (b) $\theta = 30^0$, (c) $\theta = 45^0$, and (d) $\theta = 60^0$. The bulk particle concentration was, ϕ =0.4. (From Reddy and Singh, 2014, *AIChE J,* ***60*** **(7)**, 2692-2704. Copyright 2014 by Wiley publishing group).

1.7 Outline of the thesis

In this work we have performed the micro-PIV/PTV experiments for single-phase Newtonian fluid and dilute suspension of two different size particles in bifurcation channels for a range of branching angle for diverging and converging flow condition. We have also conducted experiments on diverging-converging channels of varying width. The flow velocity profile was measured by micro-PIV and local concentration was measured by image processing method and micro-PTV. This will help to identify and quantify the effect of particle size, branching angle, type of flow on the velocity and concentration profiles. Results from this work will provide an unprecedented level of detail about the effect of shear-induced particle migration on unequal distribution of the phases in the downstream branches. These observations have important consequences in the development of microfluidic devices handling transport of suspension in bifurcating microchannels.

In Chapter 1, the origin of our studies is illustrated. A review of relevant literature survey on shear-induced migration phenomena and suspension flow in bifurcation channel was discussed. In Chapter 2 we have discussed about working principle of Particle Image Velocimetry (PIV), Micro Particle Image Velocimetry (μ-PIV) and Micro-Particle Tracking Velocimetry (μ-PTV) technique to study the flow of suspension in bifurcating channels. In Chapter 3, the diverging flow of suspension in bifurcation channels for a range of branching angle were discussed. Micro-PIV/PTV experiments were performed for simultaneous measurement velocity and concentration profile. Here we have also elaborated on the fabrication of microchannels, post-processing of captured images before PIV/PTV analysis. Particle counting MATLAB program was used to study qualitatively the concentration profile. In Chapter 4, results for converging flow of suspension in the same microchannels keeping the experimental parameter same as diverging flow was reported. In Chapter 5, the flow of suspensions in diverging-converging channels of varying width were examined. In Chapter 6, we have discussed the fidelity of developing “Turn in Corner” type velocity based micro rheometer for online monitoring and measurement of rheological properties of the complex fluid using symmetric bifurcating channel. In Chapter 7, the free surface flow of concentrated suspension in T and Y bifurcation channels were investigated. Finally, the main conclusion and overall impact of the work are discussed, as well as opportunity for extending our research works are presented in Chapter8.

Chapter 2

Experimental details and methodology

2.1 Introduction

In this research work, we have used Particle Image Velocimetry (PIV), Micro-Particle Image Velocimetry (μPIV), Micro-Particle Tracking Velocimetry (μPTV) technique to study the flow of suspension in bifurcating channels. Details of working principle of each method and its components are described in this chapter.

2.1.1 Particle Image Velocimetry

Particle Image Velocimetry (PIV) is a non-intrusive, indirect, full field optical technique to determining velocity fields from images of seeded flows. PIV techniques are still developing, a number of review papers and books have already been published, some of important papers are-[Adrian (1991, 2005), Tropea et al. (2007), Wereley and Meinhart (2010), Katz and Sheng 2010)] and two books are [Raffel et al. (1998), Adrian and Westerweel (2011)] which together illustrate the historical development, measurement technique, and applications of PIV. The main components of PIV setup are light source such as laser or fluorescence lamp, CCD camera, frame grabber, tracers etc. as shown in Figure 2.1. Here in this Figure 2.1 the light source of the optical system is a double pulse laser and operates at a wavelength of 532 nm. Plane mirrors are used to reflect the beam and a cylindrical lens is used to generate a light sheet to illuminated test region (shown in Figure 2.1). In modern PIV a synchronizer is used to synchronize pulsed light source with a digital camera. The images are captured by using a CCD camera in conjugation with a macro zoom lens. The camera can either operate in fixed mode (video mode) or in double shutter mode to capture images. Displacement of a particle between two successive images ascertains the motion of the fluid. Flow can be visualized by seeding the flow with micron size tracer particles. Flow velocity can be calculated from a pair of images by using the PIV analysis software. The captured images

are interrogated using two-frame cross-correlation technique [Adrian et al. (1995)] to get velocity vector field.

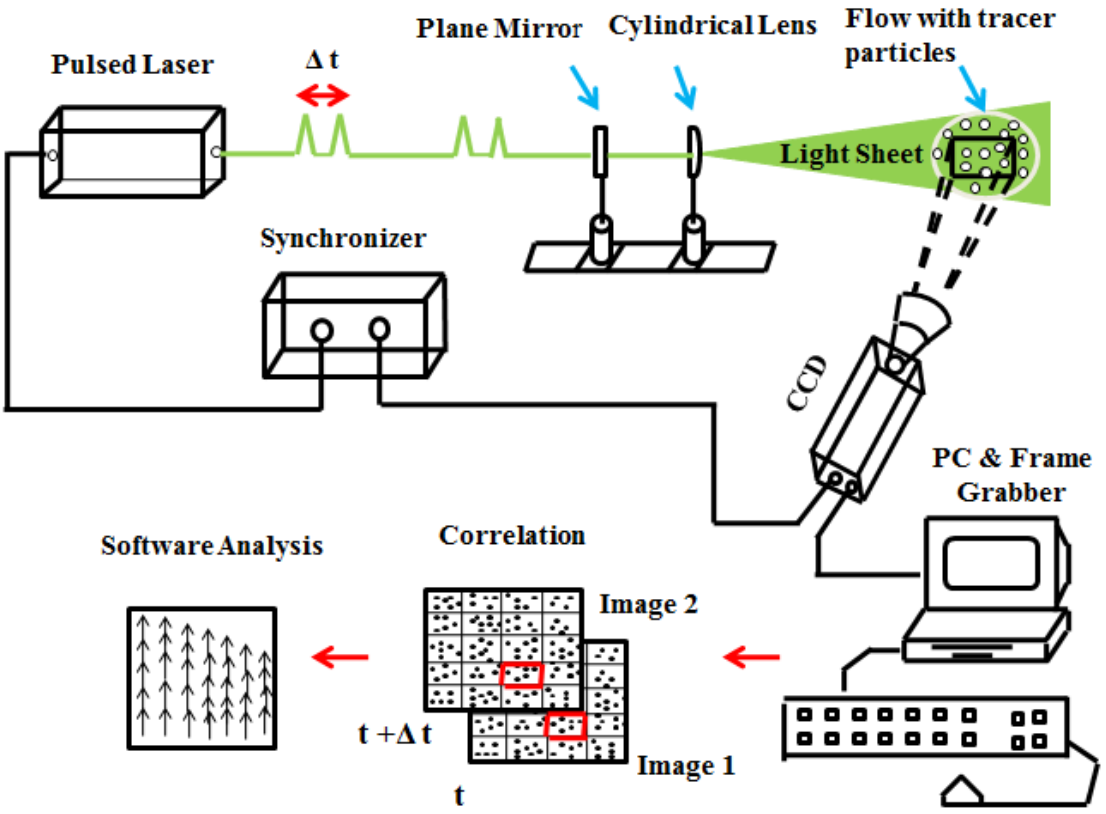

Figure 2.1. Experimental arrangement for Particle Image Velocimetry.

The theory behind a PIV system is easy and simple: The fluid of interest is seeded with neutrally buoyant tracer particles, which are illuminated by a light source and the images of these tracer particles at different times are recorded by a recording medium CCD camera. Displacement of a particle between two successive images ascertains the motion of the fluid. The captured images are divided into identical grid known as interrogation windows (IWs) and data are calculated by the correlation technique. The size of the IW should be small enough such that particle displacement in the area is consistent, additionally, IW should be large enough so that it contains an adequate number of particles.

The density of tracer particle images is one of the important parameters for success of any optical measurement method. The density represents the mean number of particle images in an interrogation region. For a successful PIV measurement, it is important that this number is

at least 10-15. Schematic representative of low and high seeding density flow is shown in Figure 2.2.

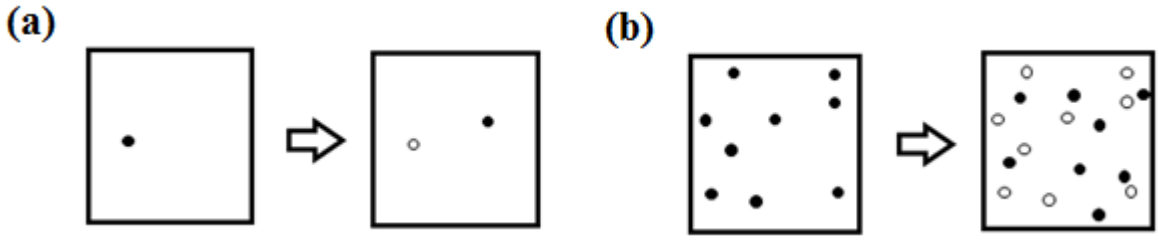

Figure2.2. Schematic representative of (a) Low seeding density (b) high seeding density flow. (From Westerweel, 1997, *Measurement Science* and *Technology*, **8,** 1379–1392. Copyright 1997 by IOP Publishing).

Low particle density $N_I << 1$ — Particle Tracking Velocimetry (PTV)

High particle density $N_I >> 1$ — Particle Image Velocimetry (PIV)

Where image density:- $$N_I = \frac{C\Delta z_0}{M_0^2} \cdot D_I^2 \quad (2.1)$$

C = tracer concentration

z_0 = light-sheet thickness

M_0 = image magnification

D_I = interrogation spot diameter

For low density of tracer particles, it is very easy to estimate displacement from individual tracer particles as the distance between tracer particles is considerably more than the displacement. This kind of procedure is normally stated as low image density PIV (or, particle tracking velocimetry). If we increase the tracer concentration, then displacement of particles becomes larger than their spacing, and it is no longer possible to recognize matching pairs clearly. This type of procedure is normally referred to as high image-density PIV (or, laser speckle velocimetry).

As stated above the captured images are divided into identical grid known as interrogation windows (IWs) and data are calculated by correlation technique. Different correlation methods are -

Auto-correlation method: This method is used for single frame multi-exposure type of images. Here correlation of interrogation window is done on the same window. The directional ambiguity of displacement occurs in this type of method due to the symmetry of correlation and also this method can't detect small displacement.

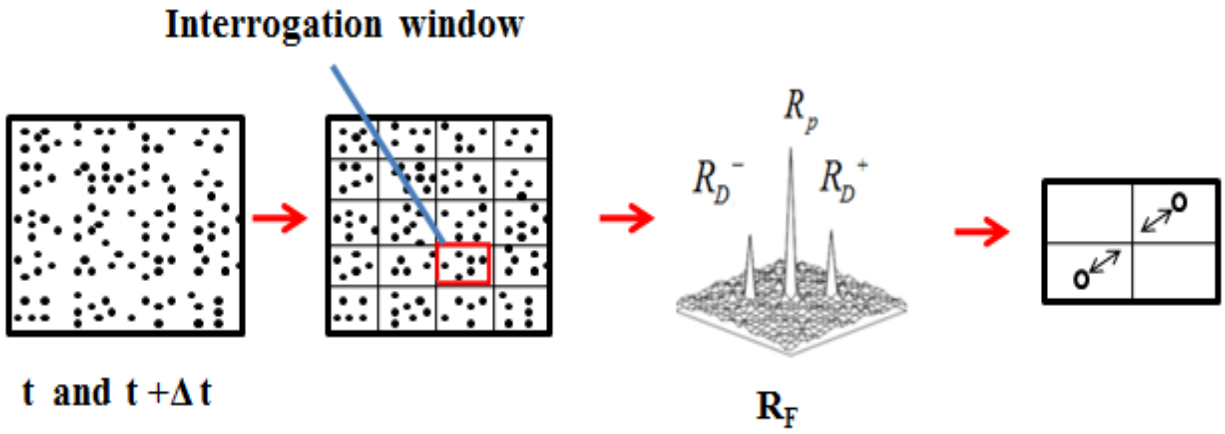

Figure 2.3. Flow chart of auto-correlation method (Conecept taken fromRaffel et al., 2007, A Practical Guide. to Particle Image Velocimetry. *Springer-Verlag*, Berlin).

Figure 2.3 presents a flowchart of the fully digital auto-correlation method, which can be implemented straightforwardly by using Fast Fourier transform (FFT). The equation for autocorrelation method can be expressed as-

$$R_{auto} = R_p + R_D^+ + R_D^- + R_F \qquad (2.2)$$

Where,

R_F = Noise for the background or noise in correlation due to the missing of particle pairs

R_p = A central self-correlation peak

R_D^+ & R_D^- = Two displacement-correlation peaks on either side of the self-correlation peak.

Two frame cross-correlation method: Now a day's two frame cross-correlation method is the most accurate method. In this method there is no directional ambiguity and also very small displacements can be measured .

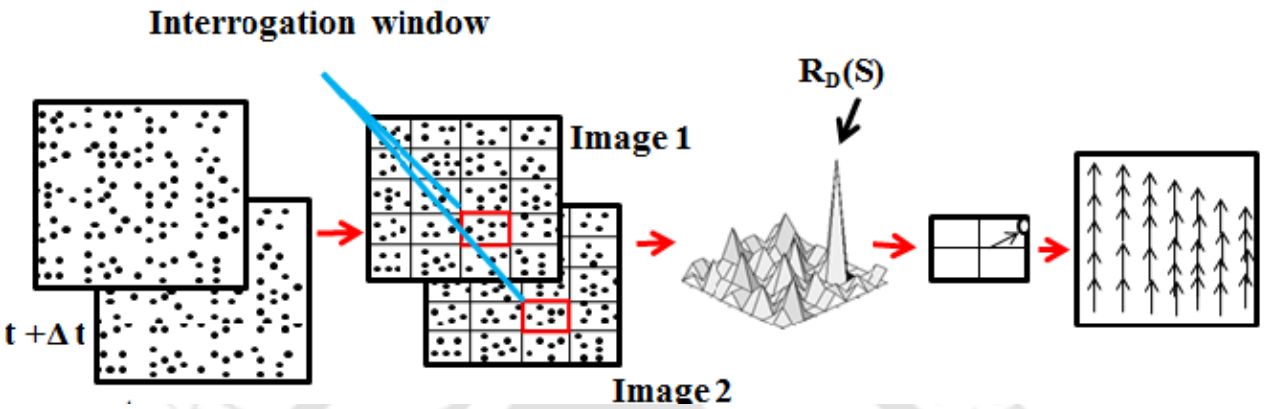

Figure 2.4. Flow chart of two frame cross-correlation method (Conecept taken fromRaffel et al., 2007, A Practical Guide. to Particle Image Velocimetry. *Springer-Verlag*, Berlin).

Figure 2.4 presents a flowchart of the fully digital two frame cross-correlation method, which can be implemented straightforwardly by using Fast Fourier transform (FFT). Spatial correlation can be written as

$$R(\mathbf{s}) = \int I_1(\mathbf{X})\, I_2(\mathbf{X}+\mathbf{s})\, d\mathbf{X}. \qquad (2.3)$$

Where, intensity

$$I = \langle I \rangle + I'$$

Here $< I >$ = Mean Intensity

I' = Intensity of fluctuation

The spatial correlation can be separated into three terms:

$$R(\mathbf{s}) = R_C(\mathbf{s}) + R_F(\mathbf{s}) + R_D(\mathbf{s})$$

R_C = Correlation between mean intensity and intensity fluctuations

R_F = Mean background correlation

R_D = Correlation of image fluctuations

When mean intensity <I> is subtracted from I_1 and I_2,

$$R_C = R_F = 0 \quad (2.6)$$

Post-processing of PIV data is needed for the cases like if the captured image has low particle density, for inhomogeneous particle seeding, if tracer particle trap within a vortex and 3D movement of particle. All these together give spurious vector (these are considered as high frequency signals) which must be minimized to get correct information of flow field. Normally filters like a temporal median filter, median local filter is use to minimize these spurious vectors. Even after that also some spurious vectors may present in the PIV data which has to replace with correct vectors. This can be done by taking mean or median of surrounding velocities, or a weighted average of surrounding velocities.

2.1.2 μ-Particle Image Velocimetry

The concept of μ-PIV (micro-PIV) borrows from modern PIV technique in order to access the small scales of microfluidic devices. In last one decade, μ-PIV has been applied by an increasing number of scientists to study flow in microfluidic devices. The theory behind a μ-PIV system is almost same as PIV: The fluid of interest is seeded with neutrally buoyant tracer particles, which are illuminated by a light source and the images of these tracer particles at different times are recorded in a recording medium such as a photographic film. Finally, images are analyzed to find the displacement of particle between two successive images which ascertain the motion of the fluid. Santiago et al. (1998) first conducted a successful μ-PIV experiment. The component of his experimental setup was a fluorescence microscope, CCD camera, a Hg-arc lamp as continuous light source and the tracer particles, which were dyed with a fluorescent material. Meinhart et al. (1999) demonstrated a μ-PIV system by replacing light source with two pulsed Nd: YAG lasers keeping other components same as Santiago et al. (1998). He studied pressure driven flow in a microchannel.

According to Wereley et al. (2002), μ-PIV can be distinguished from macroscopic measurement by the following ways-

- In μ-PIV, if tracer particle size falls below 1 μm Brownian motion may occur, creating a significant error in velocity determination. There is no effect of Brownian motion in PIV technique.

- In PIV a thin sheet of laser light is generated in order to illuminate the measured area within the flow. Due to the small length scales associated with μ-PIV thin laser sheet generation is not feasible so the entire volume of the flow is illuminated.

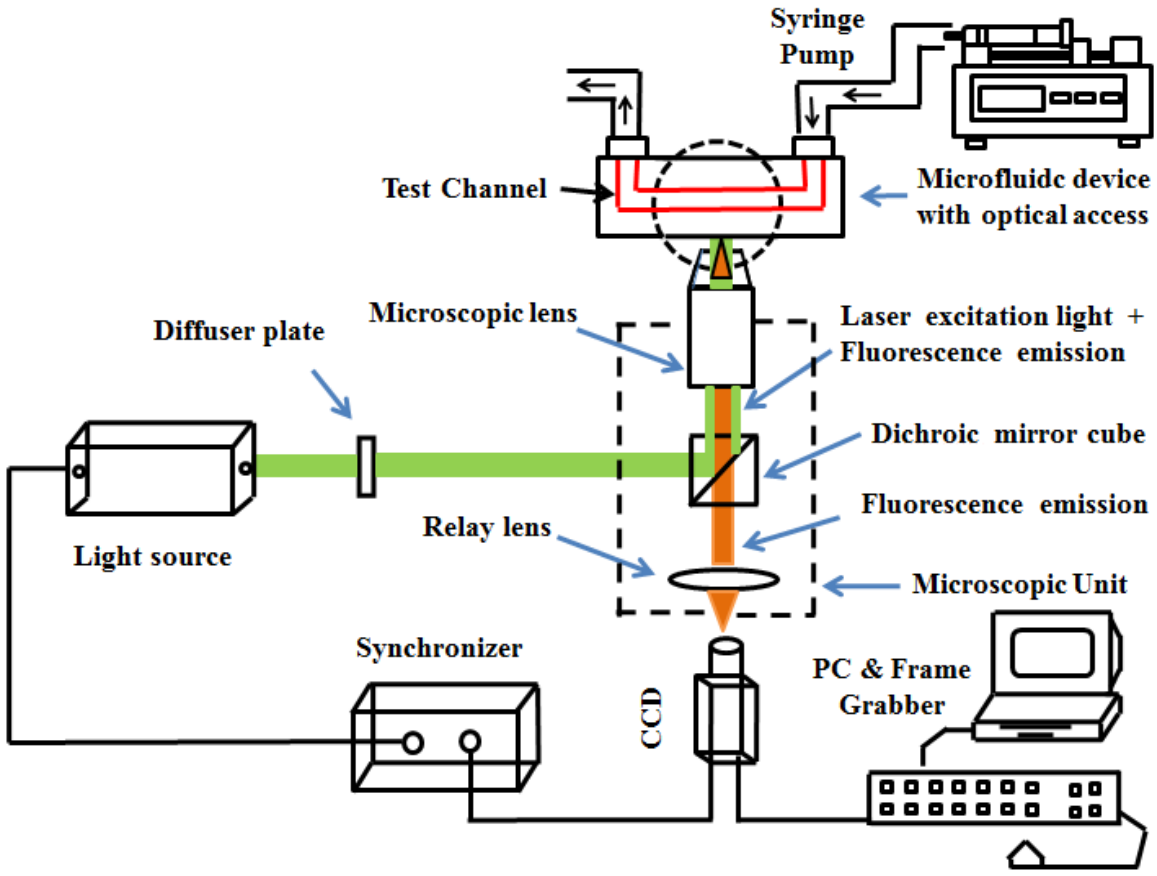

Figure 2.5. Schematic diagram of a typical μ-PIV experimental setup (Concept taken from Lindken et al. 2009*, Lab on a Chip*, **9(17)**, 2551-67).

The schematic of a typical μ-PIV experimental setup shown in Figure 2.5 and it consists of flow, optical and recording systems**.** A physical model of microchannel generally made of

glass or PDMS gel to ensure optical transparency. The test fluid is seeded with fluorescent tracer particles which are illuminated by a light source. Preferably a syringe pump should be used to circulate the fluid in the channel. The illuminated images captured using a CCD camera attached with a microscope. Once images were captured post-processing and analysis of images should be done similar to PIV. Some of the important components of a μ-PIV experiment are as follows-

Seeding

Seeding flow with tracer particles is essential to generate a durable fluorescent signal. It makes the excitation and emission wavelengths of seeding particles are compatible with the rest of the optical system, which significantly improves the signal to noise ratio. In μ-PIV, these seeding particles size must have density closely matching with the suspending fluid and it's being small enough to faithfully follow the flow without disturbing the flow field or clogging the device. At the same time, particles need to be large enough to be effectively imaged and to reduce the effects of Brownian motion. Due to optical constraint, Lindken et al. (2009) has suggested tracer particle size of 0.5-1.5μm, with particle image diameter same as 2-3 pixels. When seeded particles size falls below 1μm, particle-fluid interactions cause random particle movement, averting the particles from following the flow faithfully. The expression for diffusion coefficient can be written as-

$$D = \frac{kT}{3\pi\mu d_p} \tag{2.7}$$

Where D is the Stokes-Einstein diffusion coefficient, d_p is particle diameter, k is Boltzman's constant, T is the absolute temperature of the fluid and μ is the dynamic viscosity of the fluid.

The response time of a tracer particle should be lesser than the smallest time-scale in the flow. Response time can estimate by below equation (Raffel et al. 2007b)-

$$\tau_p = \frac{d_p \rho_p}{18\mu} \tag{2.8}$$

Where τ_p is response time, d_p diameter and ρ_p density of the tracer particle and μ is the dynamic viscosity of the fluid.

As stated earlier, when seeded tracer particles size falls below 1µm, Brownian motion occurs and the error in measurement can be express as -

$$\varepsilon_B = \frac{1}{u}\sqrt{\frac{2D}{\Delta t}} \tag{2.9}$$

Santiago et al. (1998) has measured the influence of Brownian motion in his work. From equation 2.9 it is obvious that as flow velocity increases the effect of Brownian motion becomes of lesser importance. Moreover, as the diffusion coefficient D is proportional to fluid temperature and inversely proportional to particle diameter, the error increases with both increasing temperature and lesser particle diameters. Similarly, the error due to Brownian motion is decay with increasing time of travel Δt.

Tracer particle concentration is another important parameter to be considered for accurate measurement. The concentration tracer particles should be such that in each IW for the cross-correlation contains at least 10-15 particles. The expression to calculate tracer particle concentration is -

$$C_{tr} = \frac{2{d_p}^2 M^2 \beta^2 (s_0 - a)(s_0 - a + L_f)}{3V_2 L {s_0}^2 \{M^2 {d_p}^2 + 1.49(M+1)^2 \lambda^2 [(\frac{n_0}{NA}) - 1]\}} \tag{2.10}$$

Where $\beta^2 = 3.67$, L_f is measured flow thickness, s_0 is the focal plane distance of the objective, a is the measurement depth, λ is the wavelength of laser, n_0 is the refractive index of the lens immersion liquid. V_z is particle visibility which is the ratio of the intensity of a focused particle image to the average intensity of the background light produced by the unfocused particles (Olsen and Adrian 2000). Raffel et al. (2007b) suggested that V_z value should be greater than 1.5 for high quality velocity measurement.

Illumination:

In typical PIV, a light sheet defines the measurement plane, the camera field-of-view (FOV) defines the measurement area and the light sheet thickness defines the thickness of the measurement volume. For µ-PIV, the illumination mode is often volume illumination, as

even a thin light sheet often has a thickness similar to the channel dimension. The microscope objective's depth-of-field determines the thickness of the measurement volume.

Pulsed light Sources:

A modern μ-PIV system consists of a pulsed light source that is synchronized with the digital camera by a timing unit. The synchronization is done in a way that the first light pulse is set at the end to the first image recording and the second pulse is set at the beginning of the second image. In this way, the time interval Δt is independent of the camera frame rate but defined by the time interval between the two synchronized light pulses. The time interval can now be adjusted according to the flow conditions. A double-pulsed, Nd: YAG laser emitting wavelength of 532nm is commonly used as light source. An optical fiber is used to deliver the beam to the microscope. Alternative light sources for μ-PIV are high power LEDs. On-going development of these laser diodes and high-power LEDs will raise the applicability of these types of light source in μ-PIV recordings.

Filter Cube:

It is located between the light collecting objective and the digital camera. Filter cube reflects light at the illumination wavelength and transmits the fluorescent light that has a longer wavelength. As a result of filter cube, light originating from the tracer particles is collected on the camera sensor, while light originating from the channel walls and other non-fluorescent disturbances are blocked by it. This significantly increases the signal to noise ratio of the μ-PIV measurement.

Depth of correlation

Thickness of the measurement plane for μ-PIV and μ-PTV analysis is one of the important parameter in this type of experiment which is normally expressed in terms of DOC (depth of correlation). The DOC depends on the depth of field of the objective and on the size of the particles. Schematic of μ-PIV volume illumination principle is shown in Figure 2.6.

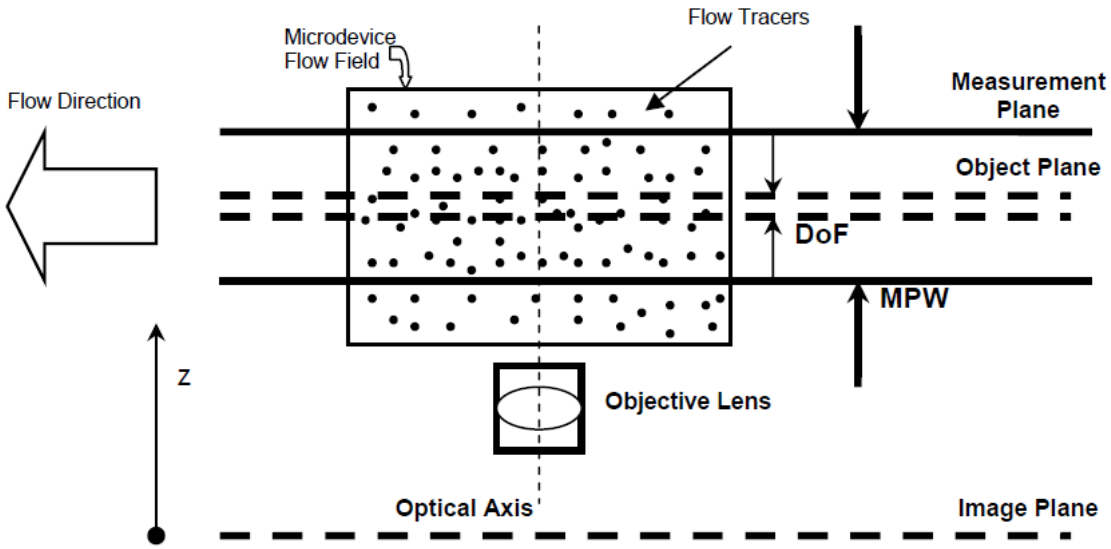

Figure 2.6. The μ-PIV volume illumination principle: the depth of focus (DoF) is always much lower than the measurement plane width (MPW) or DOC. (From Koutsiaris, 2012, *The Particle Image Velocimetry - Characteristics, Limits, and Possible Applications.* Copyright 2012 by InTech).

The expression to calculate DOC for μ-PIV was derived by Olsen and Adrian (2000)

$$DOC = 2\left[\frac{(1-\sqrt{\varepsilon})}{\sqrt{\varepsilon}}\left(\frac{n_0^{\,2} d_p^{\,2}}{4NA^2} + \frac{5.95(M+1)^2 \lambda^2 n_0^{\,4}}{16M^2 NA^2}\right)\right]^{1/2} \qquad (2.11)$$

where ε is the relative threshold below which the defocused particle images no longer contribute significantly to the displacement correlation peak, normally set to be equal to 0.01., n_0 is the refractive index, d_p is the diameter of the particle, M is magnification number, NA is numerical aperture of the objective lens (Koutsiaris, 2012), λ is the laser wavelength.

2.1.3 Particle Tracking Velocimetry

As the name suggests Particle Tracking Velocimetry (PTV), individual particles are tracked, so this technique is a Lagrangian approach. In contrast to Particle Image Velocimetry (PIV), which is an Eulerian method that measures the velocity of a fluid by dividing the test area into a rectangular grid. In the PTV method typically a single phase particle is tracked and particle center detection is used with the nearest neighbor matching particles. This is to determine the most probable single particle displacement allowed for tracking each of them individually in several frames. For PTV, low particle seeding density is necessary to ensure good tracking between IWs.

In this work, we have used μ-PIV/PTV method to study the suspension flow in bifurcation channels. In our μ-PIV/ PTV experiment objective was to simultaneously measure the fluid phase and particle phase velocities with one camera system. Researchers have used various PIV/ PTV technique to measure fluid and particle phase velocity. Some of the important works are-

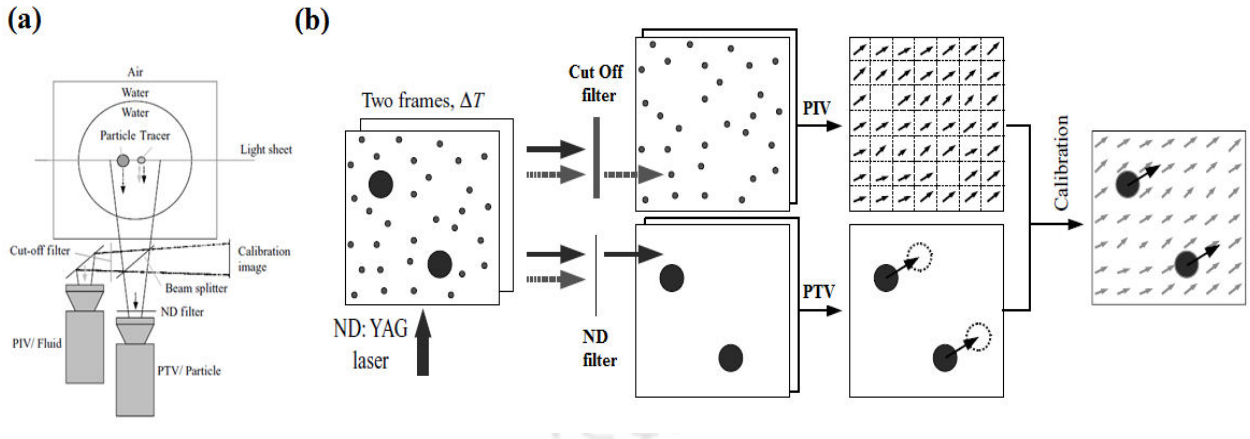

Figure 2.7. Schematic illustration of the (a) simultaneous measurement of the fluid and dispersed phases using fluorescent tracer particles (b) data processing to obtain to simultaneously velocity measurement of particle and fluid phase. (From Poelma *et.al* 2007, *Journal of Fluid Mechanics,* **25(589)**, 25–56. Copyright 2007 by Cambridge University Press).

Poelma et.al (2007) used a duel camera system for simultaneous fluid- and particle-phase measurements (Figure 2.7). In this measurement system consists of two cameras that are focused on the same field of view, using a mirror and a beam splitter plate, Figure 2.7(a). To ensure that each camera only records one phase, tracer particles containing a fluorescent dye and an appropriate wavelength cut off (i.e.'color') filter are used. Devasenathipathy et al. (2003), Kiger and Pan (2000) also used a single camera in their μ-PIV/ PTV experiment. Finally, image processing was done to separate the images based on tracer size to estimate both phase velocity. Noguchi and Nezu (2009), Nezu and Sanjou (2011) carried out single camera PIV/ PTV (Figure 2.8) experiment for sediment-laden flows in open channel to study particle turbulence interaction and local particle concentration.

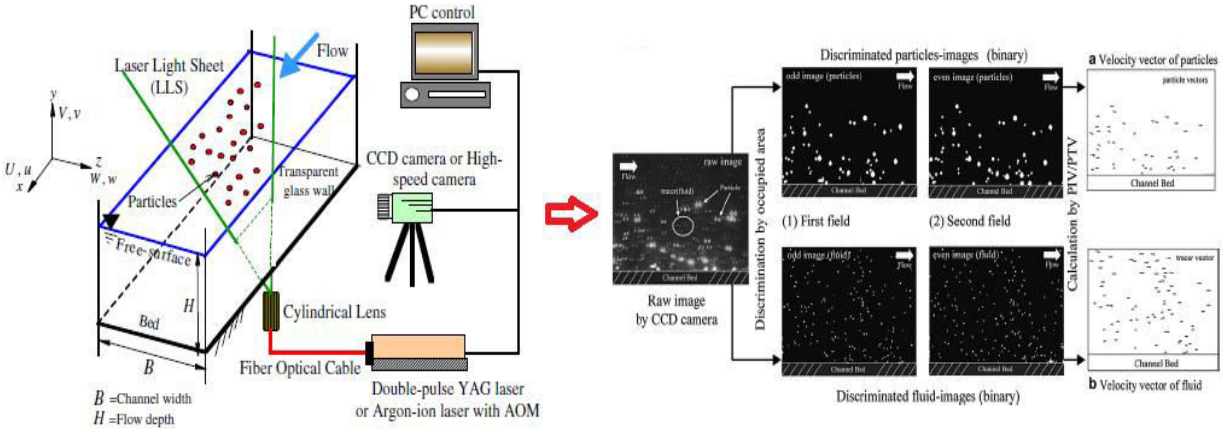

Figure 2.8. Schematic diagram of experimental setup and image processing between sediment particle and fluid tracer. (From Nezu and Sanjou, 2011, *Journal of Hydro-environment Research*, **5(4)**, 215-230. Copyright 2011 by Elsevier).

Chapter 3

Suspension flow in diverging channel

3.1 Introduction

In this work, experiments were carried out in bifurcation channels for a range of branching angles for low Reynolds number diverging flow of single-phase Newtonian fluid and dilute suspension of two different size particles. Shear-induced migration of particles in bifurcating channels can significantly alter the flow field which may have important consequences in physiological flows. Some recent studied [Xi and Shapley(2008), Ahmed and Singh (2011), Reddy and Singh (2014), Yadav et al. (2016)] reported that the particle partitioning in the daughter branches does not follow the flow partitioning due to shear-induced particle migration. The velocity and concentration profile for suspension flow was observed to be symmetric in the inlet branch but asymmetric in the daughter branches. In this work flow velocity profile was measured by μ-PIV and local concentration was measured by image processing method and μ-PTV.

3.2 Experimental Procedure

The bifurcation geometry signifies a structure where a parent branch divides into two daughter branches with an angle (θ). Experiments were carried out with both symmetric and asymmetric bifurcation channels. The symmetric channels were of two types: T-shape and Y-shape with 180 and 120° bifurcation angle. The asymmetric channels had oblique bifurcations with angles of 90°, 60 °, and 30°. The width of daughter branches (500 μm) in all the channels was the same as that of the parent branch. The volume fraction of dispersed particle (ϕ) was 0.05 in all the experiments. Reason for working with dilute suspension is that experimental variable can be well-controlled and getting accurate measurements much easier. In the present study, the relative lengths of different sections (parent branch and daughter branches) were taken to be equal (L=7 cm) and the ratio of the half width of the channel (B) to the particle radius (a) was taken to be 25. An extension of pipe was attached to the inlet of the test channel to connect the syringe pumps which allow a sufficient entrance length for fully developed flow to establish. This kind of bifurcation geometry has several relevant applications in biological and industrial

systems. Schematic of symmetric and asymmetric bifurcation channels used in our experiment is shown in Figure 3.1. The locations at which profiles were evaluated are also shown in the images.

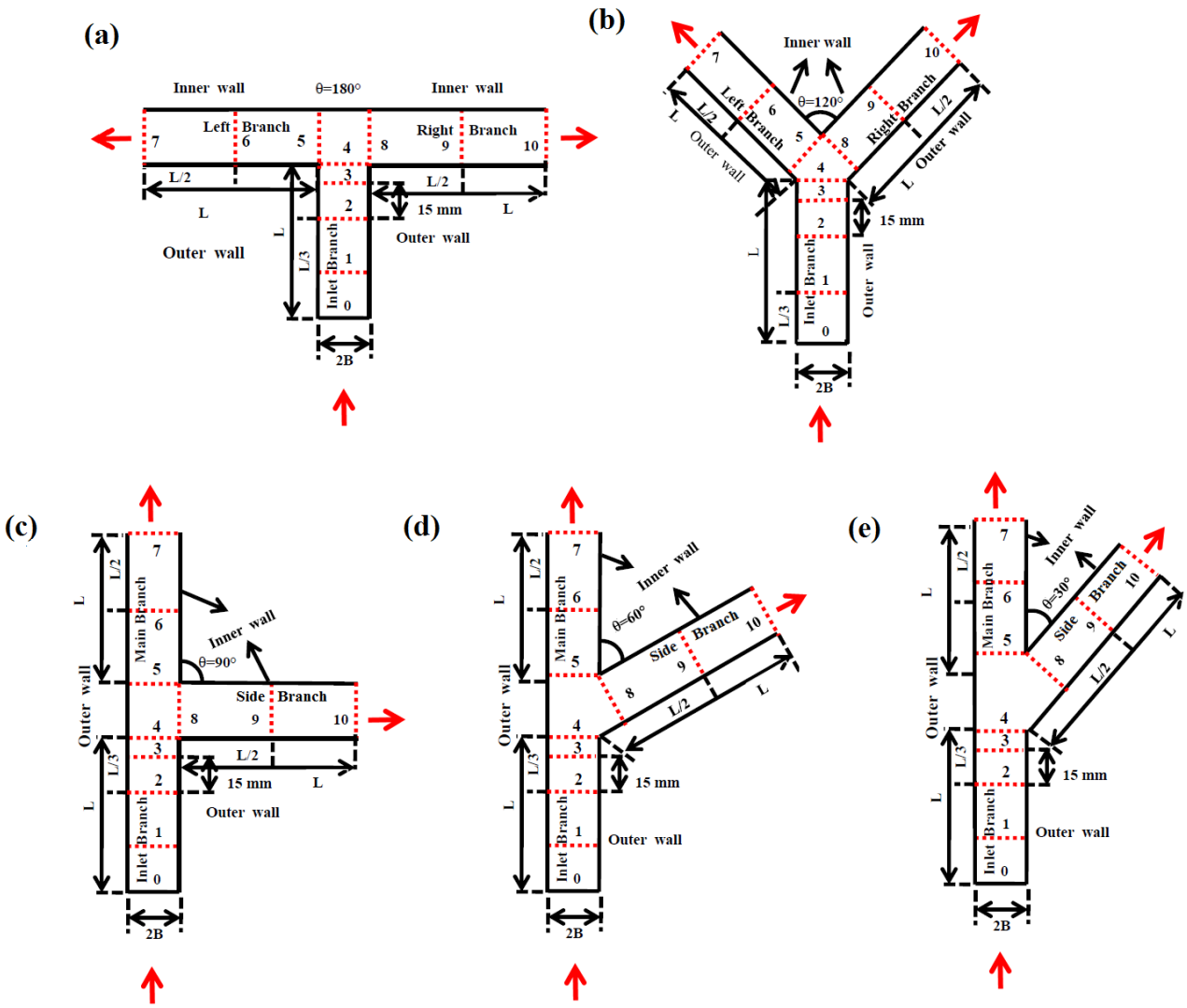

Figure 3.1. Schematic diagram of bifurcating channels used in our experiment: (a) θ =180°, (b) θ =120°, (c) θ =90°, (d) θ =60° and (e) θ =30°.

Figure 3.2 shows the schematic diagram of our experimental setup. It consists of an epi-fluorescent microscope (IX 83, Olympus), Fluorescence illumination light source (U-HGLGPS, Olympus) and a continuous acting syringe pump (DUEL-NE-1000, New Era Pump System). Experiments were carried out with a neutrally buoyant suspension of two different sizes of particles. PMMA particles of mean diameter 6 and 10 μm dispersed in the

glycerol-water mixture were used. The size of the PMMA particles selected was close to the diameter of red blood cells (RBC, 6-8 µm diameter), white blood cells (WBC, 10-12 µm diameter) respectively, which will mimic the blood suspension and help to quantify flow and particle dynamics. In blood we see particle volume fraction is 40-45 % but in our experiments particle volume fraction was 5% due to experimental limitation. So, we admit that there is considerable difference from the particle volume fraction view. The inlet and outlet end of the micro-channels were connected to the syringe pump through silicon pipe. The speed of the pump could be adjusted to get the desired flow.

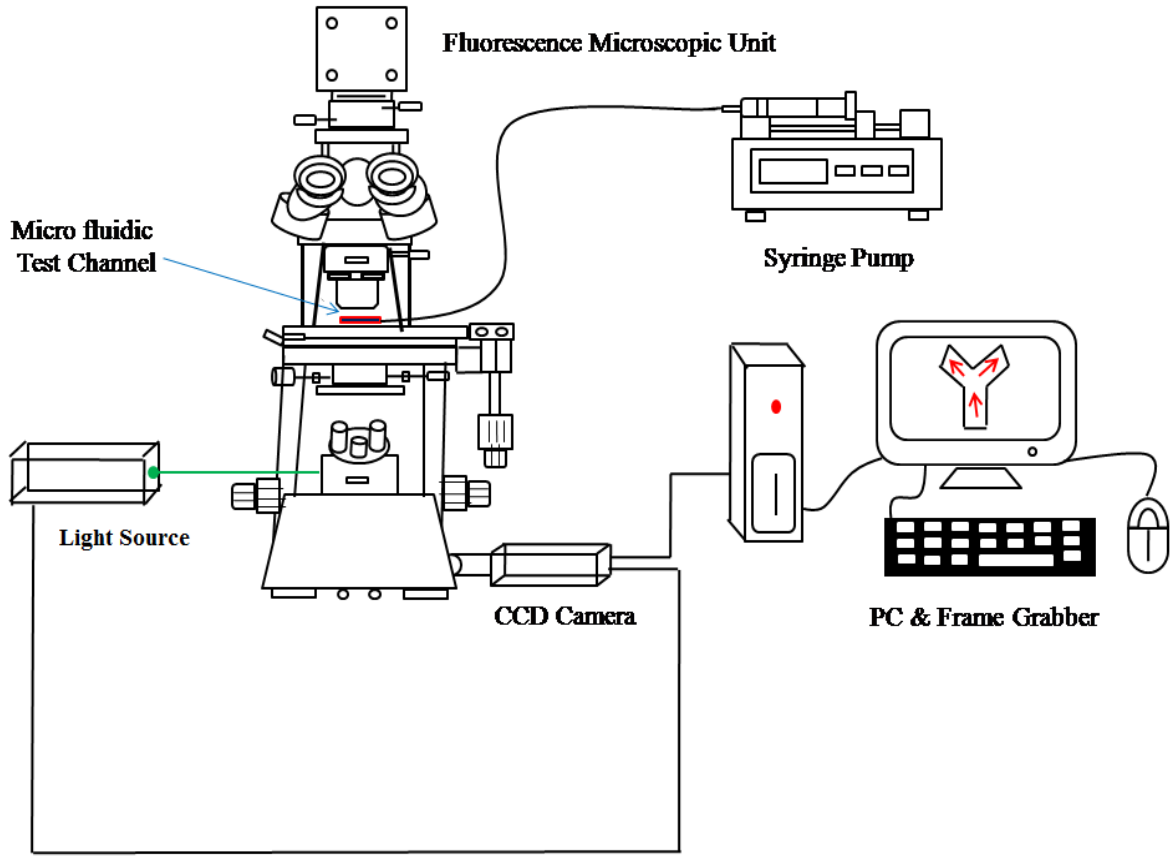

Figure 3.2. Schematic diagram of the experimental setup.

The images were captured using 12 bit, 1376 x 1040 pixel CCD camera (Sensicam qe from PCO) and were transferred via frame-grabbing board (PCI interface 520/525) to the computer. One hundred particle image frames were recorded for each set of experiment at a particular flow condition. The recorded images were analyzed using the two-frame cross-correlation method to obtain velocity fields. The size of interrogation window (IW) was 32 x 32 with 75% overlap. In our experiments the maximum (centerline) velocity in the channel varied from 0.0161cm/s to 0.0284 cm/s. The particle and flow Reynolds number was O (10^{-4})

and O (10^{-2}) respectively; and the Stokes number for 1µm, 6µm, and 10µm was found to be O (10^{-9}), O (10^{-8}) and O (10^{-7}) respectively. To investigate the particle phase velocity and concentration profile using µ-PTV analysis small amount of the suspended particles were colored with a dye (rhodamine 6G from Sigma Aldrich), while tracer particles (diameter, d_p= 1 micron) were mixed with the suspension for measuring the velocity field of the bulk suspension from the µ-PIV analysis. The volumetric concentration of tracer for µ-PIV and µ-PTV analysis was in the range of 0.011-0.025 % (v/v) and 0.002-0.005 % (v/v) respectively. Fluorescently labeled microspheres in the flow field had an emission peak of about 570 nm. The emitted light passes through the cooled-CCD camera via barrier filter, where the scattered light from the green light is filtered out and the red fluorescence from the particle is recorded.

3.3 Post processing of images for µ-PIV/ PTV analysis

In post-experimental work, one of the most important parts is processing the image in a required manner and to get required velocity and concentration profile. In case of micro-Particle Image Velocimetry (µ-PIV) image filtering (removing noise from the images) is very much essential as it suffers a range of imperfection and noises such as non-uniform contrast and low frequency background noise etc. Once large particles were identified, it can separate to calculate velocity and concentration profile. As in micro-PIV volume, illumination is used, a separated image also contains out-of-focus particles which causes a wrong value of particle velocity and concentration. Particles which are at more distance from focal plane are more defocused. Various steps of processing of images to improve the accuracy of micro PIV experiments are described as follows-

3.3.1 Separation of Large Particles

There are many techniques which can be used to separate particles based on size. ‘Dilation' and ‘Erosion' is one of the most common methods which are being used. But one of the main disadvantages of this algorithm is to define a structural element which is a very tedious task in case of a spherical particle with a small radius. This problem can be overcome by the method "Circular Hough Transform" which is a feature extraction technique for detecting circles. The purpose of this technique is to find circles in imperfect image inputs. The circle candidates are produced by "voting" in the Hough parameter space and then select the local maxima in a so-called accumulator matrix.

In a two dimensional space a circle has parametric representation of:

$$x = a + r\cos\theta \tag{3.1}$$

$$y = b + r\sin\theta \tag{3.2}$$

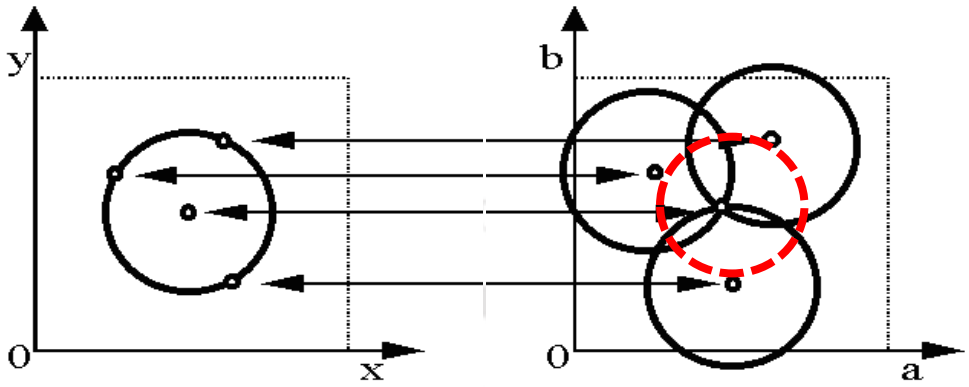

Figure 3.3: Schematic showing a Circular Hough Transform from Image to Hough space.

When the angle θ sweeps through the full 360^0 range the points (x, y) race the perimeter of a circle (Shown in Figure 3.3). If an image contains many points, some of which fall on perimeters of circles, then the job of the search program is to find parameter triplets (a, b, r) to describe each circle. In μ- PIV experiment since the radius of suspended particles are known, so a problem of finding parameter triplet reduces to finding the locus of (a, b) which would fall on a circle of known radius 'r' centered at (x, y). The true center point will be common to all parameter circles and can be found by using Hough Accumulation Array.

3.3.2 Steps of the algorithm:

1) The idea being simple is to use the above detailed algorithm with some radius range suppose (r_m,r_h), where actual radius r (radius of the large particle in the image) lies between (r_m,r_h). However, taking a radius range instead of a constant radius increases the time complexity but it also ensures calculating almost every circle as radius might get differ due to noise and on the basis of height from the focal plane.

2) By choosing values of r_m and r_h carefully defocused particles also can be removed easily up to some extent using this algorithm. Generally, it is expected that the radius

of defocused particles has a greater radius than the focused particle. So greater the difference between the actual radius and expected radius, greater the degree of defocusing. r_m and r_h should be chosen such that radiuses which are differed by some noise should not be missed and particles which are defocused should not be selected.

3) After then center of every circle is known it is an easy task to separate that circle from the image by using the equation shown below. Every point in square of side 2*r need to be selected with center of square is same as center of circle and check whether the point is inside the circle or not.

$$x^2 + y^2 = r^2 \quad (3.3)$$

4) Then every suspended particle is separated from the image the left out image would be tracer particle image.

3.3.3 Removal of overlapped large particles

A simple method has been used to remove overlapped large particles. For any particle pair if the distance between centres is less than sum of their radius than only one particle should be kept and other one should be removed. Selection of particle could be done by using the information of difference of actual radius and expected radius. A particle with large difference with actual radius should be removed and other one should be kept.

For n particles, this method takes O (n^2) time to check each and every pair but this algorithm could be modified to improve time complexity to O (n). Starting the loop from the first pixel and for every center of the circle to be found , mark every neighbour pixel at distant r from that center. Next time in running the loop, center which comes in the marked area should be removed on the basis of method described earlier by using the information of difference between actual radius and expected radius.

3.3.4 Filtering of particle based on a particle mask co-relation method

A particle mask is typically a type of brightness pattern which is expected in particles. In this study two dimensional Gaussian distribution has been used for particle mask as shown by Ushijima et al. [1996]:

$$(x,y) = a.exp(-\frac{(x-x_0)^2 + (y-y_0)^2}{2\sigma^2}) \quad (3.4)$$

Where I(x,y) is the peak value of brightness, a is the peak brightness, σ is the representative radius and x_0,y_0 is the location of the center of particle image.

In the calculation of co-relation value particle mask is kept fixed. As shown by 'Takehara et.al [2014] co-relation coefficient can be calculated by:

$$r(x_0,y_0) = \frac{\sum_{i=x_0-\frac{m}{2}}^{x_0+\frac{m}{2}} \sum_{j=y_0-\frac{n}{2}}^{y_0+\frac{n}{2}} (I(i,j)-\hat{I})(I_m(i,j)-\widehat{I_m})}{\sqrt{\sum_{i=x_0-\frac{m}{2}}^{x_0+\frac{m}{2}} \sum_{j=y_0-\frac{n}{2}}^{y_0+\frac{n}{2}} (I(i,j)-\hat{I})^2} \sqrt{\sum_{i=x_0-\frac{m}{2}}^{x_0+\frac{m}{2}} \sum_{j=y_0-\frac{n}{2}}^{y_0+\frac{n}{2}} (I_m(i,j)-\widehat{I_m})^2}} \quad (3.5)$$

Where I (I, j) is the brightness pattern of image and I_m(I, j) is the brightness of particle mask at (I, j). m and n are the coefficients for interrogation area and they should be chosen equal to $1.5\sigma_m$. $\hat{I}$ and $\widehat{I_m}$ are the spatial averages of respective brightness pattern over the interrogation area.

It could be easily seen that co-relation coefficient does not depend on peak brightness and it depends only on brightness pattern that any particle has. This calculated co-relation coefficient can be binarized by using some threshold to remove undesired particles. In this study value of this threshold is taken as 0.7 as suggested by 'Takehara et.al (2014). Elements which are linear in image lead to low brightness value and therefore can be eliminated by using this threshold value.

A sample image from our μ-PIV experiment is shown in Figure 3.4(a). All these kind of images contains fluorescence tagged one of the test particle having a diameter (D_p) 6 or 10 μm and tracer particles with diameter (d_p) 1 μm. For standard micro-PIV/PTV system particle with a larger diameter is used to investigate the particle phase phenomena using μ-PTV, while small particles are used for measuring the background fluid velocity with μ-PIV technique.

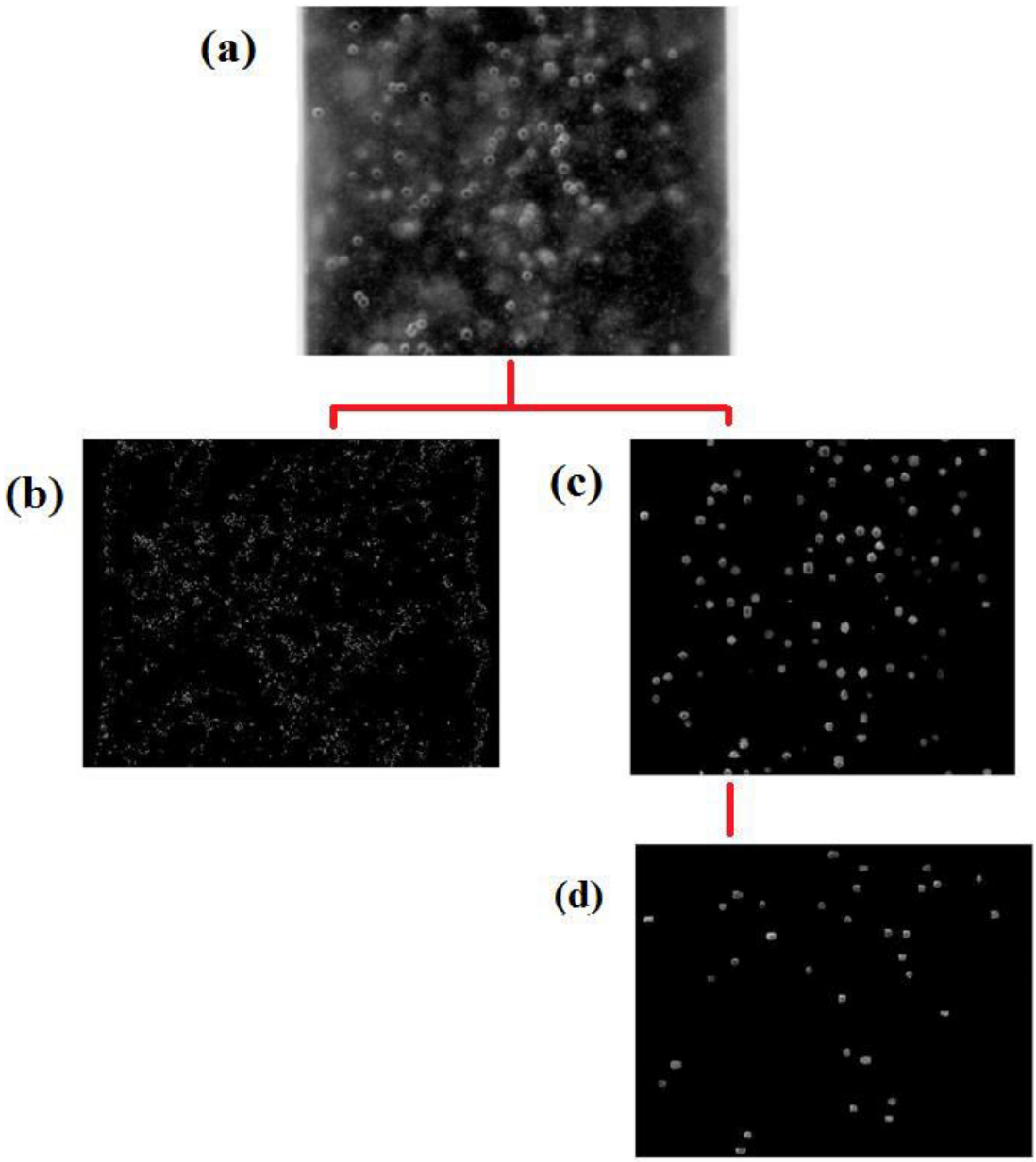

Figure 3.4. (a) Sample μ-PIV image (b) separated image containing 1μm tracer (c) focused and defocused particle (d) separated focused particle.

In this study, we have separated the Figure 3.4 (a) image base on the particle size with our in-house developed MATLAB code before μ-PIV/PTV analysis. Now Figure 3.4 (b) & (c) contains separated 1μm tracer and 10μm test particles respectively. The image is shown in Figure 3.4 (c) contains both focused and defocused particles. Therefore we have performed further post-processing to separate the focused and de-focused particles. Focused test particle extracted from Figure 3.4 (c) which is shown in Figure 3.4 (d). Finally, the μ-PTV analysis was carried out for image Figure 3.4 (d) using PTV lab Beta software to get the information

of particle phase phenomena. The μ-PIV analysis was carried out for the separated 1μm tracer image, Figure 3.4(b) using PIVlab_1.32 software to get the information about carrier fluid velocity.

Both PIVlab_1.32 [Thielicke and Stamhuis (2014)] and PTV Beta [Brevis et al.(2011)] has user-friendly graphical user interface (GUI) which makes both PIV and PTV data post-processing, analyses fast and efficient. For both micro PIV and PTV analysis we have used smoothing, outlier-rejection, interpolation filter to remove erroneous vectors which show up due to poorly illuminated regions in the image or out-of-plane flow. PTV method directly tracks single particles and the PIV method uses the cross-correlation function to derive the local motion statistically. Therefore, the accuracy of the PTV algorithm depends on the accuracy of the detection of particle positions, whereas for the PIV method it depends on the accuracy of locating the correlation peak.

3.4 Preparation of microchannels

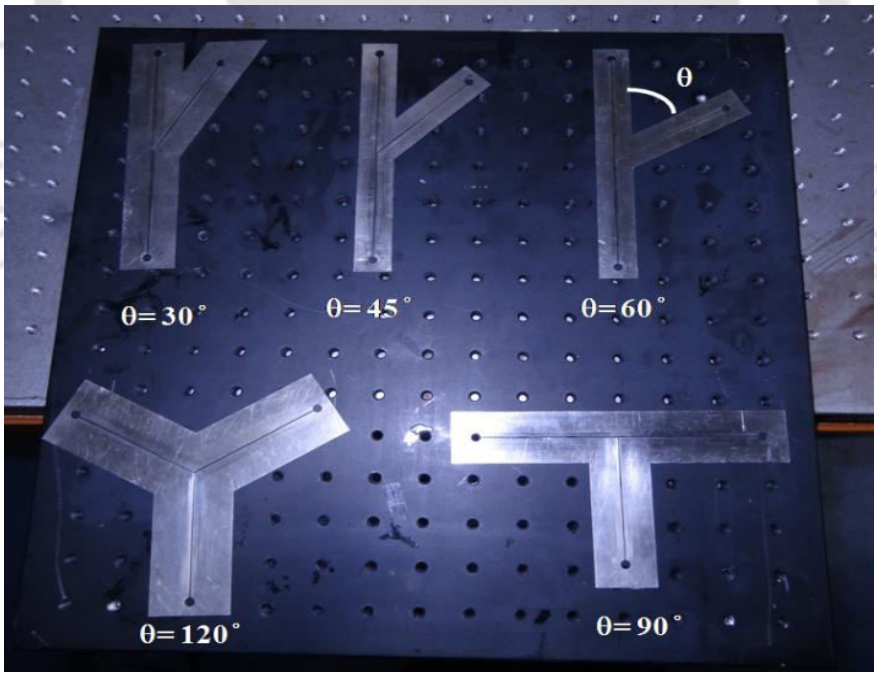

Figure 3.5. Microchannel with various branching .

The microchannel of rectangular cross-section (500μm x 500μm) with various branching angles were fabricated at the Tool Room Training Centre, Amingaon Branch (Guwahati,

India) shown in Figure 3.5. Electric Discharge Machining (EDM) cutting was used to fabricate our channels from stainless steel. Micro-milling was used to fabricate diverging-converging microchannels at Achria Lab (Bangalore).

3.4.1 Preparation procedure of super hydrophobic surface:

After EDM cutting we have covered the top and bottom surface of a microchannel with a super hydrophobic coated glass surface. Super hydrophobic surfaces have the potential to reduce drag both in the laminar and turbulent regimes will give no-slip boundary condition at the top and bottom wall with good optical transparency.To coat the glass surfaces we have used ZXL-CSS nanocoating from Laiyang ZiXiLai Environmental Protection Technology Co. Ltd China. It has a high contact angle 130°-140° on glass. A double sided tape was used to fix the top and bottom glass surface with the stainless steel microchannel. Schematic of microchannel preparation steps are shown in Figure 3.6.

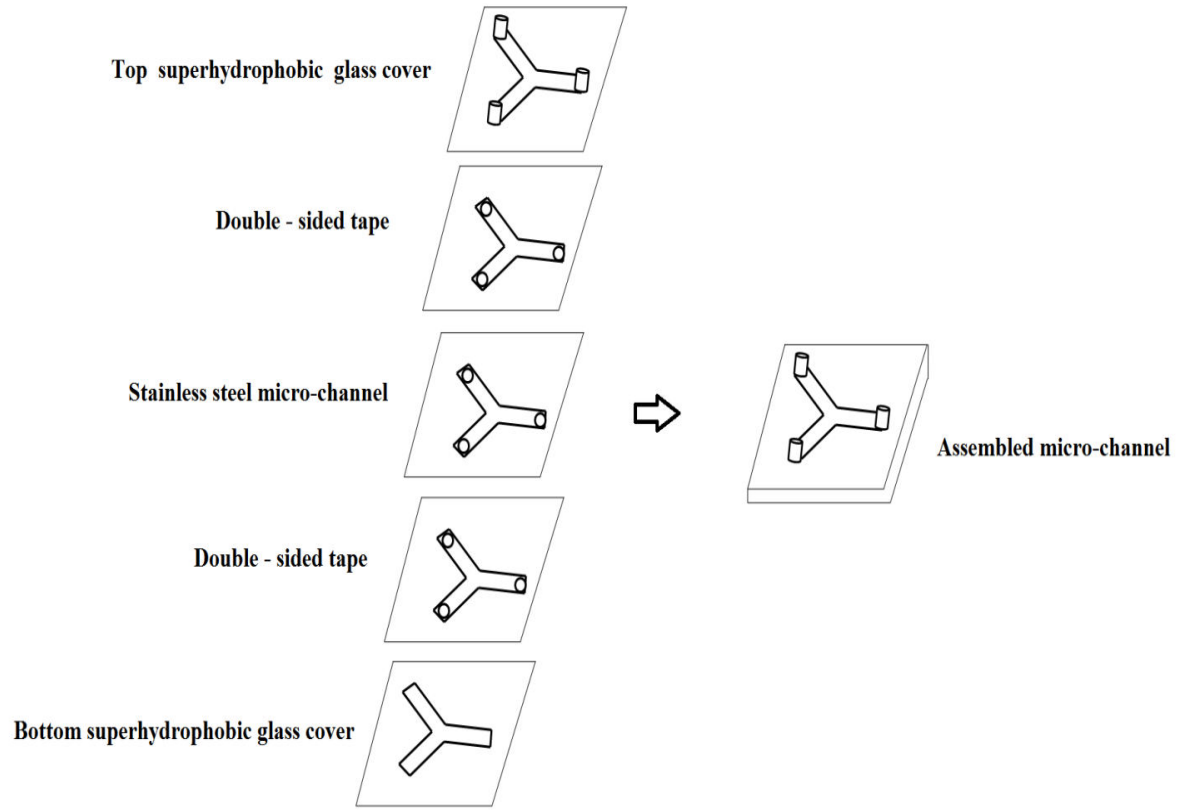

Figure 3.6. Schematic of micro channel preparation steps.

Spraying method: First surface of glasses was cleaned by water or ethanol to ensure no water stain and visible particles on its surface. Then spray the ZXL-CSS nanocoating on it followed by drying under room temperature environment for 10-30 minutes.

3.5 Preparation of Suspension

All the experiments were carried out with a neutrally buoyant suspension which required density matching of fluid and particles. Two different sizes of particles were used in this study. In one study suspension of PMMA spheres of mean diameter 6 and 10 μm dispersed in a glycerol-water mixture was used. To achieve density matching with PMMA particles of density 1.18 g/cc, the suspending fluid was prepared by mixing of 74% glycerol and 26% water (volume%). This fluid had a viscosity of 19.5 cP and its surface tension was 60.4 mN/m at 24 °C. Approximately 10 ml of suspension was prepared. To prepare the suspension required amount of particles and appropriate liquid were added in a beaker and stirred vigorously to achieve homogeneous mixing and dispersion. However, during the mixing small air bubbles were formed which needed to be removed. This was achieved by keeping the suspension under vacuum for overnight, allowing the bubbles to rise up. Suspension cleared of air bubbles was then gently transferred into the microchannel.

3.5.1 Selection and Preparation of Tracer

Fluorescent tracers are made from the PMMA particles having diameters 1μm, 6 μm and 10 μm using the procedure described in Lenoble et al. (2005). The particles are dyed with rhodamine 6G fluorophore from Sigma Aldrich.

Preparation procedure: We first dissolve 0.07g of rhodamine 6G in 200 mL of pure ethanol. The solution is vigorously stirred at 35℃ for 45 minutes. Next, we add 3-4g of particles (the future tracers) and continue mixing for about 15 minutes, with moderate stirring. This time interval was sufficient for the dye to impregnate the particles.

3.6 Results and discussion

3.6.1 Velocity field

Sample velocity vector maps for suspension of 10μm particles in symmetric and asymmetric bifurcation channels are shown in Figure 3.7

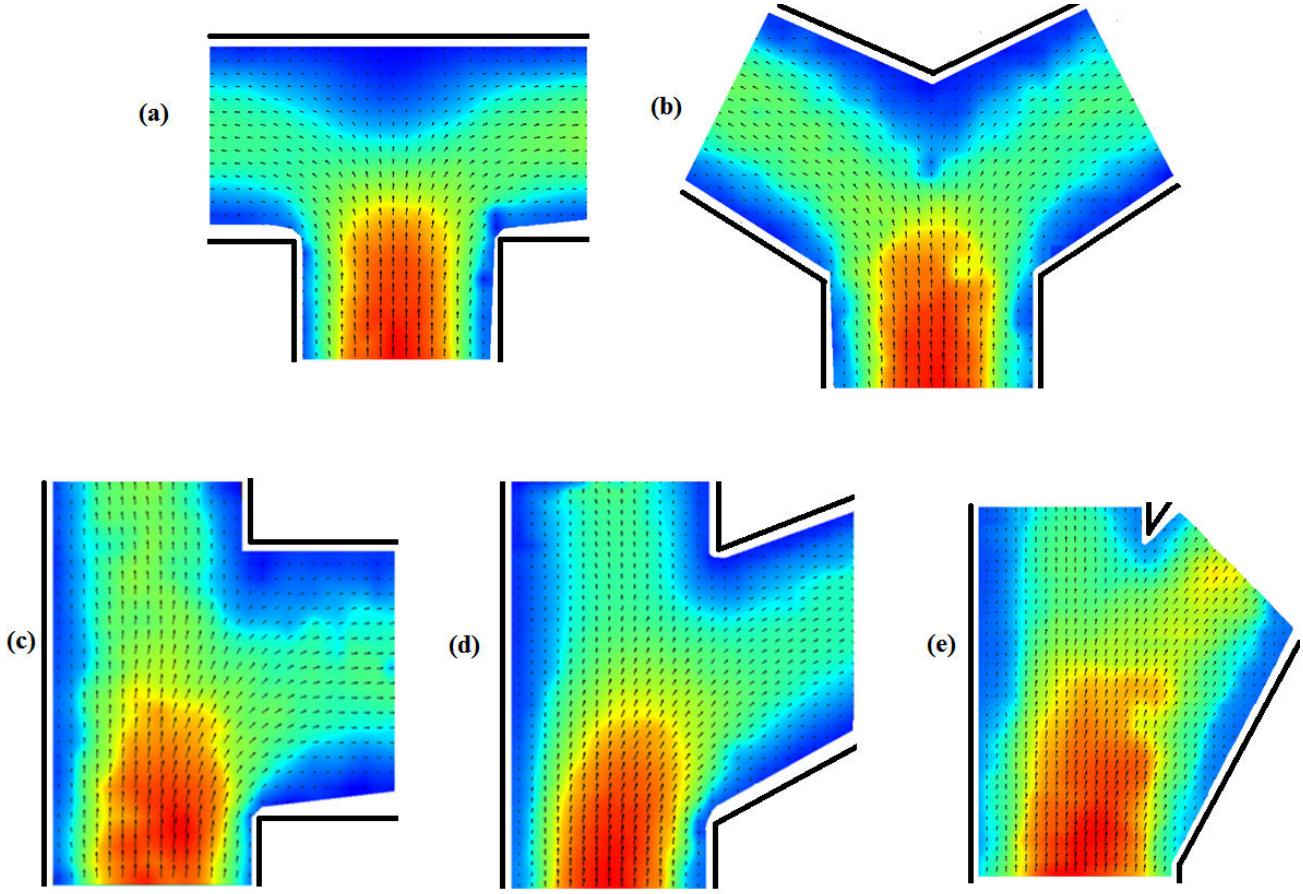

Figure 3.7. Velocity vector map of suspending fluid phase for 10μm suspension in the different bifurcation channels (a) θ =180°, (b) θ =120°, (c) θ =90°, (d) θ =60°, and (e) θ =30°.

The mean velocity profiles for pure suspending fluid and suspensions of two different particle sizes (6 and 10 μm) at various locations in the bifurcating channels are plotted in Figure 3.8. The experiments were conducted for particle volume fraction (ϕ=0.05) in a Newtonian fluid. The velocity magnitude (U) is normalized relative to the maximum velocity (U_{max}) for each case. Figure 3.8 shows the velocity profiles in the symmetric T-bifurcation channel at three

positions in the inlet branch (location 1, location 2 and location 3). These locations can be identified in the schematic diagrams of the channels (Figure3.1).

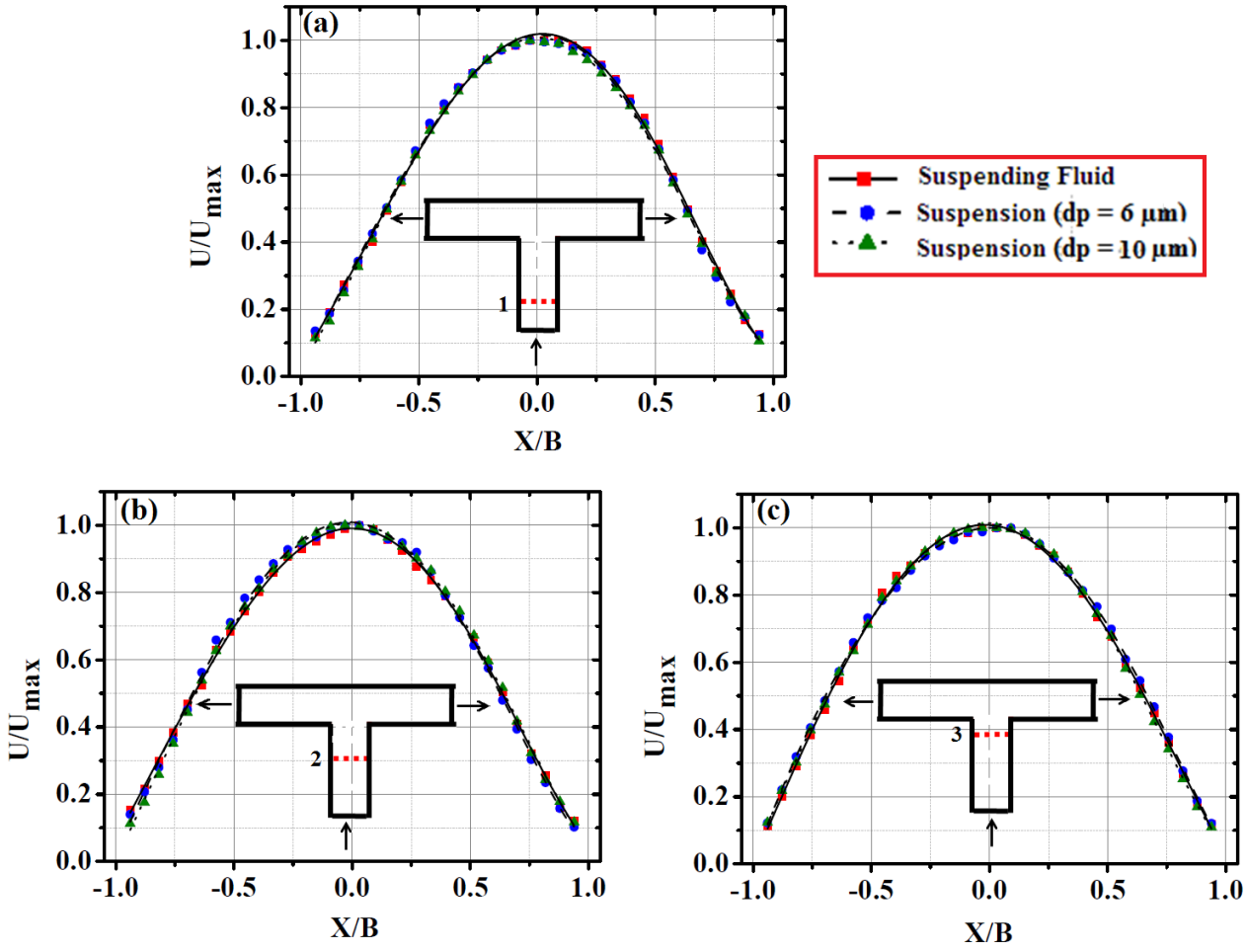

Figure 3.8. Velocity profiles in the inlet branch of symmetric T- shape channel (θ =180°) at (a) location 1 (b) location 2 and (c) location 3 before the junction.

At location 2 and 3, the velocity profiles were symmetric and fully developed. For the experimental study, some data points are missing near the walls. This was due to the difficulty in locating the channel wall, curvature effect and the irregularity in the velocity near the walls. To the location 3, the velocity profiles in the inlet branch are identical for all bifurcation channels. This is because the effect bifurcation angle was not experienced up to location 3. After location 3 the nature of velocity profile depends on the bifurcation angle and bulk particle concentration.

Figure 3.9 (a) shows the velocity profile at location 4 (bifurcation position) for symmetric T-shaped bifurcation, whereas Figure3.9 (b) shows the profile for the symmetric Y-shaped bifurcation. Peak-valley-peak patterns were observed for pure suspending fluid and suspensions of two different particles in both the channel. This peak-valley-peak pattern results from the division of flow into the left and right branches. It can be observed that peak-valley-peak pattern is more prominent for suspension of larger particles.

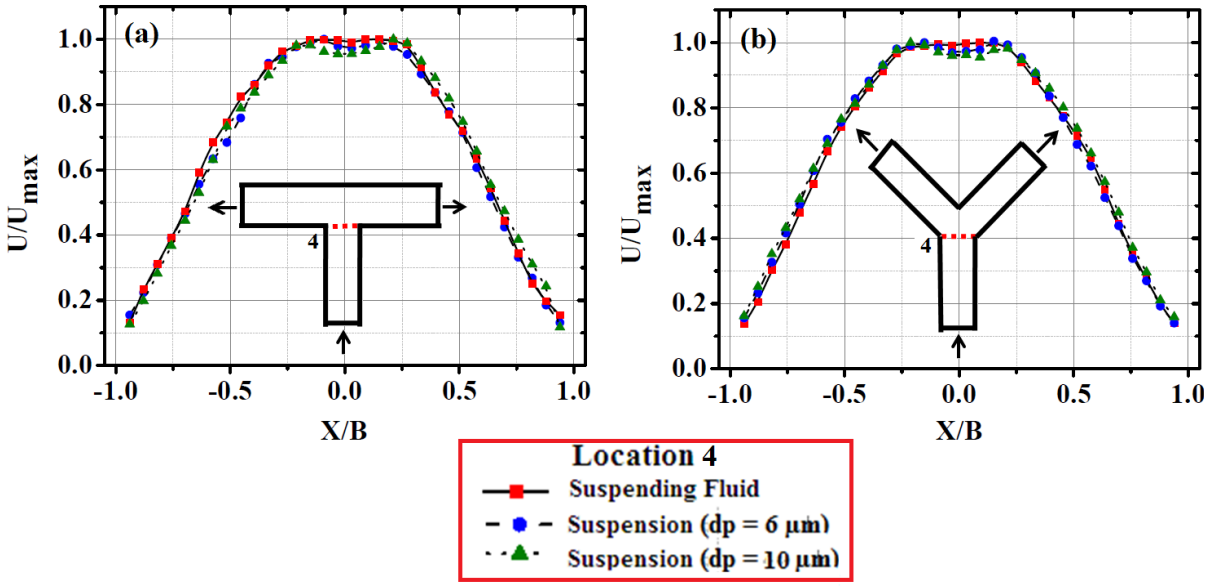

Figure 3.9. Velocity profiles at the location 4 in the symmetric bifurcation channels: (a) θ=180°, (b) θ =120°.

The velocity profiles at the bifurcation position (location 4) in the asymmetric bifurcating channels are shown in Figure 3.10. No peak-valley-peak pattern was observed here but there a small skewing of profiles towards the side branch was observed for both pure fluid as well as suspension in all the channels. We have calculated skewness of velocity profile at bifurcation position in all the asymmetric channels. This will help us to evaluate the effect variables such as particle size and bifurcation angle on asymmetry of the profile. For suspension of 10µm size calculated skewness for 90°,60° and 30°.bifurcation channel are 0.1465, 0.1364 and 0.0937 respectively. Here we have observed that as the bifurcation angle decreases the velocity profiles skewness towards the side branch decreases. Moreover, skewness for pure suspending fluid and suspensions of two different particle sizes (6 and 10 µm) at 30° bifurcating channels are 0.0485, 0.0922 and 0.0937 respectively. We can conclude

that skewness is slightly more for suspension flow in comparison to that of pure suspending fluid (without particles). Moreover, suspension of larger particles size has marginally higher skewness in profile for all cases. As we have conducted experiments for dilute suspension it is expected to give more insight into the role particle size and bifurcation angle on skewness of profile in future experiments at higher particle concentration.

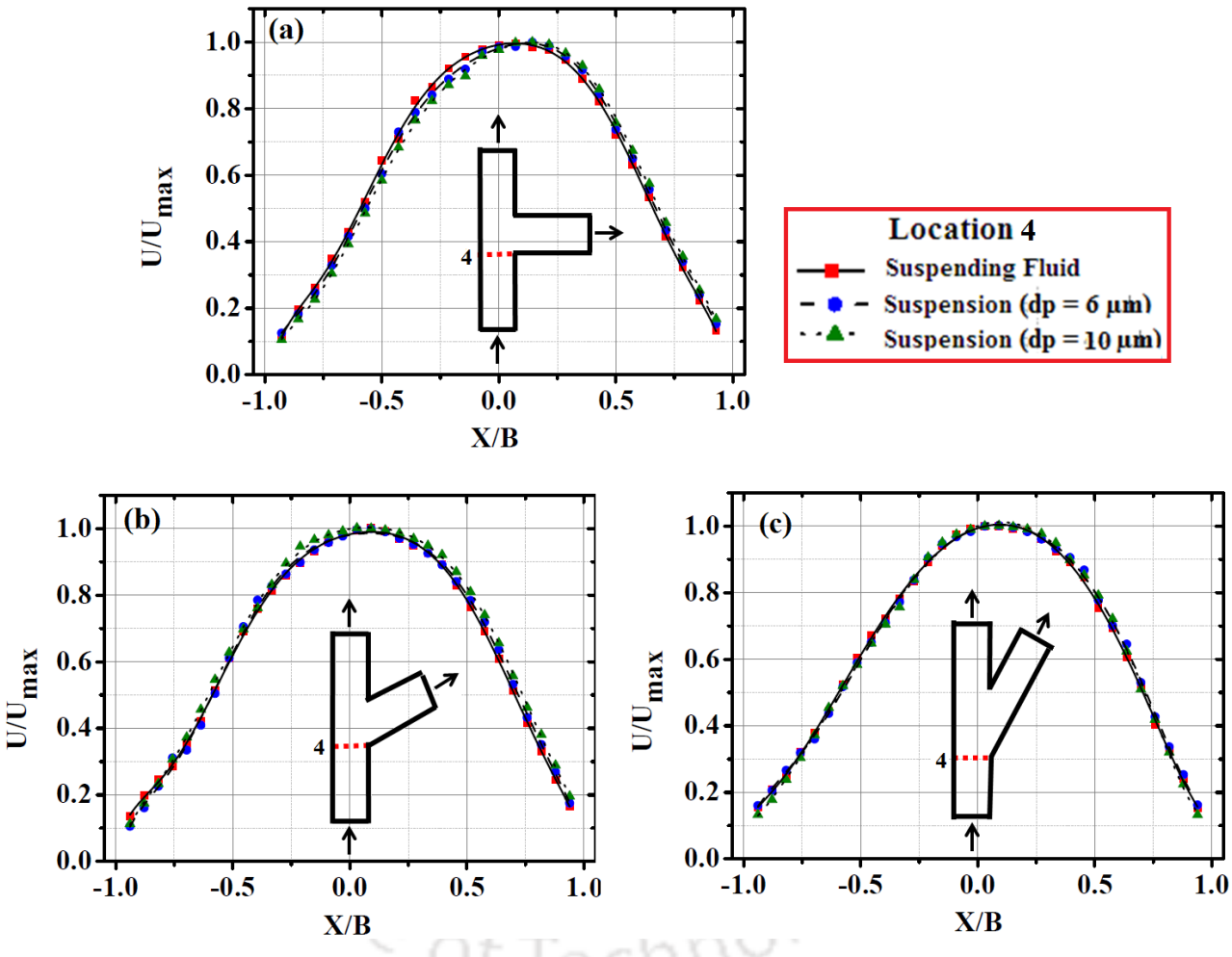

Figure 3.10. Velocity profiles at the location 4 in the asymmetric bifurcation channels :(c) θ =90°, (d) θ =60°, and (e) θ =30°.

The comparative velocity profiles at the beginning of respective daughter branches of symmetric and asymmetric bifurcation channels are shown in Figure 3.11 and 3.12 respectively. For the clarity of plots, the outer wall of the left branch is at the location x/B = -1, whereas that of the right branch has x/B= +1. It can be observed that in symmetric

channels the velocity profile at location 5 in the left branch is almost mirror image of the profile at location 8 in the right branch. In both the daughter branches for T and Y bifurcation the peak in velocity profiles are shifted towards the outer walls. Shifting of velocity profile was more for suspension compared to the suspending fluid. The skewness of the velocity profile is more for the suspension of 10 µm particles in comparison to that of 6 µm particles. For asymmetric channel ($\theta = 90^{o}$) the velocity profile in the main branch is nearly symmetric with a peak located at the center of the channel, and at the same location in the side branch, a shift towards the outer wall was observed. Whereas, for the channel with bifurcation angles of 60^{0} and 30^{0} the velocity profiles in both main and side branch are asymmetric and skewed towards the outer walls in the main and side branch.

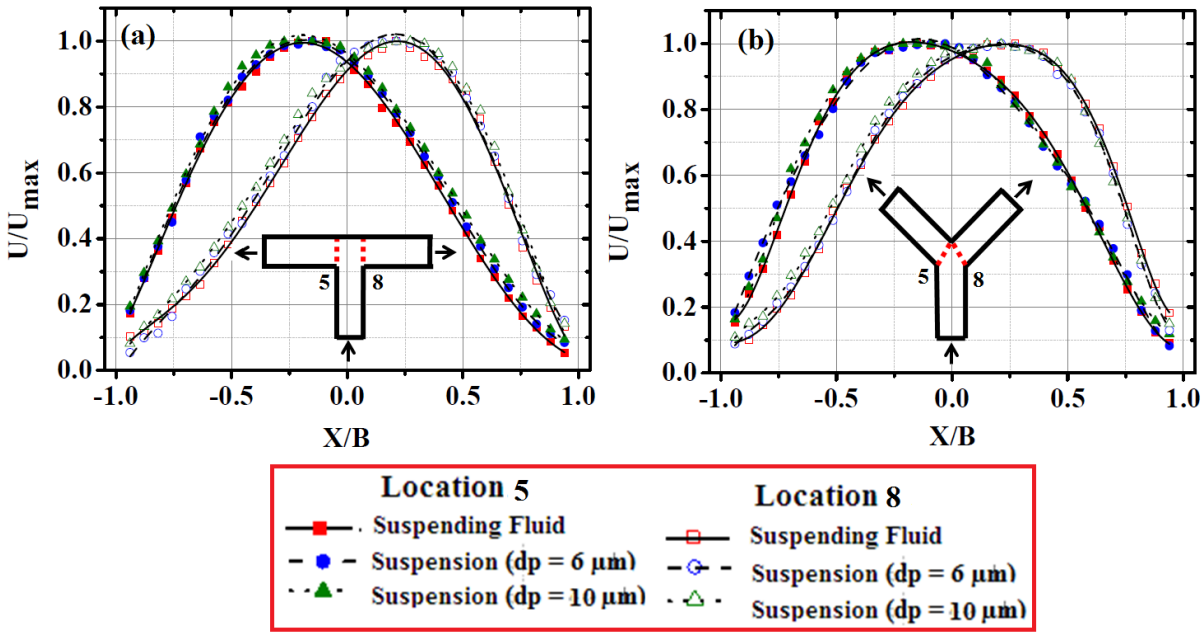

Figure 3.11. Velocity profiles at the beginning (location 5 and 8) of daughter branches in the symmetric bifurcation channels :(a) θ =180° and (b) θ =120°.

In Figure 3.11and 3.12 it is clearly noticeable that profiles at the beginning of daughter branches have higher shifting in symmetric channels than the asymmetric. This is due to sharp turn encounter by the suspension after crossing the bifurcation in a symmetric channel.

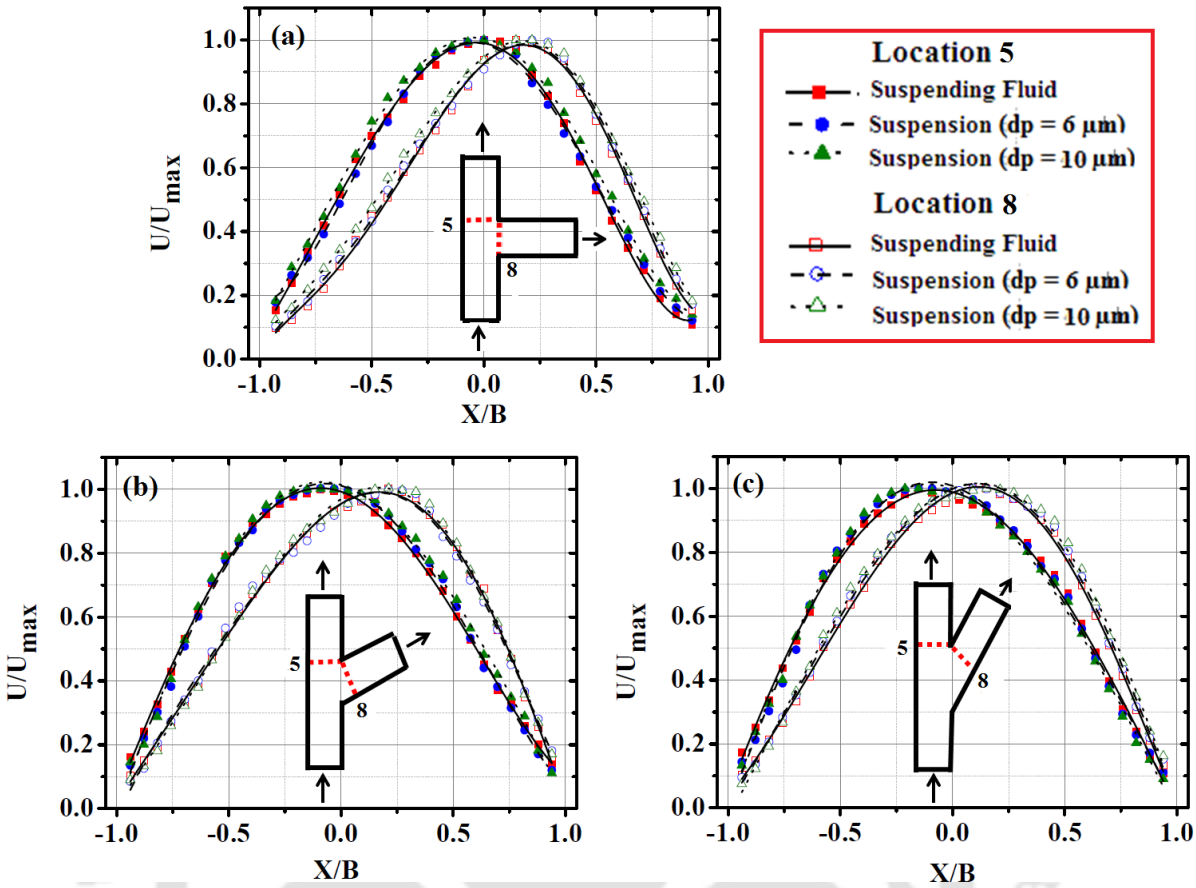

Figure 3.12. Velocity profiles at the beginning (location 5 and 8) of daughter branches in the asymmetric bifurcation channels: (c) θ =90°, (d) θ =60° and (e) θ =30°.

As we move downward positions in the daughter branches the velocity profile tried to become stable and shifts toward the center of the channel, while the profile is still asymmetric. Figure 3.13 and 3.14 shows comparative velocity profiles of Newtonian fluid with suspensions in daughter branches for symmetric (T and Y) bifurcation and in the side and main branch for the asymmetric (θ) 90°, 60 ° and 30° channels at the location 6 and 9. It was observed that as the bifurcation angle decreases the asymmetry in the velocity profile reduces.

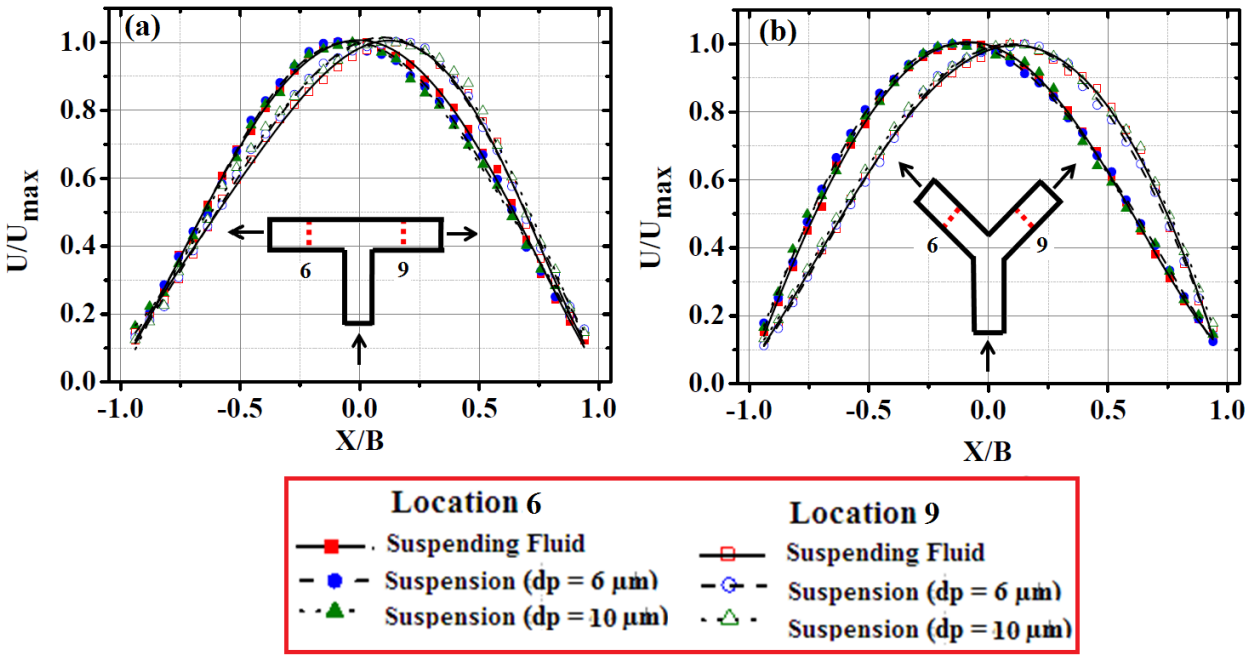

Figure 3.13. Velocity profiles at location 6 and location 9 in the symmetric bifurcation channels: (a) θ =180° and (b) θ =120°.

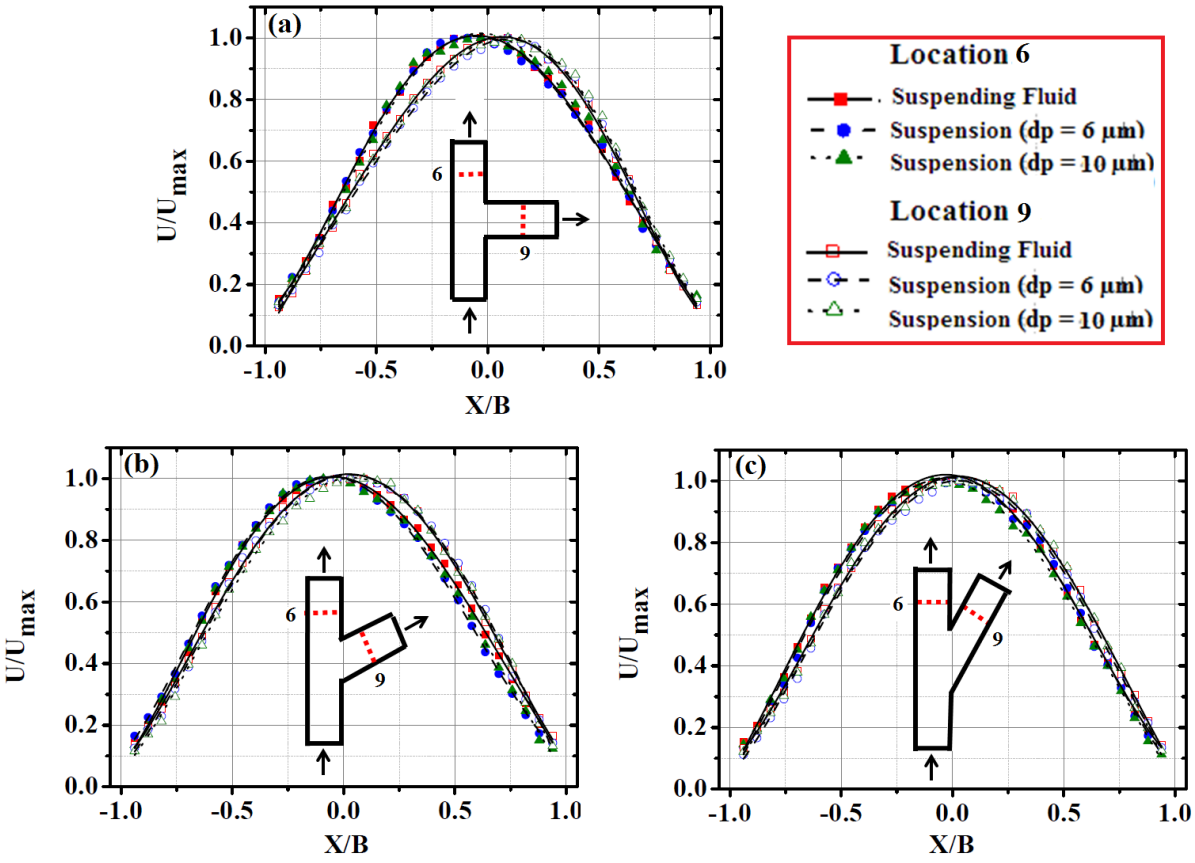

Figure 3.14. Velocity profiles at location 6 and location 9 in the asymmetric bifurcation channels: (a) θ =90°, (b) θ =60° and (c) θ =30°

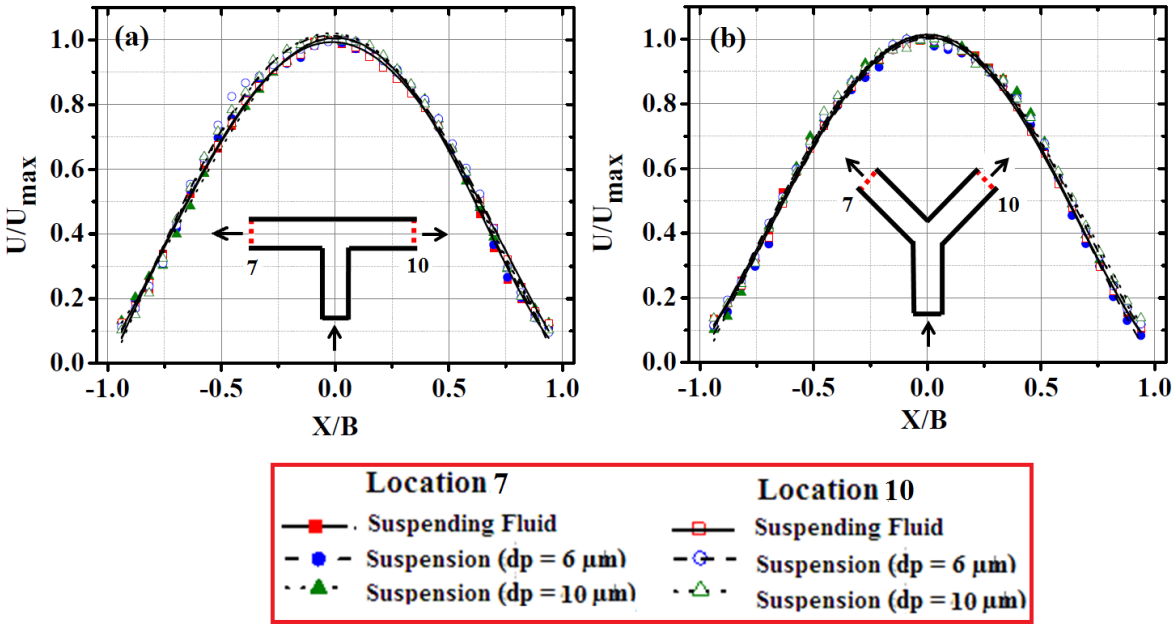

Figure 3.15. Velocity profiles at the end (location 7 and 10) of daughter branches in the symmetric bifurcation channels: (a) θ =180° and (b) θ =120°.

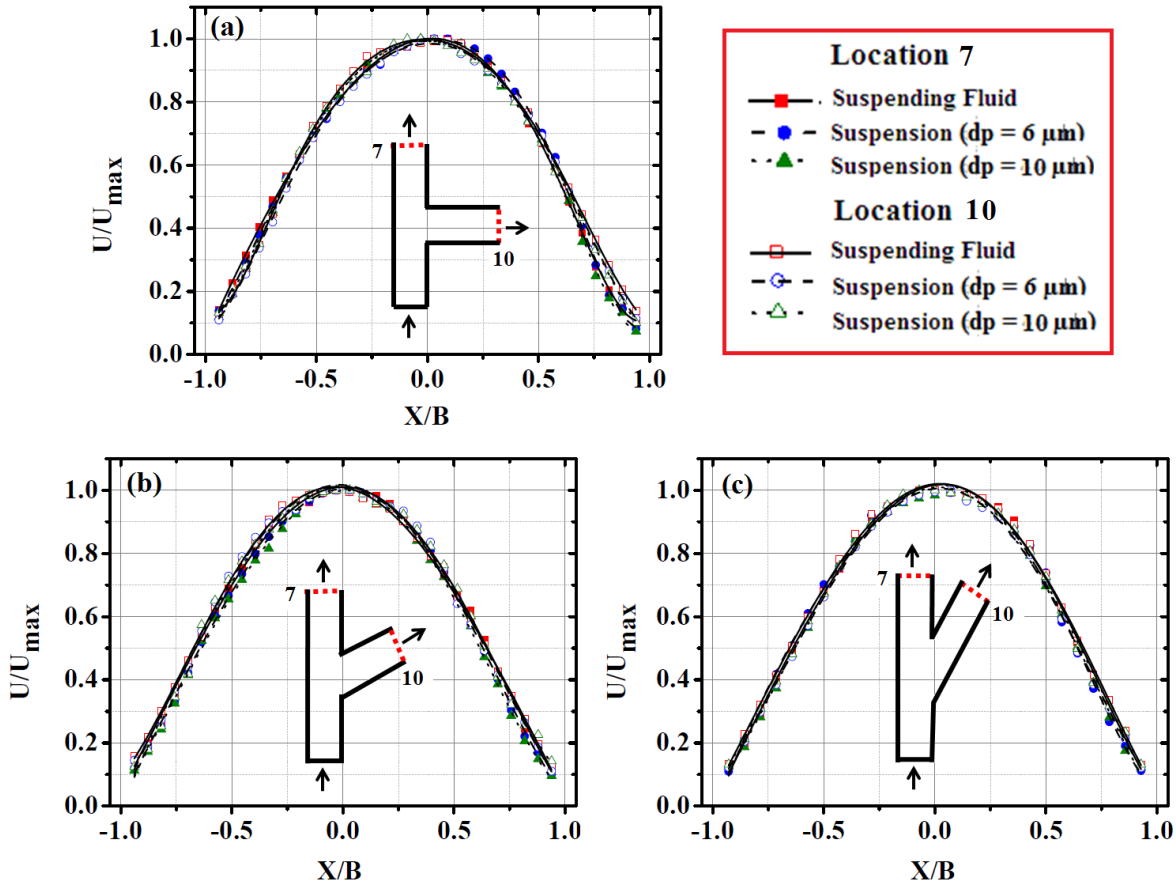

Figure 3.16. Velocity profiles at the end (location 7 and 10) of daughter branches in the asymmetric bifurcation channels: (a) θ =90°, (b) θ =60° and (c) θ =30°.

Figure.3.15 and 3.16 shows comparative velocity profiles of Newtonian fluid with suspensions at the end positions of daughter branches for symmetric (T and Y) bifurcation and in the side and main branch for the asymmetric (θ) 90°, 60 °, and 30° channels. Moreover, for all cases, the velocity profile at location 10 (side branch) was almost mirror image of location 7 (main branch). It was observed that in the downstream locations velocity profiles were symmetric.

Streamlines can be constructed from the velocity fields obtained from PIV and PTV analysis. In our study, the streamlines for the carrier fluid was obtained from μ-PIV analysis of 1 μm tracer particles and for the particles, μ-PTV analysis of the particles making the bulk suspension was carried out. Figure 3.17 shows these streamlines superimposed over the same grid for suspension of 10 μm particles. The streamlines shown in red color are for the carrier fluid and the blue lines are the streamlines obtained from the particle phase velocity. From the knowledge of the position of dividing streamlines the fluid and particle partitioning in the daughter branches can be known. For symmetric T and Y-shape channel, the position of the dividing streamline is almost at the middle of the junction point of daughter branches. The fluid and particle streamlines are nearly the same before the bifurcation (junction) point but deviate significantly thereafter. This shows that the larger particles which make the bulk suspension do not follow the smaller tracer particles indicating a difference in the fluid and particle velocities in the bifurcation region. The position of the dividing streamlines for both fluid and particle phase was shifted more towards the main branch in case of asymmetric bifurcation channels with angles 90°and 60°. But for the 30° bifurcation channel, it is shifted more towards the side branch. It should be noted that the width of the inlet, main and side branches in all the bifurcation channels were the same. Therefore, the junction part leading to daughter branch have unequal opening for the channels of 60^0 and 30^0 angle. As angle decreases the ratio of side branch to the main branch opening for the flow increases. For 30° bifurcation, the opening for the flow is more compared to 90°and 60° bifurcation channels. This is why both the fluid and particle phase streamlines are shifted more towards the side branch.

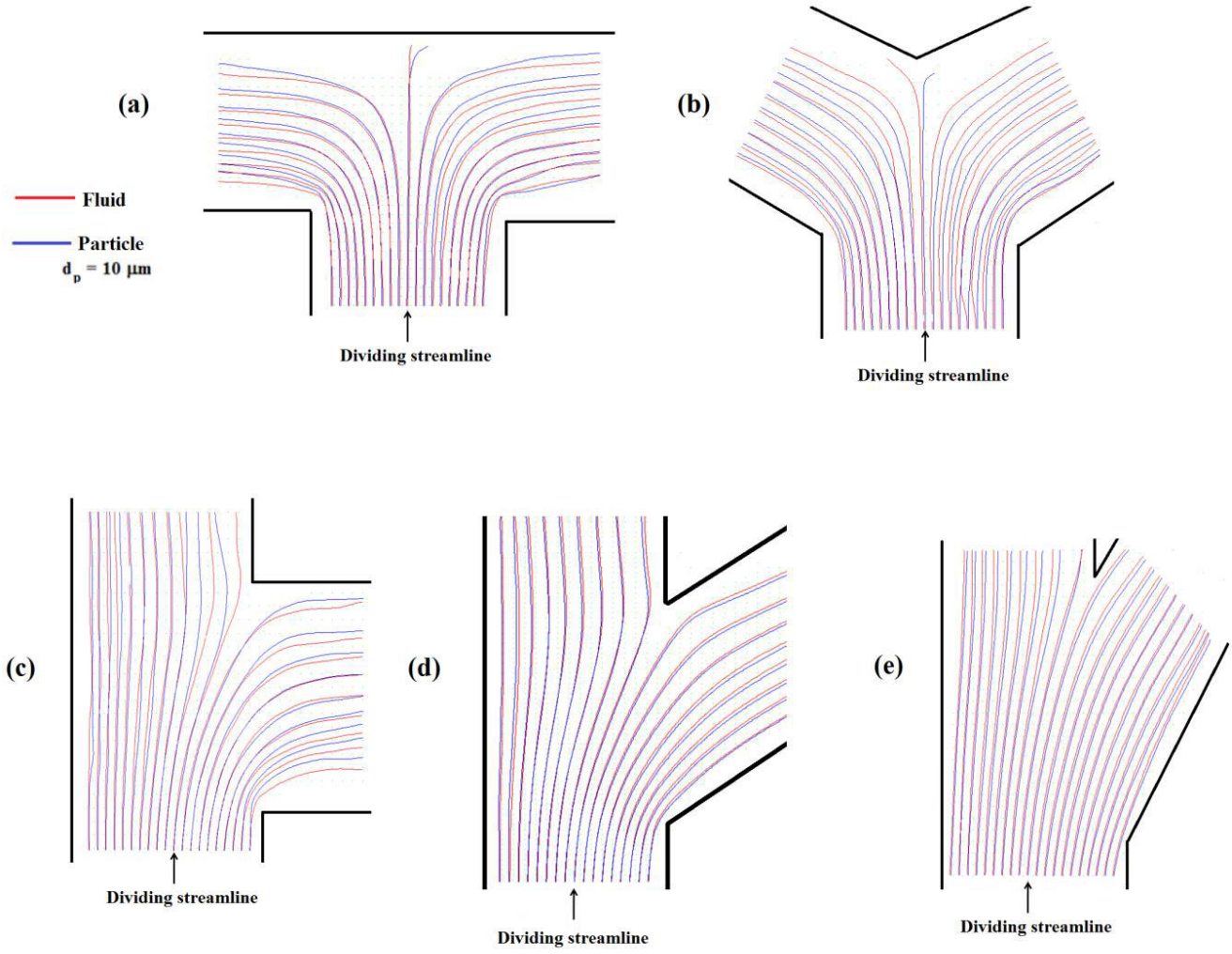

Figure 3.17. Streamlines of fluid phase velocity (obtained from PIV analysis of tracer particles) and the particle phase velocity (obtained from PTV analysis of suspended particle of 10 lm size) in various channels for diverging flow: (a) symmetric T-shape, (b) symmetric Y-shape; asymmetric channels: (c) θ =90°, (d) θ =60° and (e) θ =30°.

3.6.2. Particle concentration

The µ-PTV analysis was based on the tracking of dispersed particles that make up the suspension. The exact locations of a particle in two consecutive frames result a velocity vector. The positions of the velocity vector are the location of the particles in those regions. Figure 3.18 shows a velocity vector map of 10µm particles in all the five bifurcation channels. For the clarity of vectors, we have shown only a small region near the bifurcation or junction. From the vector map, it can be clearly observed that more number of vectors is located at the center of the channel in the inlet branch. The higher concentration of particles

in the center of the channel is due to the shear-induced migration. It can be observed that the particle concentration is relatively higher in the region close to the inner walls of the daughter branches. This is due to the fact that the inlet section had already high concentration of the particles in the center and these particles move closer to the inner wall of the side branches.

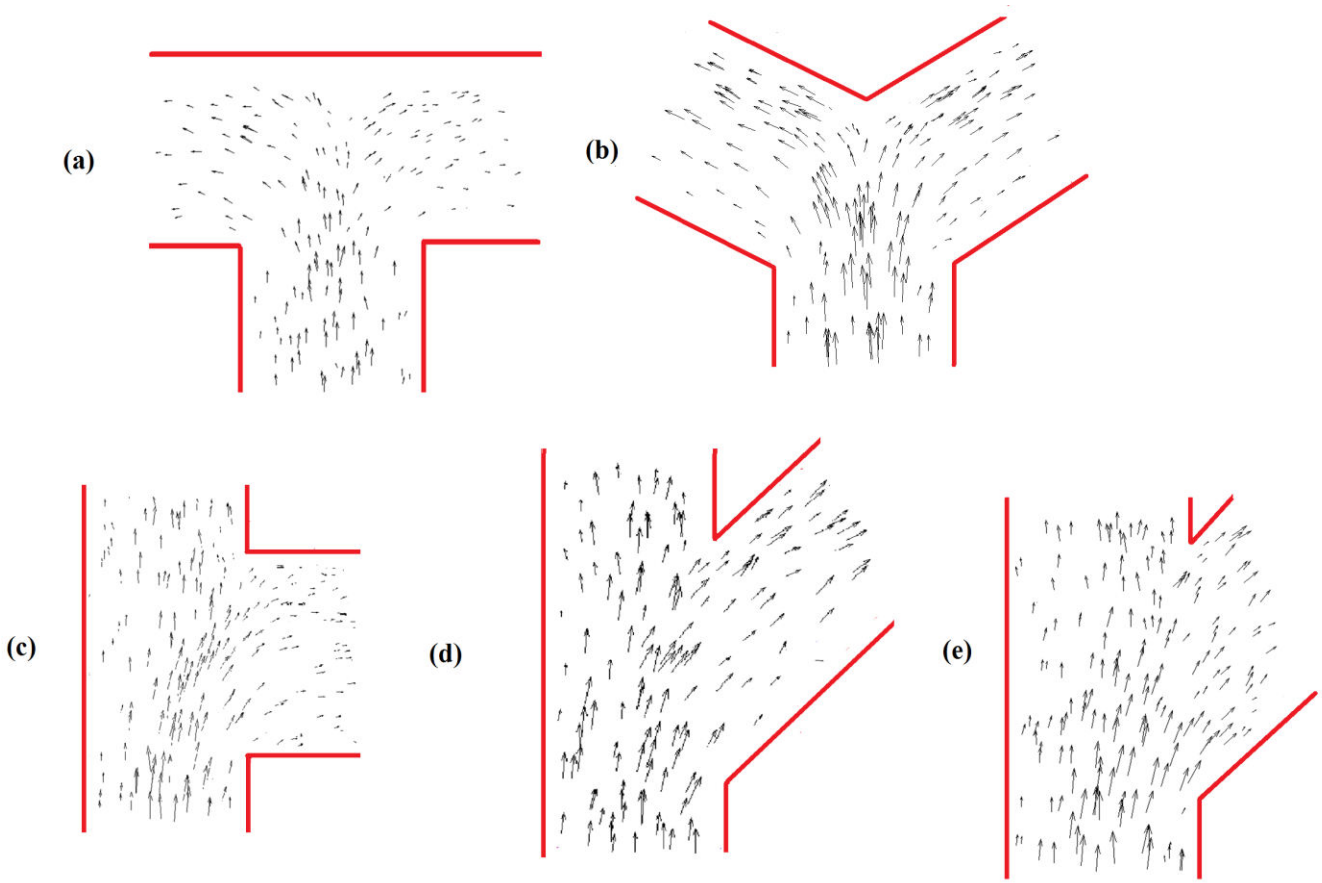

Figure 3.18. Velocity vector map of particle phase of size 10μm in the different bifurcation channels (a) θ =180°, (b) θ =120°, (c) θ =90°, (d) θ =60°, and (e) θ =30°.

The qualitative measurement of particle concentration was carried out using a particle counting program written in MATLAB. Figure 3.19 (a) shows a sample raw image of 10 μm particles distributed across the width of the channel. The rectangular section of the images that were chosen for the analysis measured 380 pixels in the velocity gradient direction and 65 pixels in the flow direction. To count the particles the whole image was divided into 11 bins of equal width as shown in Figure3.19 (b). The concentration of particles in each bin is represented as N_p/N_T where, Np denotes the number of particles in a bin and N_T is the total

number of particles present in the whole image. The average value of N_p/N_T was obtained by performing an average over 100 images. The normalized particle count in the inlet section of symmetric T- channel is shown in Figure 3.19(c). Due to shear-induced migration the particles move from walls (higher shear rate region) to the center of the channel (lower shear rate region) which is clear from inverted V-shape of the profile. As we move from location 1 to location 4 the peak concentration also increases

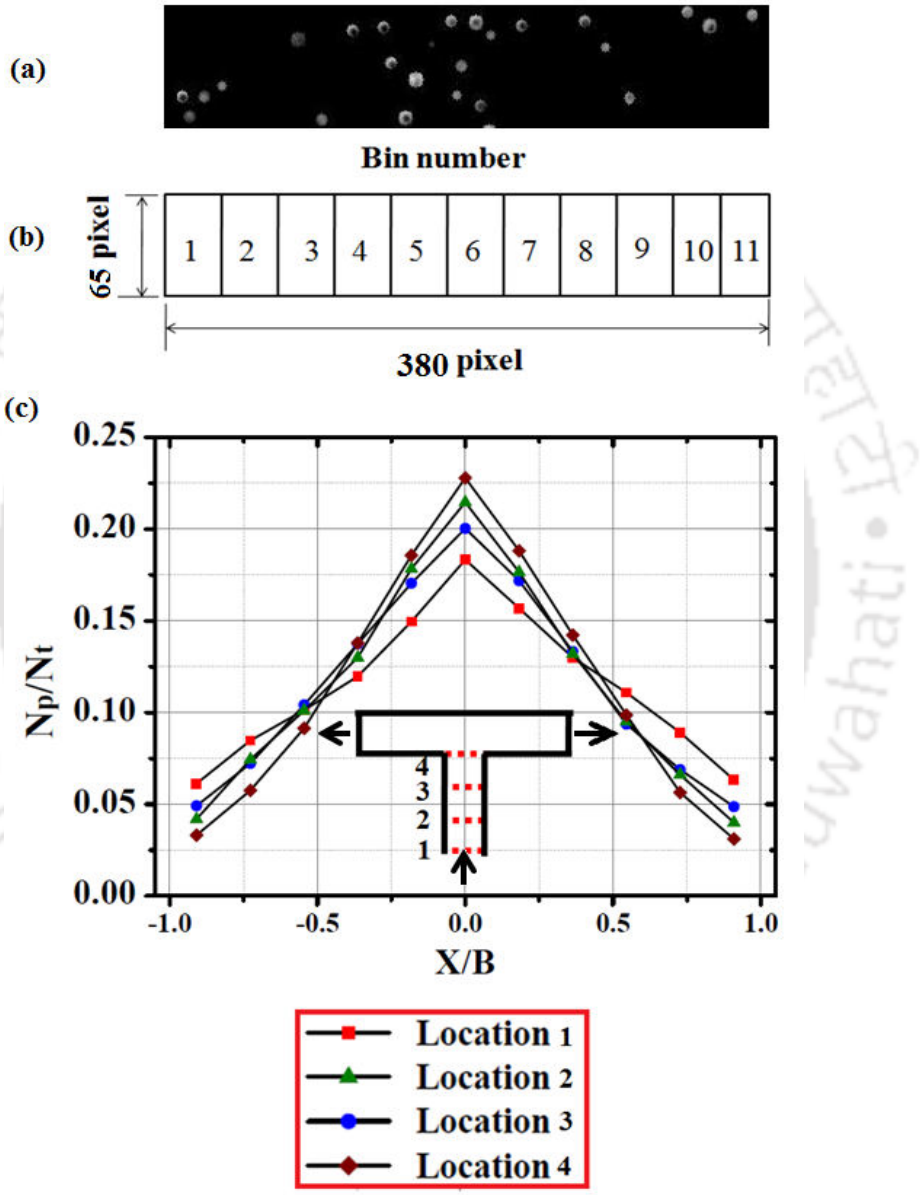

Figure 3.19. (a) Sample image for determining the concentration of particle, (b) Schematic representation of 11 spatial bins (B1 to B11) created across the width of the channel to count the number of particles in each bin, (c) Profiles of the particle count in the bins (normalized with the total particle count) at the inlet sections of symmetric T-shape channel in diverging flow.

Figure 3.20 and 3.21 shows the normalized particle count in the daughter branches of the symmetric and asymmetric bifurcation channels. We would like to mention that for the clarity of profiles x/B = -1 represents the inner wall of the left branch and x/B = +1 represents the inner wall of the right branch. At location 5 of the left branch and the corresponding location 8 of the right branch, the particle concentration is highest near the inner walls. The profile of the left branch is similar to the right branch for all the locations. As we move to downstream locations the particle concentration near the wall gradually decreases and the peak concentration shifts to the center of the channel. This is again due to shear-induced particle migration. Similar behavior was also observed for asymmetric bifurcation channels except for the fact that the profile at any location in the main branch is not the mirror image of the corresponding location in the right branch. For 90^0 bifurcations the concentration near the inner wall of the left branch is slightly larger compared to that of the right branch. However, for 30^0 bifurcation channel reverse was observed.

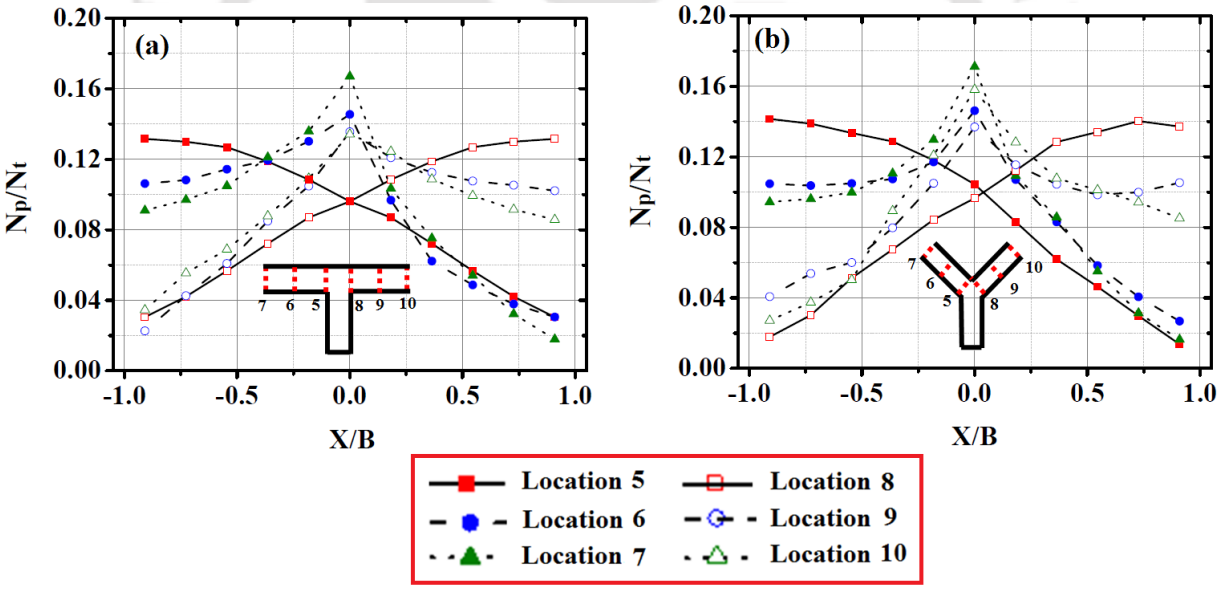

Figure3.20. Profiles of the particle count in the bins (normalized with the total particle count) in the left and right branches in diverging flow through symmetric bifurcation channels: (a) T-shape; (b) Y-shape.

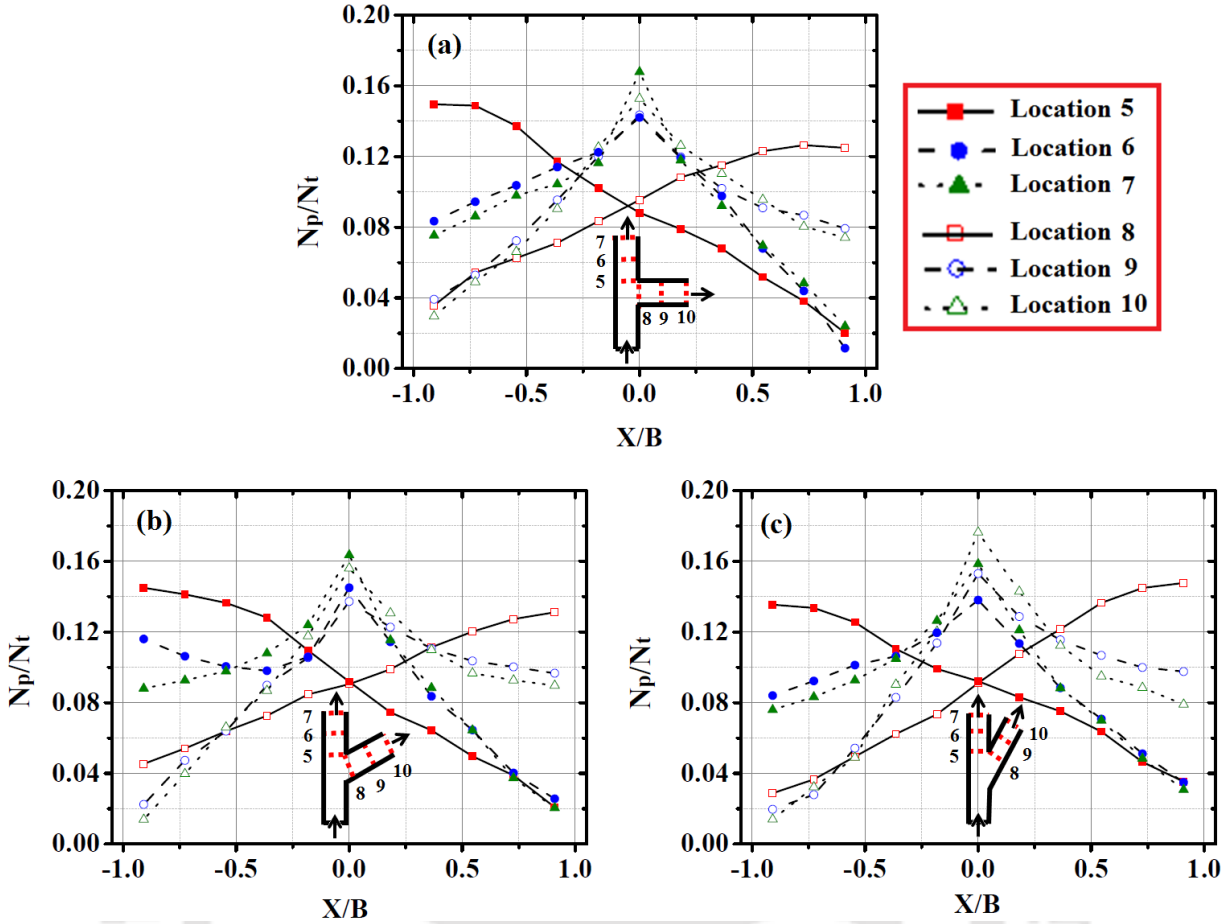

Figure 3.21. Profiles of the particle count in the bins (normalized with the total particle count) in the left and right branches in diverging flow through asymmetric bifurcation channels: (a) θ =90°; (b) θ =60°; (c) θ =30°.

3.7 Conclusions

We have carried out micro-PIV/PTV experiment of non-colloidal neutrally buoyant suspensions both in symmetric and asymmetric bifurcation channel. We have observed that due to shear-induced migration phenomena particles move toward the center of the channel and shows blunting of velocity profile before junction. It was observed that after the bifurcation the peak of velocity profile move in the direction of outer wall whereas disperse particle is distributed near the inner wall of the channel. As we move descendent positions in the daughter branches both the velocity and concentration profile become stables and shifts towards the middle of the channel. From the velocity vector map (μ-PTV) of particle phase, it is clearly observed that more number of vectors located at the center of the channel in the

inlet branch bifurcation. This can be directly related to shear induce migration phenomena for which particles migrate from the wall to the middle of the channel. In addition to this, it was also observed that in the respective daughter branches of microchannel, vectors shifted towards the inner wall after the bifurcation. So finally it can be concluded that after the bifurcation dispersed particles distributed near the inner wall of the channel. To verify the above findings we have used a Particle counting MATLAB program to study qualitatively the concentration profile, which also verifies the above findings. Flow and particle partitioning in daughter branches ware studied from the position dividing streamline. It was observed that for both fluid and particle phase was shifted more towards left branch than the right branch in for bifurcation angle (θ) 90°and 60 °. But for (θ) 30° both fluid and particle phase was shifted more towards the right branch than the left branch. Whereas for symmetric T and Y-shape fluid and particle phase separates equally in the daughter branches. It can be concluded that solid particles do not follow the fluid path near the bifurcation which leads to unequal flow and particle distribution in daughter channels.

Chapter 4

Suspension flow in converging channel

4.1 Introduction

In this chapter, we have conducted similar micro-PIV/PTV experiments as in Chapter 3 for converging flow. Although studies have been conducted for solid-liquid two phase flows in micro bifurcations for converging flow in past but many aspects were not reported. Majority of the studies limited to mixing of suspensions or pure fluids in the outlet branch.

4.2 Experimental Procedure

In these experiments, two syringe pumps were used to pump the samples from two inlets and finally it leaves from a single outlet. Schematic diagram of our experimental setup is same as the previous chapter (Chapter 3) except here we used another syringe pump to pump the sample from both inlets. We have conducted converging flow experiments in the same microchannels keeping the experimental parameter same as diverging flow. Schematic of symmetric and asymmetric bifurcation channels used in our experiment is shown in Figure 4.1. The locations at which profiles were evaluated are also shown in the images.

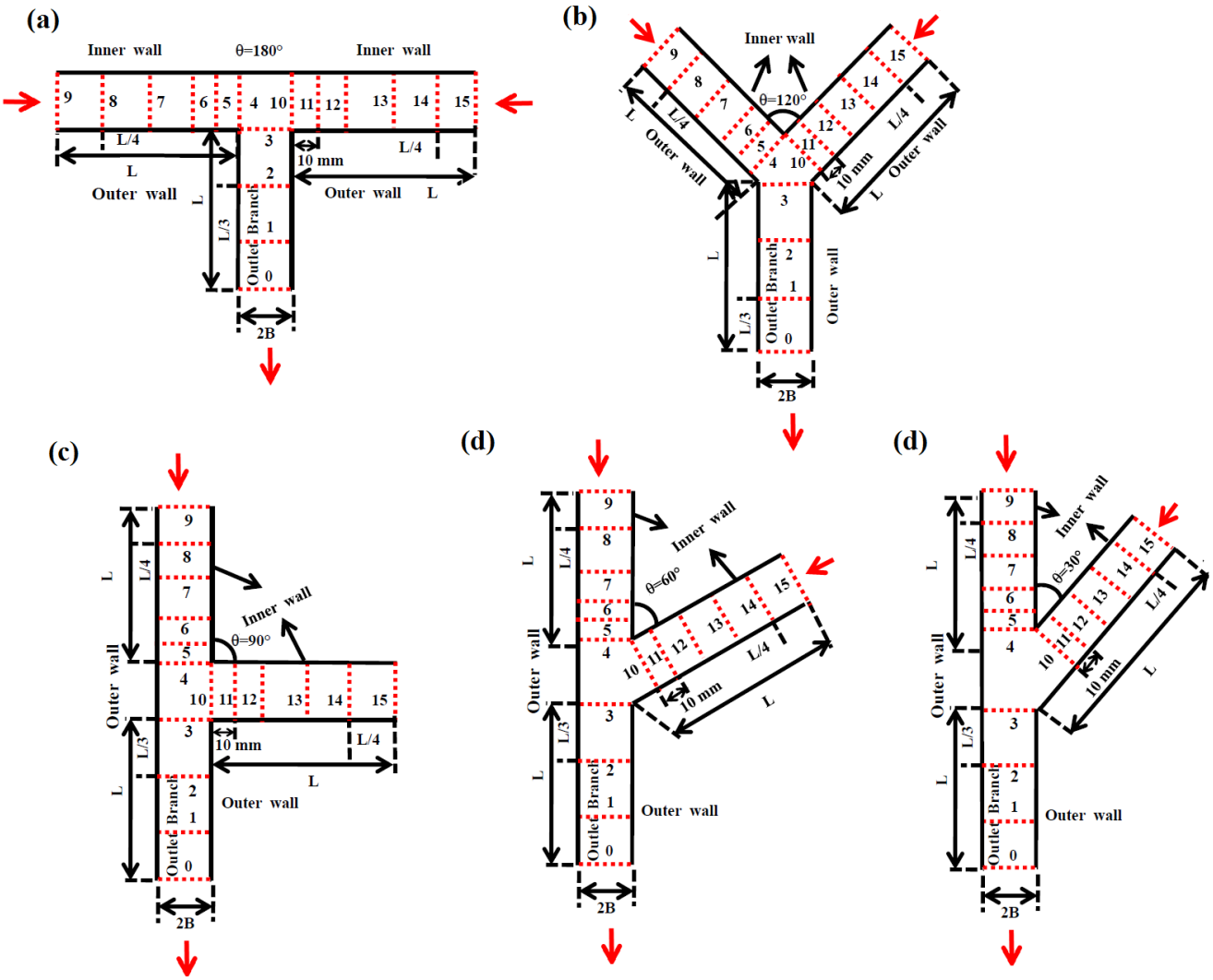

Figure 4.1. Schematic diagram of bifurcating channels used in our experiment.

4.3 Results and discussion

4.3.1 Velocity field

Velocity vector map of suspending fluid phase for 10μm suspension at the all the bifurcation is shown in Figure 4.2.

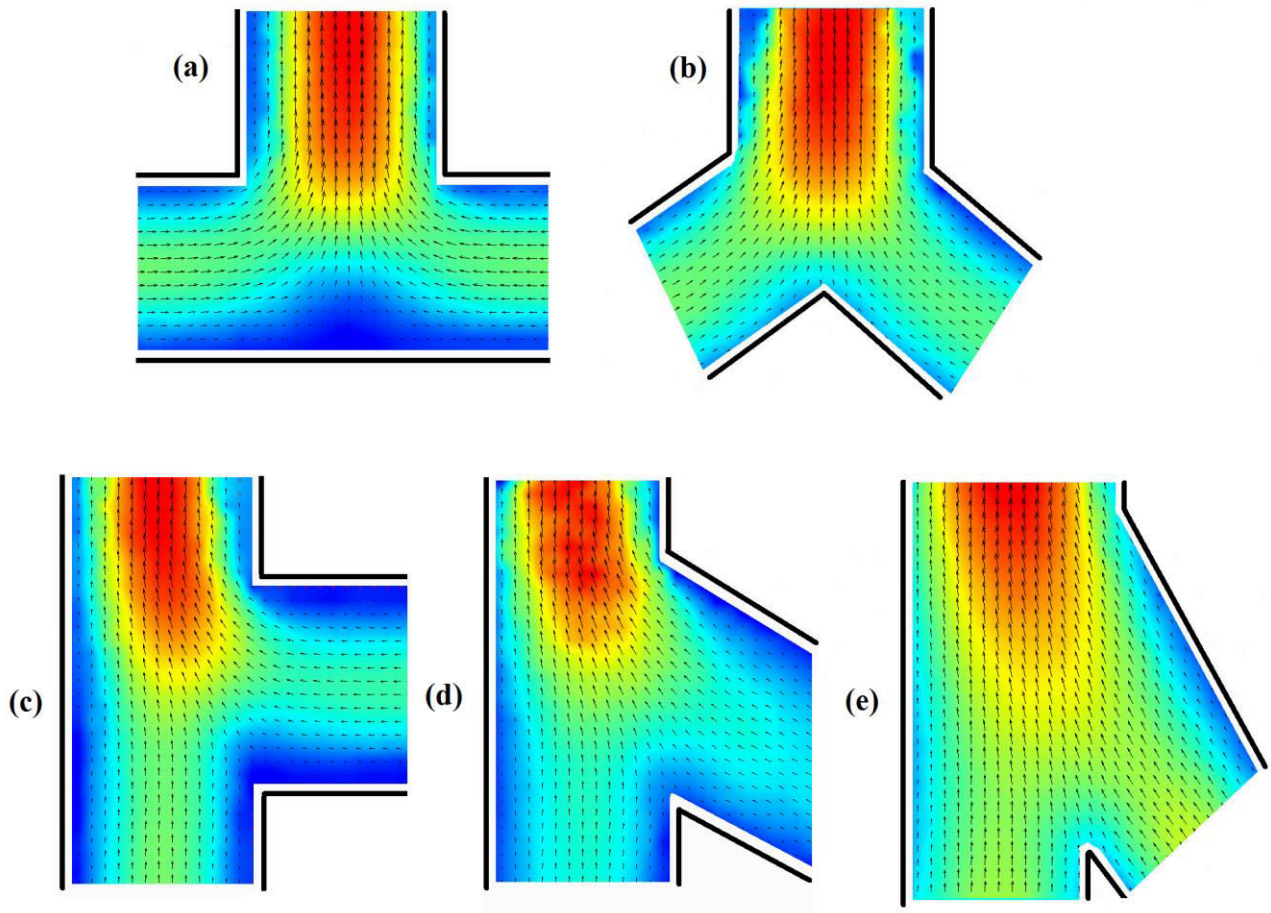

Figure 4.2. Velocity vector map of suspending fluid phase for 10μm suspension in the different bifurcation channels (a) θ =180°, (b) θ =120°, (c) θ =90°, (d) θ =60°, and (e) θ =30°.

The mean velocity profiles for pure suspending fluid and suspensions of two different particle sizes (6 and 10 μm) at various locations in the bifurcating channels are plotted. The velocity magnitude (U) is normalized relative to the maximum velocity (U_{max}) for each case. Figure 4.3 shows the velocity profiles in the symmetric T- bifurcation channel at three positions in one of inlet branch (location 8, location 7 and location 6). These locations can be identified in the schematic diagrams of the channels (Figure 4.1). At location 7 and 6 the velocity profiles are symmetric and fully developed. It was observed that up to location 6, the velocity profiles in the inlet branches were nearly parabolic and same for all bifurcation channels. This is because the effect of bifurcation angle is not felt up to location 6. After location 6 the nature of velocity profile depends on the bifurcation angle.

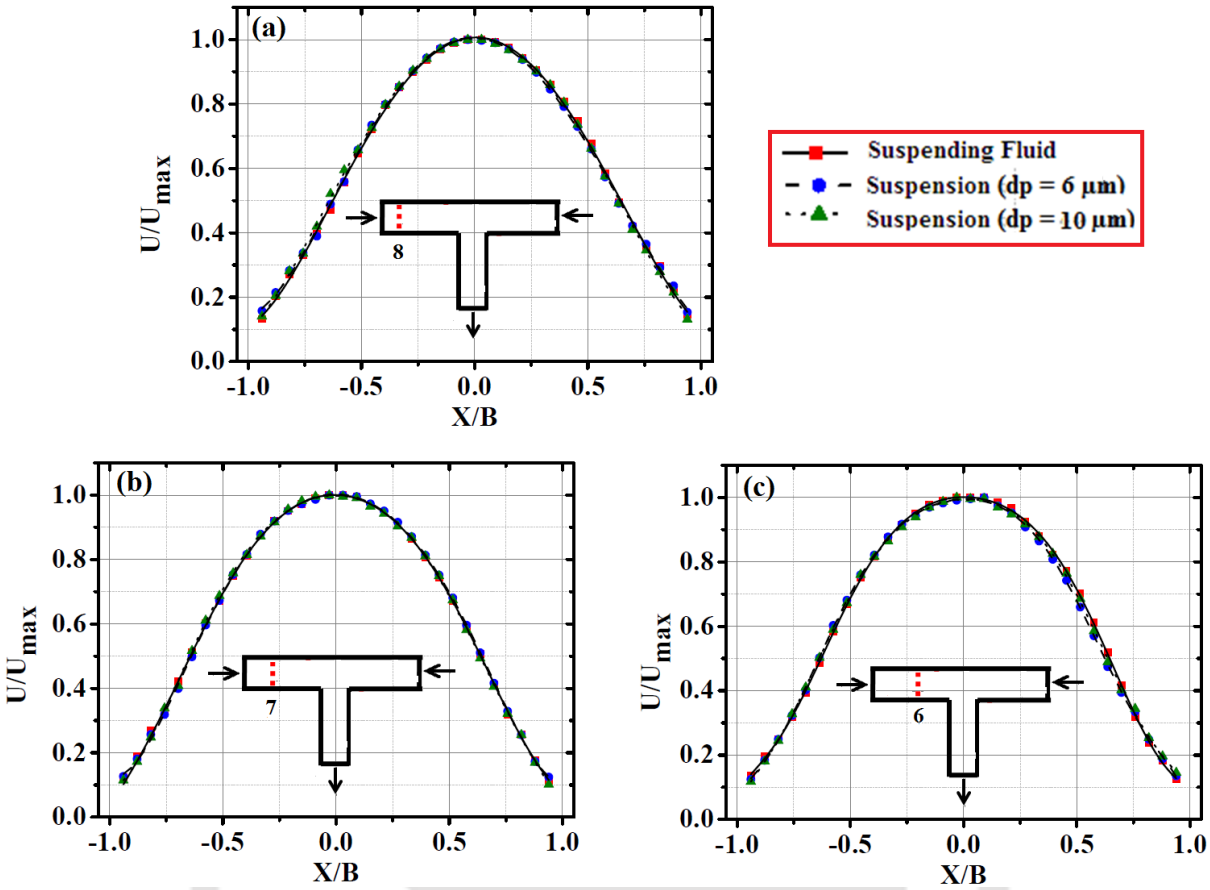

Figure 4.3. Velocity profiles in the inlet branch of asymmetric T- shape channel (θ =90°) at (a) location 8 (b) location 7 and (c) location 6.

Figure 4.4 and 4.5 shows the comparative velocity profiles of Newtonian fluid with suspensions at a location 10 mm ahead of the end of both the inlet (location 5 and Location 11) in symmetric and symmetric bifurcation channels respectively. In Figure 4.4 it was observed that at this location velocity profile slightly shifted towards the downward direction as this location is very near to the converging section and profile become asymmetric for both the symmetric bifurcation channels.

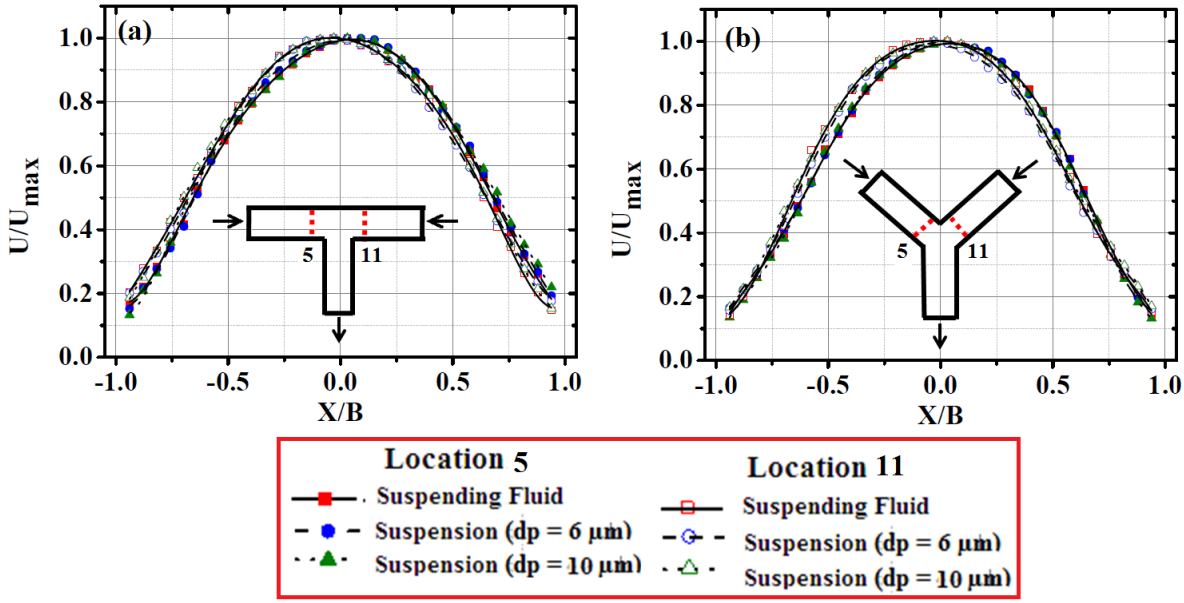

Figure 4.4. Velocity profiles at the location 5 and location 11 in the asymmetric bifurcation channels symmetric bifurcation channels: (a) θ =180°, (b) θ =120°.

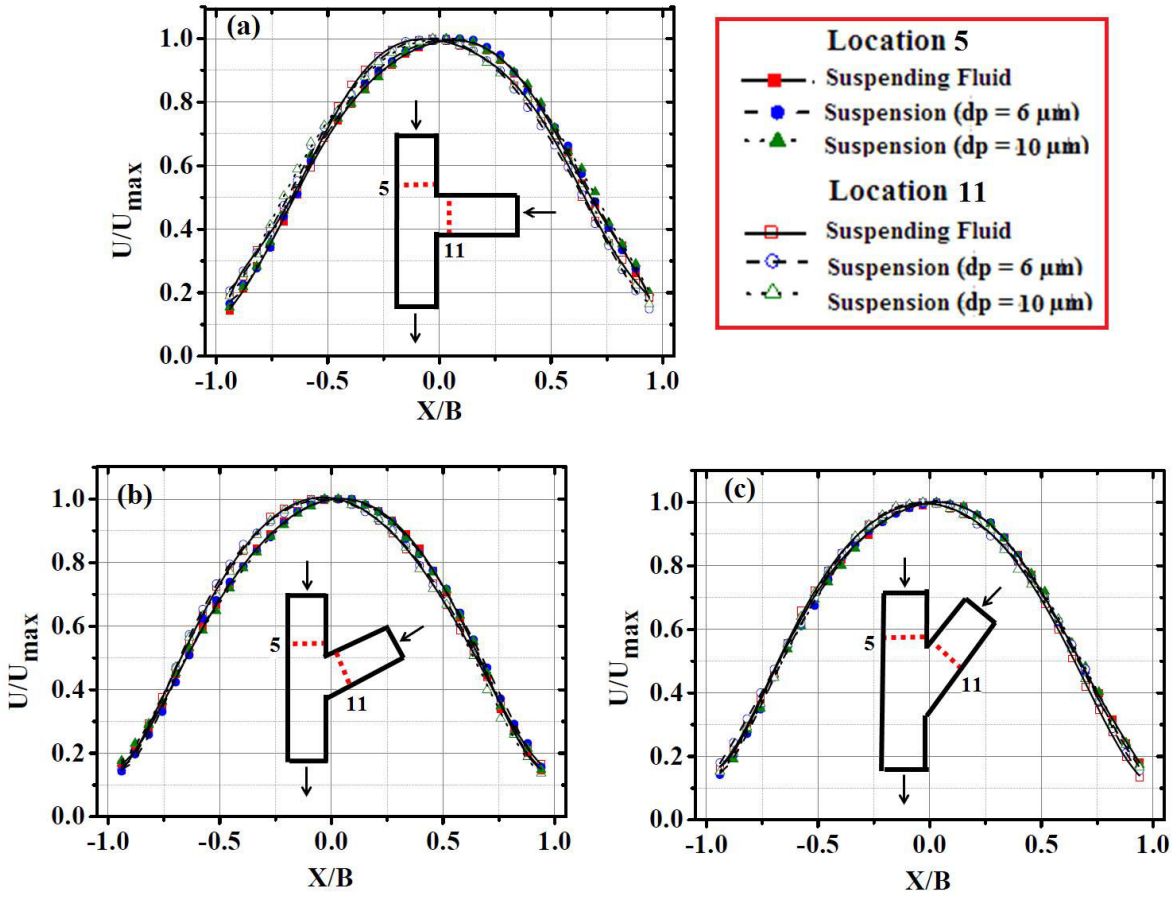

Figure 4.5. Velocity profiles at the location 5 and location 11 in the asymmetric bifurcation channels: (a) θ =90°, (b) θ =60° and (c) θ =30°.

For asymmetric channels, we have observed faintly asymmetric velocity profile in the side branch. On the other hand, velocity profiles in the main branch are symmetric. Also, we have observed that as the bifurcation angle decreases asymmetry in velocity profile reduces.

Velocity profiles at the end of inlet sections for symmetric and asymmetric bifurcation channels are shown in Figure 4.6 and 4.7 respectively. It was observed that in both symmetric channels the velocity profile at location 4 in the left branch is almost mirror image of location 11 in the right branch. In both, the daughter branches for T and Y -bifurcation the peaks in velocity profiles are shifted towards the converging section (inner wall) in contrast to diverging flow, where velocity profiles were shifted towards the outer wall. This shows that velocity profiles at these locations are reversible for diverging and converging flow conditions. For asymmetric channels, the velocity profile is asymmetric in the side branch but symmetric in the main branch. The asymmetry of the velocity profile is more pronounced in 90^0 channel compared to 60^0 and 30^0.

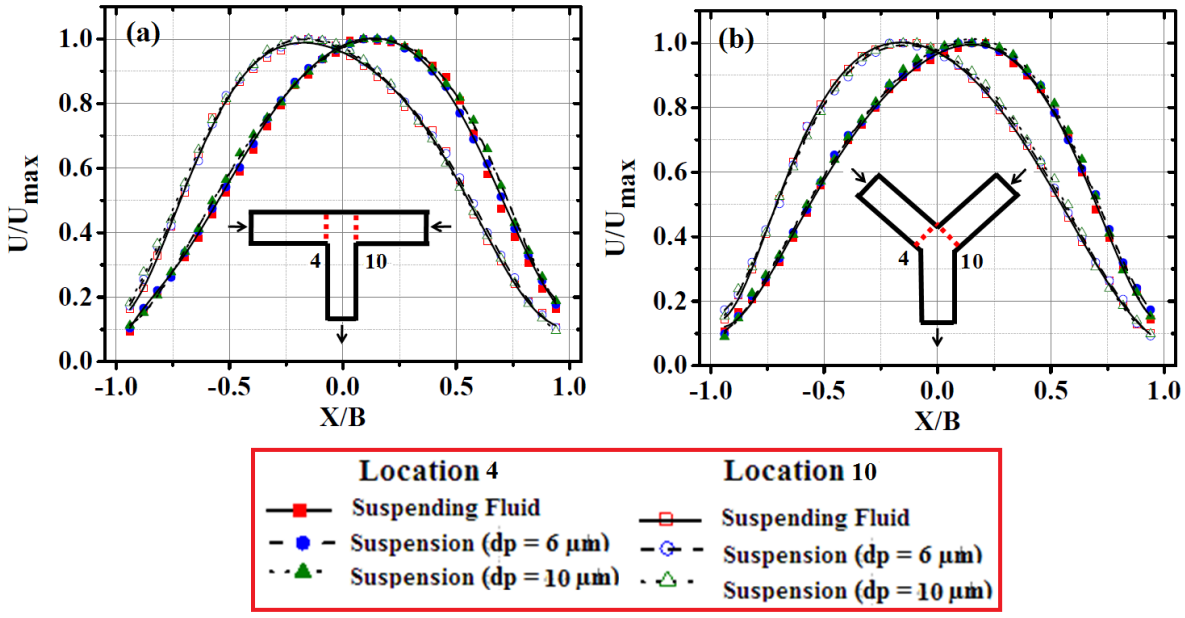

Figure 4.6. Velocity profiles at the end of inlet sections (location 4 and location 10) in the symmetric bifurcation channels: (a) θ =180°, (b) θ =120°.

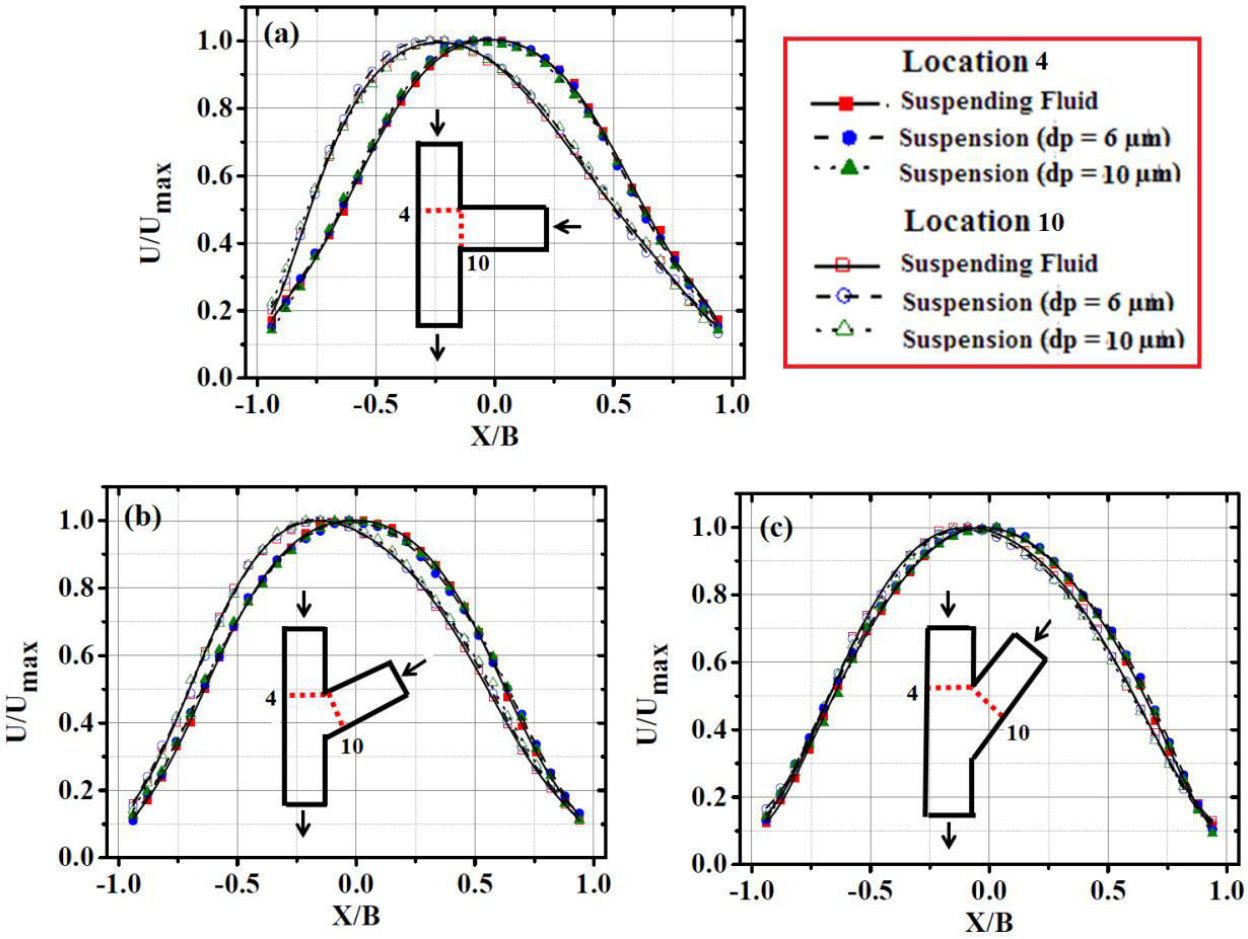

Figure 4.7. Velocity profiles at the end of inlet sections (location 4 and location 10) in the symmetric bifurcation channels: (a) θ =90°, (b) θ =60° and (c) θ =30°.

Figure 4.8 and 4.9 shows the velocity profiles at the junction of both the inlet streams, which is also the beginning of the outlet section (location 3) for the symmetric and asymmetric bifurcation channels. We have observed symmetric but slightly blunted velocity profile in both the symmetric channels. However, unlike the diverging flow, no peak-valley-peak type of profile was observed. In case of the asymmetric channels, the profiles are skewed towards the left. For suspension of a 10μm size calculated skewness for 90°, 60° and 30° bifurcation channel are 0.0404, 0.091 and 0.246 respectively. Here we have observed that as the bifurcation angle decreases the velocity profiles skewness towards the side branch decreases.

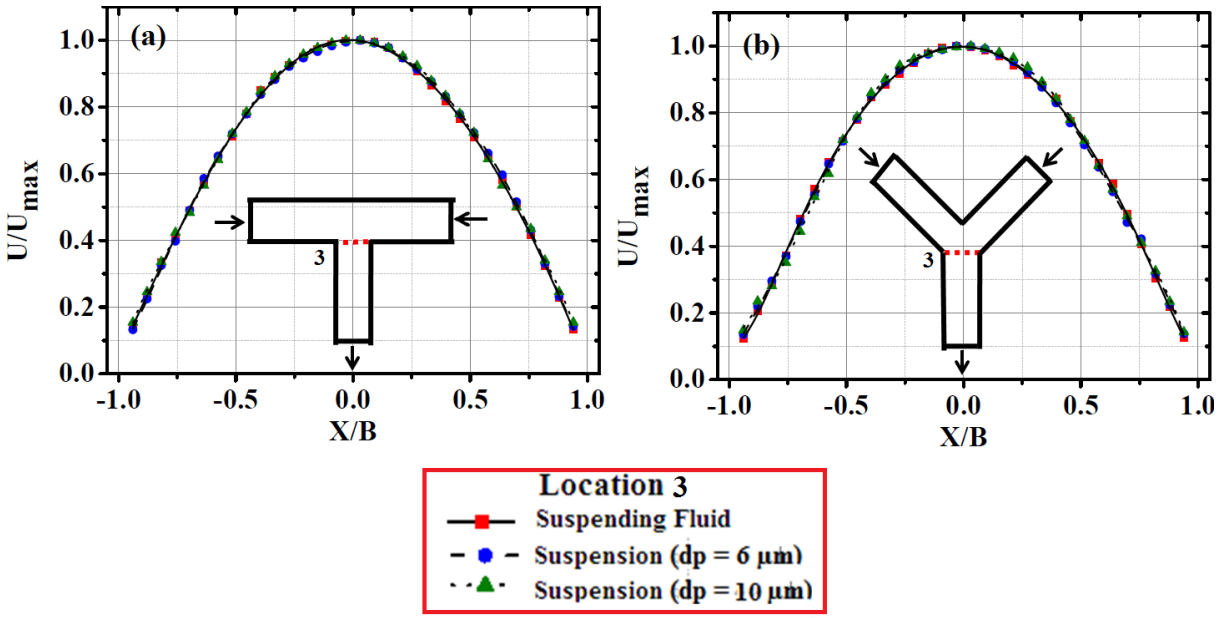

Figure 4.8. Velocity profiles at the junction point (location 3) in the symmetric bifurcation channels: (a) θ =180°, (b) θ =120°.

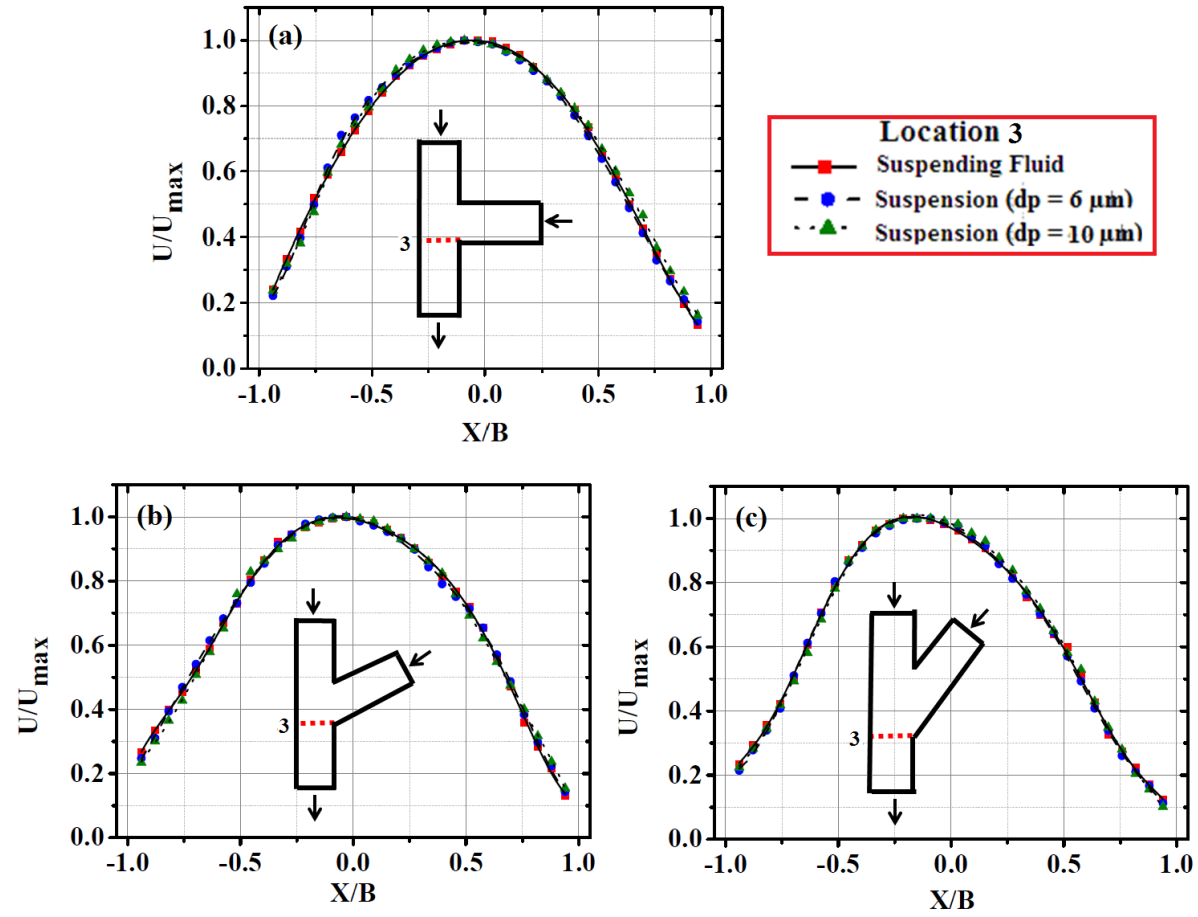

Figure 4.9. Velocity profiles at the junction point (location 3) in the symmetric bifurcation channels: (a) θ =90°, (b) θ =60° and (c) θ =30°.

We have observed that as the bifurcation angle decreases the asymmetry in the velocity profile increases. This is expected since for asymmetric channel as the bifurcation angle decreases the side branch to the main branch opening for the flow increases. As the opening for the flow is more, downward flow from the side branch will push the flow coming from the main branch towards the left. Moreover, skewness for pure suspending fluid and suspensions of two different particle sizes (6 and 10 μm) at 30°.bifurcating channels are 0.2152, 0.2179 and 0.246 respectively. Skewness is slightly more for suspension flow in comparison to that of pure suspending fluid. Moreover, suspension of larger particles size has marginally higher skewness in profile for all cases.

As we move downward positions in the outlet branch the velocity profile tries to become stable and shifts toward the center of the channel. Velocity profiles at location 2 for symmetric and asymmetric channels are shown in Figure 4.10 and 4.11 respectively. We have observed that in both channels, blunting of velocity profile decreases and profile were tries to become parabolic. Slight asymmetry in the profiles persists up to this location for (θ) 60° and 30° whereas for 90° channel profile become symmetric.

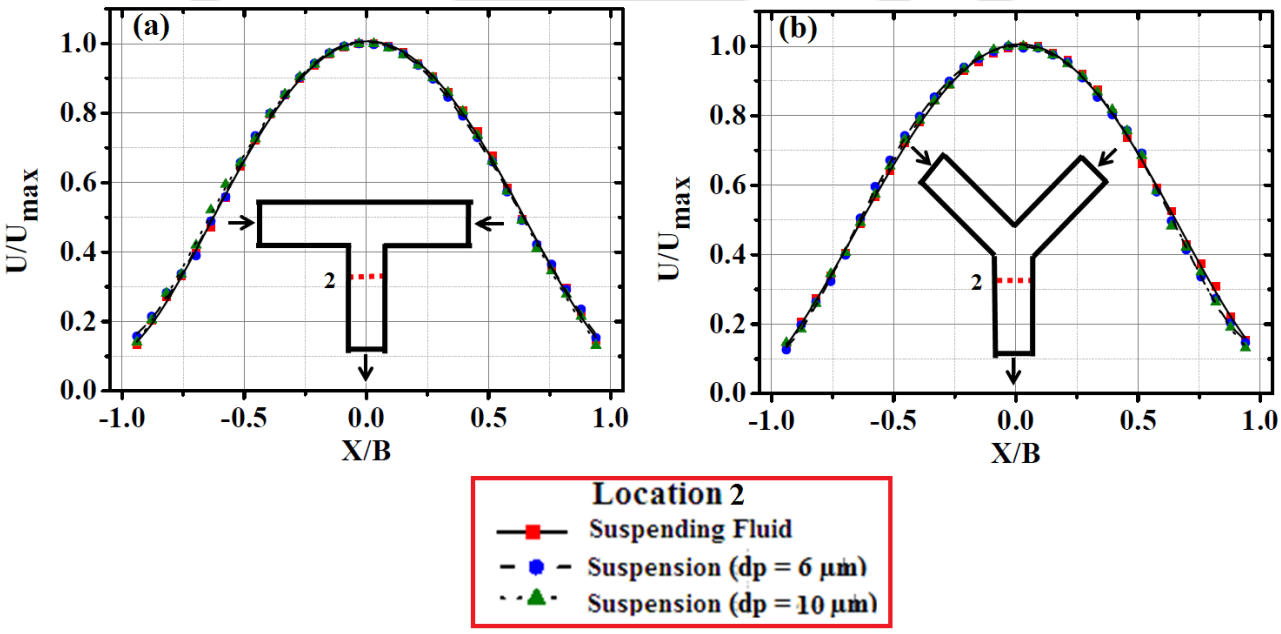

Figure 4.10. Velocity profiles at the outlet section (location 2) in the symmetric bifurcation channels: (a) θ =180°, (b) θ =120°.

.

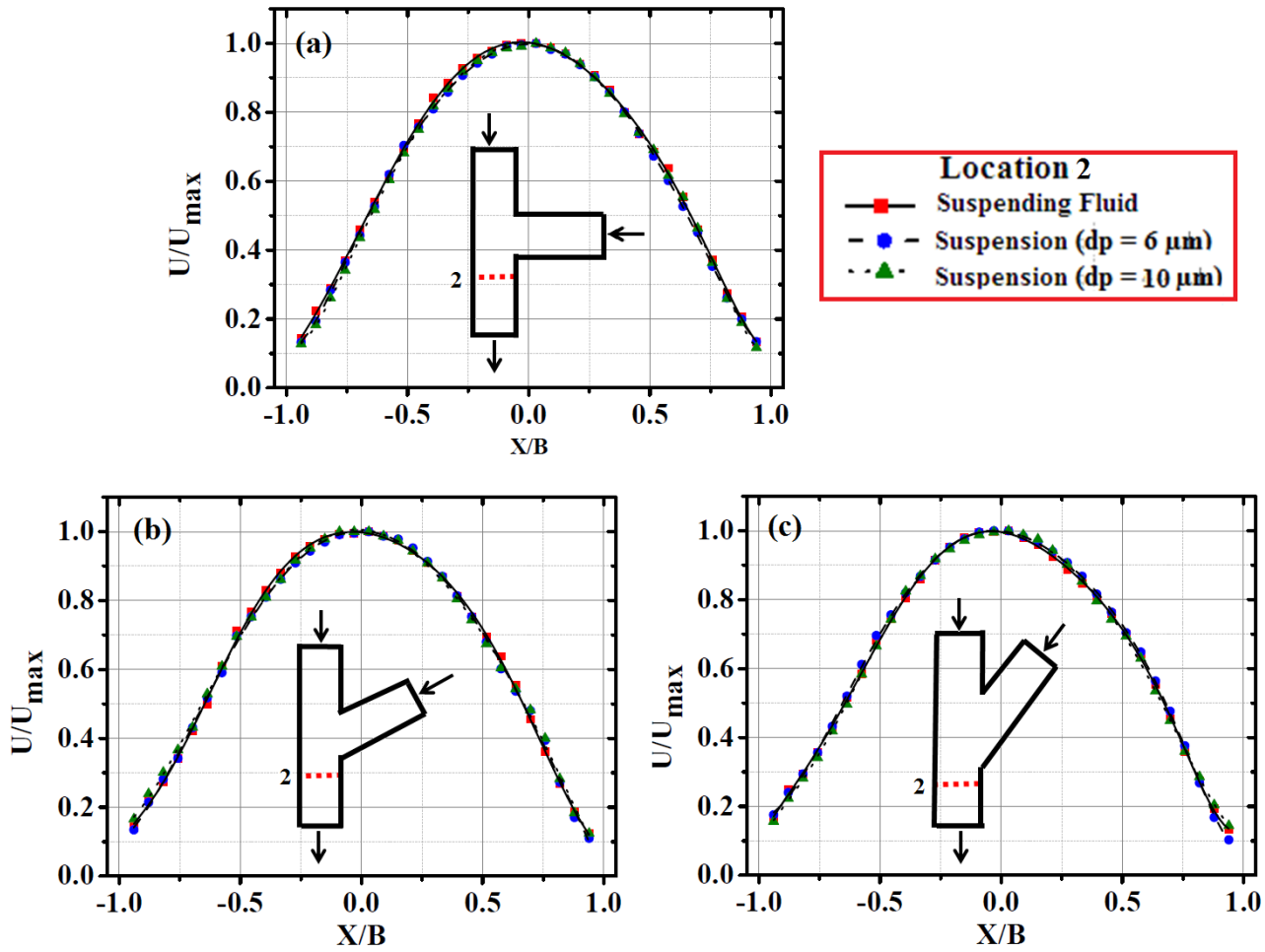

Figure 4.11. Velocity profiles at the outlet section (location 2) in the asymmetric bifurcation channels: (a) θ =90°, (b) θ =60° and (c) θ =30°.

In Figure 4. 12, 4.13, 4.14 and 4.15 we have noticed that the velocity profiles at locations away from the bifurcation are again symmetric and parabolic which resembles the corresponding profiles of the diverging flow.

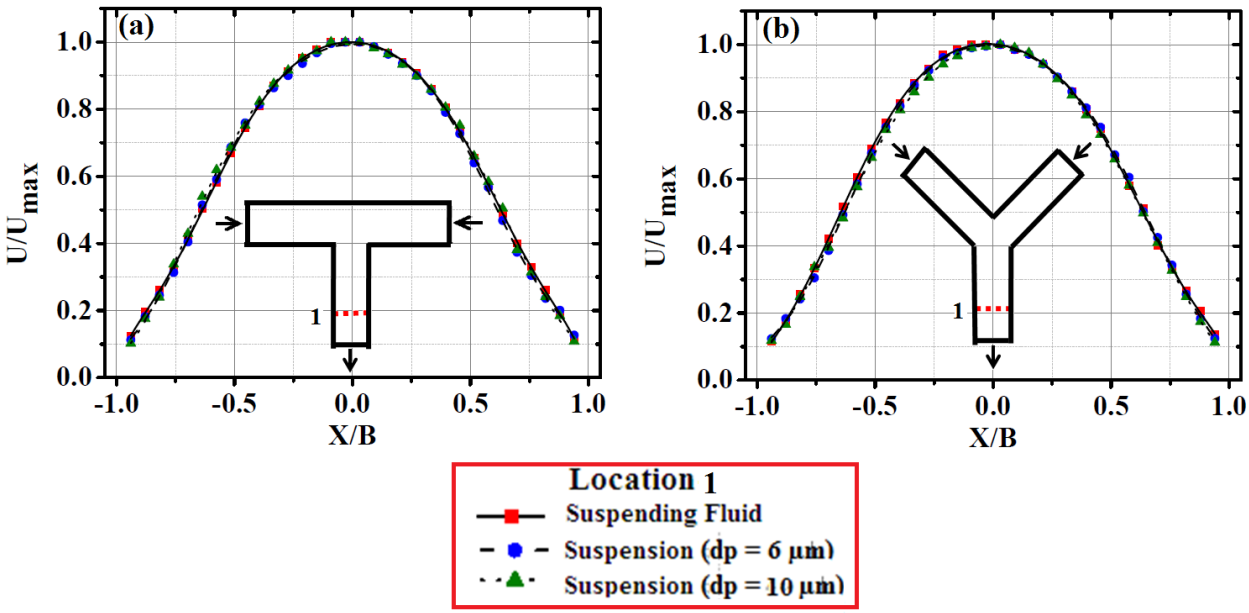

Figure 4.12. Velocity profiles at the outlet section (location 1) in the symmetric bifurcation channels: (a) θ =180°, (b) θ =120°.

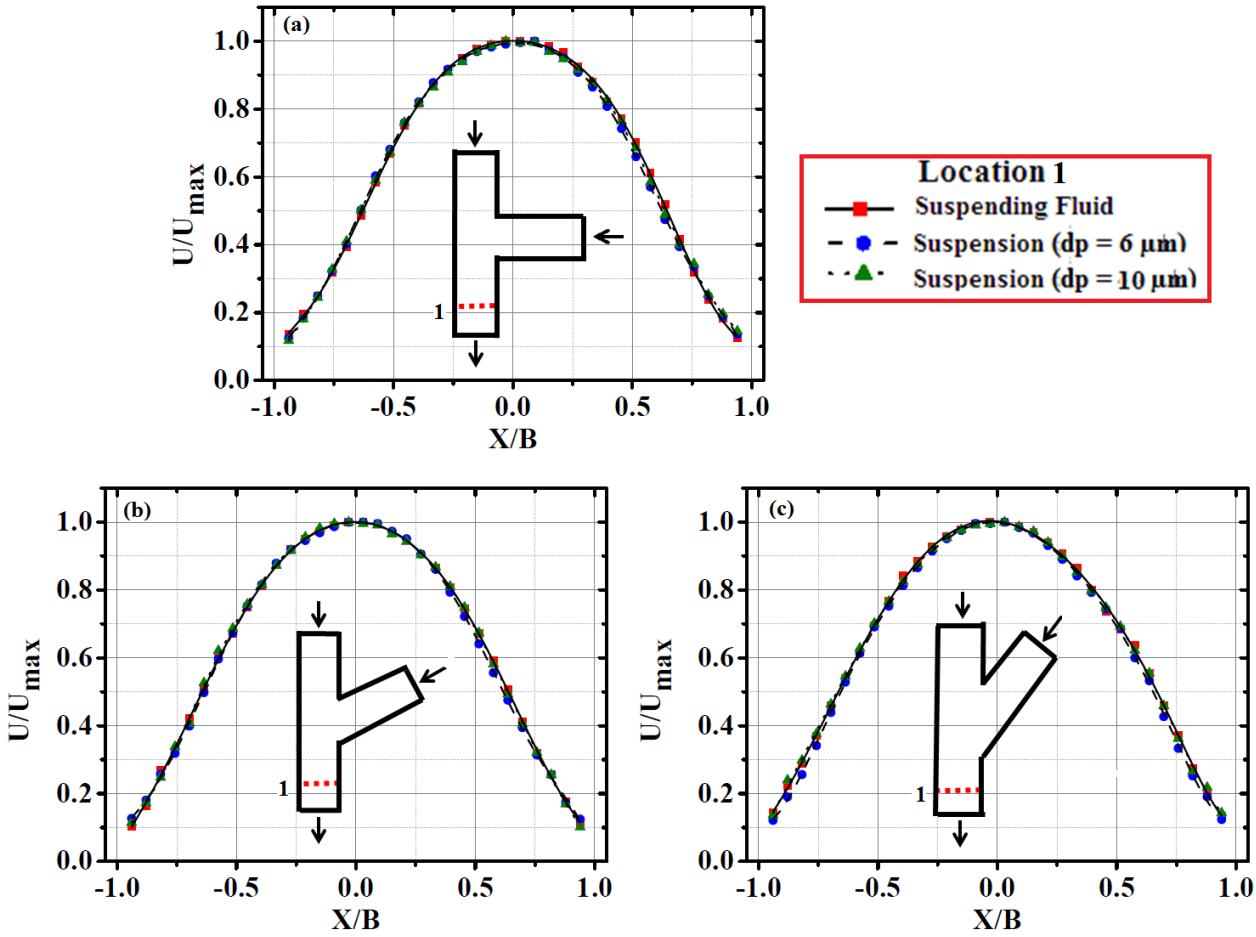

Figure 4.13. Velocity profiles at the outlet section (location 1) in the asymmetric bifurcation channels: (a) θ =90°, (b) θ =60° and (c) θ =30°.

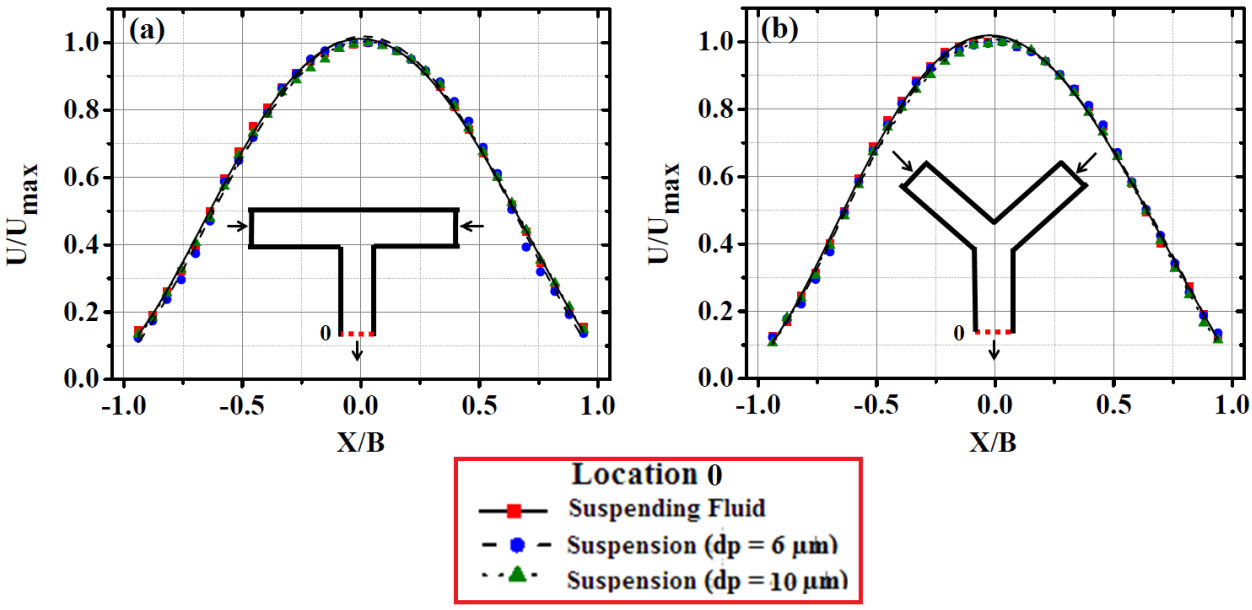

Figure 4.14. Velocity profiles at the outlet section (location 1) in the symmetric bifurcation channels: (a) θ =180°, (b) θ =120°.

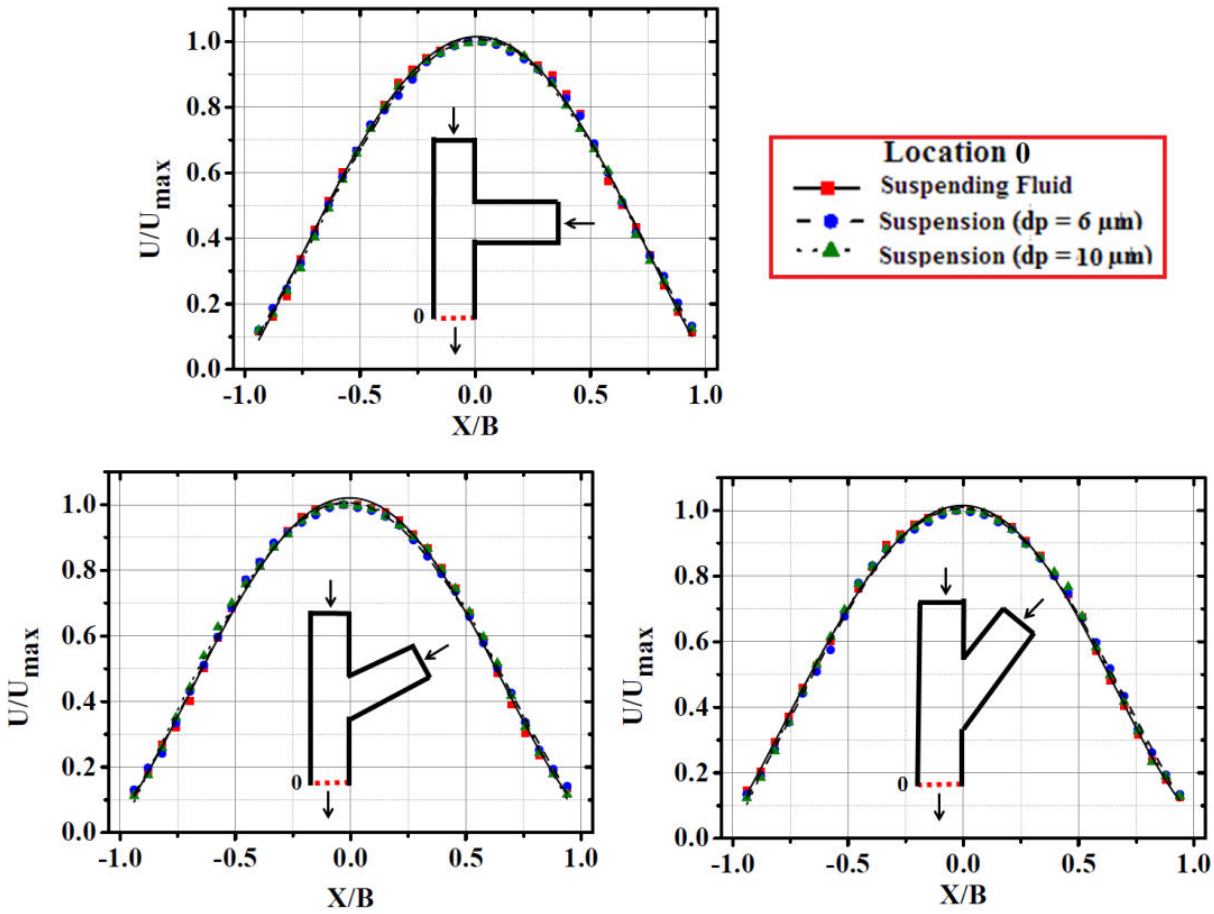

Figure 4.15. Velocity profiles at the outlet section (location 0) in the asymmetric bifurcation channels: (a) θ =90°, (b) θ =60° and (c) θ =30°.

Streamlines construction from the horizontal velocity fields of PIV and PTV analysis was explained in previous chapter (Chapter 3). Figure 4.16 shows the streamlines near the bifurcation of all the microchannels for suspending fluid and particle of diameter of 10μm. The streamlines shown in red color are for the carrier fluid and the blue lines are the streamlines obtained from the particle phase velocity. The comparison of the streamlines for the bulk flow and the particles showed significant deviation near the bifurcation region due to particle-particle interaction.

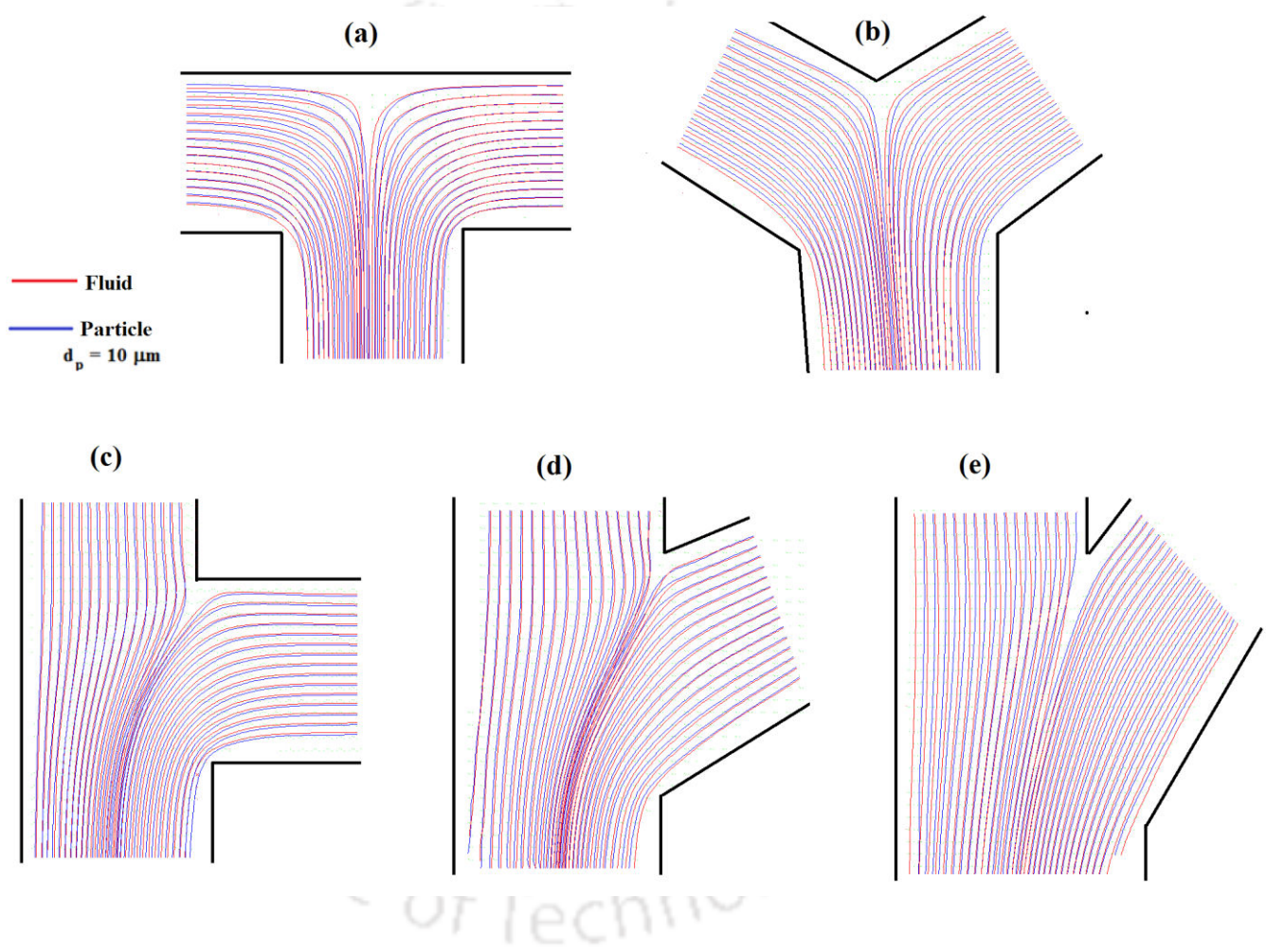

Figure 4.16. Comparison of streamlines of bulk suspension (obtained from PIV analysis of tracer particles) with the suspension particles (10μm) obtained from PTV analysis for various channels: (a) θ =180°, (b) θ =120°, (c) θ =90°, (d) θ =60° and (e) θ =30°

4.3.2 Particle concentration

Here Figure 4.17 shows the velocity vector map of 10µm size particle in all the five bifurcation channels. From the vector map, it was clearly observed that a greater number of vectors were located at the center of the channel in the two-inlet branch. This can be directly related to shear induce migration phenomena for which particles migrate from the wall to the center of the channel. As the flow moves downward in the converging section, velocity vector map near the junction shows bend towards the outlet section. Another interesting observation is that for symmetric T and Y shape channel two separate sharp vector stream is clearly seen in the outlet section. For asymmetric (θ) 90°, 60 °, and 30° channels also we can see two separated vector streams. It was observed that two streams of particles coming from the two inlet branch do not merge at the centre at the beginning of the outlet section. This gives rise to peak-valley-peak pattern in concentration profile which will be discussed next.

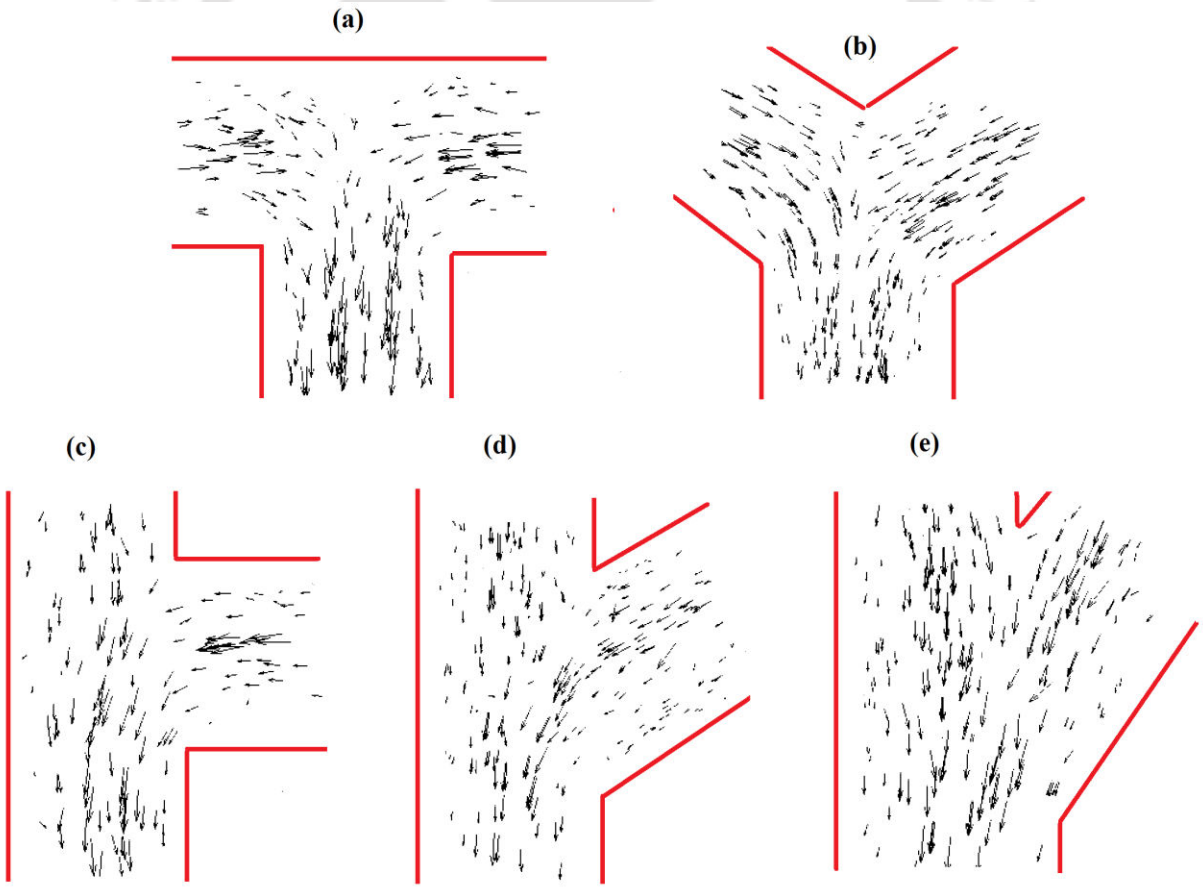

Figure 4.17. Velocity vector map of particle phase (10µm size) in the different bifurcation channels: (a) θ =180°, (b) θ =120°, (c) θ =90°, (d) θ =60°, and (e) θ =30°.

Then we have studied qualitatively the concentration profile at different locations of bifurcation channels using Particle counting MATLAB programme. Working Principle of MATLAB Particle counting programme described in the previous chapter (Chapter 3).

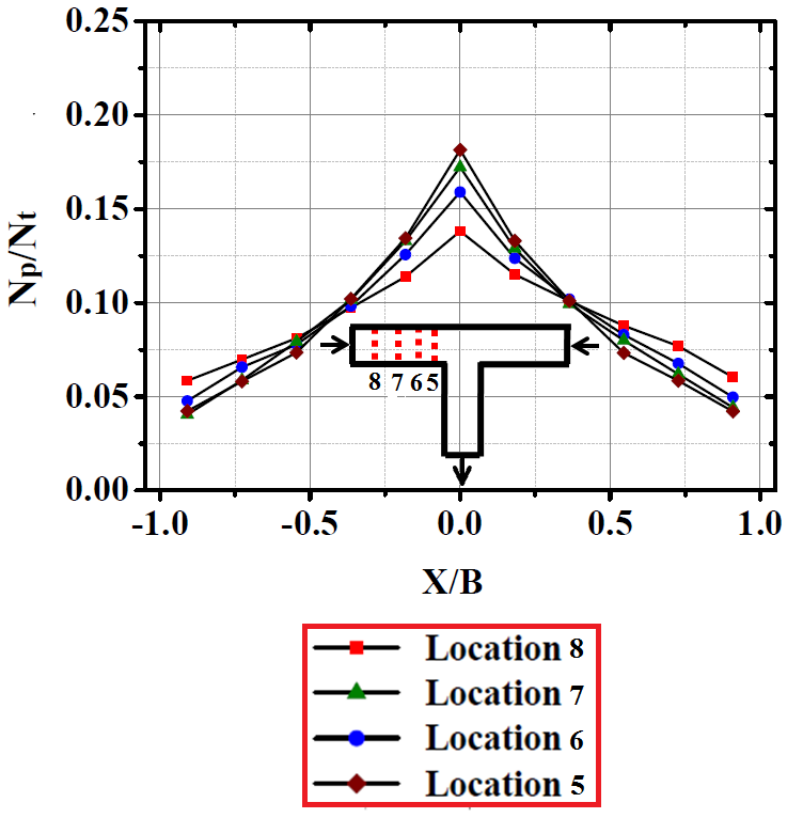

Figure 4.18. Profiles of the particle count in the bins (normalized with the total particle count) in the inlet section of the main branch (Locations 8-5) of asymmetric T-shape channel.

Particle volume fraction profile for suspension at the left inlet section (Locations 8-5) in symmetric T-shape channel is shown in Figure.4.18. Due to shear-induced migration phenomena the particles move from walls (higher shear rate region) to the center of the channel (lower shear rate region) and finally gives higher concentration in the central bin (6), which represent the middle part of the test channel. As the particles move from location 8 to location 5 the concentration near the central region increases and near the wall decreases. Up to location 5, upturned V-shape in the concentration profile is detected (Figure 4.18) and profiles are identical for all bifurcation channels.

Figure 4.19 and 4.20 shows the comparative particle volume fraction profile at the end of both the inlet branch for symmetric and asymmetric channels. As we move further downstream of the inlet sections asymmetry in concentration profile are seen and we found that at location 4 the concentration profiles shifted towards the downward direction.

The shifting in concentration profile is more intense in the case of symmetric (T and Y) shape than asymmetric channels. The shifting of profiles towards the downward direction is due to the fact that this location is very near to the converging section. We have observed that for an asymmetric channel (θ =30°) the concentration profile in the main branch is symmetric and identical for both the inlets.

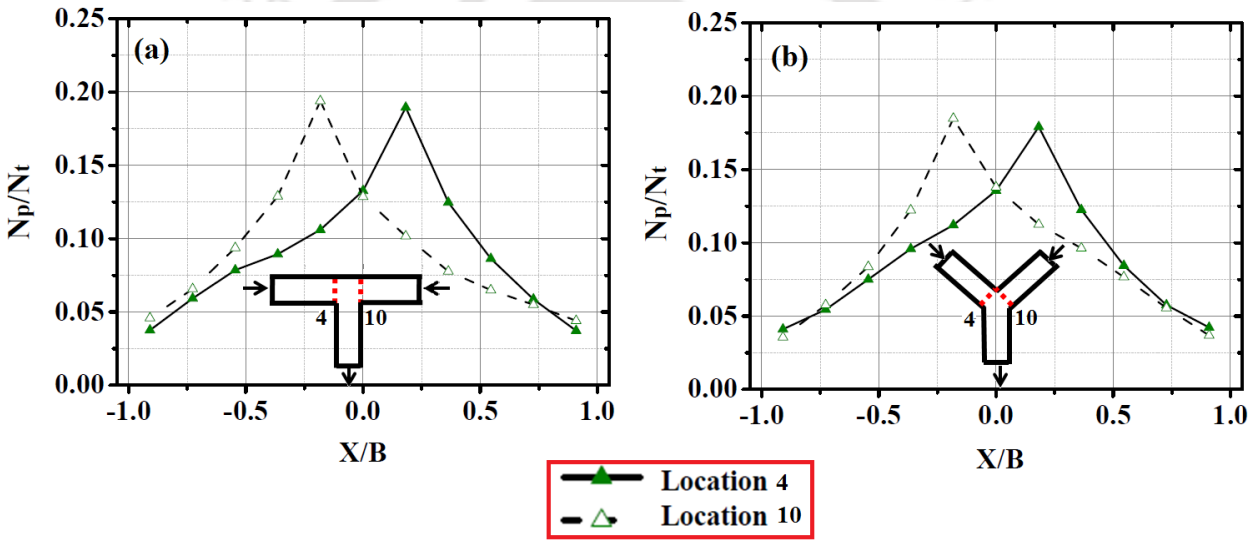

Figure 4.19. Profiles of the particle count in the bins (normalized with the total particle count) at the end of inlet sections (location 4 and location 10) for symmetric bifurcation channels: (a) θ =180°; (b) θ =120°.

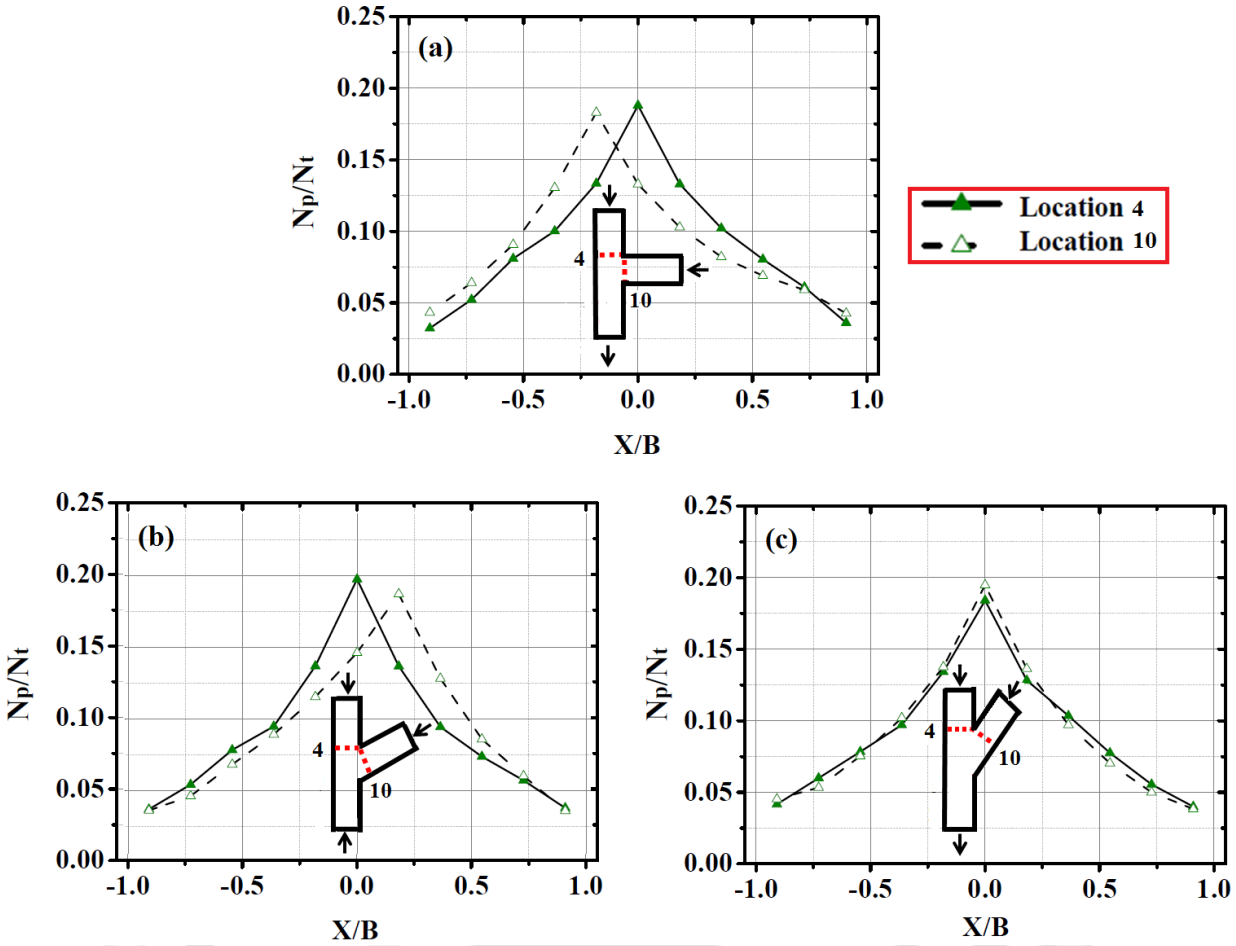

Figure 4.20. Profiles of the particle count in the bins (normalized with the total particle count) at the end of inlet sections (location 4 and location 10) for asymmetric bifurcation channels: (a) θ =90°; (b) θ =60°; (c) θ =30°.

Figure 4.21 and 4.22 shows the concentration profiles at various locations in the outlet section of symmetric and asymmetric bifurcations channels during converging flow condition. At location 3 and 2 we observe peak-valley-peak pattern in all the channels and this is due to combining of two streams in the outlet section. As we move further downstream locations, the peak-valley- peak pattern in the concentration profile gradually vanishes and only a single peak in the concentration profile emerges. At location 1 and 0 profiles are fully symmetric and showing maximum concentration at the center. These results clearly establish that due to the irreversible nature of shear-induced migration the profiles near the bifurcation region are not same in converging and diverging flow conditions.

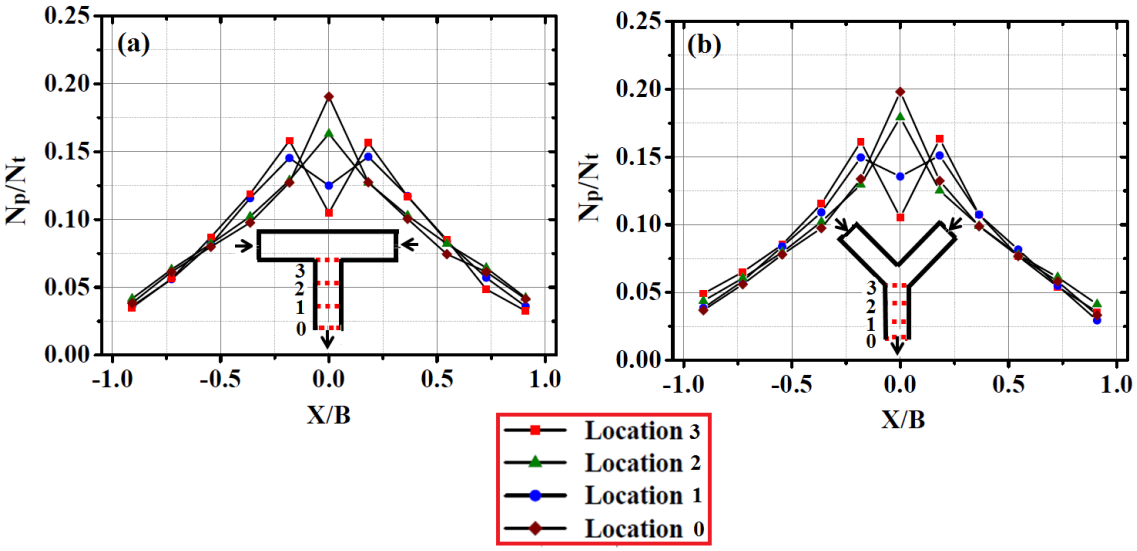

Figure 4.21. Profiles of the particle count in the bins (normalized with the total particle count) at different locations in the outlet section in the symmetric bifurcation channels (a) θ=180°, (b) θ=120°.

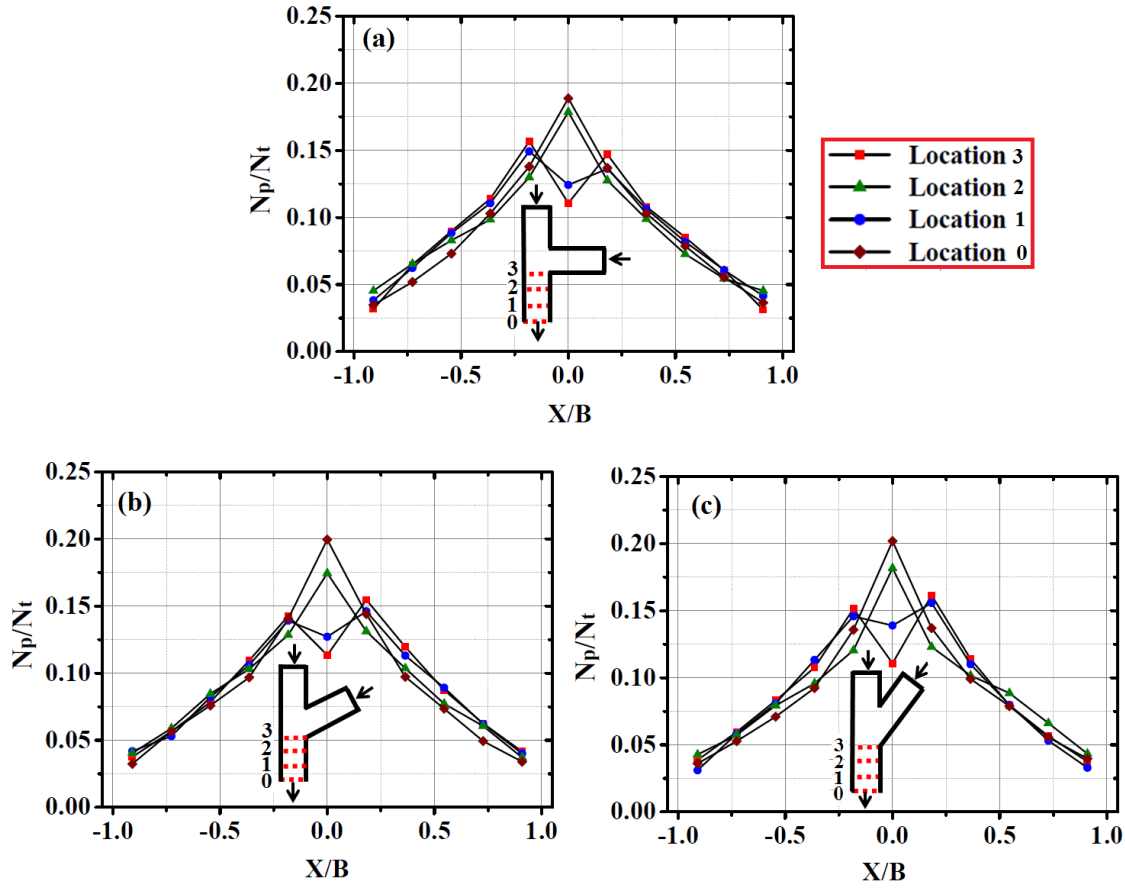

Figure 4.22. Profiles of the particle count in the bins (normalized with the total particle count) at different locations in the outlet section in the asymmetric bifurcation channels (a) θ=90°, (b) θ=60°, (c) θ=30°.

4.4 Conclusion

We have performed the micro-PIV experiments for both symmetric and asymmetric bifurcation channels for converging flow of equal inlet conditions (velocity and concentration). It was observed that at the end of inlet of both the daughter branches the crests in velocity profiles are shifted towards the converging section for symmetric T and Y bifurcation. Shifting of velocity profile was more for suspension flow compared to the Newtonian fluid. It was also observed that for asymmetric bifurcation channels velocity profiles of the main branch remains symmetric whereas profiles in the side branch are shifting towards the downward converging section. The shifting of profiles reduces with decrease of bifurcation angle. For converging flow we observed reversibility in results with diverging flow for velocity profiles at the end of inlet branches for symmetric bifurcation channels but for the asymmetric channels the profiles at the same locations were not same due to irreversible nature of shear-induce particle migration. From the velocity vector map (μ-PTV) of particle phase, it is clearly observed that more number of vectors are located at the center of the channel in both the inlet branch .This can be directly related to shear induced migration phenomena for which particles migrate from the wall to the center of the channel. One interesting observation is that for symmetric T and Y shape channel two separated sharp vector streams are clearly seen in the outlet section. For asymmetric (θ) 90°, 60 ° and 30° channels also we can see two separated vector streams. To verify the above findings we have used a Particle counting MATLAB program to study qualitatively the concentration profile, which also verifies the above findings. From the comparison of concentration profiles in outlet sections (location 3- location 0) for symmetric and asymmetric bifurcations channels, we have observed the peak-valley- peak concentration profile and this is due to combining of two streams in the outlet section. As we move to downstream locations in the outlet section, the peak-valley peak pattern in concentration profile gradually decreases and only a single peak in the concentration profile emerges. Another interesting observation is that at location 1 the two peaks in concentration profiles completely merge and then it resembles like an inverted V shape profile. We have observed from streamline comparison that disperse solid particles do not follow the fluid path near the bifurcation due to particle-particle interaction.

Chapter 5

Suspension flow in diverging-converging channel of varying width

5.1 Introduction

Blood microvasculature is a widespread network, consisting of continually bifurcate (i.e., diverging bifurcation) and merges with other microvessels (i.e., converging bifurcation). The abnormality of the micro vasculature can also cause a disorder of particles movement in suspension flow. Presence of diverging-converging bifurcations and short-length shunts may increase the speed flow, aggregation of particles near the apex of bifurcation etc. Therefore, it is significant and helpful to study the flow of suspension in bifurcate microvessels for a better understanding of the effect of branching angle, width of daughter branches, size of dispersed particles on distribution of fluid and particles in the daughter branches. Recently several studies were reported for flow in the diverging-diverging channel. Li et al. (2012) investigated the motion of red blood cells (RBCs) in converging-diverging bifurcating microfluidic channels using dissipative particle dynamics of healthy and unhealthy blood at low Reynolds number. Their results predicted that RBC flux in bifurcation channel depends on the deformability of RBCs and the feed hematocrit level of blood. Ishikawa et al. (2011) have investigated experimentally the behavior of RBC cells and adhesion of cancer cells for low Reynolds number. They revealed that there is a strong asymmetry in the trajectories of RBC cells and cancer cells at the diverging and converging section although the trajectories of tracer particles in pure water were almost symmetric. Subsequent to this Leble et al. (2011) had investigated experimentally the red blood cell motions in a microchannel with a diverging and converging bifurcation. They observed an asymmetry in velocity profiles of RBC's. Wang et al. (2016) carried out numerical simulation in the diverging and converging channel to investigate the effects of RBC shape, the deformability of membrane and hematocrit on rheological nature and the hemodynamics. They also reported the lateral

migration of RBC in the inlet branch and blunted velocity profiles in the inlet as well as daughter branches. Ye et al. (2018) carried out dissipative particle dynamics simulation for three-dimensional motion and deformation of a red blood cell (RBC) in a bifurcated microvessel with diverging and converging bifurcations. They have studied the effect of bifurcated angle, diameter of branch, as well as the RBC's properties on flow behaviour.

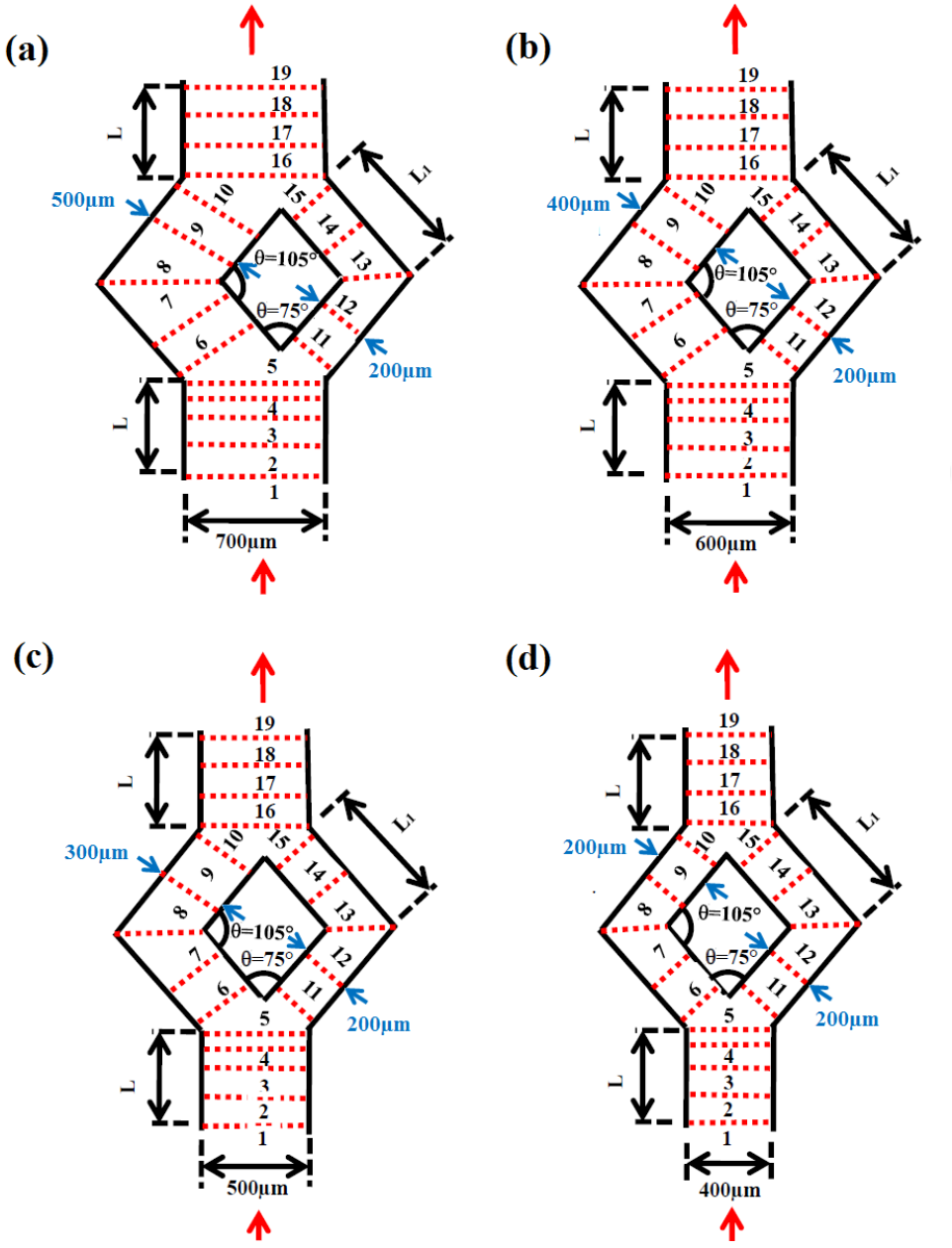

Figure 5.1. Schematic diagram of diverging-converging channels of equal right daughter branch width (200µm) and varying left daughter branch width (a) 500µm (b) 400µm (c) 300µm (d) 200µm respectively.

5.2 Experimental Procedure

We have performed micro-PIV/PTV experiments for diverging-converging channels of varying width. Schematic of channels used in our experiment is shown in Figure 5.1. The locations at which profiles were evaluated are also shown in the images. The widths of left daughter branch were varied keeping right daughter branch constant in all channels. We have varied the width of left daughter branches from 200µm to 500 µm keeping width in right daughter branch constant 200µm (Shown in Figure5.1). The relative lengths of inlet and outlet sections were taken to be equal (L=4 cm) and the length of left and right daughter branch were taken L_1=1.5 cm. An extension of pipe was attached to the inlet of the test channel to connect the syringe pumps which allow a sufficient entrance length for fully developed flow to establish before flow enter to inlet section of the channel. In this work, we have conducted experiments keeping particle concentration low 5% so that particle to-particle impacts can be ignored. Moreover, at low concentration experimental variables can be control nicely and getting accurate measurements easier. Schematic of our experimental setup and description of components are same as in Chapter 3. The inlet velocity and particle concentration were assigned at the inlet. The maximum (centreline) velocity in the channel varied from 0.0157 cm/s to 0.0277 cm/s. Reynolds number based on suspending fluid and particle for 10 µm particle size was $O(10^{-2})$ and $O(10^{-4})$ respectively. In our µ-PIV/ PTV experiment objective was to simultaneously measure the fluid phase and particle phase velocities. All images contain fluorescence tagged larger particle having a diameter (D_p) 6 or 10 µm and smaller particles with a diameter (d_p) 1 µm. Details of separation of images based on tracer particle size were discussed in Chapter 3. After separation of images, µ-PTV analysis was carried out for the images of larger particles to get the particle velocity and concentration field using PTV lab Beta software and µ-PIV analysis was performed for 1µm tracer image (Figure 3.4c, Chapter 3) using PIVlab_1.32 software to measure the fluid phase velocity. Velocity vector map of suspending fluid phase for 10µm suspension at the all the bifurcation is shown in Figure 5.2.

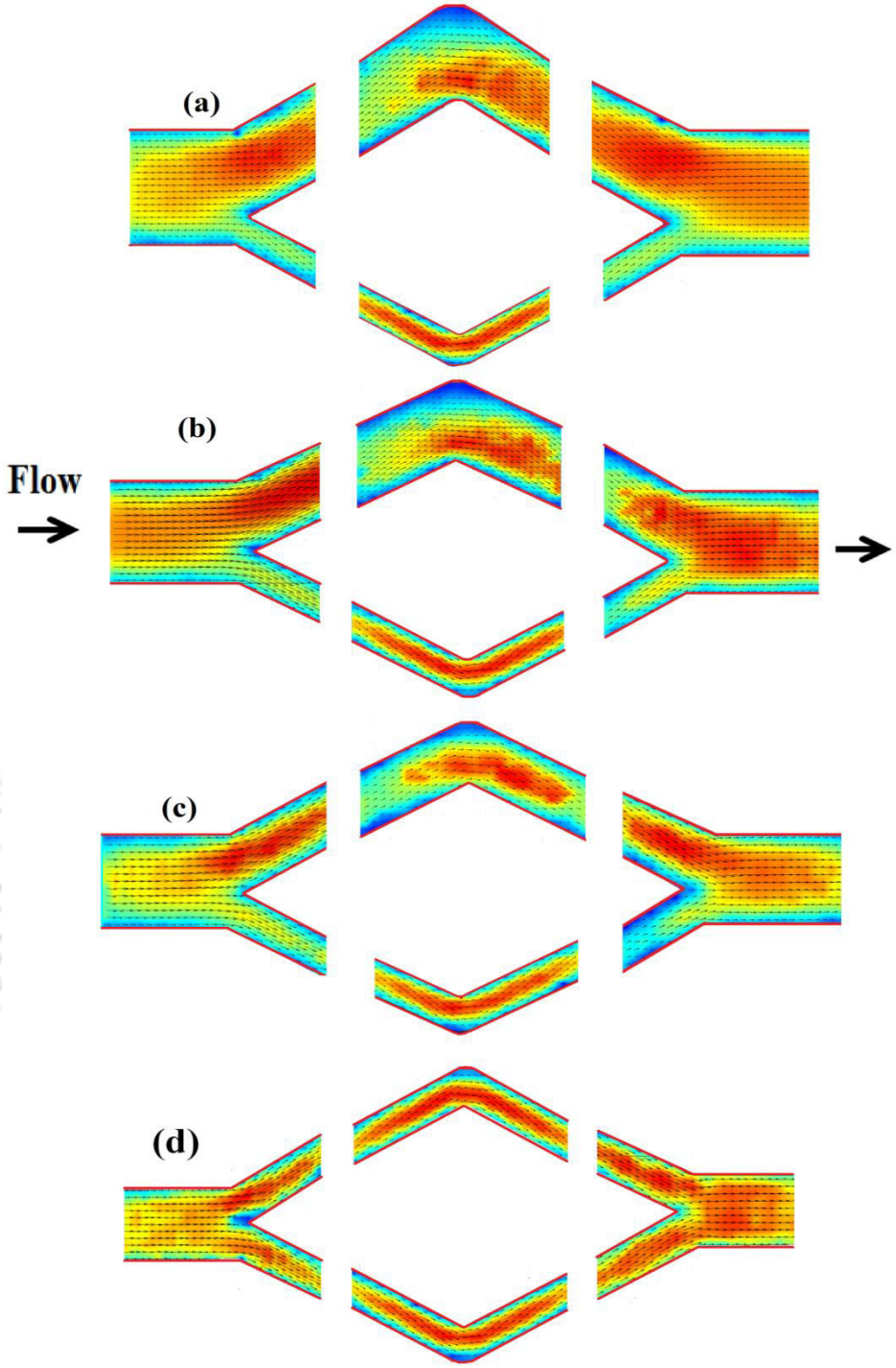

Figure 5.2. Velocity vector map of suspending fluid phase for 10µm suspension in the different diverging-converging channels of equal right daughter branch width (200µm) and varying left daughter branch width (a) 500µm (b) 400µm (c) 300µm (d) 200µm respectively.

From the velocity vector map, we have observed that in both the daughter branches of the diverging-converging channels, the velocity magnitude is high in the region where the flow takes sharp turn and changes its direction from diverging to converging. So, increase in velocity is primarily due to the geometry effect. Moreover, the length of the daughter branch in the

diverging section is short for the velocity and concentration profile to get fully developed. The particle in the diverging branch already migrated towards the inner wall and continue to move along the inner wall. Before the particles completely migrate to the center of the channel, they again faces a sharp turn at the meeting point of converging and diverging section. This sharp turn increases the velocity of the suspension and in the vector map we notice high velocity region. This can be related with the inhomogeneity of particle distribution, and there is no significant effect of inertial forces

5.3 Results and Discussion

5.3.1 Velocity field

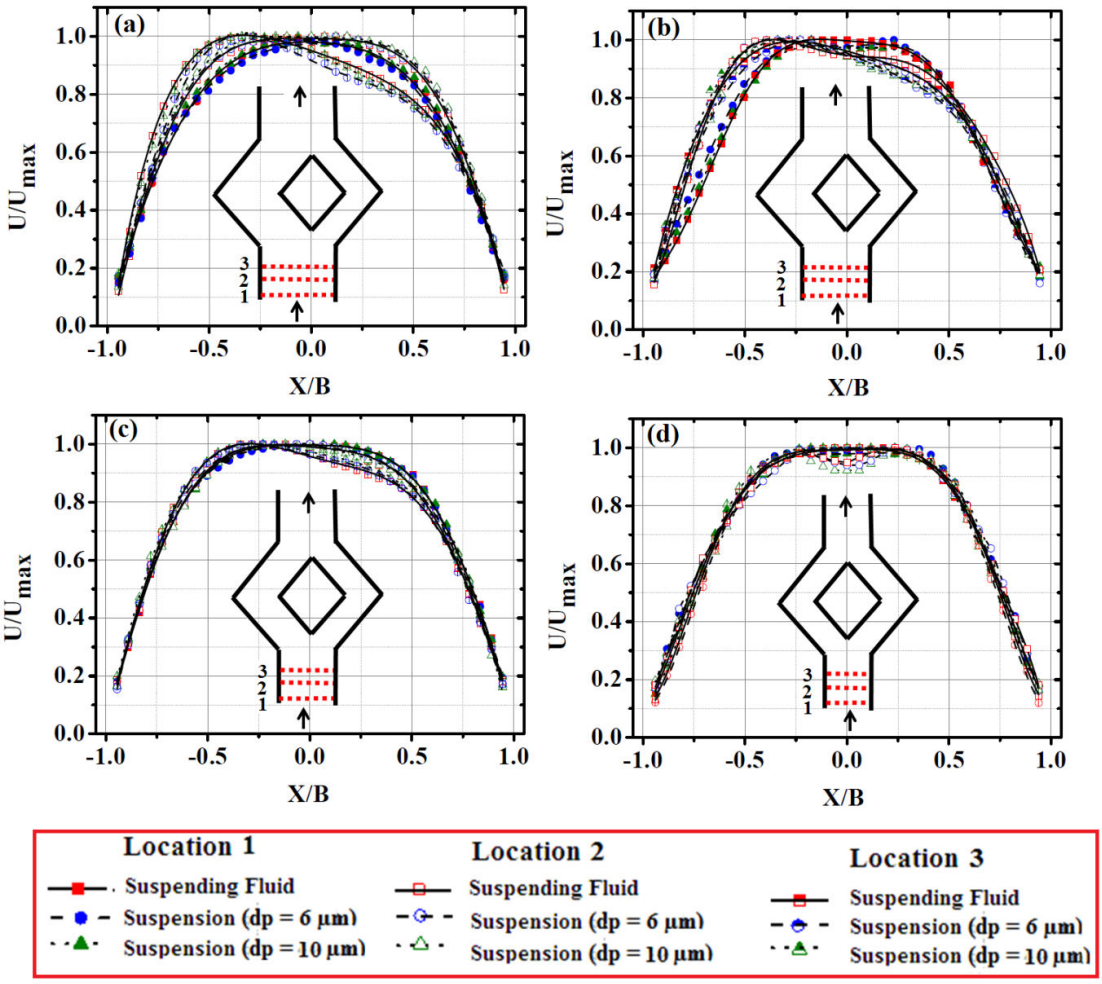

Figure 5.3. Velocity profiles in the inlet branch at location 1, location 2 and location 3 of diverging-converging channels of equal right daughter branch width (200µm) and varying left daughter branch width (a) 500µm (b) 400µm (c) 300µm (d) 200µm respectively.

The mean velocity profiles for pure suspending fluid and suspensions of two different particle sizes (6 and 10 μm) at various locations in the inlet section (locations 1, 2 and 3) are plotted in Figure 5.3.

The velocity magnitude (U) is normalized relative to the maximum velocity (Umax) for each case. At location 1 velocity profiles are blunted in all the channels, which indicate that flow is fully developed before location 1. It was observed that at location 2, the velocity profiles become asymmetric and it shifted towards the left branch which further increases in Location 3. This observation was made for all the three bifurcation channels except Figure 5.3 (d).This is obvious as left daughter branches have a higher opening for the flow compared to right daughter branch. It should be noted that the width of the right daughter branch in all the channels was the same. The shifting is more for channel having 500μm width in left daughter branch and it gradually decreases with reducing width. In 200 μm channel, we can observe a formation of peak-valley-peak profile at location 3.

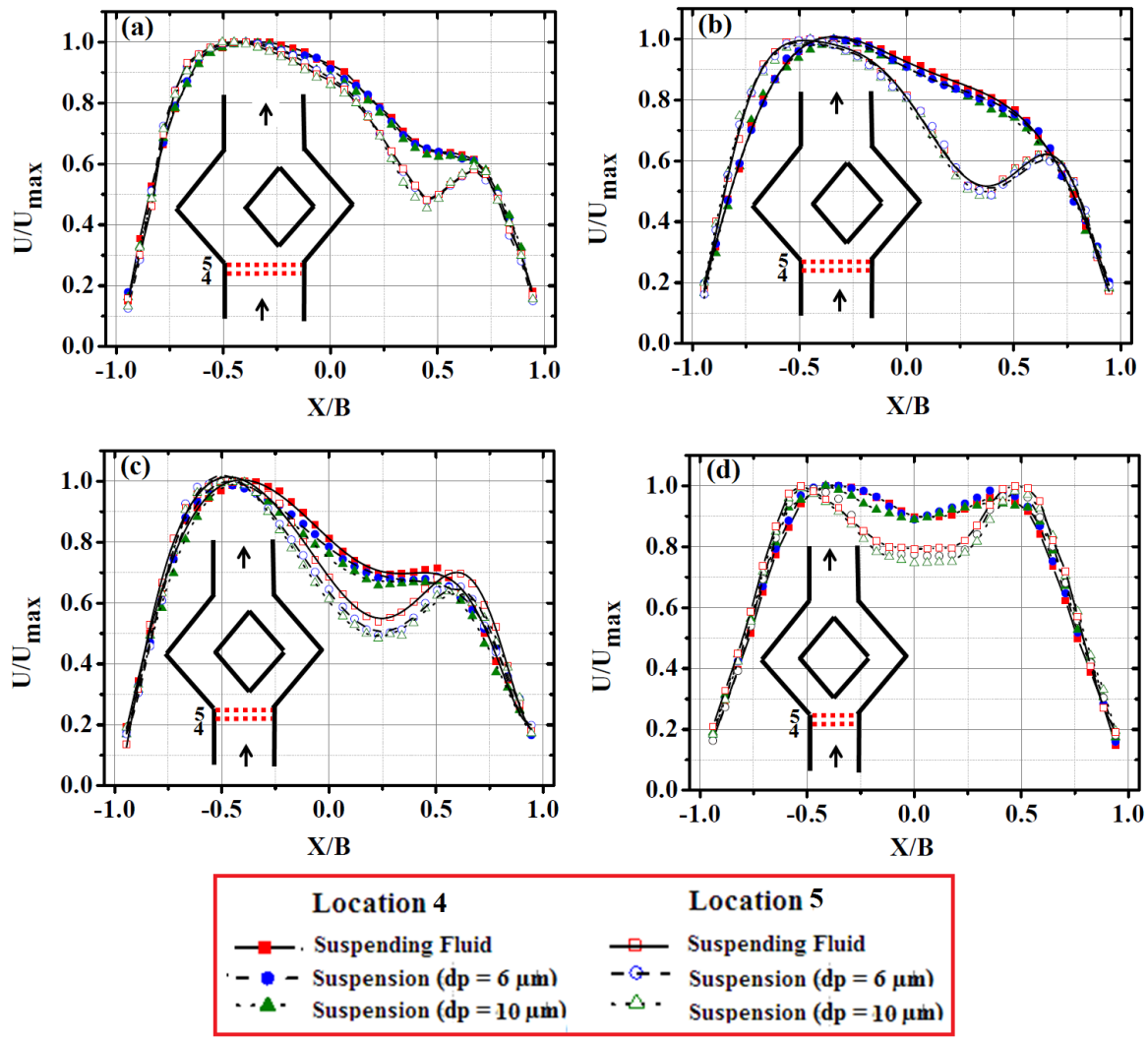

Figure. 5.4. Velocity profiles in the inlet branch at location 4 and location 5 of diverging-converging channels of equal right daughter branch width (200µm) and varying left daughter branch width (a) 500µm (b) 400µm (c) 300µm (d) 200µm respectively.

Figure 5.4 shows the comparative velocity profiles of Newtonian fluid with suspensions at a location which is 5 mm ahead of bifurcation (Location 4) and at the bifurcation point (Location 5) of diverging-converging channels. It was observed that at this location velocity profile skewed towards left branch and profile become highly asymmetric. The shifting of profiles towards the left side direction is due to the fact that this location is very near to the bifurcation section. A shifting peak-valley-peak profile was noticeable at this location and profile become sharp at location 5 as flow divides unequally at this location. With the decrease of width of left daughter branch sharpness in the dip of peak-valley-peak profile

reduces and peak-valley-peak pattern become symmetric in channel having equal width daughter branches.

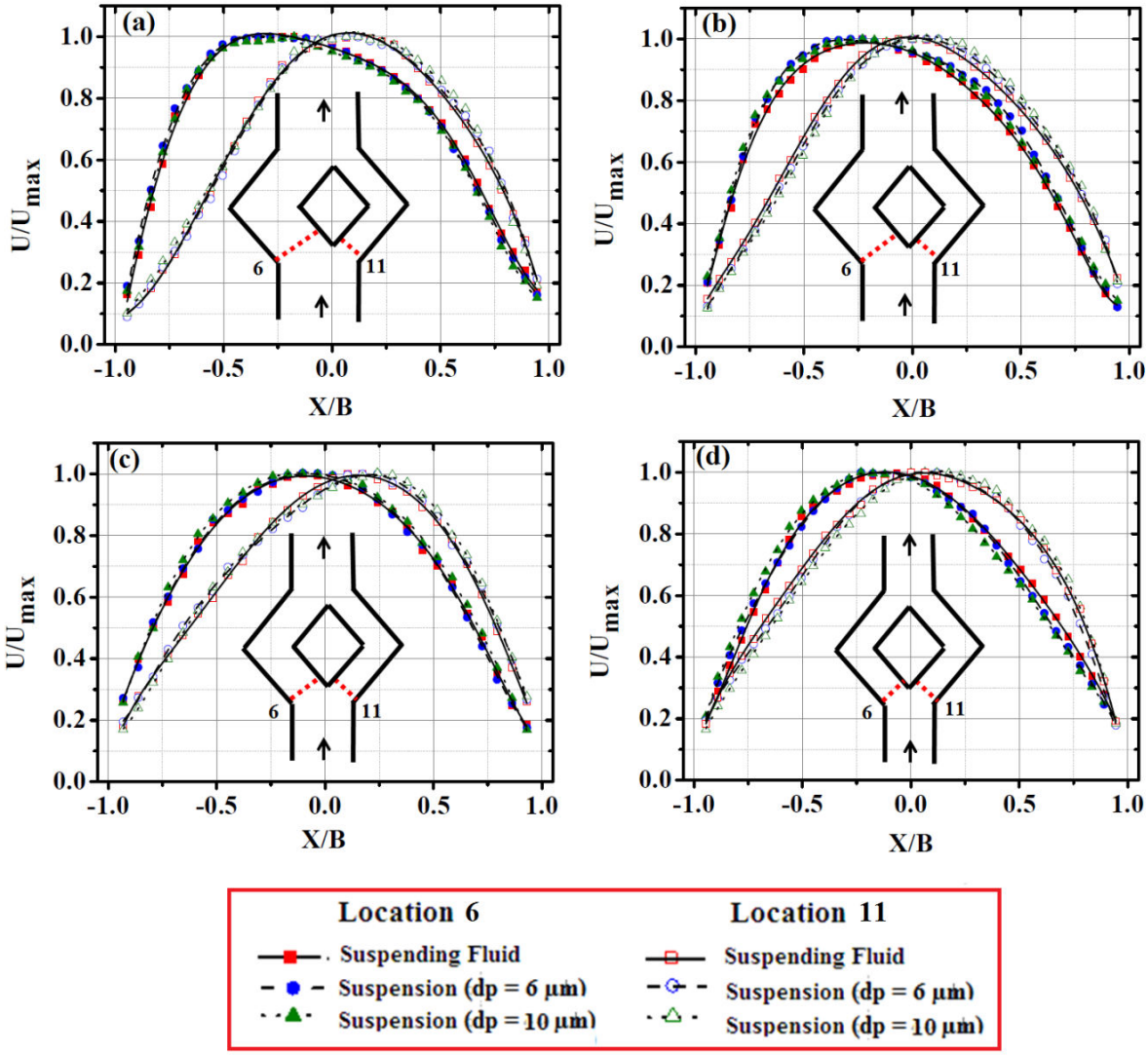

Figure 5.5. Velocity profiles of Newtonian fluid with suspensions at location 6 (left daughter branch) and at location 11 (right daughter branch) of the diverging-converging channels of equal right daughter branch width (200)µm and varying left daughter branch width (a) 500µm (b) 400µm (c) 300µm (d) 200µm respectively.

After the bifurcation, the flow enters into the daughter branches. Figure 5.5 shows velocity profiles of Newtonian fluid with suspensions at location 6 (left daughter branch) and at location 11 (right daughter branch). For all the channels we have observed shifting of velocity profile towards the outer wall direction. Shifting of the profile in the left branch is

more for the channel having higher width than the other channels. Moreover shifting of profiles in left daughter branches decreases with the decrease of width.

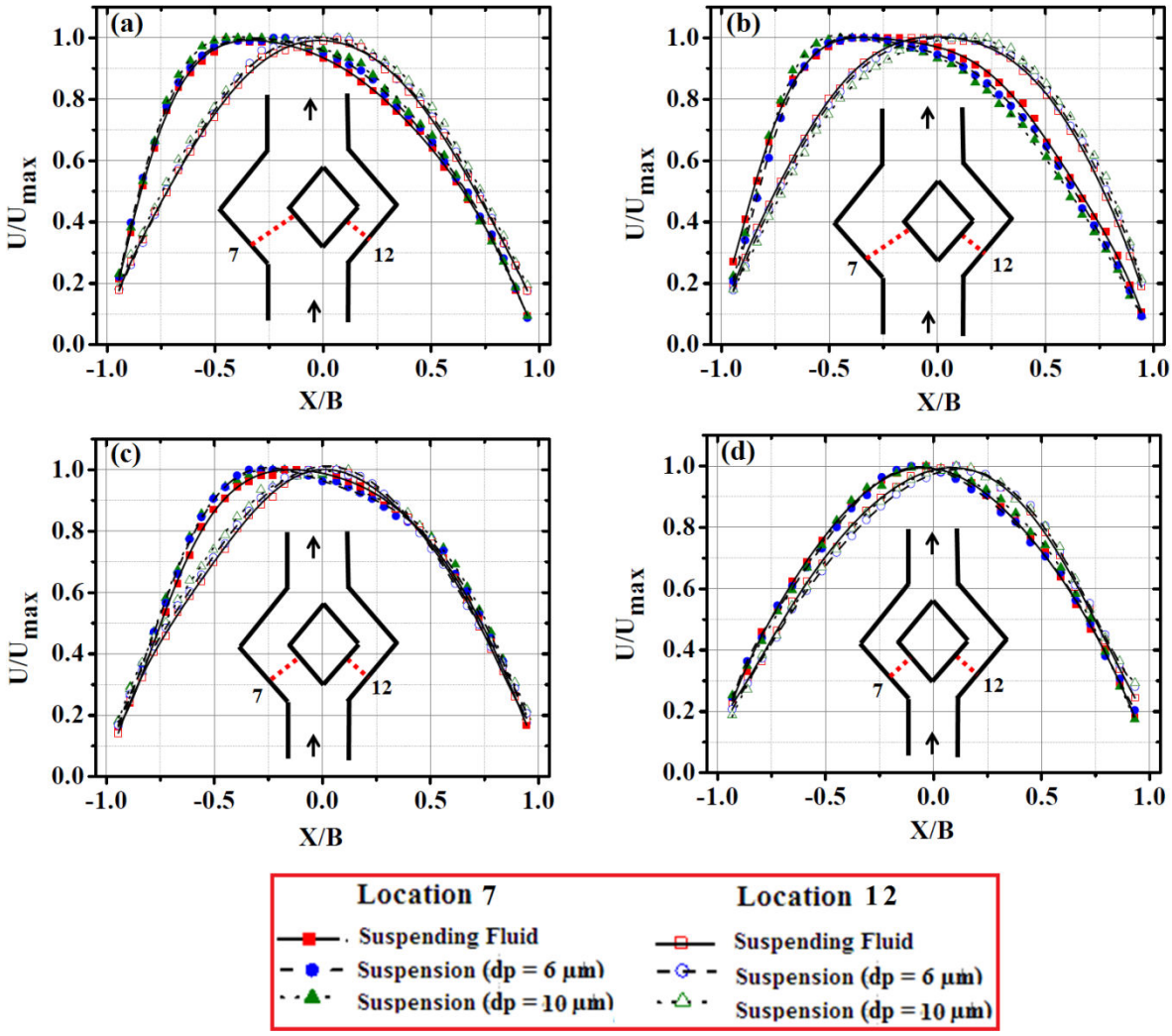

Figure 5.6. Velocity profiles of Newtonian fluid with suspensions at location 7 (left daughter branch) and at location 12 (right daughter branch) of the diverging-converging channels of equal right daughter branch width (200µm) and varying left daughter branch width (a) 500µm (b) 400µm (c) 300µm (d) 200µm respectively.

Velocity profiles at the middle of daughter branches for diverging flow shown in Figure 5.6. It was observed that the skewness in velocity profile persists in the left branch but the profiles become nearly symmetric and parabolic in the right branch.

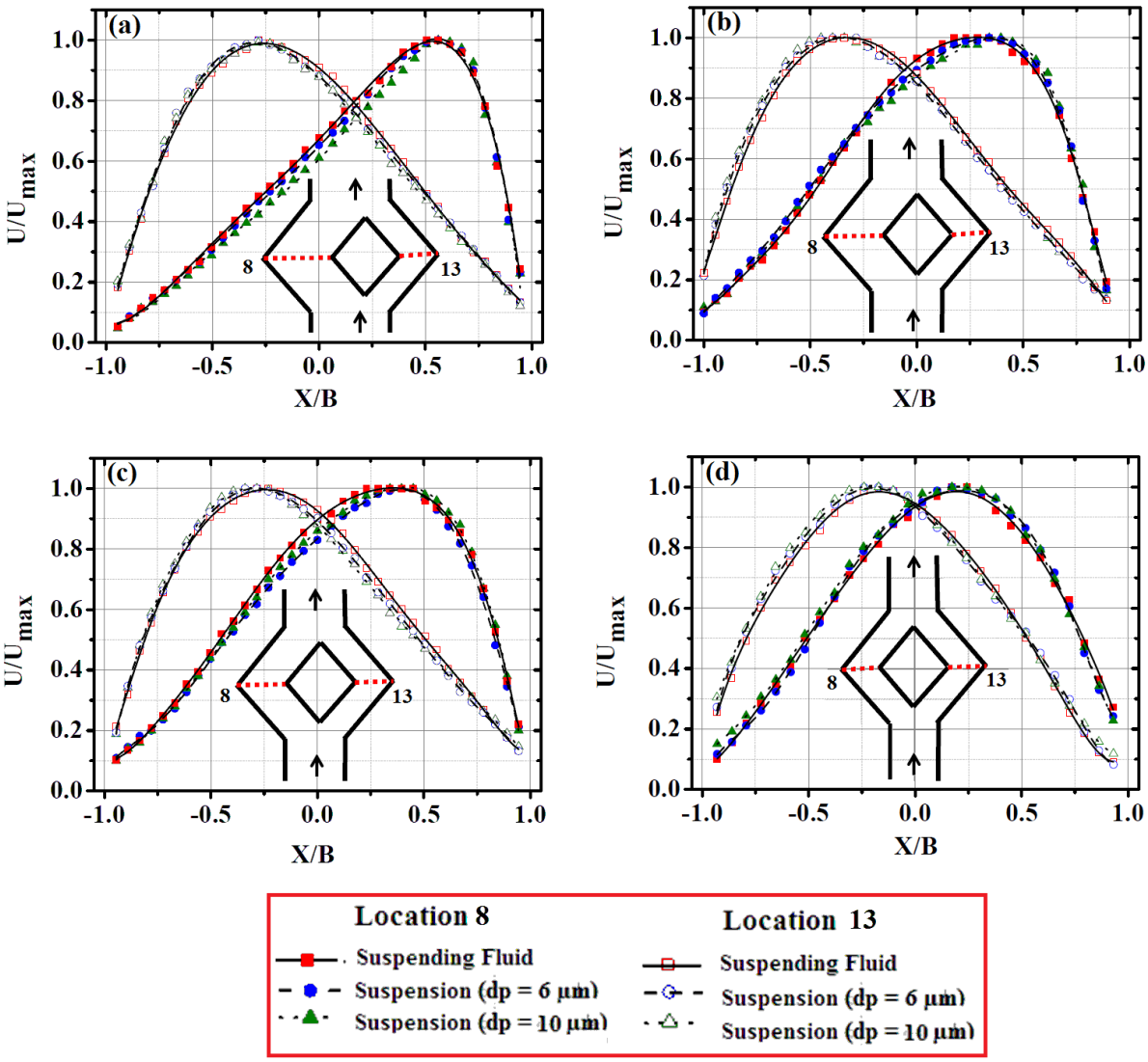

Figure 5.7. Velocity profiles at the end of diverging section and beginning of converging section at location 8 (left daughter branch) and at location 13 (right daughter branch) of the diverging-converging channels of equal right daughter branch width (200µm) and varying left daughter branch width (a) 500µm (b) 400µm (c) 300µm (d) 200µm respectively.

The locations 8 and 13 are the end position for diverging flow and beginning of converging flow. In both the daughter branches crests in velocity profiles are shifted towards the converging section. Here flow changes its direction in both the locations. As obvious tilting of velocity profiles are sharper in the channel having higher width than the other channels. Shifting of profile was more for suspension flow compared to the Newtonian fluid. It was also observed that in all the test channels, with the increase of dispersed particle diameter the shifting of velocity profile towards the downward direction is higher. It was detected that in

Figure 5.7 (c), (d) velocity profile at location 8 in the left branch is almost mirror image of location 13 in the right branch.

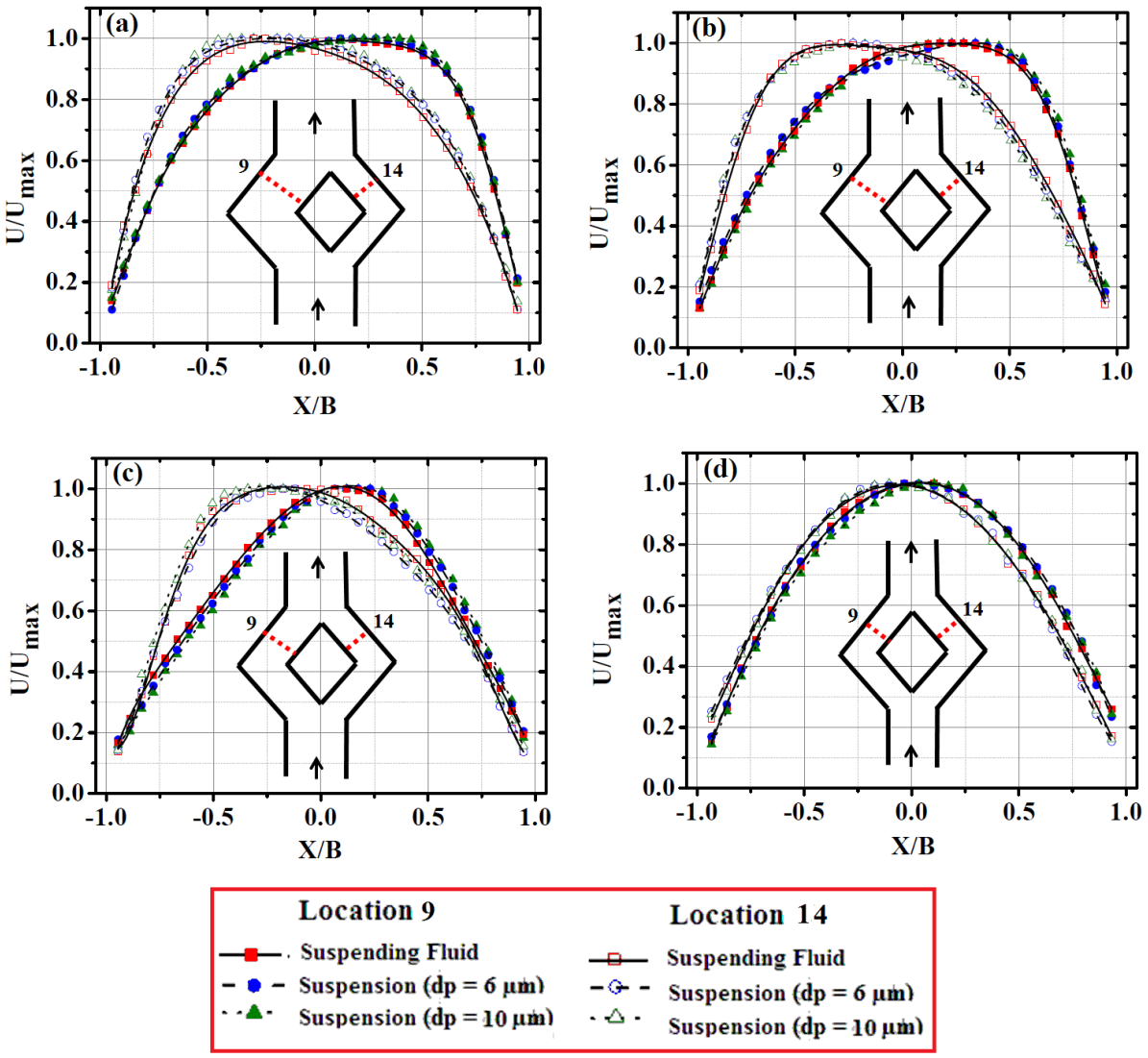

Figure 5.8. Velocity profiles at the location 9 (left daughter branch) and at location 14 (right daughter branch) of the diverging-converging channels of equal right daughter branch width (200µm) and varying left daughter branch width (a) 500µm (b) 400µm (c) 300µm (d) 200µm respectively.

Velocity profiles at the locations 9 and 14 shown in Figure 5.8. In both the locations asymmetry in velocity profile decreases compared to previous locations (Figure 5.7) and profiles tries to shifted towards centre. Shifting in profiles is more in first two channels and it reduces with decrease in width.

The velocity profiles at the end of converging section, location 10 in left branch and location 15 in the right branch are shown in Figure 5.9. At these locations profiles in both the daughter branches shifted towards the confluence of two streams. Moreover, shifting of profiles decreases with decrease of width. Profiles were faintly asymmetric for the 200µm equal width channel Figure 5.9 (d).

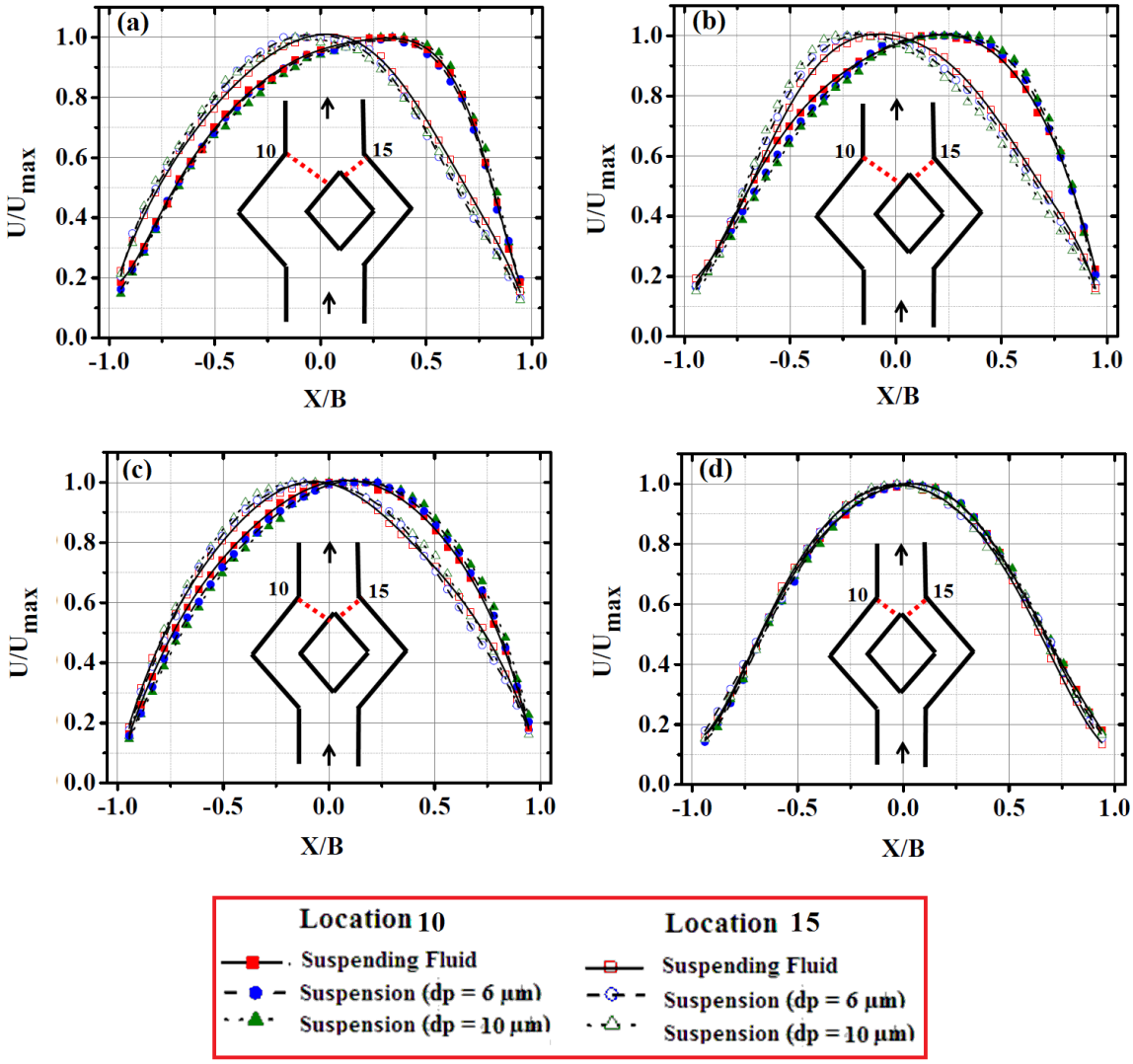

Figure 5.9. Velocity profiles at the end of diverging section and beginning of converging section at location 10 (left daughter branch) and at location 15 (right daughter branch) of the diverging-converging channels of equal right daughter branch width(200)µm and varying left daughter branch width (a) 500µm (b) 400µm (c) 300µm (d) 200µm respectively.

Figure 5.10 shows the comparative velocity plot at the confluence of flow streams (location 16) and at the outlet section (location 17, location 18 and location 19). It was observed that at

the confluence of flow streams (location16) velocity profile skewed towards left branch and profile become highly asymmetric for all three channels having unequal width Figure 5.10(a), (b) (c).

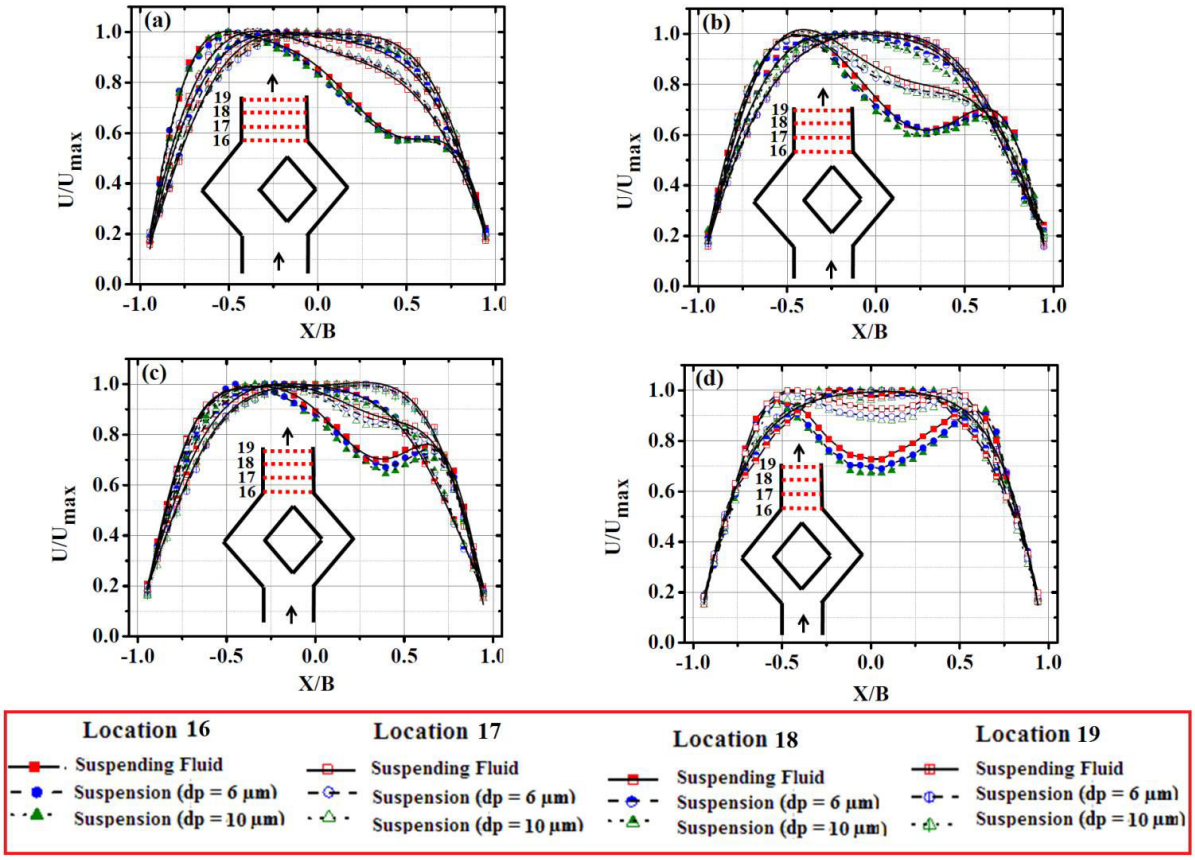

Figure 5.10. Velocity profiles at the junction point (location 16) and the outlet section, location 17, location 18 and location 19 of the diverging-converging channels of equal right daughter branch width (200µm) and varying left daughter branch width (a) 500µm (b) 400µm (c) 300µm (d) 200µm respectively.

The shifting of profiles towards the left direction is due to higher opening in the left branch compared to right branch results more flow coming towards the junction trough left branch and pulling the total outlet flow towards left side. For the 200µm equal width channel we observed symmetric peak-valley-peak profile. This is due to meeting two fluid streams of equal flow rate and equal volume. As we move further downstream locations in the outlet section, both shifting and symmetric peak-valley-peak pattern in the profiles gradually vanishes and only a blunting velocity profile emerges at the last location (location 19).

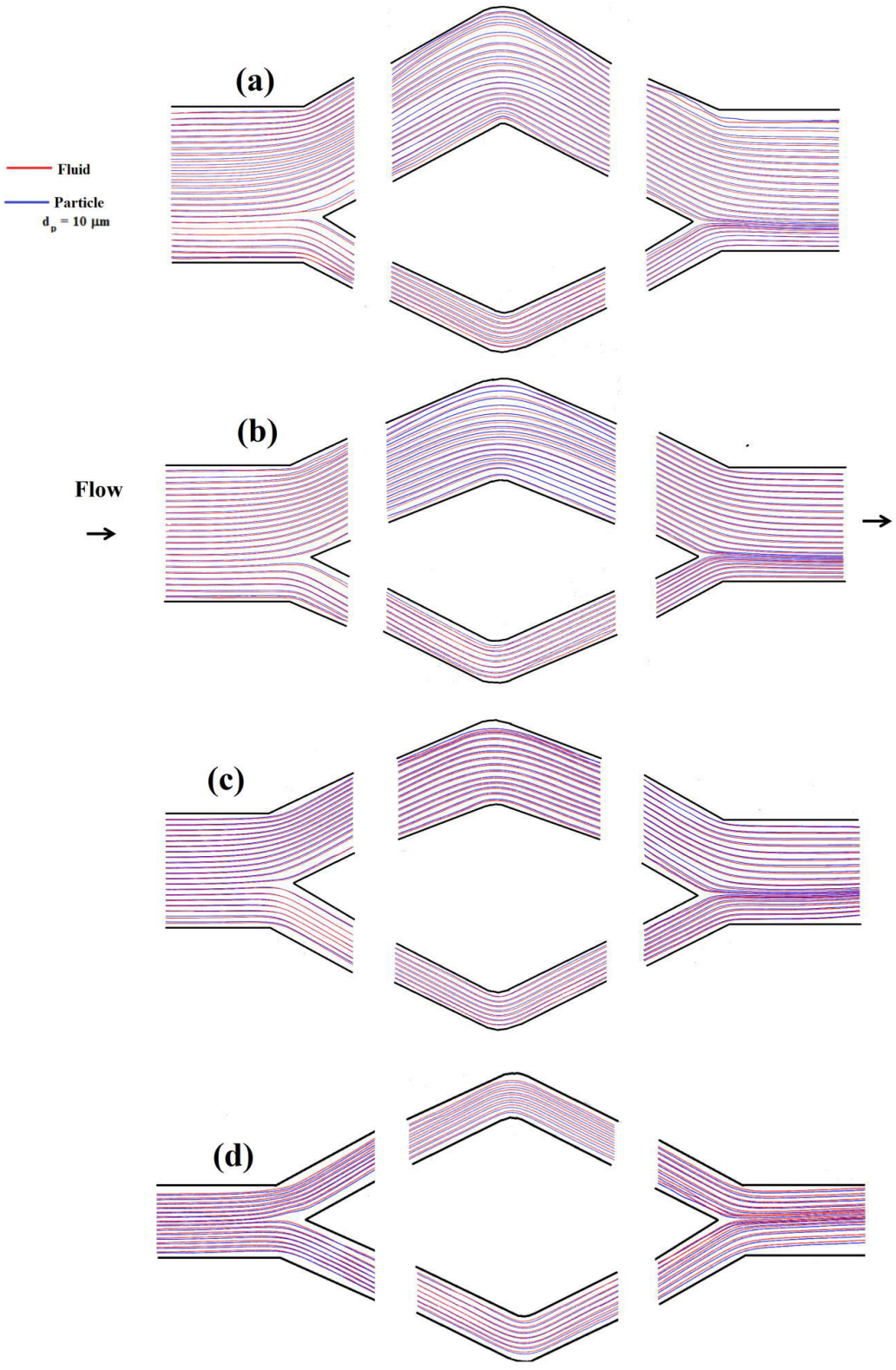

Figure 5.11. Comparison of streamlines of bulk suspension (obtained from PIV analysis of tracer particles) with the suspension particles (10µm) obtained from PTV analysis in diverging-converging channels of equal right daughter branch width (200µm) and varying left daughter branch width (a) 500µm (b) 400µm (c) 300µm (d) 200µm respectively.

Figure 5.11 shows the streamlines in all the diverging - converging channels for suspending fluid and particle having a diameter of 10μm. Construction of streamlines from the horizontal velocity fields of PIV and PTV analysis was same as discussed in Chapter 3. The streamlines shown in red color are for the carrier fluid and the blue lines are the streamlines obtained from the particle phase velocity. The comparison of the streamlines for the bulk flow and the particles showed significant deviation near the bifurcation region for the diverging section and near the confluence region for the converging section for all the channel. The deviation is slightly less for 200μm equal width channel than compared to other channels. The region near the end position for diverging flow and beginning of converging flow showing some noticeable deviation. This is because near the bifurcation and confluence particle-particle interaction is more and these interactions perturb the trajectory of particles near the bifurcations resulting dissimilar fluid and particle streamline near the bifurcation.

5.3.2 Particle concentration

Figure 5.12 shows the velocity vector map of 10μm size particle in all the four diverging-converging channels. From the vector map, it was clearly observed that more number of vectors located at the middle of the channel in the inlet section. This is due to shear induce migration phenomena for which particles migrate from the wall to the middle of the channel. After bifurcation point, it can be observed that the particle concentration is relatively higher in the region close to the inner walls of the daughter branches both in the diverging and converging section. This is due to the fact that, in the inlet section particle has already moved to the middle of channel and these particles favour to move closer to the inner wall of the side branches. Finally, particles from the both branches meet at the confluence of converging section and come out from the outlet section. Here we have observed two separated vector stream in the outlet section. This velocity vector map of particle phase qualitatively gave particle concentration over the whole section of diverging-converging channels.

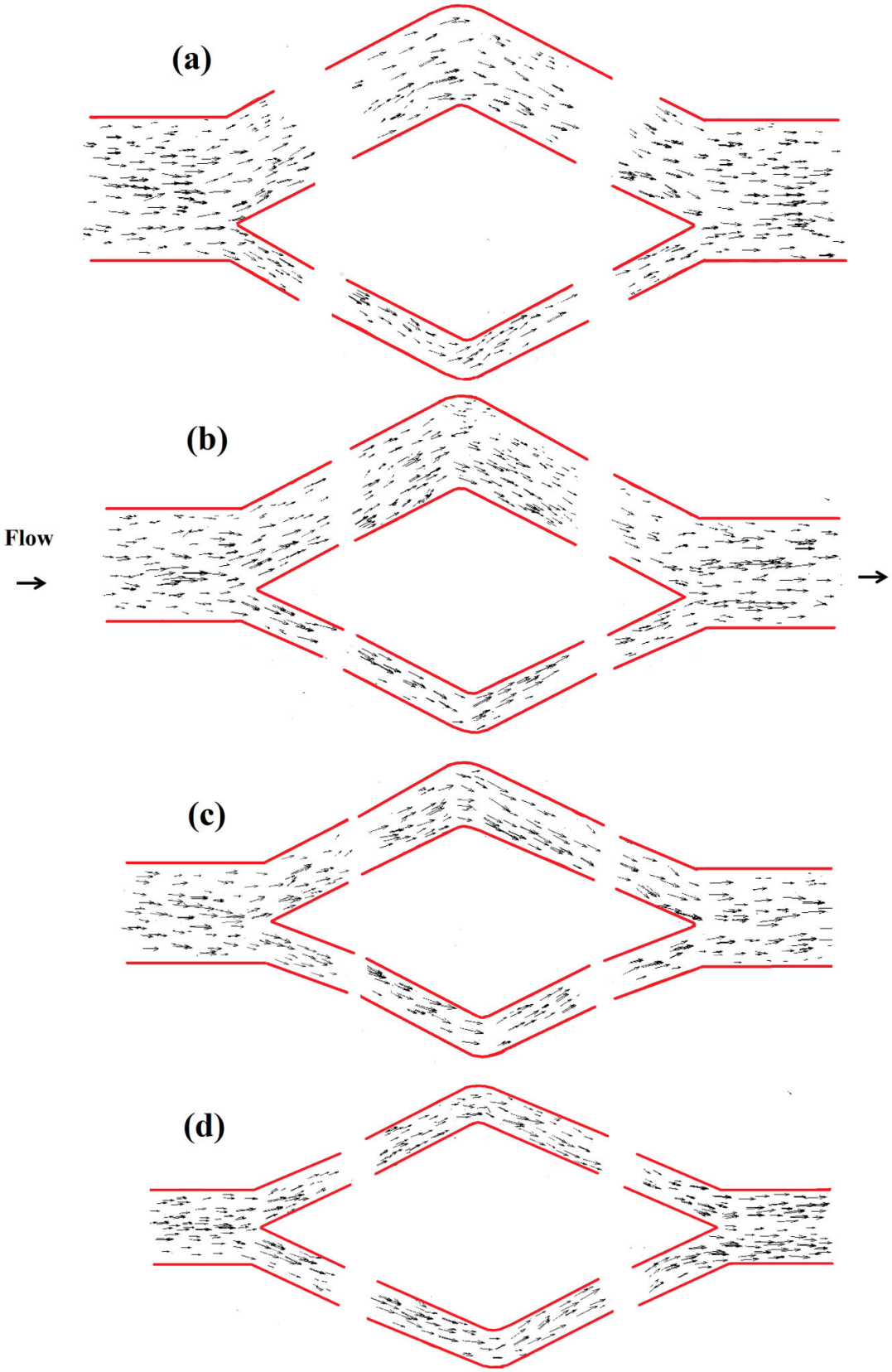

Figure 5.12. Velocity vector map of particle phase (10µm size) in diverging-converging channels of equal right daughter branch width (200µm) and varying left daughter branch width (a) 500µm (b) 400µm (c) 300µm (d) 200µm respectively.

After that, we have qualitatively studied the concentration profile at different locations of all the channels using the Particle counting MATLAB programme. Working Principle of MATLAB Particle counting programme described in the previous chapter (Chapter 3).

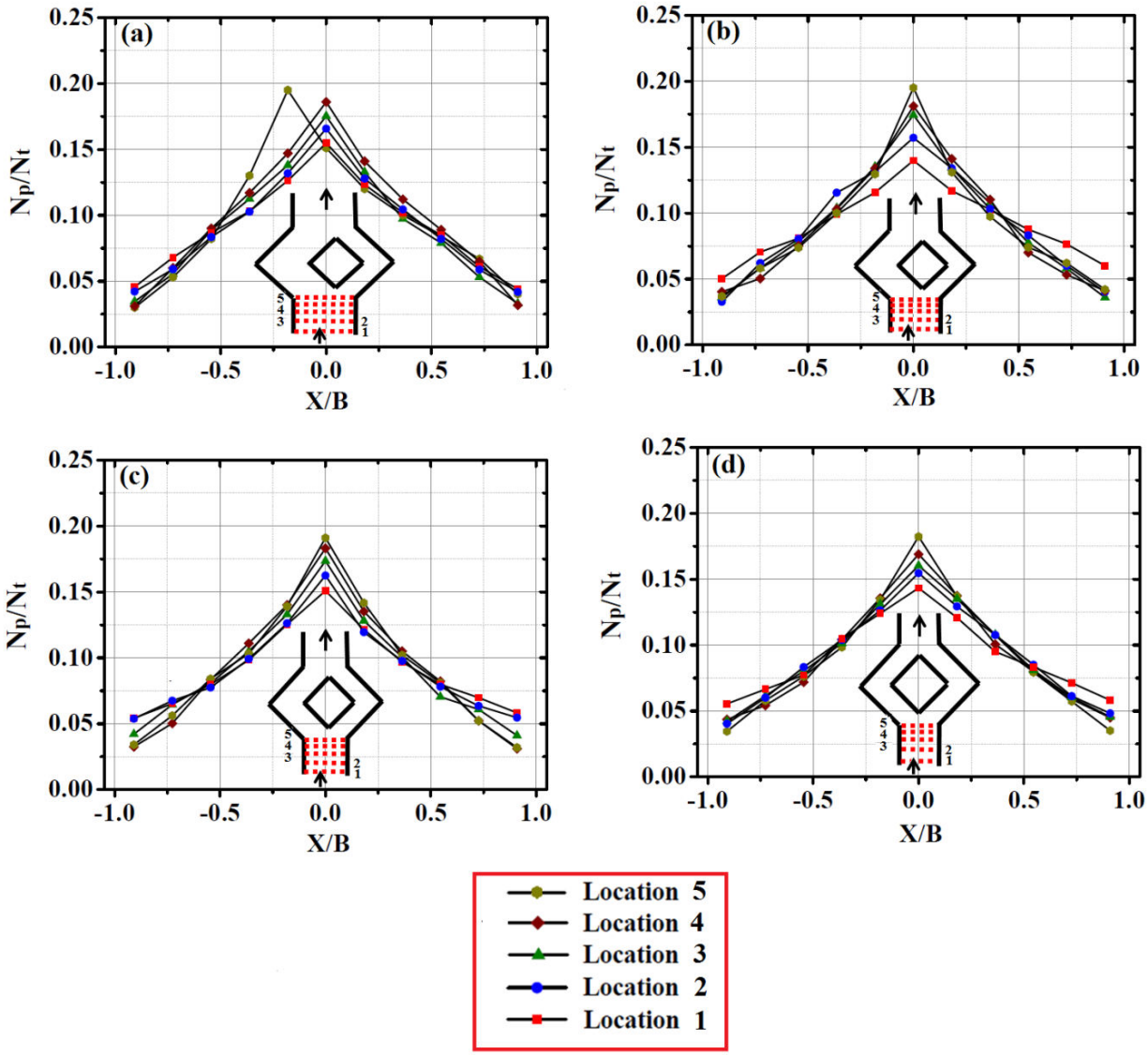

Figure 5.13. Profiles of the particle count in the bins (normalized with the total particle count) in the inlet section (Location 1, location 2, location 3 , Location 4 and Location 5) of diverging-converging channels of equal right daughter branch width(200µm) and varying left daughter branch width (a) 500µm (b) 400µm (c) 300µm (d) 200µm respectively.

The normalized particle count in the inlet section (Location 1, Location 2, Location 3, Location 4 and Location 5) shown in Figure 5.13. Due to shear-induced migration the particles move from walls to the center of the channel, which gives inverted V-shape of the

profile. As we move from location 1 to location 5 the peak concentration also increases in the entire channel. We detected an interesting observation for the channel having 500µm width in left daughter branch that the concentration profile at Location 5 shifted towards the left branch. This might be due to the fact that the opening of the left branch is 2.5 times higher than the right branch and as suspension approaches near the bifurcation flow preferentially move towards the higher opening.

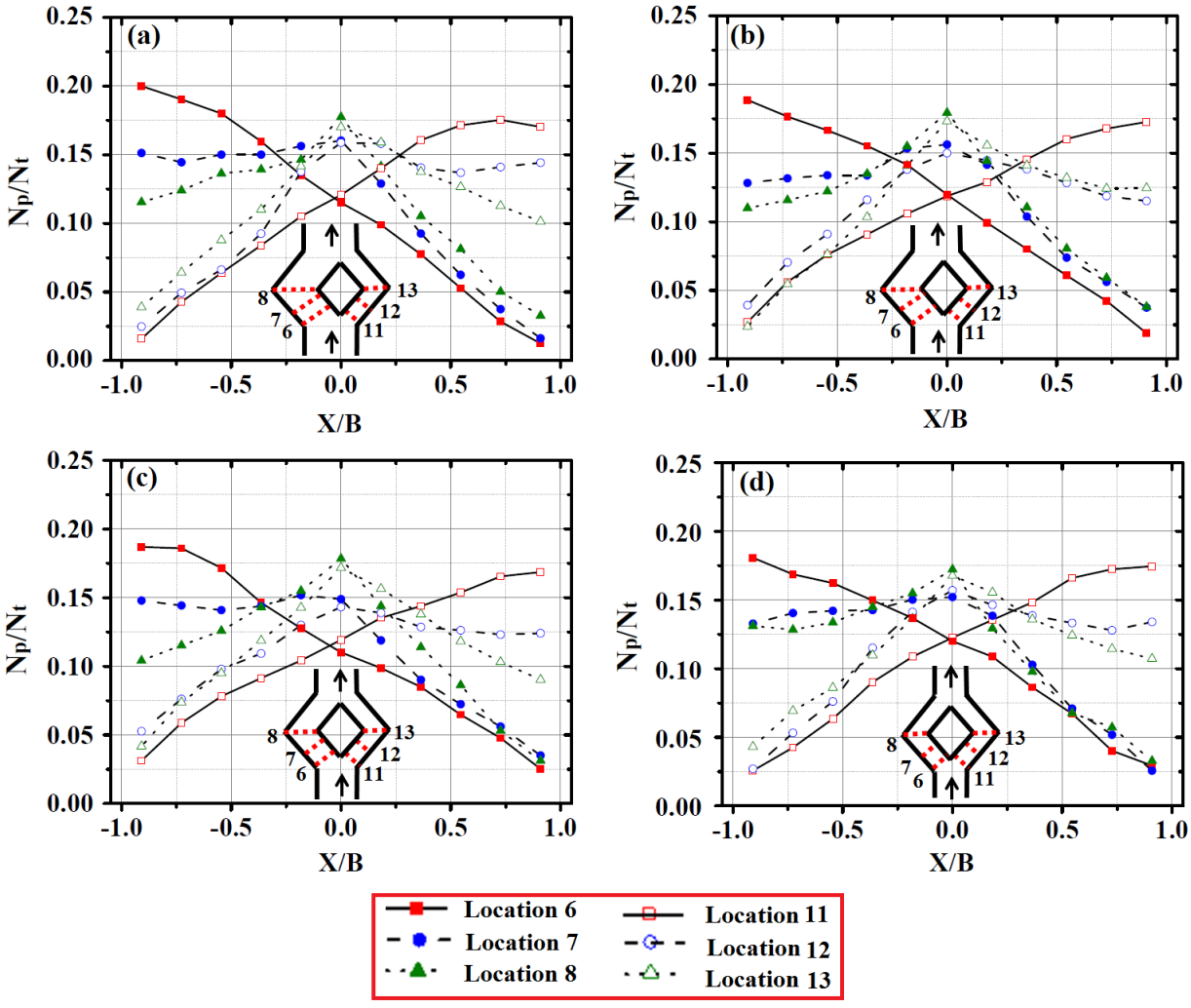

Figure 5.14. Profiles of the particle count in the bins (normalized with the total particle count) in equal width right daughter branch (Location 11, Location 12, Location 13) and at varying width of (a) 500µm (b) 400µm (c) 300µm (d) 200µm in left daughter branch (Location 6, location 7, location 8).

Figure 5.14 showed the normalized particle count in the daughter branches for diverging flow. At location 6 of the left branch and the corresponding location 11 of the right branch, the particle concentration is highest near the inner walls. As we move to downstream locations the particle concentration near the wall gradually decreases and the peak concentration shifts to the middle of the channel. As the flow leaves the diverging section and enters into converging section at location 8 of the left branch and at location 13 of the right branch profiles were still asymmetric. This is due to shorter length of daughter branches in the diverging section for fully developed symmetric profile.

Flow changes its direction in the converging section and profiles at the middle and at the end of converging section is shown in Figure 5.15. In the converging section redistribution of particles and migration towards the middle of daughter branches continue and finally asymmetric profile leaving diverging section become symmetric at location 9 and location 14 in the converging section. We found that at the end of daughter branches in the converging section (location 10 and location 15) the concentration profile shifts towards the downward direction. The shifting of profiles towards the downward direction is due to the fact that this location is very near to the converging section. We have observed that for equal width channel the concentration profile in the daughter branch is identical.

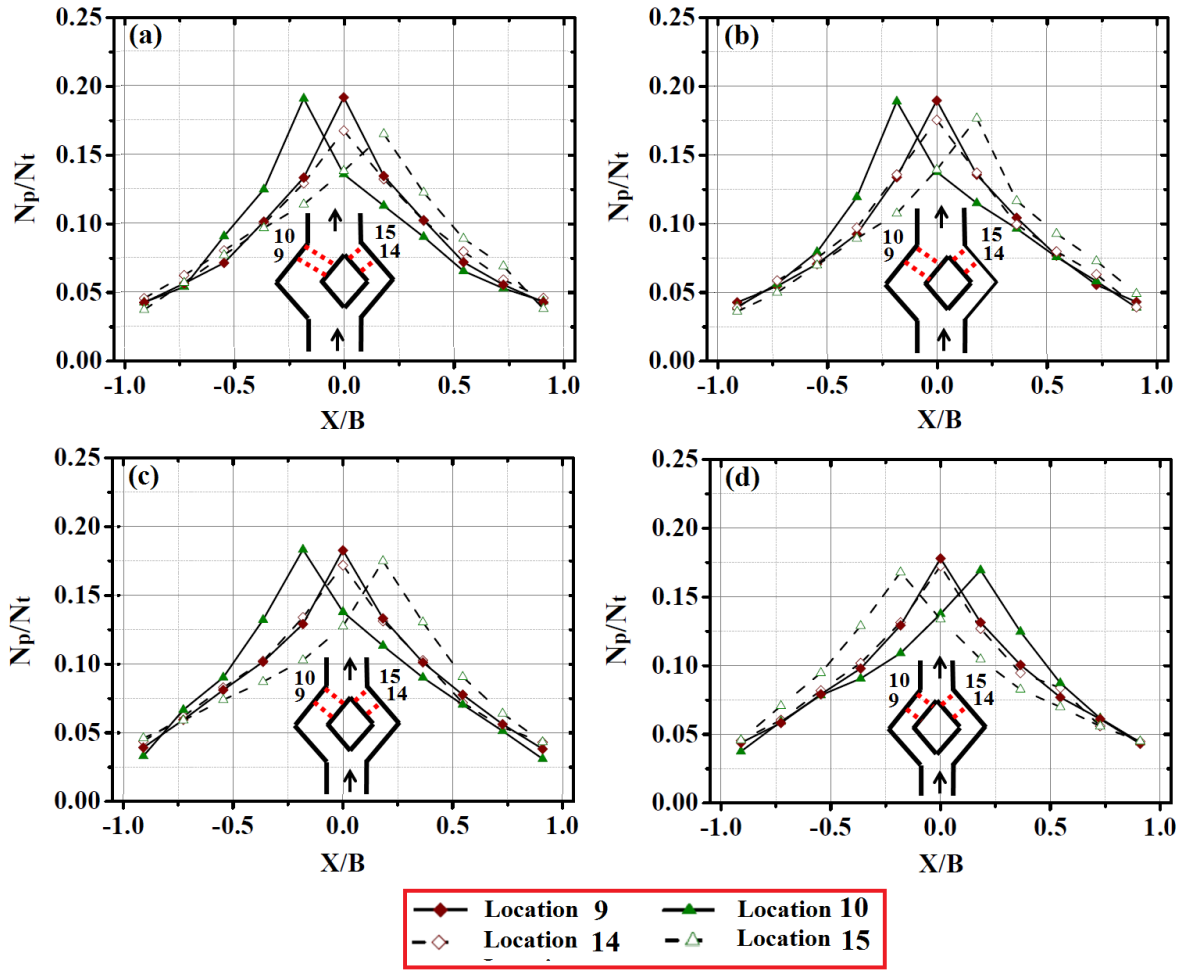

Figure 5.15. Profiles of the particle count in the bins (normalized with the total particle count) in equal width right daughter branch (Location 14, Location 15) and at varying width of (a) 500µm (b) 400µm (c) 300µm (d) 200µm in left daughter branch (Location 9, location 10).

Figure 5.16 shows the concentration profiles at various locations in the outlet section for converging flow. At location 16 and 17 we observe shifting peak-valley-peak pattern in Figure 5.16 (a), (b) and (c) i.e. for channels with dissimilar daughter branch width. This is due to merging of two unequal fluid streams at the confluence. For symmetric width channel, we observed peak-valley-peak in profile at location 16 and 17.As we move further downstream locations in the outlet section, the peak-valley- peak pattern in the concentration profile gradually vanishes and only a single peak in the concentration profile emerges. At location 18 and 19 profiles are fully symmetric and showing maximum concentration at the

center for the channels except for 500µm width channel. Where profile still asymmetric up to location 18 and become single peak symmetric at the end of the outlet (Location 19).

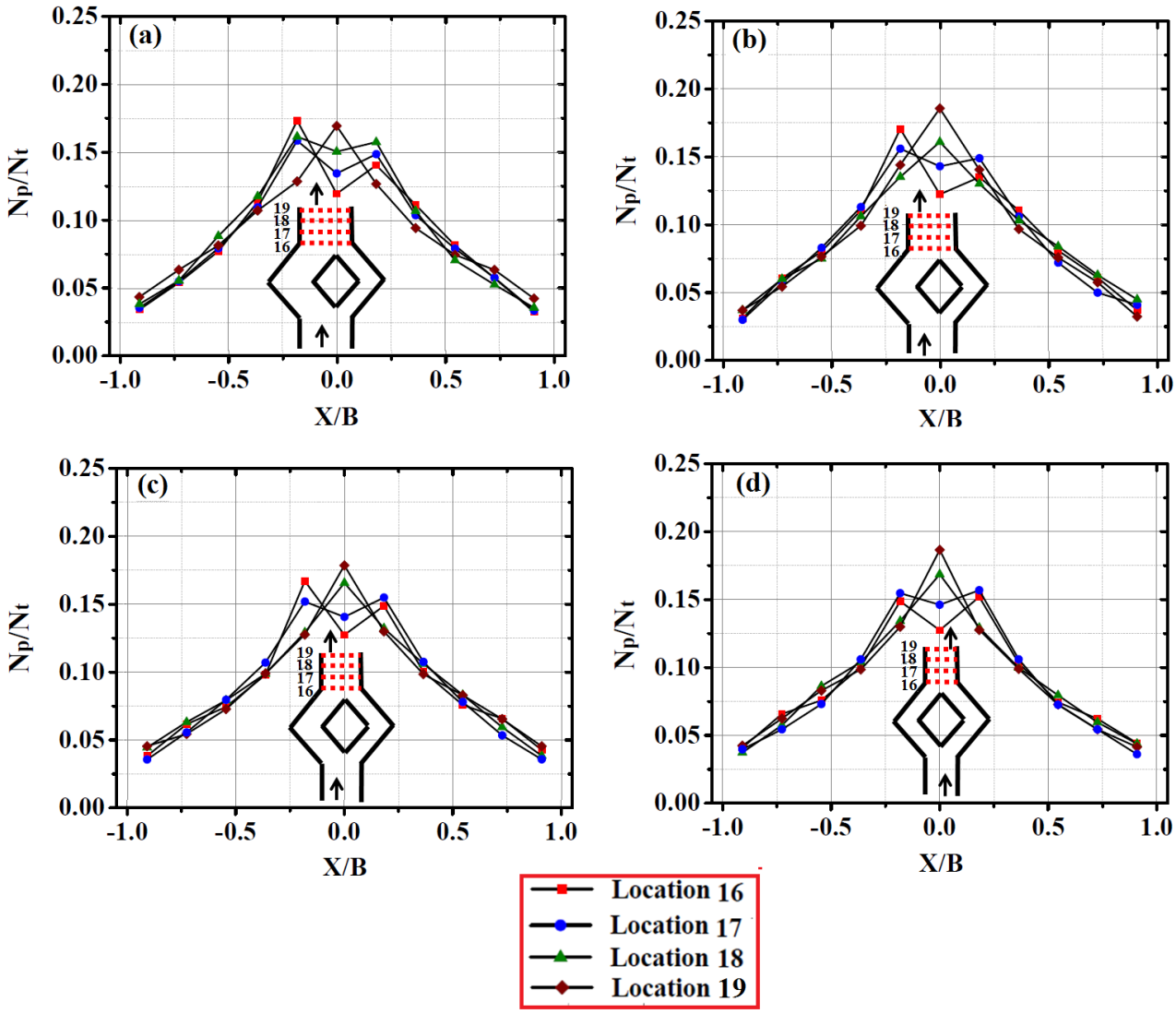

Figure 5.16. Profiles of the particle count in the bins (normalized with the total particle count) in the outlet section (Location 16, location 17, location 18 and Location 19) of diverging-converging channels of equal right daughter branch width (200µm) and varying left daughter branch width (a) 500µm (b) 400µm (c) 300µm (d) 200µm respectively.

5.4 Conclusion

We have performed the micro-PIV experiments for diverging-converging channels of varying width. The width of the left daughter branch was varied keeping right daughter branch constant in all channels. We have observed shifting peak-valley-peak profile at the bifurcation point (location 5). It was observed that for both the daughter branches the crests in velocity profiles are shifted towards the outer wall for the diverging side in contrast to converging flow where profiles are shifted towards inner side. Shifting of the profile was more for the channel with a higher width and reduces with a decrease of channel width. Also shifting of profiles is more for suspension flow in compare to the Newtonian fluid. From the comparison of profiles in outlet sections (location 16-location19), we have observed the shifting peak-valley-peak profile and this is due to combining of two streams in the outlet section. As we move downstream locations in the outlet section, the peak-valley-peak pattern in profiles gradually decreases and only a blunted velocity profile emerges. We have qualitatively studied the concentration profile from PTV analysis vector map and also by using the particle counting MATLAB program. We have noticed the effect of shear induced migration phenomena in distribution of particles across the channels. An interesting observation noted for the channel having 500µm width in left daughter branch that the concentration profile at Location 5 shifted towards the left branch which is due to the highest opening towards left branch intent to move a major portion of the fluid in that branch. At various locations in the outlet section, we observe shifting peak-valley-peak profile up to location 17 for all channels with dissimilar daughter branch width except for 500µm channel where peak-valley-peak profile persist up to location 18. As we move to further downstream locations in the outlet section, the peak-valley- peak pattern in the concentration profile gradually vanishes and only a single peak in the concentration profile emerges. From streamline comparison, we observed dissimilar fluid and particle streamline near the bifurcation and confluence. The region near the end position for diverging flow and beginning of converging flow in the daughter branches shows some noticeable deviation. This is because near the bifurcation and confluence particle-particle collision is more which results deviation

Chapter 6

Micro rheometry using bifurcation channel

6.1 Introduction

In rheometry, flow and deformation of materials being studied under applied forces, which are measured using a rheometer. The measurement of rheological properties is relevant to all material processing industries such as polymer, paints, drilling mud and pharmaceuticals. In addition to this measurement of rheological properties is important in molecular biology blood cell separation, DNA analysis, proteomics, drug delivery etc. Rheological properties can be measured from bulk sample deformation using a mechanical rheometer or on a micro-scale by using a micro capillary viscometer or an optical technique such as Micro rheology. With the recent advances in micro fabrication , microfluidics have prompted the development of novel tools to investigate the rheology of complex fluids.

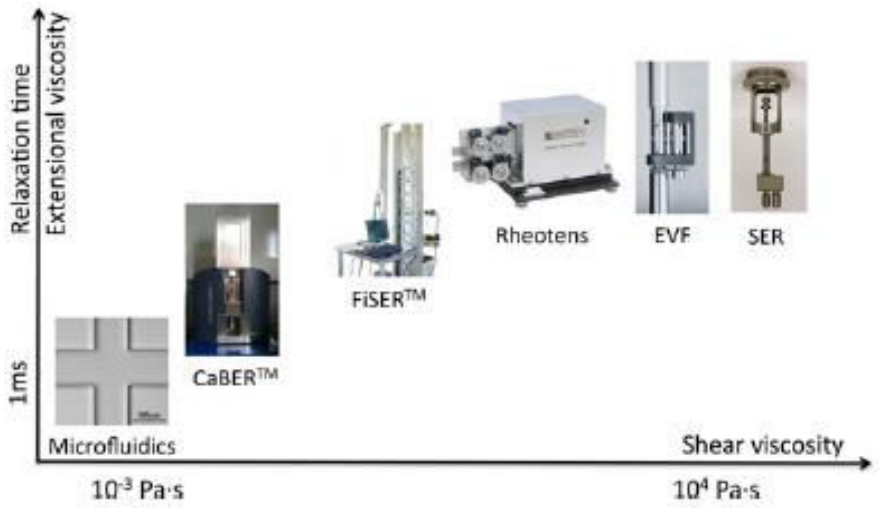

Figure 6.1. Operability diagram of range of viscometer in terms of shear viscosity and extensional viscosity (From Rosales et al., 2013, *Microfluidics and Nanofluidics*, **14**, 1–19. Copyright 2013 by Spinger publishing group).

Figure 6.1 shows operability diagram of range of viscometer in terms of shear viscosity and extensional viscosity. From figure we can observed that with microfluidic rehometry researchers are able to accurately measure the deformation rate up to 0.001 Pa.s which is difficult with the traditional viscometer. The advantages of micro rheometry can be summarize as follows-

Small length scales and geometric confinement

Understanding the rheology of complex fluids at these small length scales is not only fundamentally rich but also important for a wide range of applications including porous media flows, blood flow in capillaries etc. The interaction of fluid forces and these deformable particles under geometric confinement can produce interesting rheological behaviours that are yet to be fully explored. Moreover "Turn in Corner" type microfluidic devices like symmetric T, Y shape can generate a range of share rate in a single experiment.

Access to unique flow regimes

From a viscometry viewpoint, the small length scales of microfluidics provide a suitable means to operate in unique flow regimes, which are difficult to access in macro scale geometries. The small characteristic length scales of microfluidics enable to dominate the viscous forces over inertial forces and generate flows with high deformation rates while keeping the Reynolds number (Re) small. Thus, using microfluidic devices, viscosity data can be obtained at high shear rates without crossing over to turbulent regimes.

Characterization of flow and microstructure

Small size of microfluidic devices and the ability to make them in optically transparent materials has made them a natural fit for local strain rate measurement along with microscopic visualization of change in structure and dynamics of complex fluids, soft particles etc. Recently several studies have integrated micro Particle Imaging Velocimetry for micro rheometry. Degré et. al (2006) use μ-PIV to measure the velocity profiles of non-Newtonian fluid and compute rheology in a straight micro channel. Masselon et.al (2008) use μ-PIV to measure the velocity profiles of semi dilute wormlike micellar systems in a straight micro channel and finally characterize their local rheology. Bandalusena et al. (2009) carried out experimental (μ-PIV) and numerical (FEM) measurement of velocity fields in a

symmetric T-junction for shear-thinning fluid. All the above stated works provide the groundwork toward the development of an inverse optical method to infer the rheological parameters of complex fluid. Overall, the potent capability to concurrently characterize the rheology and structure of complex fluids is becoming one of the main driving forces for using microfluidic devices rather than macroscale rheometric methods.

Technological benefits

Micro devices offer the advantage of consuming fewer samples compared to traditional viscometers. This is especially important for biological fluids like blood, protein ,DNA samples . In microfluidics, it is possible to control the composition of fluids, allowing combinatorial viscometry. For example, microfluidic combinatorial viscometry has been successfully employed for evaluating the intrinsic viscosities of polymer solutions and biofluids by measuring their viscosities over a range of dilutions on a single chip.

There are different microfluidic rheometers reported in literature eg- Pressure sensing rheometers, Flow rate sensing rheometers, Surface-tension rheometers, Co-flowing stream rheometers, Diffusion rheometers .Here we have described principle underlying measurement technique and its methodology of three most common type of micro rheometer.

(a) Velocity type rheometers

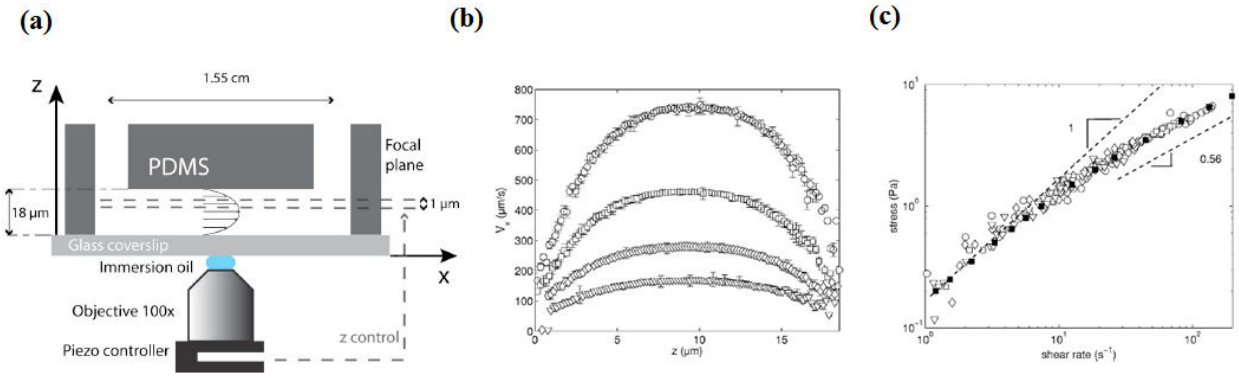

Figure 6.2. Velocimetry based rheometry (a) Experimental set up viscosity measurement of complex fluid using µ-PIV (b) Velocity profile for different pressure drop (c) Shear rate vs. Strain rate for correspondence velocity (From Degre et al., 2006, *Applied Physics Letter*, **89**, 024104.Copyright 2006 AIP Publishing).

Main working principle of a velocity type rheometer is based on measuring the velocity profile for a fluid in a microchannel at a specified pressure drop, Figure. 6.2(a). When the flow field inside the microchannel has been obtained the local shear rate can be estimate from the gradient of the velocity profile as-

$$\gamma = \frac{dv_x}{dz} \qquad (6.1)$$

Here, v_x is the fluid velocity along flow direction and z is the channel height. For a fully developed flow, the local shear stress can be related to the imposed pressure gradient as-

$$\tau = -\frac{\Delta p}{L}(z - z_0) \qquad (6.2)$$

Here, Δp is the applied pressure, L is the micro channel length, and z_0 denotes a reference position which need not to overlap with the mid plane of the micro channel. For every Δz, (horizontal portion) the local shear rate and shear stress can be calculated and plotted [Figure 6.2(c)]. Finally viscosity can be calculated as-

$$\eta = \frac{-\frac{\Delta p}{L}(z - z_0)}{\frac{dv_x}{dz}} \qquad (6.3)$$

(b) Pressure sensing rheometers

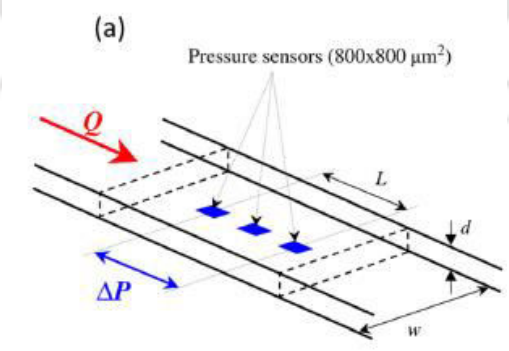

Figure 6.3. Flush-mounted pressure transducers on the floor of the micro rheometer channel (From Baek and Magda ,2003, *Journal of Rheology*, **47**,1249–1260. Copyright 2003 by Society of Rheology).

These kind of viscometers based on pressure sensors involve measuring pressure drop Δp across a straight micro channel for known imposed flow rates (Q).

For Newtonian fluid the equation for viscosity measurement is

$$\eta = \frac{wd^3\Delta P}{\left[2LkQ(1+\frac{z}{w})\right]}$$

Where ΔP is the applied pressure drop, w is the width of micro channel, z is the channel height, Q is the flow rate, k is the numerical factor and its value is 6 for $\frac{z}{w} \leq 1$ and 14.3 for $\frac{z}{w} \geq 1$, L length of sensor area.

For non Newtonian fluid viscosity can be measured by using Weissenberg-Rabiowitsch equation

$$\eta = \frac{\left[2+\frac{d(\ln Q)}{z(\ln \Delta p)}\right]}{3}$$

Measurement of pressure in microfluidic channels can be done by three different ways: (i) inserting flush-mounted pressure transducers on the floor of the micro channel [Figure. 6.3(a)] (ii) oblique tapping into the micro channel and (iii) mounting an external pressure sensor at the upstream of the channel. Out of these three flush-mounted pressure transducers are widely used due to its commercial availability (www.rheosense.com) over a wide range of viscosities and high shear rates (80 000 s^{-1}).

(c) Co-flowing stream rheometers

In this type shear viscosity of complex fluids measured by flowing two laminar fluids through the daughter branches in a Y-shaped micro channel (Figure 6.4).

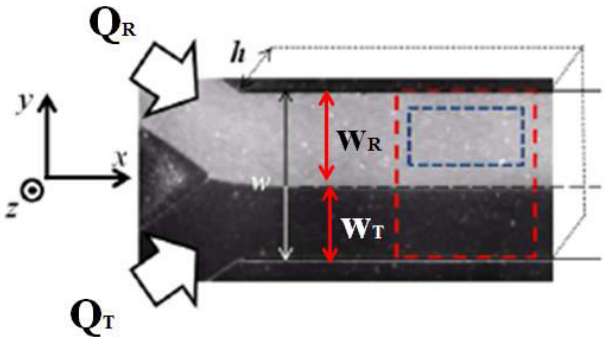

Figure 6.4. Time averaged image of co-flowing stream rheometer (From Gachelin et al., 2013, *Physical Review Letters*, **110**, 268103. Copyright 2013 by American Physical Society).

The basic principle in co-flowing stream viscometer includes flowing a fluid of known viscosity (reference fluid) though one daughter branch and fluid of unknown viscosity (test fluid) through the other daughter branch. By recording the position of the fluid-fluid interface between the two streams in the test region for a range of pumping flow rates (Q), the viscosity curve for a complex fluid can be determined. Governing equation for calculating the viscosity is given by

$$\frac{\mu_T}{\mu_R} = \frac{Q_R w_T}{Q_T w_R} \tag{6.6}$$

Where the subscripts T and R refer to the test and reference fluids, respectively. w_R and w_T is the fraction of the channel width occupied by reference and test fluid.

The significance of the current work comes from the above cited works and also some recent studies in measurent rheological properties in bifurcation T and Y shape geometry. Zimmerman et al. (2006) carried out finite element simulations for non -Newtonian fluid in symmetric T-junction and reported viscosity from the measured pressure profile. In Gachelin et al. (2013) viscosity of an active suspension of E-coli bacteria is determined experimentally as a function of the shear rate using a Y-shaped microfluidic channel. Guillot et. al (2007) experimentally determined the viscosity of Newtonian and non Newtonian fluid as a function of the shear rate using a symmetric T-shaped microfluidic channel. As per our knowledge there is no reported study on micro rheology using μ-PIV technique for neutrally buoyant suspension in symmetric bifurcation channel. More over there is no reported work on Y-

shape bifurcation for diverging flow. To know the effect of bifurcation angle and particle size on rheological measurements we have conducted experiments in symmetric T, Y shape bifurcation channel for pure suspending fluid and suspensions of two different particle sizes (6 and 10 μm) at six different locations. Our approach of viscosity measurement is similar to velocity type rheometer. The purpose of this work is to develop an efficient "Turn in Corner" type rheometer for complex fluids. Moreover it will provide fidelity for development of online monitoring and measurement of rheological properties.

6.2 Experimental Procedure

Schematic diagram of our experimental setup is same as Chapter 3. Schematic of bifurcation channels used in our experiment is shown in Figure 6.5

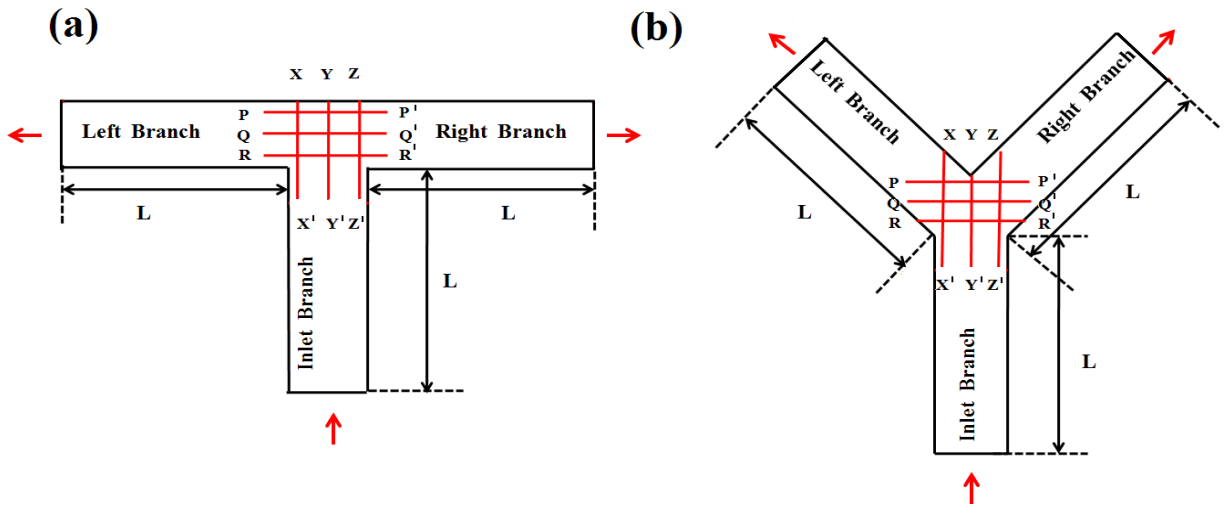

Figure 6.5. Schematic diagram of bifurcation channels used in our experiment.

The locations at which profiles were evaluated are also shown in the images. The width of daughter branches (500 μm) in all the channels was same as that of the parent branch. The volume fraction of dispersed particle (ϕ) was 0.05 in all the experiments. The relative lengths of different sections (parent branch and daughter branches) were taken to be equal (L=7 cm). Velocity vector map of suspending fluid phase for 10μm suspension in the T and Y bifurcation channel shown in Figure 6.6. From vector map we can notice that there is minimum velocity at the upper side of symmetry line (YY`) and its neighbour area. This is due to presence of stagnation point in that region.

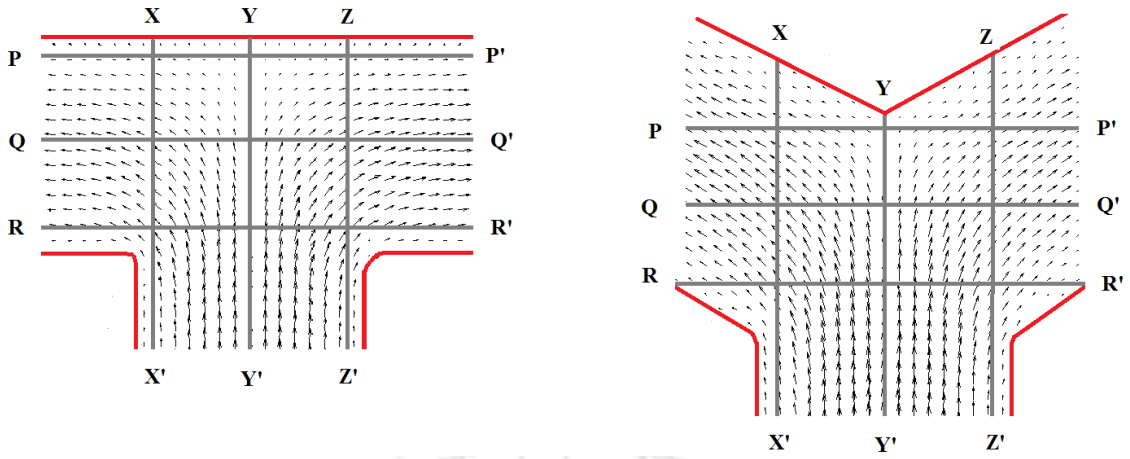

Figure 6.6. Velocity vector map of suspending fluid phase for 10µm suspension in the T and Y bifurcation.

6.3 Results and discussion

6.3.1 Velocity field

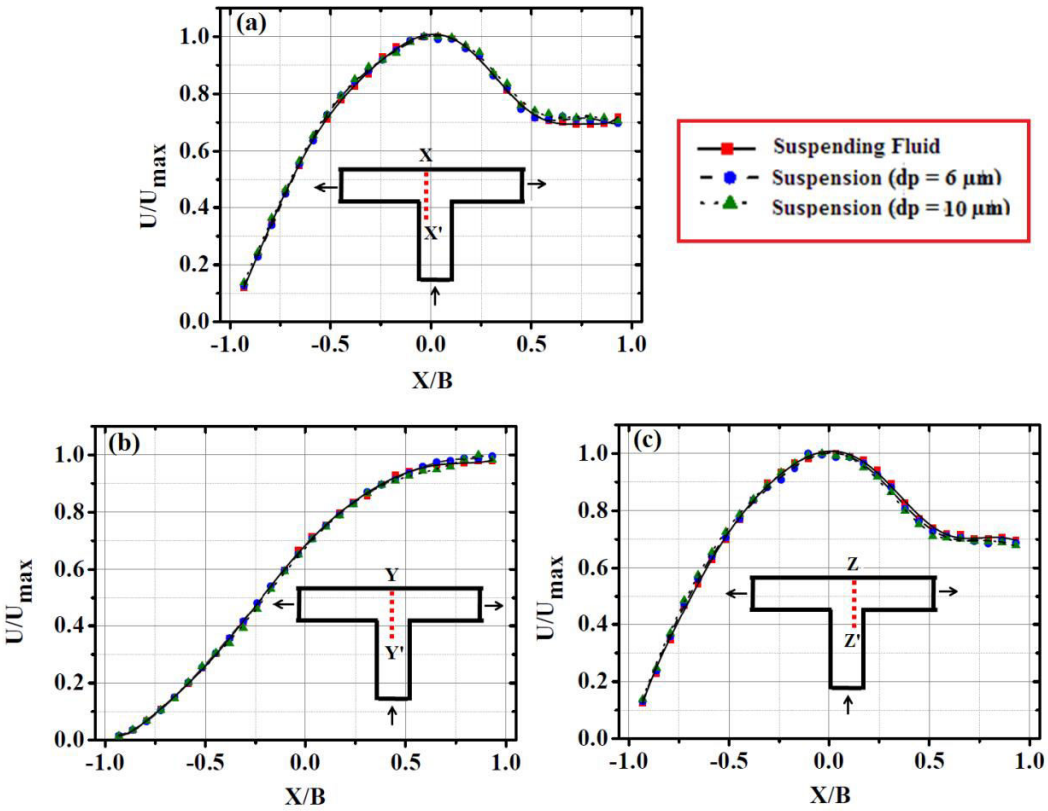

Figure 6.7. Velocity profiles in the vertical location of symmetric T- shape channel (θ =180°) at (a) XX` (b) YY` and (c) ZZ`.

The mean velocity profiles for pure suspending fluid and suspensions of two different particle sizes (6 and 10 μm) at various vertical locations in the symmetric T and Y shape channels are plotted. The velocity magnitude (U) is normalized relative to the maximum velocity (Umax) for each case. Figure 6.7 and 6.8 shows the velocity profiles along the lines XX`, YY` and ZZ` positioned at 0.3W, 0 W, 0.3W, respectively, from the line of central symmetry in T and Y shape channel respectively. The slight difference in YY` profiles for T and Y shape geometry might be due to presence of stagnation point along the symmetry line, at the intersection point of the channel sidewall and the separating streamline. Velocity gradients at the stagnation point are zero and generate extensional flow in near region. The profiles in the position XX` and ZZ` is symmetric for both the channels.

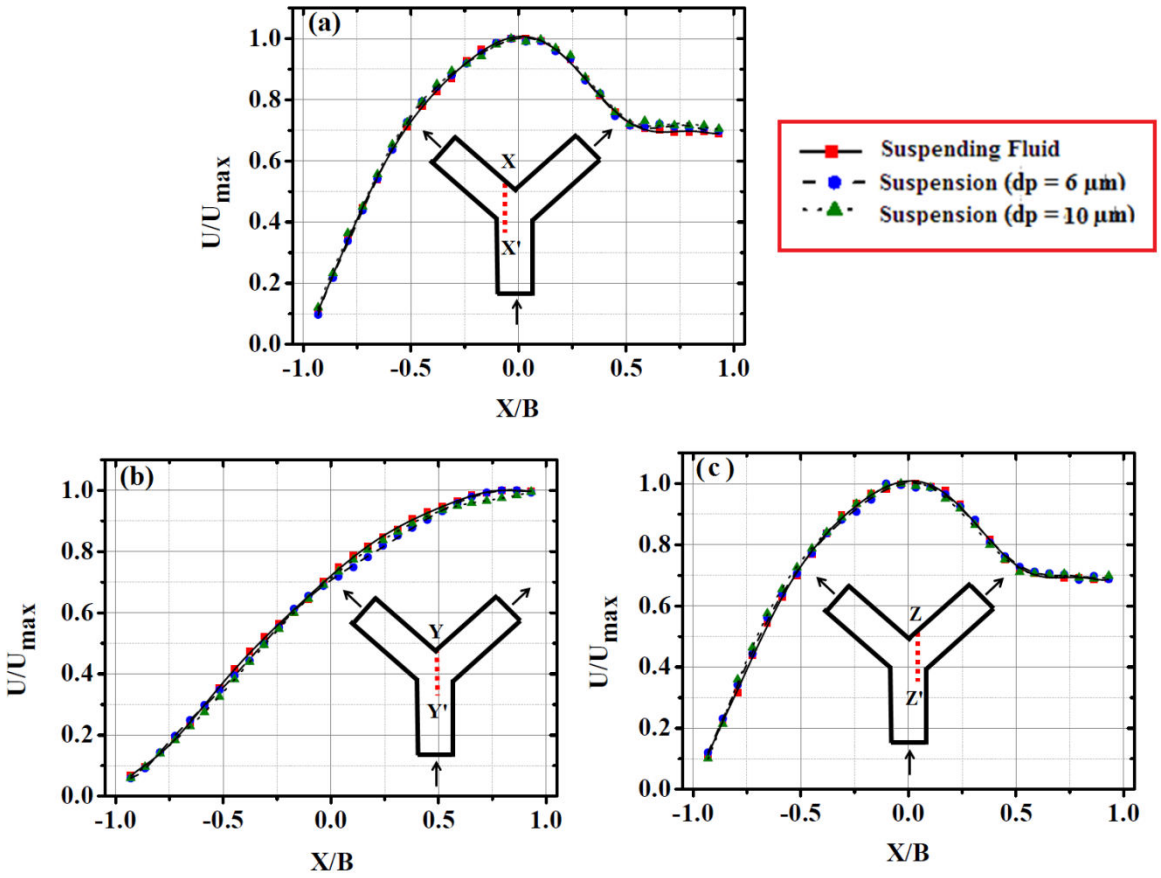

Figure 6.8. Velocity profiles in the vertical location of symmetric Y- shape channel (θ =120°) at (a) XX` (b) YY` and (c) ZZ`.

Figure 6.9 shows streamline and location of stagnation point in both the channels. It is observed from the figure that in case of T shape channel region near the stagnation point is more flat than Y shape leads to generate extensional flow.

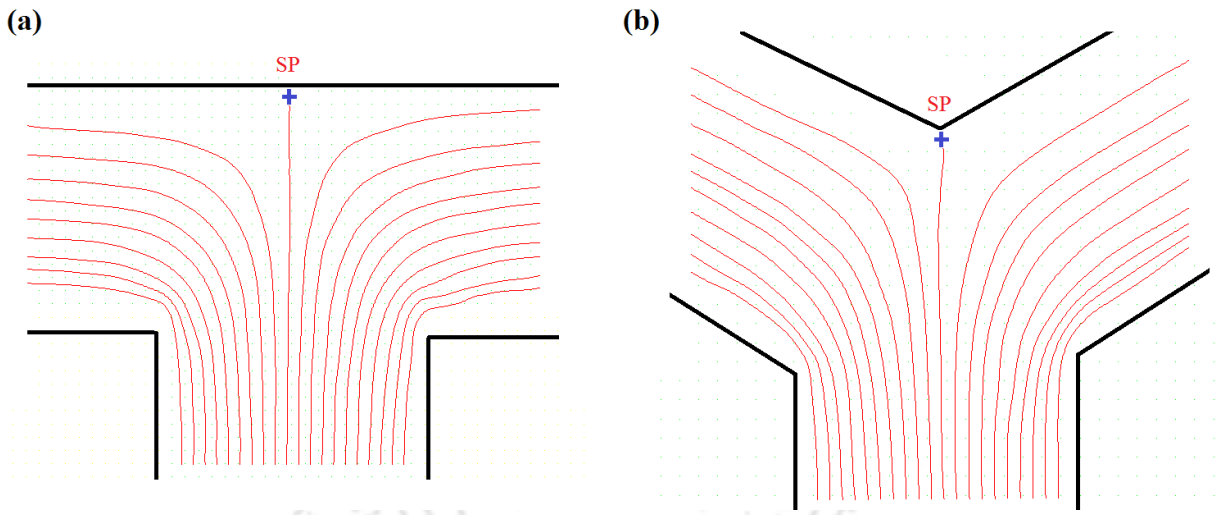

Figure 6.9. Streamline and location of stagnation point at (a) T and (b) Y bifurcation.

Figure 6.10 and 6.11 shows velocity profile for the horizontal lines PP`, QQ` and RR` positioned at same distance, from the line of central symmetry like the previous case for T and Y shape bifurcation channel.

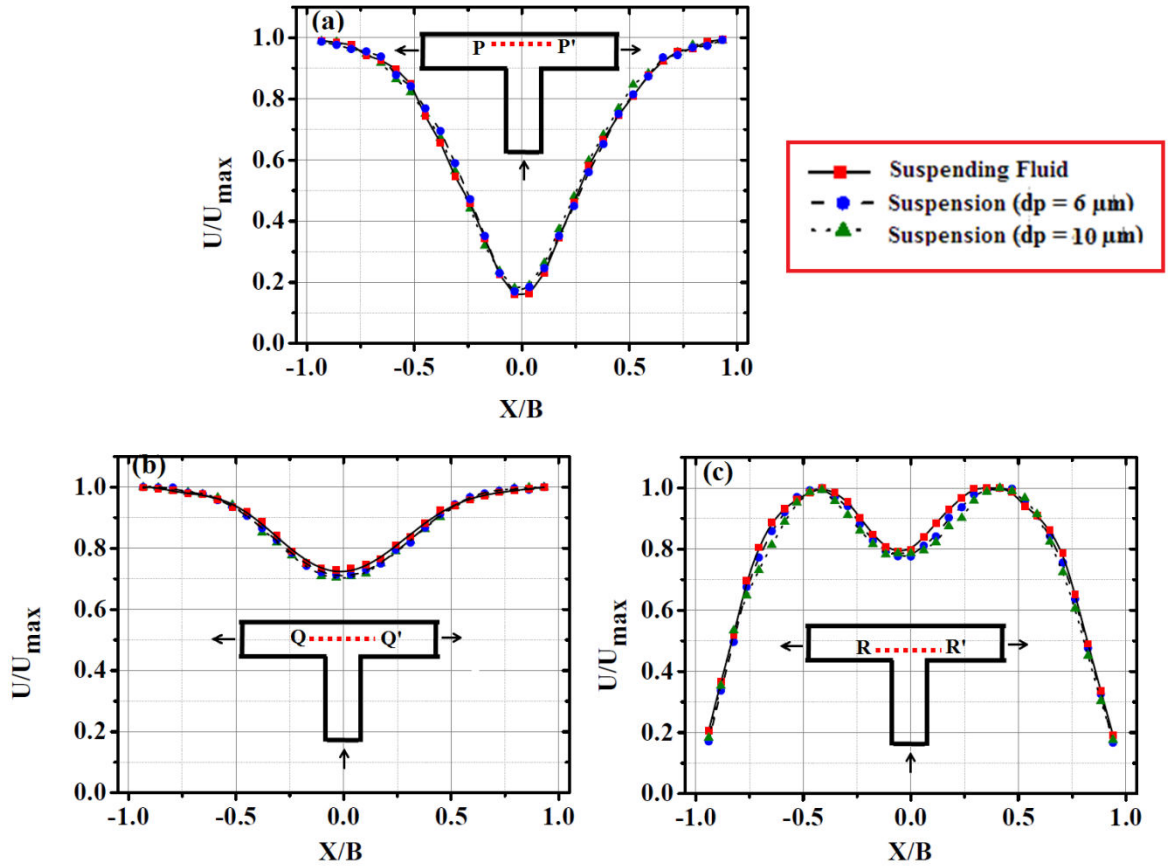

Figure 6.10. Velocity profiles in the vertical location of symmetric T- shape channel (θ =180°) at (a) PP` (b) QQ` and (c) RR`.

For T- shape channel the at location PP` and QQ` we have observed inverted normal profile but the downward peak is more at PP` location. Here also we can see the effect of stagnation point on the velocity profile. Location PP` is very near to stagnation point, where velocity gradient is very minimum resulting negative peak in the velocity profile. The location QQ` (the central location) is little far from stagnation point as a result effect on velocity is less, giving small negative peak. The profile at PP` and QQ` location in the Y-shape channel is almost similar to T-shape channel. The difference we have observed in T-bifurcation that, there is an extension in profile at the both corner. At location RR` for both T and Y shape a Peak-valley-peak patterns were observed for pure suspending fluid and suspensions of two different particles in both the channel. This peak-valley-peak pattern results from the division of flow into the left and right branches. It can be observed that peak-valley-peak pattern is more prominent for suspension of larger particles.

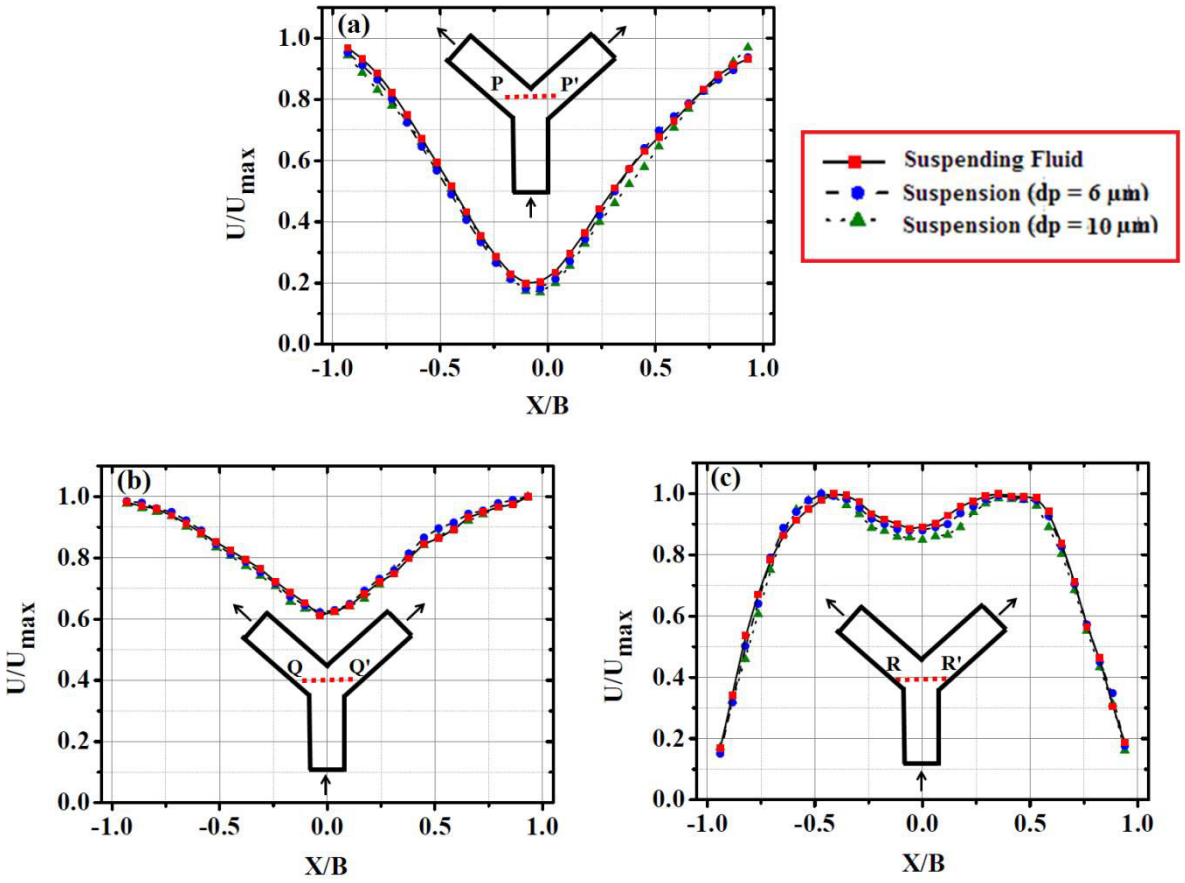

Figure 6.11. Velocity profiles in the vertical location of symmetric Y- shape channel ($\theta = 120°$) at (a) PP` (b) QQ` and (c) RR`.

We can use these velocity profiles to measure viscosity at all the locations XX`, YY`,XX` ,PP`, QQ`, RR` trough a single experiment using velocity type rheometer with equation 6.3. Here in this equation we know the value of L, z , z_0 from our experimental parameter. Gradient in velocity $\frac{dv_x}{dz}$ can be evaluate from the measured velocity profile. To calculate viscosity pressure drop Δp across the XX`, YY`, XX`, PP`, QQ` and RR` is needed. In this work due to experimental limitation we are not able to record Δp across the above stated lines during our μ-PIV experiment. But simultaneously measurement of pressure drop across the different lines is possible by putting pressure measuring sensors in those locations. In Figure 6.12, we have shown the experimental arrangement for simultaneous measurement of pressure gradient (Δp) and velocity to develop velocity type micro rheometer. This work provides ground for using bifurcation channel as a micro rheometer for measurement of rheological properties of complex fluids in future experiments.

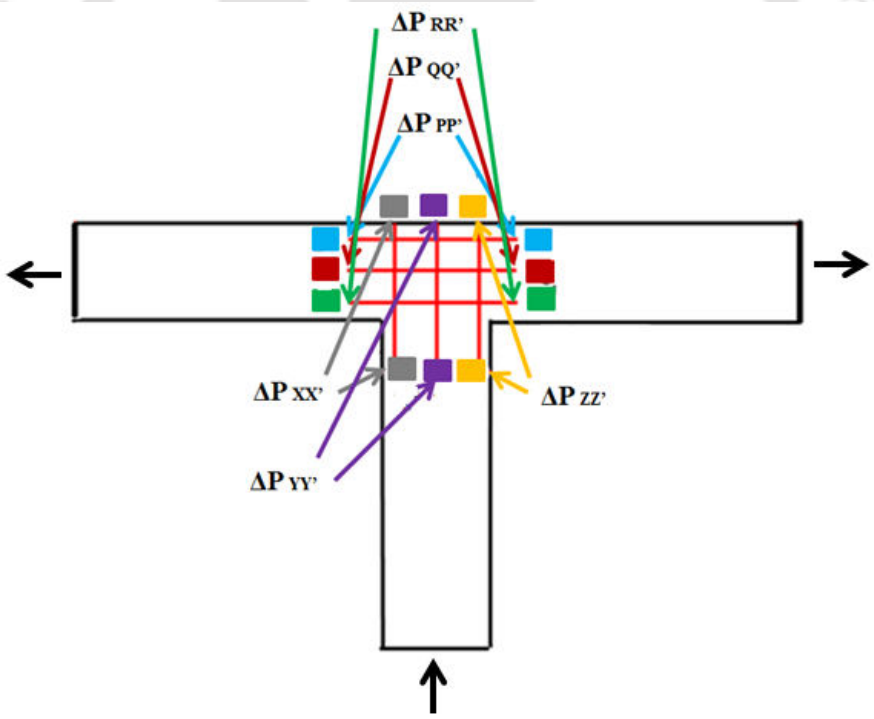

Figure 6.12. Schematic of T-bifurcation channel with pressure measuring sensors for velocity type micro rheometer.

6.4 Conclusion:

In this chapter we have measured velocities at six different locations in the bifurcation region of symmetric T and Y shape channel. Here due to experimental limitation we are not able to record Δp across the different lines during our μ-PIV experiment. But simultaneously measurement of velocity and pressure drop across the different lines is possible by putting pressure measuring sensors in those locations. This work provides ground for using bifurcation channel as a micro rheometer for complex fluids in future experiments.

Chapter 7

Flow of concentrated suspension in bifurcating open channel

7.1 Introduction

In hydraulic and environmental engineering, free surface flow in branching channel is commonly encountered in river bifurcation, river delta, spillway etc. The behavior of suspension flow in a bifurcation channel under varying geometrical conditions leading to the distribution of flow and sediment is yet to be completely understood. The control of flow and sediment separation in bifurcation plays a significant role in the development of deltaic systems. Therefore, the knowledge of the dynamics of a multi-phase system in this kind of bifurcation geometry is of paramount importance to understand the various flow behavior and macroscopic features. Moreover, it will also help in forecast and management of flood risks and understand the development of river delta.

The significance of the current work comes from some recent studies in open bifurcation geometries for the flow of concentrated suspensions. Thomas et al. (2011) carried out an experimental study in symmetric Y-bifurcation channel using Ultrasonic Doppler Velocity Profiling (UDVP) to investigate the influence of bifurcating angle on the flow division and flow structure in the daughter branches for a range of discharge division's ratios. They reported about the development of secondary flows near the bifurcation move towards the inner bank. Marra et al. (2014) also carried out experiments in Y-bifurcations using PIV and UDVP varying three important factors (discharge ratio, width-to-depth ratio, and bed roughness) to investigate the secondary flow field and its effect on the splitting of flow, specifically near-bed and surface flow. They also reported about the evaluation of secondary flow near the bifurcation which causes dissimilar flow portioning. Neary et al. (1993) and Ramamurthy et.al (2007) from their experiment study also confirmed the formation of secondary flow in the upstream of the open T-bifurcation channel. Muste et al. (1997) carried out Discriminator Laser-Doppler Velocimeter (DLDV) experiment in open geometry to determine the mean velocity and turbulence features

with and without suspended sediment. They reported slip between fluid and sediment. This work reports the experimental study of velocity profiles for suspension of neutrally buoyant particles in both symmetric Y-shape and asymmetric T-shape bifurcating channel

7.2 **Experimental procedure**

Figure 7.1 demonstrates the schematic drawing of our PIV experimental facility and Figure7.2 shows the photograph of asymmetric T-shape and symmetric Y-shape bifurcating channel.

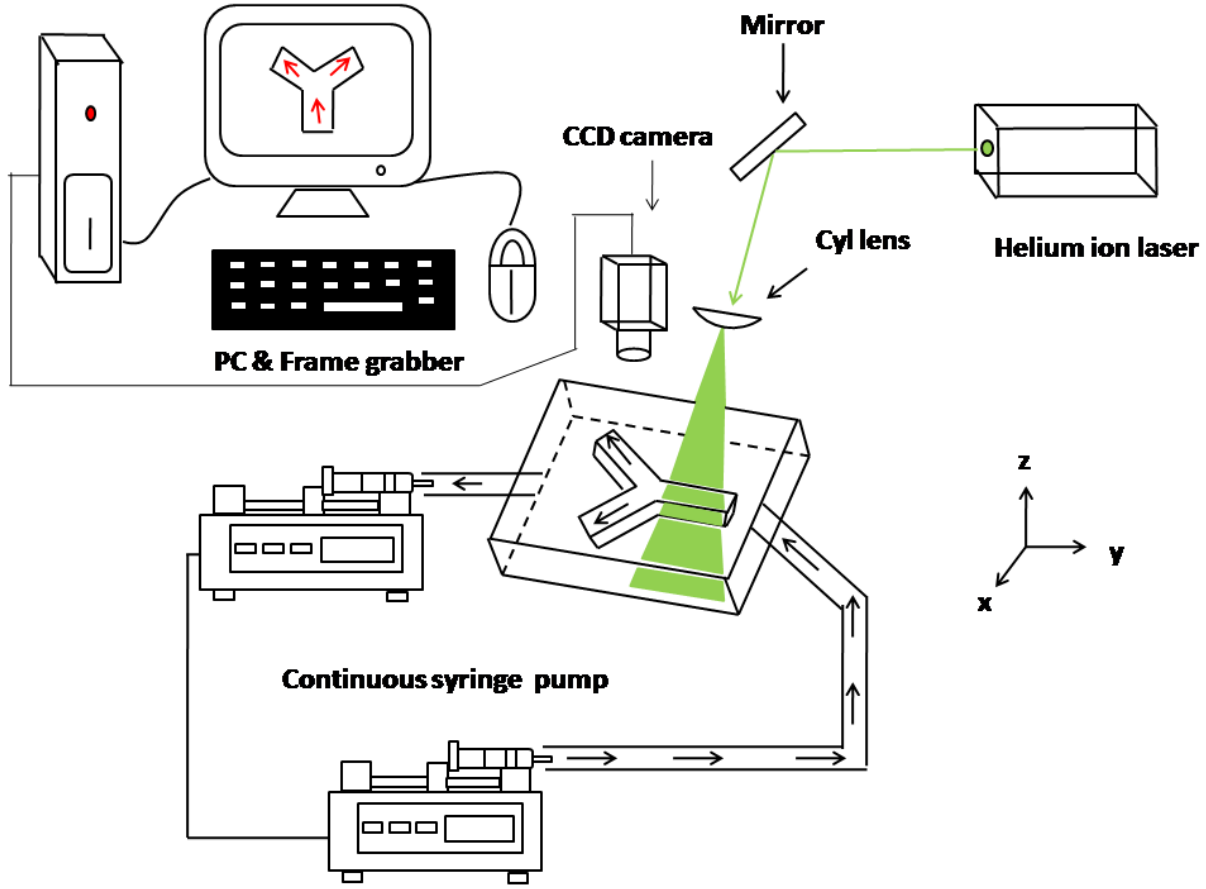

Figure 7.1. Schematic diagram of an optical arrangement for PIV experiment.

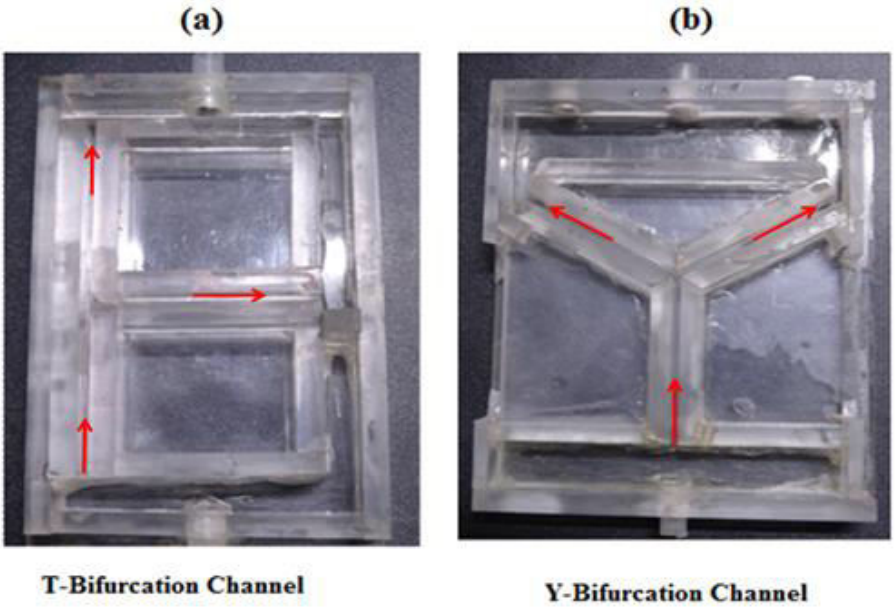

Figure 7.2. Photograph of (a) T- bifurcating channel and (b) Y- bifurcating channel.

Experiments were carried out in a rectangular geometry that was 8 cm long, 0.2 cm wide and 0.5 cm deep. The length of each side branch was equal to 4 cm. The channels were made of 5 mm thick Perspex material. An extension of pipe of 24 cm long was attached to the inlet of the test channel to connect the syringe pump. A helium ion solid state continuous laser from Coherent (actual power 25 mW, k = 635 nm) was used as light source. A plane mirror was used to guide the laser beam to the test channel and a cylindrical lens produced a horizontal light sheet to illuminate from the side of the channel (shown by the dark area in the x-y plane of the Fig.1). A continues syringe pump from New Era Pump System was used to circulate the suspension in the test channel. To reduce the slight instabilities created by the syringe pump throughout the flow, the upstream and downstream end of the channel was coupled with the reservoirs. In the Fig. 1, x is the length-wise direction, y is the direction of flow, and z is the gravity direction. Experiments were conducted for neutrally buoyant suspension of two different sizes of particles. Polystyrene particle of mean diameter 80 μm dispersed in a glycerol-water mixture was used to prepare the suspension. The suspending fluid was prepared by mixing 25% glycerol and 75% water (volume %). The density and viscosity of the solution were 1050 Kgm^{-3} and 0.00205 Pa.s respectively. About 200 ml of suspension was prepared and gently transported to test channel via the syringe pump. The inlet and outlet ends of the channels were connected to the syringe pump through silicon pipe of inner diameter 7 mm which pump the suspension in the test channels. The speed of the pump could

be adjusted to get the expected flow. The range of centerline velocity for the experiments was varied from 0.85 cm/s to 2.7 cm/s. The Reynolds number based on particle size and suspending fluid viscosity was O (10^{-3}). Schematic of bifurcation channels used in our experiment is shown in Figure 7.3. The locations at which profiles were evaluated are also shown in these images.

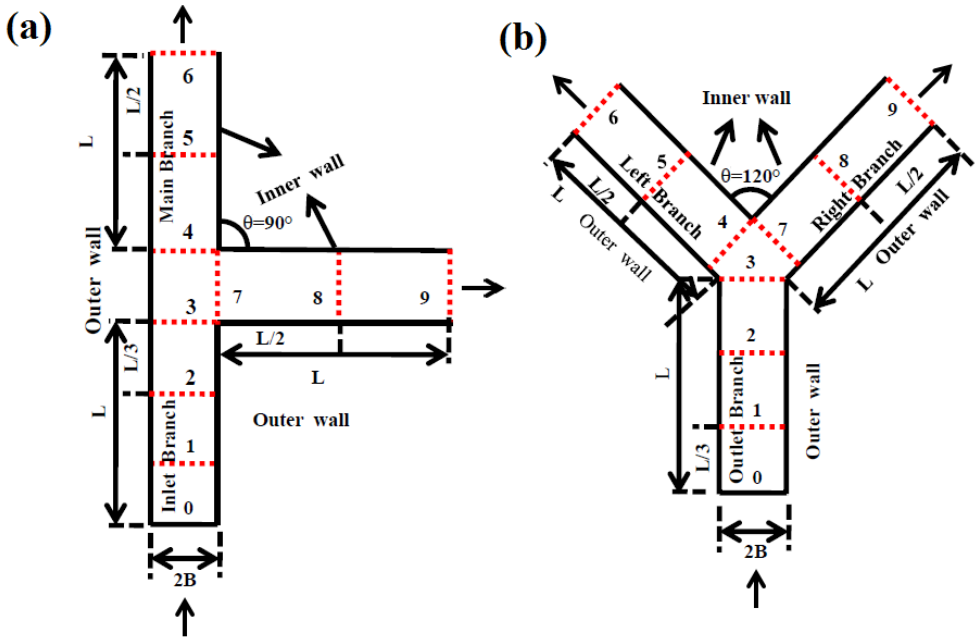

Figure 7.3. Schematic diagram of bifurcating channels used in our experiment (a) T shape (b) Y shape.

7.3. Results and discussion

7.3.1 Velocity field

The flow of both single-phase Newtonian fluid and non-colloidal suspensions through the bifurcation geometries were studied experimentally. Single-phase flow experiments were carried out with Newtonian fluid (glycerol + water mixture) while neutrally buoyant suspensions in Newtonian fluids of matching densities were investigated for particle volume fractions (ϕ) 0.3 and 0.4. The velocity profiles for Newtonian fluids and corresponding suspensions at different locations in the bifurcating channels are plotted for quantitative comparison. The velocity magnitude (U) at each position is normalized by the maximum velocity Umax. Figure 7. 4 and 7.5 shows the velocity plot of Newtonian fluid and suspension (

$\phi = 0.3$ and $\phi = 0.4$) in T and Y bifurcation channel at the inlet branch (location 1 and location 2 and location 3).

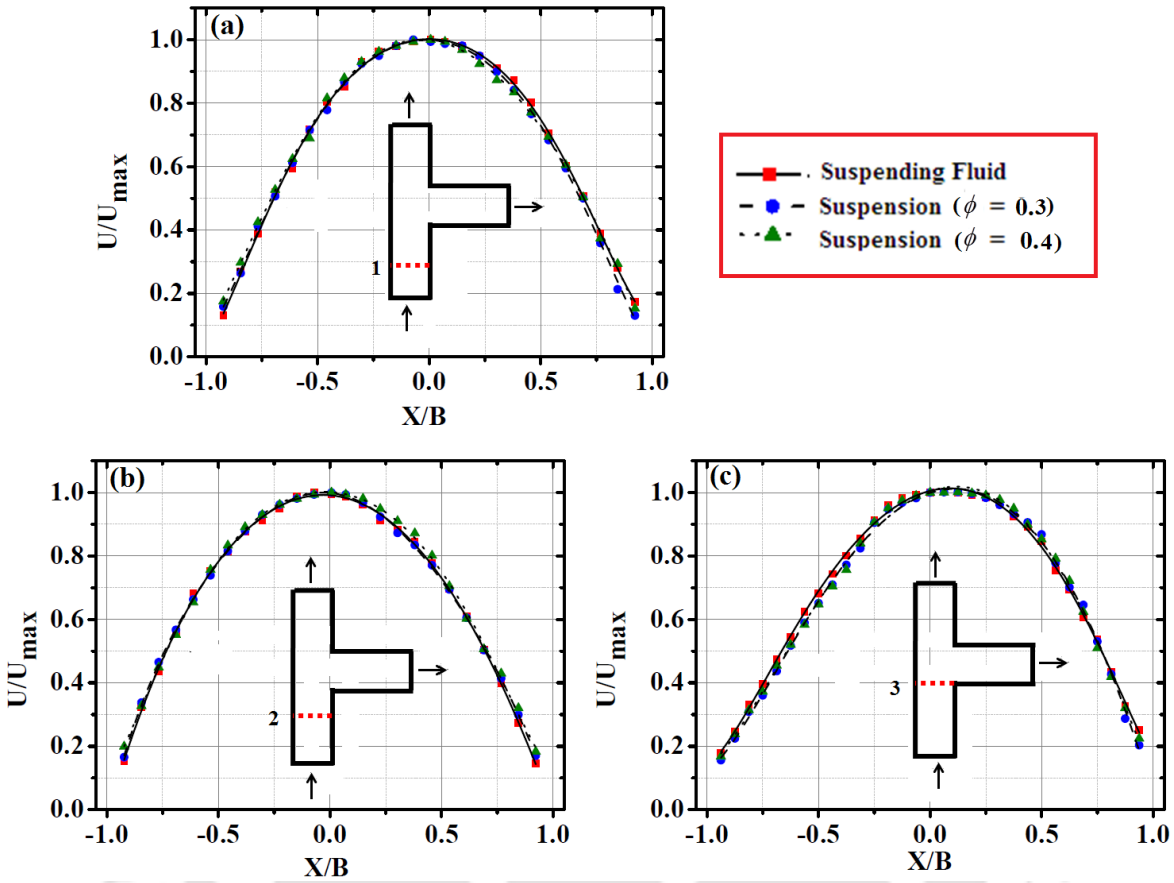

Figure 7.4. Comparative velocity profiles of Newtonian fluid with suspensions at the inlet section (a) Location 1 (b) Location 2 and (c) Location 3 of T-bifurcation channel.

At location 1 and 2, the velocity profiles were symmetric and fully developed for both the channels. In this experimental study, some data points are missing near the walls. This was due to the difficulty in locating the channel wall, curvature effect and the irregularity in the velocity near the walls. Up to the location 2, in the inlet branch velocity profiles are identical in both bifurcation channels. This is because the effect of bifurcation angle was not experienced up to location 2. After location 2, the nature of velocity profile depends on the bifurcation angle and bulk particle concentration. At the location 3 (bifurcation point) we have observed a small shift of profile in the direction of side branch for Newtonian as well as suspension flow in asymmetric T-bifurcation channels. For Y-bifurcation the flow has to divide into left and right branches, the profile near the center becomes smeared and as a

result, small bluntness in velocity profile was observed. The skewness coefficients of velocity profile at bifurcation point for Newtonian fluid and suspension ($\phi = 0.3$ and $\phi = 0.4$) in T channels are 0.857, 0.915, and 0.9835 respectively. Similarly, for Y shaped channels the corresponding values were found to be 0.423, 0.462, and 0.47. It can be observed that as the bifurcation angle increases the skewness toward the side branch also decreases. Moreover with the increase of particle concentration skewness in profile increases.

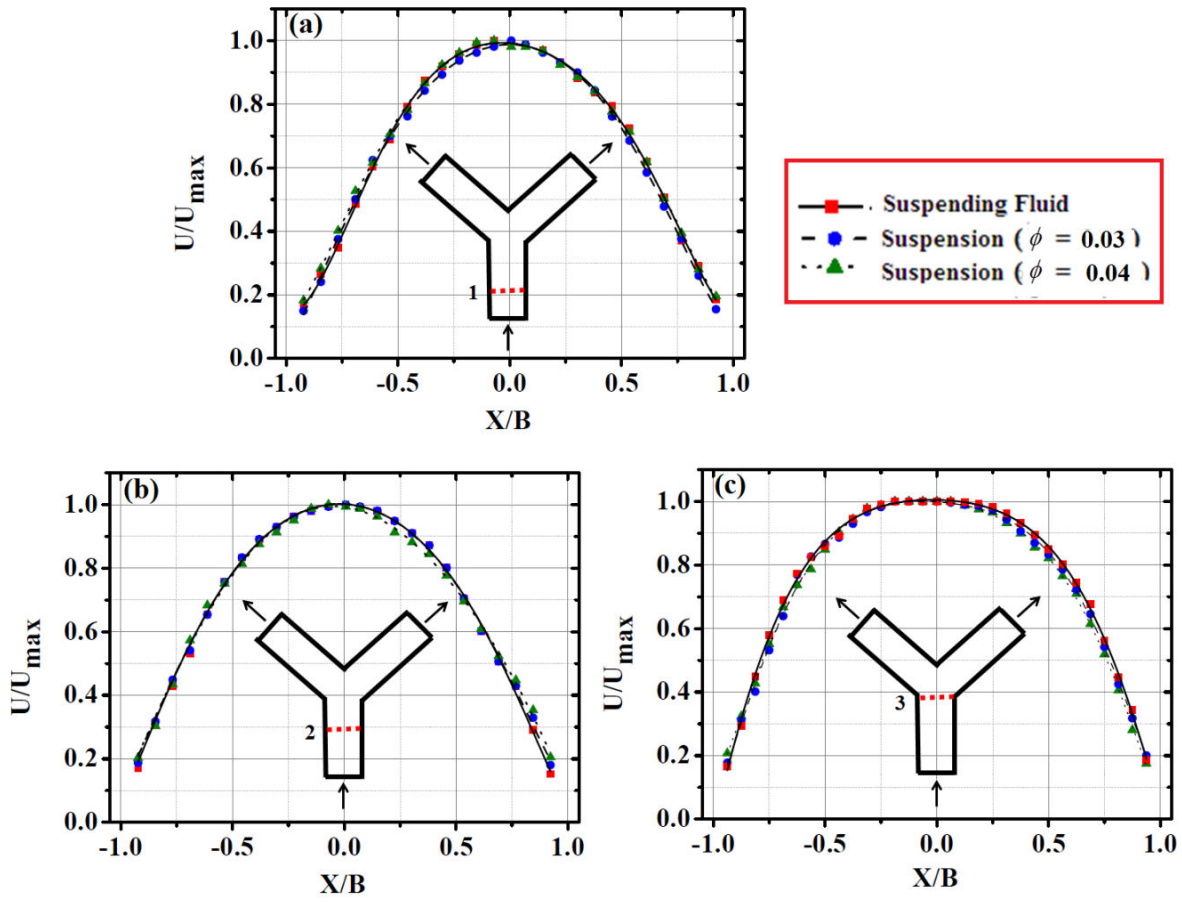

Figure 7.5. Comparative velocity profiles of Newtonian fluid with suspensions at the inlet section (a) Location 1 (b) Location 2 and (c) Location 3 of Y-bifurcation channel.

After the bifurcation, the flow enters into the daughter branches. The velocity profiles at the entrance and exit locations of the daughter branches of asymmetric T shape and symmetric Y shape bifurcation channels are shown in the Figure 7.6 and Figure 7.7 respectively. It was observed that for both the channels the velocity profile at location 4 in the left branch is almost mirror image of location 7 in the right branch. In both, the daughter branches of the T

and Y -bifurcation the peaks in the velocity profiles were shifted towards the outer wall. The skewness of the experimental profiles in the T- shaped channel for the Newtonian fluid and suspensions ($\phi = 0.3$ and $\phi = 0.4$) at the location 4 was found to be 0.562, 0.59 and 0.643. The corresponding values of skewness at the location 7 was 0.663, 0.7 and 0.728 respectively. Similarly, for the Y-shape channel, the skewness value of the velocity profiles at the location 4 for the Newtonian fluid and suspension suspensions ($\phi = 0.3$ and $\phi = 0.4$) was calculated as 0.689, 0.768 and 0.79. The corresponding values at the location 7 was 0.658, 0.72941 and 0.73676 respectively. It is apparent that the skewness of the velocity profile was more for suspension compared to the Newtonian fluid. Moreover, in both the channel with the increase of particle concentration the shifting of velocity profile towards the outer wall was found to increase.

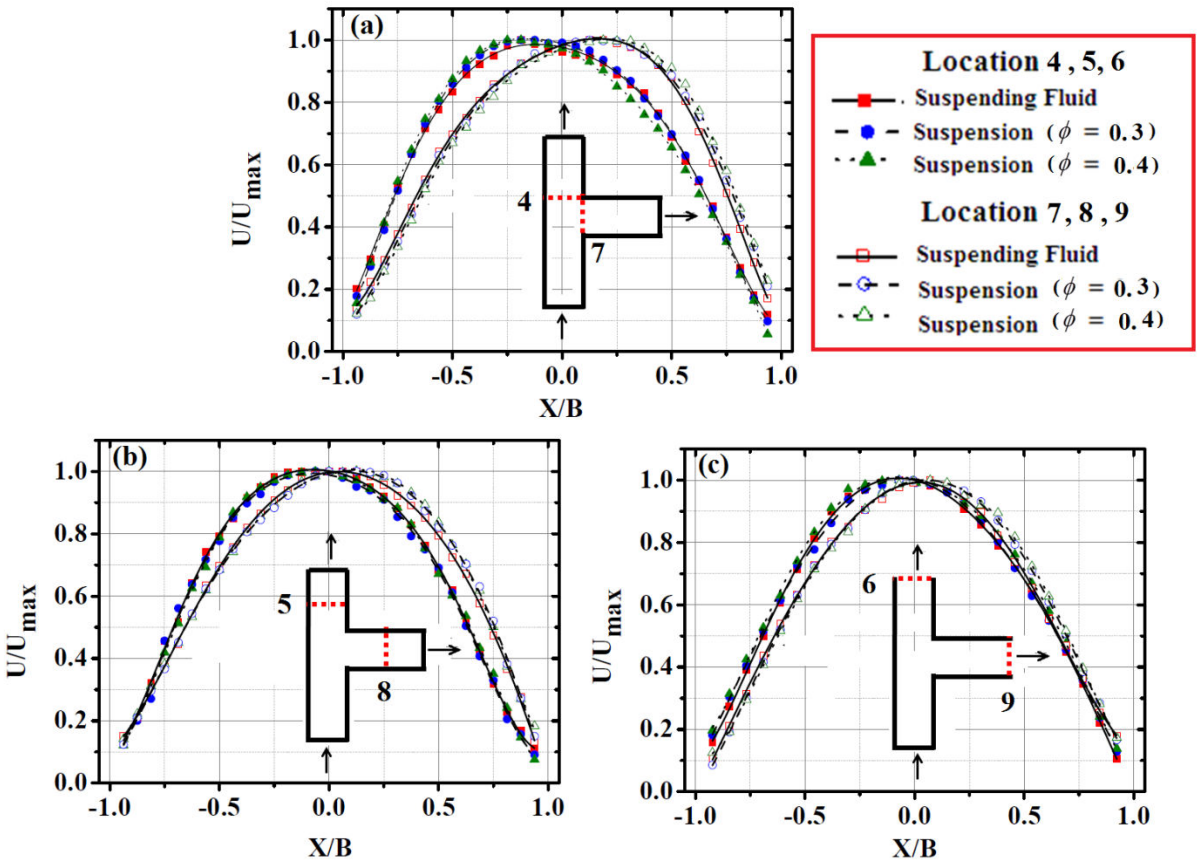

Figure 7.6. Comparative velocity profiles of Newtonian fluid with suspensions at different locations of the main branch and a side branch of T-bifurcation channel.

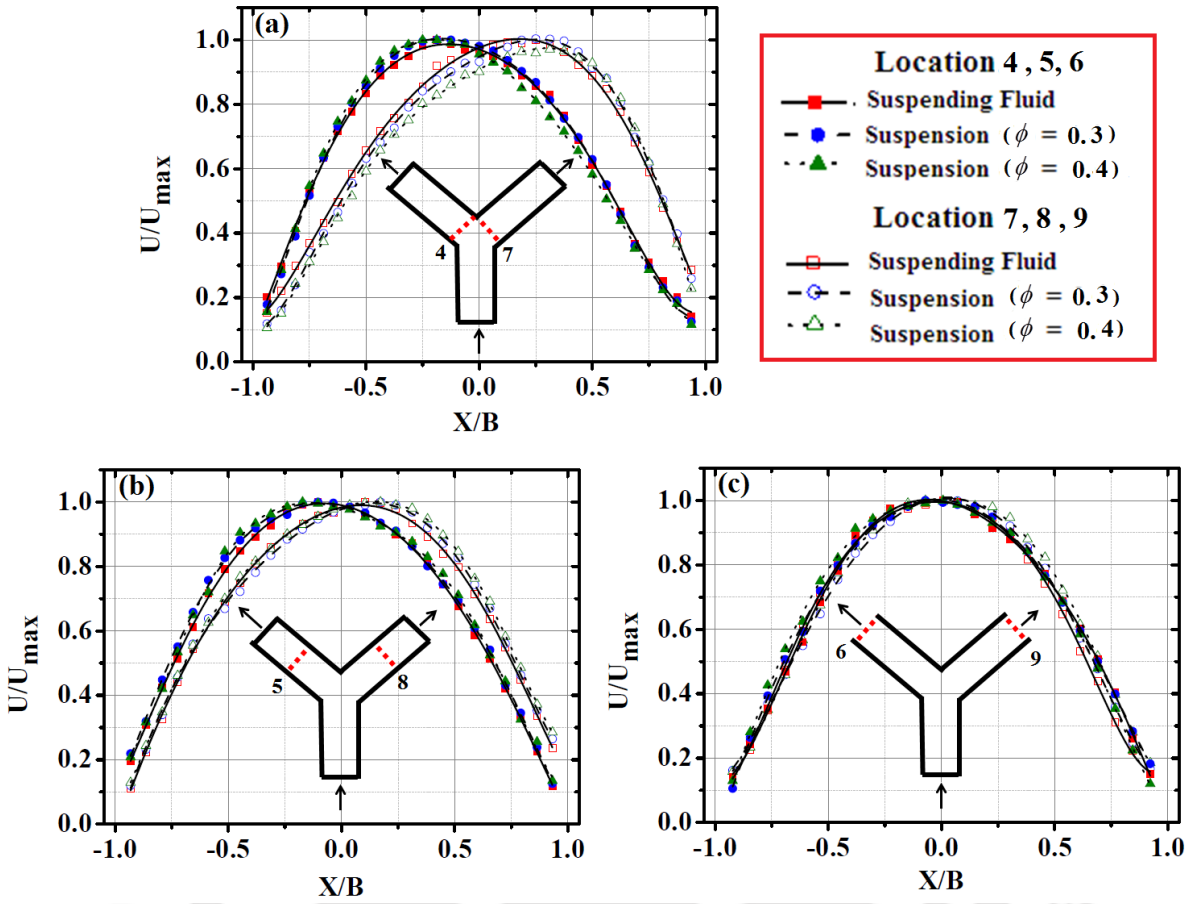

Figure 7.7. Comparative velocity profiles of Newtonian fluid with suspensions at different locations of the left and at right daughter branch of Y-bifurcation channel.

Again due to the shear-induced migration ,particles moves towards the center of the channel., As we move downward positions in the daughter branches the peak of the velocity profile shifts towards the center of the channel and asymmetry in velocity profile reduces. It was observed that for both the channels the velocity profile at location 5 (in the left branch) and location 8 (in the right branch) is shifted closer to the center of the channel. The velocity profile at the exit of both the branches (location 6 and location 9) was nearly symmetric for the T and Y bifurcations. However, due to the short length of the daughter branches, the profiles were not fully developed.

Figure 7.8 shows streamlines in the T and Y-bifurcation channel. Streamlines can be constructed from the horizontal velocity fields. The average particle concentration was $\phi = 0.4$ and the particle diameter was 80μm. Streamlines were generated using the PIVlab_1.32 software. It was observed that the position of the dividing streamline is shifted more towards the main branch of the T-shaped channel. For the symmetric Y-shape channel, the position of the dividing streamline in both the cases is almost in the middle of the junction point of the daughter branches.

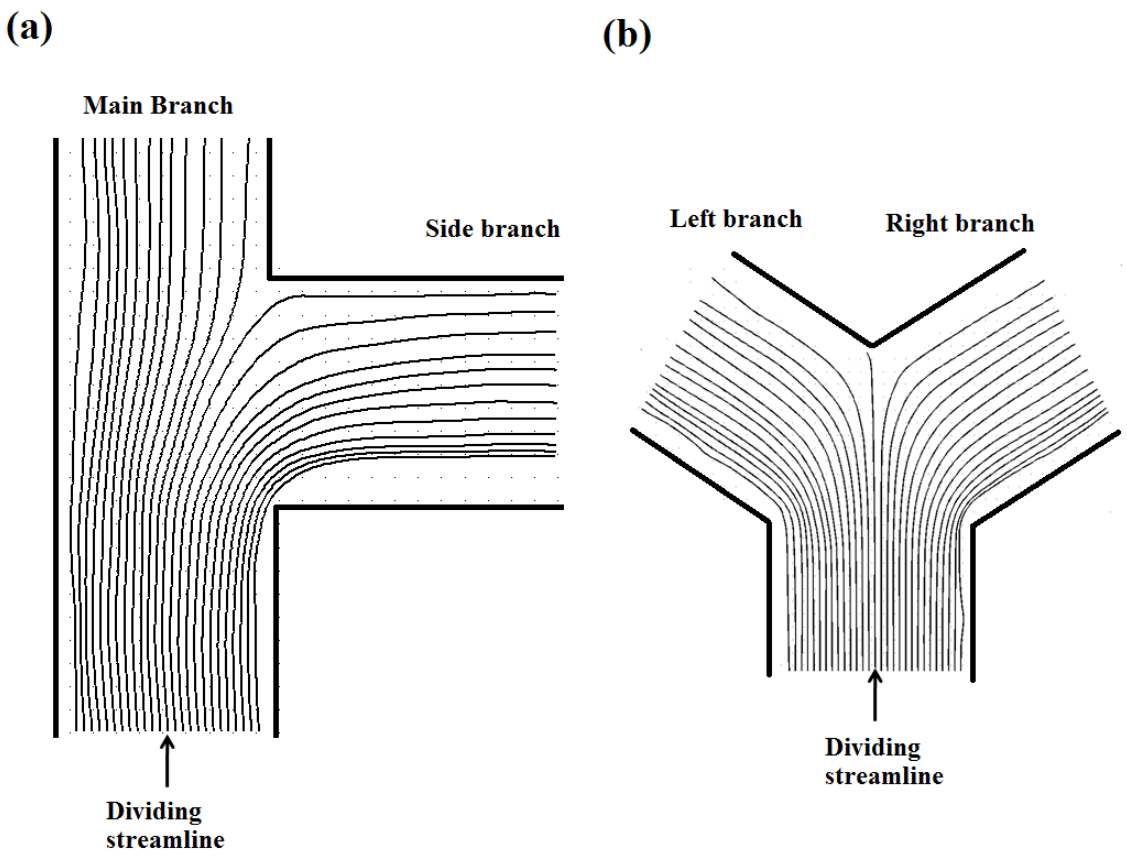

Figure 7.8. Streamlines near the bifurcation section of (a) T and (b) Y- shaped channel. The average particle concentration was $\phi = 0.4$.

7.3.2 Particle concentration

From the captured images we can obtain the qualitative measurement of the particle concentration by plotting the typical pixel intensity variation of the reflected light across the width of the channel. Light intensity can be correlated with the concentration. More intensity of the reflected light means the higher concentration of the particles at that location. Figure

7.9 shows the intensity distribution at the inlet branch (Locations 1-3) corresponding to the sample image shown in the Figure. The images were recorded by the CCD camera using the cold light source at different locations in the inlet branch of the T-shaped channel. The images were stored in gray scale whose intensity varied between 0 and 255. At a given axial location the intensity of the pixels along the horizontal direction is shown. Here we have noticed that as we move from the location 1 to location 3, the peak intensity profile also increases forming the inverted V-shape of the profile. This can be linked with shear-induced migration phenomena due to which particles move towards the center of the channel and gives rise to the higher intensity reflected light. As the concentration profiles for Y-shape channel is qualitatively similar to the T-shape at these three locations which we have not included here.

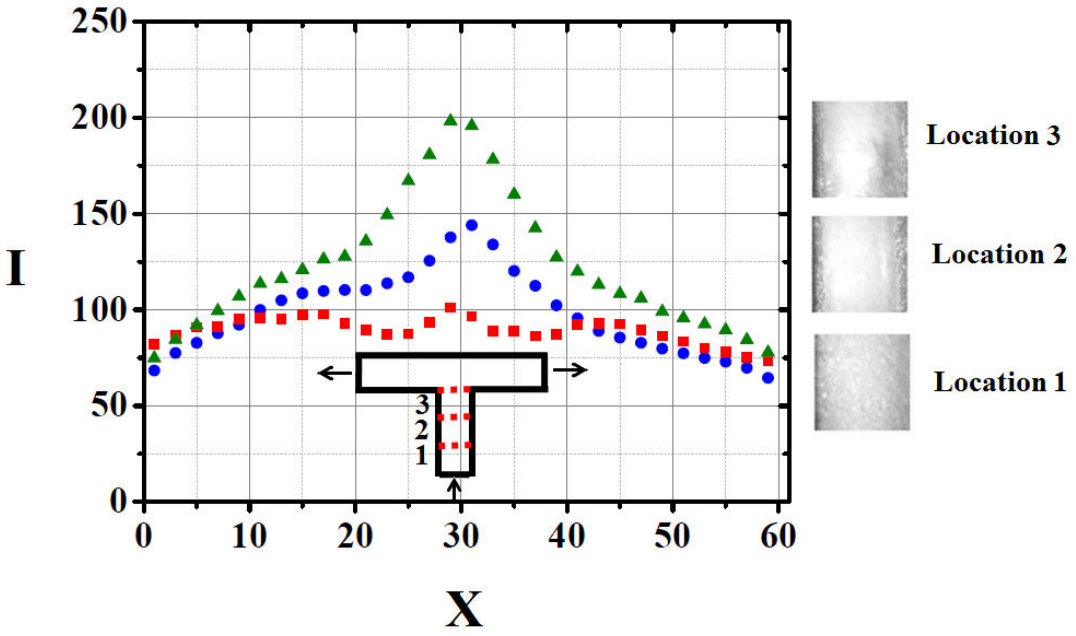

Figure 7.9. (a) Profiles of reflected light intensity for the suspension at the inlet branch (Locations 1-3) in T bifurcation channel (b) sample image recorded by CCD camera.

Figures 7.10 and 7.11 show intensity profile at the daughter branches of the asymmetric T and asymmetric Y-bifurcation channels. For T shape bifurcation, at location 4 of the main branch and the corresponding location 7 of the side branch, the profiles are nearly linear and the particle concentration is highest near the inner wall. As we move to the downstream locations the particle concentration near the wall gradually decreases and due to particle migration the peak concentration shifts to the center of the channel.

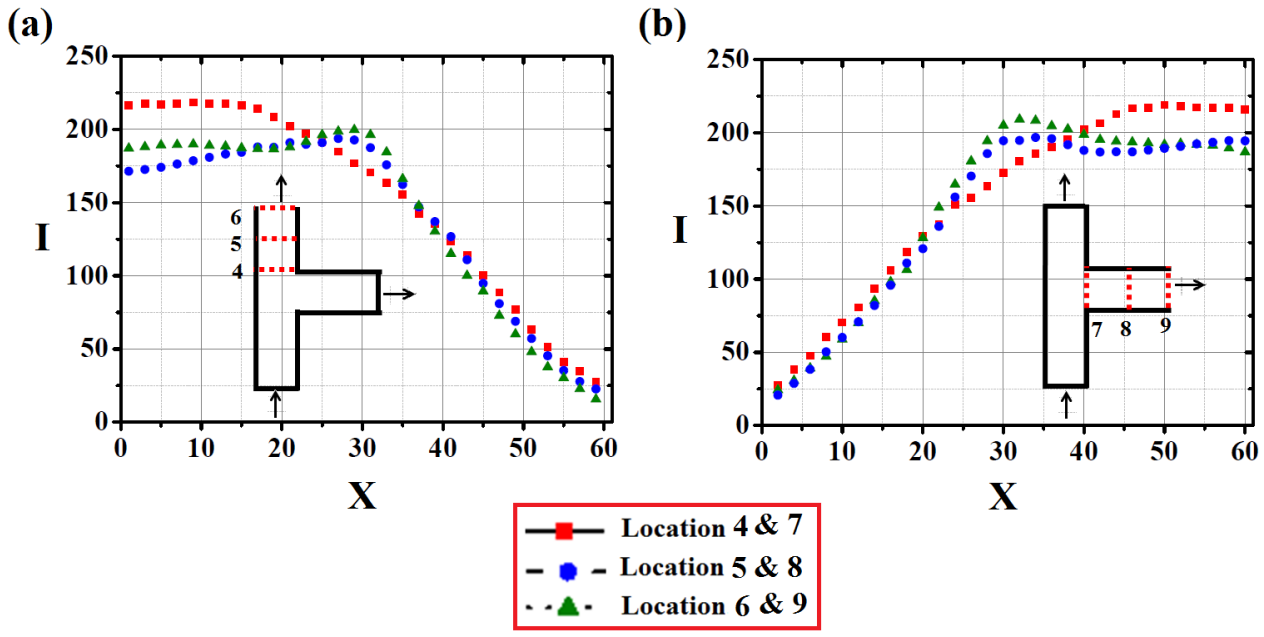

Figure 7.10. Profiles of reflected light intensity for the suspension in the T- shaped channel at different locations in (a) main branch, and (b) side branch.

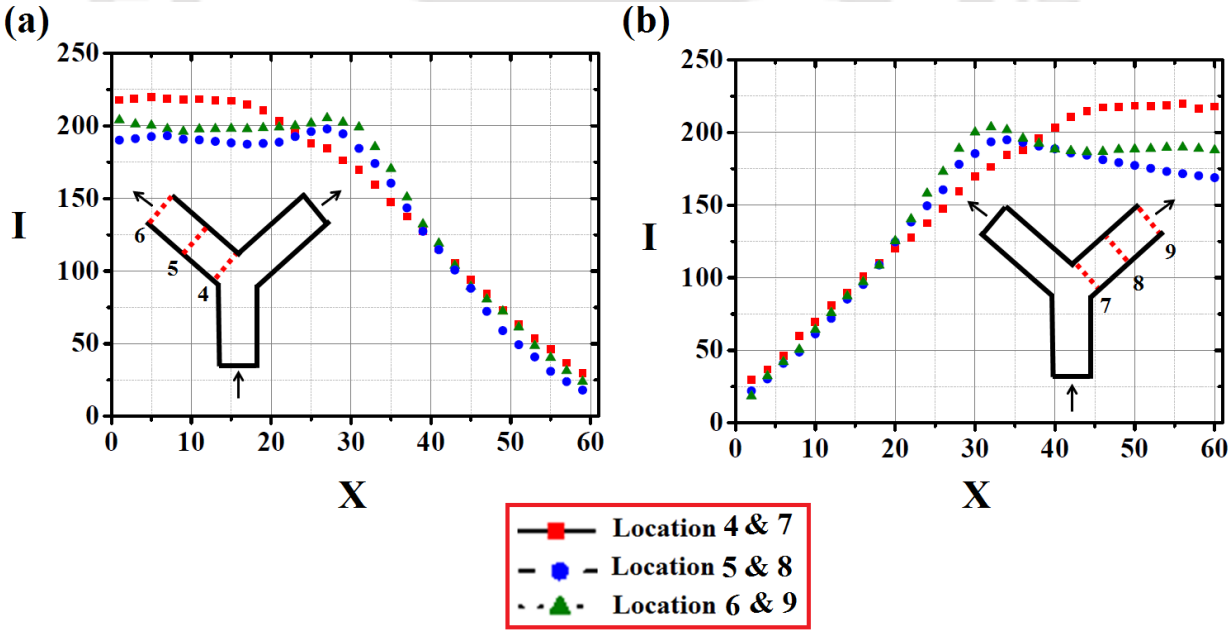

Figure 7.11. Profiles of reflected light intensity for the suspension in the Y- shaped channel at different locations in (a) left branch, and (b) right branch.

7.4 Conclusion:

Transport of suspension in T- and Y- shaped bifurcation channels was studied experimentally using the PIV technique. We have observed that due to the shear-induced migration phenomena the particles move towards the center of the channel and this gives rise to the blunting of velocity profile before the junction. After the bifurcation, the peak of velocity profile moves in the direction of the outer wall, whereas, the maxima in particle concentration was observed near the inner walls. This causes asymmetry in the velocity and concentration profiles in the daughter branches. As we move towards the downstream positions the maxima in velocity and concentration profiles again shifts toward the center of the channel. The velocity and concentration profiles were found to be strongly influenced by the bifurcation geometry.

Chapter 8

Conclusion and future work

8.1Conclusion:

This work was aimed at providing insight into identify and quantify the effect of particle size, branching angle, type of flow on the velocity and concentration profiles in bifurcation channels. Micro-PIV/PTV experiments were performed for single-phase Newtonian fluid and dilute suspension of two different particles in bifurcation channels for diverging and converging flow condition. It was observed that solid particles do not follow the fluid path near the bifurcation which leads to unequal flow and particle distribution at this region. Also due to the irreversible nature of shear-induced particle migration, the profiles were not the same near the bifurcation location for converging and diverging flow conditions.

In Chapter 2 we have discussed about working principle of Particle Image Velocimetry (PIV), Micro Particle Image Velocimetry (μPIV), Micro-Particle Tracking Velocimetry (μPTV) technique to study the flow of suspension in bifurcating channels.

In Chapter 3 we have elaborated the fabrication of microchannels, post-processing of captured images before PIV/PTV analysis. Results from the experiment on diverging flow in bifurcation channels for a range of branching angle showed that migration of particles occurs across the streamline and symmetric velocity and concentration profile in the inlet branch becomes asymmetric in the daughter branches. Further migration of particles towards the center of the channel in the daughter branches again makes the profiles symmetric. In this work flow velocity profile was measured by μ-PIV and local concentration was measured by image processing method and μ-PTV. From streamline comparison, it can be concluded solid particles do not follow the fluid path near the bifurcation which leads to unequal flow and particle distribution in daughter channels.

In Chapter 4 we have carried out converging flow experiments in the same microchannels keeping the experimental conditions same as diverging flow. Some interesting results we have observed for converging flow, velocity profiles at the end of inlet section are reversible for

diverging and converging flow conditions in symmetric T and Y shape channel. At the confluence of two streams for converging flow or at the bifurcation point for diverging flow velocity profiles are reversible for asymmetric channels. Concentration profile obtained from Particle counting MATLAB programme shows peak-valley-peak profile at the outlet section for converging flow this is due to combining of two streams in the outlet section. As we move downstream locations in the outlet section, the peak-valley peak pattern in the concentration profile gradually decreases and only a single peak in the concentration profile emerges.

The flow of suspensions in diverging-converging channels of varying width were examined in Chapter 5**.** The width of left daughter branch was varied from 200µm to 500 µm keeping width in right daughter branch constant 200µm. This kind of geometry is often seen in blood microvasculature network, consisting of continually bifurcate (i.e., diverging bifurcation) and merge with other micro vessels (i.e.,converging bifurcation). The abnormality of the microvasculature can also cause a disorder of particles moving in suspension flow. Presence of diverging-converging bifurcations and short-length shunts may increase the speed flow, aggregation of particles near the apex of bifurcation etc. Shifting peak-valley-peak type of velocity profile is noticeable at the inlet and outlet section. This is due to the unequal division of flow in the diverging section and merging of two unequal fluid stream. Shifting of the profile was more for a channel with a higher width and reduces with a decrease of channel width. Also shifting of profiles is more for suspension flow in comparison to the Newtonian fluid. It was observed that for both the daughter branch the crests in velocity profiles are shifted towards the outer wall for the diverging side in contrast to converging flow where profiles are shifted towards inner side. From streamline comparison, we observed dissimilar fluid and particle streamline near the bifurcation and confluence. The region near the end position for diverging flow and beginning of converging flow in the daughter branches showed some noticeable deviation. This is because near the bifurcation and confluence particle-particle interaction is more, which causes deviation.

In Chapter 6 we have discussed fidelity of developing “Turn in Corner” type velocity based micro rheometer for online monitoring and measurement of rheological properties of complex fluid. In this turn in corner type geometry range of shear rate can be generated in a single experiment. We have measured velocity profiles across six different lines. Here due to experimental limitation we are not able to record Δp across the above stated lines during our µ-PIV experiment. But simultaneously measurement of velocity and pressure drop across the

different lines is possible by putting pressure measuring sensors in those locations. This work provides ground for development of a micro rheometer using bifurcation channel.

Up to Chapter 6 we have discussed results from μ-PIV/PTV experiments for single-phase Newtonian fluid and dilute suspension of two different size particles. For single camera μ-PIV/PTV experiment it is difficult to work in higher concentration as it will be challenging to separate the tracer bases on sizes with our existing particle separating code. Moreover handling dense suspension in micro channel is also one issue to limit our particle volume fraction to 5%. So we have carried out free surface PIV experiment for concentrated suspension in symmetric Y and asymmetric T channel in Chapter 7. We have reported results for particle volume fraction 30 % and 40 %. Experimental observations for velocity and concentration from PIV experiments has not shown significant difference compared to μ-PIV/PTV experiments.

Overall we have studied the suspension flow in bifurcation channels. Results from this work will provide an unprecedented level of detail about effect of shear-induced particle migration on unequal distribution of the phases in the downstream branches. Moreover, it will also help to understand the effect of bifurcation angle, size of the particles (relative to the channel width), concentration of particles on distribution of flow as well as particles in these kinds of complex geometry. These observations have important consequences in the development of microfluidic devices handling the transport of suspension in bifurcating microchannels.

8.2 Future work

There are several opportunities for extending this research work using the combination of micro PIV and PTV technique, which are as follows-

- In this research work we have performed single camera micro-PIV/PTV experiments for dilute suspension (ϕ=0.05).Further investigation can include the study of velocity and concentration profile for dense suspension flow. Experiments at higher particle concentration is expected to give more insight into the role of shear induced particle migration, on the flow and particle partitioning in the asymmetric bifurcation channels.

- We can study the suspension flow in bifurcation channel having one daughter branch blocked. This is a very relevant problem for biological system, process industries etc. dealing with suspension flow (Figure.8.1) This will help to investigates the hydrodynamics in microbifurcations where remarkable vortices are developed in the closed branch.

Figure 8.1. Bifurcation geometry having one daughter branch blocked. (Image source: Google Image).

- We have discussed fidelity of developing "Turn in Corner" type velocity based micro rheometerr for online monitoring and measurement of rheological properties of complex fluid using bifurcation channel. This work can be extending by simultaneous measurement of velocity and pressure drop (Δp) across the different lines by putting pressure measuring in those locations.

- We can carried out a similar experiment for bi-disperse suspension to identify and quantify the effect of particle size, particle volume fraction, branching angle, type of flow on the velocity and concentration profiles.

References

Aarts, P.; Vandenbroek, S. A. T.; Prins, G. W.; Kuiken, G. D. C.; Sixma, J. J.; Heethaar, R. M., Blood-platelets are concentrated near the wall and red blood cells, in the center in flowing blood. *Arteriosclerosis.* **1988,** *8* (6), 819-824.

Abbott, J.R.; Tetlow, N.; Graham, A. L.; Altobelli, S. A.; Fukushima, E.; Mondy, L. A.; Stephens, T. S., Experimental observations of particle migration in concentrated suspensions-Couette-flow. *Journal of Rheology.* **1991,** *35* (5), 773-795.

Adrian, R. J., Particle Imaging Techniques for Experimental Fluid Mechanics. *Annual Review of Fluid Mechanics*.**1991**, 23, 261-304.

Adrian, R.J.; Keane, R.D.; Zhang, Y., Super-resolution particle-imaging velocimetry. *Measurement Science and Technology* .***1995,*** 6, 754–768.

Adrian, R.J. Twenty years of particle image velocimetry. *Experiments in Fluids*.**2005**, 39 ,159-169.

Adrian, R.J.; Westerweel, J., Particle image velocimetry. *Cambridge University Press Cambridge.* **2011**.

Ahmed, G. M. Y.; Singh, A., Numerical simulation of particle migration in asymmetric bifurcation channel. *Journal of Non-Newtonian Fluid Mechanics.* **2011,** *166* (1-2), 42-51.

Anastasiou, A.D.; Spyrogiannia, A.S.; Koskinasb K.C.; Giannogloub, G.D.; Paras S.V., Experimental investigation of the flow of a blood analogue fluid in a replica of a bifurcated small artery. *Journal of Medical Engineering & Physics*. **2012,** 34, 211-218.

Argall, R.; Mulchandani, V.; Brenner, G., Optical measurement and numerical analysis of mono- and bidisperse coarse suspensions in vertical axisymmetric sudden-expansion. *International Journal of Multiphase Flow*. **2015,** 69, 63-80.

Arola, D, F.; Powell, R. L.; McCarthy, M.J.; Li, T.Q.; Odberg, L., NMR Imaging of Pulp Suspension Flowing through an Abrupt Pipe Expansion. *AIChE J.* **1998**, 44(12), 2597-2606.

Audet, D. M.; Olbricht, W. L., The motion of model cells at capillary bifurcations. *Microvascular Research.* **1987**, 33, 377–396.

Baek, S. G.;Magda, J. J., Monolithic rheometer plate fabricated using silicon micromachining technology and containing miniature pressure sensors for N1 and N2 measurements, *Journal of Rheology*.**2003**, 47(5), 1249–1260.

Batchelor, G. K., The effect of Brownian motion on the bulk stress in a suspension of Spherical particles. *Journal of Fluid Mechanics* .**1977,** 83, 97–117.

Balan, C.M.; Balan, C., Investigations of vortex formation in micro bifurcations. *Microfluidics and Nanofluidics*. **2012**, 13, 819-833.

Barber, J. O.; Alberding, J. P.; Restrepo, J. M.; Secomb, T. W., Simulated two-dimensional red blood cell motion, deformation, and partitioning in microvessel bifurcations. *Annals of Biomedical Engineering.* **2008,** *36* (10), 1690-1698.

Brader, J. M., Nonlinear Rheology of Colloidal Dispersions. *Journal of Physics: Condensed Matter.* **2010**, 22 (36), 363101.

Brevis. W.; Niño, Y.; Jirka, G.H., Integrating cross-correlation and relaxation algorithms for particle tracking velocimetry. *Experiments in Fluids*. **2011**, 50 (1),135-147.

Bushi, D.; Grad, Y.; Einav, S.; Yodfat, O.; Nishri, B.; Tanne, D., Hemodynamic evaluation of embolic trajectory in an arterial bifurcation: an in-vitro experimental model. *Stroke*. **2005**,36, 2696-2700.

Chapman, B., Shear-induced migration phenomena in concentrated suspensions. **1990**, Ph.D. thesis, University of Notre Dame.

Chow, A. W.; Sinton, S. W.; Iwamiya, J. H.; Stephens, T. S., Shear-induced particle migration in Couette and parallel-plate viscometers - NMR imaging and stress measurements. *Physics of Fluids.* **1994,** *6* (8), 2561-2576.

Claesson, J.; Rasmuson, A.; Wiklund, J.; Wikstrom, T., Measurement, and Analysis of Flow of Concentrated Fibre Suspensions through a 2-D Sudden Expansion Using UVP, *AIChE J*. **2012** ,59,1012-1021.

Coussot, P.; Ancey, C., Rheophysical Classification of Concentrated Suspensions and Granular Pastes. *Physical Review E* .**1999**, 59 (4), 4445–57.

Davis, J.M.; Pozrikidis, C., Hydrodynamic instability of a suspension of spherical particles through a branching network of circular tubes. *Acta Mechanica*. **2012**,223(3),529-540.

D'Avino, G.; Hulsen, M.A.; Maffettone, P. L., Separation of particles in non-Newtonian fluids flowing in T-shaped microchannels. *Advanced Modeling and Simulation in Engineering* Sciences. **2015**, 9, 2-23.

Degré,G.; Joseph,P.; Tabeling,P ; Lerouge,S.; Cloitre,M.; Ajdari. A., Rheology of complex fluids by particle image velocimetry in microchannels. Applied Physics Letters.**2006**, 89, 024104.

Devasenathipathy, S.; Santiago, J.G.; Werely, S.T.; Meinhart, C.D.; Takehara, K., Particle imaging techniques for microfabricated fluidic systems. *Experiments in Fluids.* **2003**,34,504

Dinther, A.M.C. van.; Schroen, C.G.P.H.; Vergeldt, F.J.; Sman, R.G.M. vander.; Boom, R.M., Suspension Flow in Microfluidic Devices - A Review of Experimental Techniques Focusing on Concentration and Velocity Gradients. *Advances in Colloid and Interface Science***. 2012**,173 (5),23-34.

Ditchfield, R.; Olbricht, W. L., Effects of particle concentration on the partitioning of suspensions at small divergent bifurcations. *Journal of Biomechanical Engineering-Transactions of the ASME* .**1996,** *118* (3), 287-294.

Doutel, E.; Pinto, S.I.S.; Campos, J.B.L.M.; Miranda., J.M., μPIV analysis and numerical simulation of the flow in mili-scale channels developed for studies in hemodynamics. *APCBEE Procedia.* ***2013***, 7, 132 – 137.

Einstein. A., For a theory of Brownian motion. *Annual of Physics*. **1906, 167**(19), 289 - 306.

Enden, G.; Popel, A. S., A numerical study of plasma skimming in small vascular bifurcations. *Journal of Biomechanical Engineering-Transactions of the ASME.* **1994,** *116* (1), 79-88.

Frank., M.; Anderson. D.; Weeks, E.R.; Morris, J.F., Particle migration in pressure-driven flow of a Brownian suspension. *Journal of Fluid Mechanics.* **2003**,493, 363-378.

Fridjonsson, E. O.; Seymour, J. D.; Cokelet, G. R.; Codd, S. L., Dynamic NMR microscopy measurement of the dynamics and flow partitioning of colloidal particles in a bifurcation. *Experiments in Fluids.* **2011,** *50* (5), 1335-1347.

Gachelin,J.; Min˜o,G.; Berthet,H.; Lindner,A.; Rousselet,A.; Cle´ment,E., Non-Newtonian Viscosity of Escherichia coli Suspensions, *Physical Review letters*.**2013**, 110, 268103.

Gadala-Maria, F.; Acrivos, A., Shear-induced structure in a concentrated suspension of solid spheres. *Journal of Rheology.* **1980,** *24* (6), 799-814.

Galindo-Rosales, F. J.; Alves, M. A.; Oliveira, M.S. N., Microdevices for extensional rheometry of low viscosity elastic liquids: a review, *Microfluidics and Nanofluidics.* **2013**, 14:1-19.

Gao, C.; Gilchrist, J.F., Shear-induced particle migration in one, two, and three dimensional flows. *Physical Review E*. **2008**, 77, 025301-4.

Genovese, D. B., Shear Rheology of Hard-Sphere, Dispersed, and Aggregated Suspensions, and Filler-Matrix Composites. *Advances in Colloid and Interface Science.* **2012** 171–172 (March), 1–16.

Gijsen, F. J. H.; van de Vosse, F. N.; Janssen, J. D., The influence of the non-Newtonian properties of blood on the flow in large arteries: steady flow in a carotid bifurcation model. *Journal of Biomechanics* **1999,** *32* (6), 601-608.

Gravesen,P.; Branebjerg, J.; Jensen, O.S., Microfluidics-a review. *Journal of Micromechanics and Microengineering*.**1993**, 3(4), 168.

Guillot, P. ; Moulin, T. ; Kotitz, R. ; Guirardel, M. ; Dodge, A. ; Joanicot, M. ; Colin, A. ; Bruneau, C.; Colin. T., Towards a continuous microfluidic rheometer, *Microfluidics and Nanofluidics*. **2008**, 5,619-630.

Ha, H.; Nam, K.H.; Lee, S.J., Hybrid PIV-PTV technique for measuring blood flow in rat mesenteric vessels. *Microvascular Research*. **2012**, 84(3),242-248.

Hampton, R. E.; Mammoli, A. A.; Graham, A. L.; Tetlow, N.; Altobelli, S. A., Migration of particles undergoing pressure-driven flow in a circular conduit. *Journal of Rheology.* **1997,** *41* (3), 621-640.

Han, X.; Bibb.R. Harries,R., Artificial Vascular Bifurcations Design and Modelling. *Procedia CIRP.* **2016** ,49 ,14 -18

Ishikawa, T.; Fujiwara, H.; Matsuki, N.; Yoshimoto, T.; Imai, Y.; Ueno, H.; Yamaguchi, T., Asymmetry of blood flow and cancer cell adhesion in a microchannel with symmetric bifurcation and confluence. Biomedical Microdevices. **2011,** *13* (1), 159-167.

Katz, J.; Sheng, J., Applications of Holography in Fluid Mechanics and Particle Dynamics. *Annual Review of Fluid Mechanics*. **2010**, 42, 531-555.

Kim, Y.W.; Yoo, J.Y., The lateral migration of neutrally-buoyant spheres transported through square. *Journal of Micromechanics and Microengineering*.**2008**, 18(6),65015.

Kim, Y.W.; Yoo, J.Y., Two-phase flow laden with spherical particles in a microcapillary. *International Journal of Multiphase Flow*. **2010**,36(6),460-466.

Krieger, I. M., Rheology of monodisperse lattices. Advances in Colloid and Interface Science. **1972**, 3, 111-136.

Kriger, I.M.; Dougherty, T, J., Concentration dependence of the viscosity of suspensions. *Transactions of the Society of Rheology*. **1959** 3, 137-152.

Kiger, K.T.; Pan, C., PIV Technique for the Simultaneous Measurement of Dilute Two Phase Flows. *Journal* of *Fluids Engineering*. **2000**, 122, 811-818.

Koh, M.G.; Kim, C., Separation of particles of different sizes from non-Newtonian suspension by using branched capillaries. *Journal* of *Chemical Engineering* of *Japan*. **2007**, 40(11), 964-972.

Koh, C. J.; Hookham, P.; Leal, L. G., An experimental investigation of concentrated suspension flow in a rectangular channel. *Journal of Fluid Mechanics.* **1994,** *266*, 1-32.

Korevaar, M.W.; Padding, J.T.; Deen, N.G.; Kuipers, JAM. (Hans).; Wang, J.; Wit, M.; Schutyser, M.A.I., Hybrid PIV/PTV Measurements of Velocity and Position Distributions of Gas-Conveyed Particles in Small, Narrow Channels. *AIChE J*.**2015**,61,3616–3627.

Koutsiaris, A.G., Digital Micro PIV (μ-PIV) and Velocity Profiles in Vitro and In Vivo. In *The Particle Image Velocimetry - Characteristics, Limits and Possible Applications*, edited by Giovanna Cavazzini. InTech. **2012**.

Leble, V.; Lima, R.; Dias, R.; Fernandes, C.; Ishikawa, T.; Imai, Y.; Yamaguchi, T., Asymmetry of red blood cell motions in a microchannel with a diverging and converging bifurcation. *Biomicrofluidics.* **2011,** *5* (4).

Leighton, D.; Acrivos, A., The Shear-Induced Migration of Particles in Concentrated Suspensions. *Journal of Fluid Mechanics.* **1987b,** *181*, 415-439.

Lenoble M., Écoulement et segregation dans des pâtes granulaires modèle, PhD Thesis, Université Bordeaux1, **2005**.

Li, X. J.; Popel, A. S.; Karniadakis, G. E., Blood-plasma separation in Y-shaped bifurcating microfluidic channels: a dissipative particle dynamics simulation study. *Physical Biology.* **2012,** *9* (2).

Lima, R.; Ishikawa, T.; Imai, Y.; Takeda, M.; Wada, S.; Yamaguchi, T., Measurement of individual red blood cell motions under high hematocrit conditions using a confocal micro-PTV system. *Annals* of *Biomedical Engineering*. **2009**,37(8),1546-1559.

Lindken, R.; Westerweel, J., Development of a self calibrating the stereo-μ-PIV system and its application to the three-dimensional flow in a T-shaped mixer. *6th international symposium on particle image velocimetry*. Pasadena, CA .**2005**.

Lindken, R.; Rossi, M.; Große, S.; Westerweed, J., Micro-particle image velocimetry (μPIV): recent developments, applications, and guidelines, *Lab Chip* . **2009** ,9 2551–67.

Lyon, M. K.; Leal, L. G., An Experimental Study of the Motion of Concentrated Suspensions in Two-Dimensional Channel Flow. Part 1. Monodisperse Systems. *Journal of Fluid Mechanics.***1998a***,* 363 (May), 25–56.

Lyon, M. K.; Leal, L. G., An Experimental Study of the Motion of Concentrated Suspensions in Two-Dimensional Channel Flow. Part 2. Bidisperse Systems. *Journal of Fluid Mechanics.* **1998b,** 363 (May), 57–77.

Maron, S.H.; Percy E. P., Application of Ree-Eyring Generalized Flow Theory to Suspensions of Spherical Particles. *Journal of Colloid Science.* **1956**, 11 (1), 80– 95.

Marra, W.A.; Parsons, D.R. ; Kleinhans, M.G. ; Keevil , G.M. , Thomas, R.E., Near-bed and surface flow division patterns in experimental river bifurcations, *Water Resource*, **2014**,50 ,1506-1530.

Medhi, B.J.; Kumar, A.; Singh, A., Apparent wall slip velocity measurements in free surface flow of concentrated suspensions, *International Journal of Multiphase Flow*. **2011**, 37, 609-619.

Medhi, B.J.; Agarwal, V.; Singh. A., Experimental investigation of particle migration in suspension flow through bifurcating micro-channels. *AIChE J*. **2018**,64(6),2293-2307.

Meinhart, C.D.; Wereley, S.T.; Gray, M.H.B., Volume illumination for two-dimensional particle image velocimetry. *Measurement Science and Technology*. **2000**, 11. 809–814.

Min. K.H.; Kim, C., Simulation of Particle Migration in Free-Surface Flows**.** *AIChE J*.**2010,** 56, 2539-2550.

Morris, J. F.; Boulay, F., Curvilinear flows of noncolloidal suspensions: The role of normal stresses. *Journal of Rheology.* **1999,** *43* (5), 1213-1237.

Muste, M.; Pate, V.C., Velocity profiles for particles and liquid in open channel flow with sediment transport. *Journal of Hydraulic Engineering*.**1997,** 123, 742-751.

Neary, V.S.; Odgaard, A.J., Three dimension flow structure at open-channel diversions, *Journal of Hydraulic Engineering* , **1993**, 119,1223-1230.

Nezu, I.; Sanjou, M., PIV and PTV measurements in hydro-sciences with focus on turbulent open-channel flows. *Journal of Hydro-environment Research*. **2011**,5(4),215-230.

Noguchi, K.; Nezu, I., Particles-turbulence interaction and local particle concentration in sediment-laden open-channel flows. *Journal of Hydro-environment Research*. **2009**, 3, 54-68.

Nott, P. R.; Brady, J. F., Pressure-driven flow of suspensions - simulation and theory. *Journal of Fluid Mechanics.* **1994,** *275*, 157-199.

Olsen, M. G.; R. J. Adrian., Out-of-Focus Effects on Particle Image Visibility and Correlation in Microscopic Particle Image Velocimetry. *Experiments in Fluids.* **2000**. 29 (1), 166–74.

Perkkio, J.; Keskinen, R., Hematocrit reduction in bifurcations due to plasma skimming. *Bulletin of Mathematical Biology.* **1983,** *45* (1), 41-50.

Phillips, R. J.; Armstrong, R. C.; Brown, R. A.; Graham, A. L.; Abbott, J. R., A constitutive equation for concentrated suspensions that accounts for shear-induced particle migration. *Physics of Fluids a-Fluid Dynamics.* **1992,** *4* (1), 30-40.

Poelma, C.; Westerweel, J.; Ooms, G., Particle–fluid interactions in grid-generated turbulence. *Journal of Fluid Mechanics.* **2007**, 25(589), 25–56.

Quemada, D., Energy of Interaction in Colloids and Its Implications in Rheological Modeling. *Advances in Colloid and Interface Science*. **2002**, 98 (1),51–85.

Raffel, M.; Seelhorst, U.; Willert, C.. Vertical flow structures at a helicopter rotor model measured by LDV and PIV. *The Aeronautical Journal of the Royal Aeronautical Society*. **1998**,102, 221–227.

Raffel, M.; Willert, C.; Kompenhans, J., A Practical Guide. to Particle Image Velocimetry. *Springer-Verlag*, Berlin, **2007**.

Ramamurthy, A.S.; Qu, J.; Vo, D, Numerical and experimental study of dividing open-channel flows, *Journal of Hydraulic Engineering*. 2007,**133**, 1135-1144.

Reddy, M. M.; Singh, A., Flow of concentrated suspension through oblique bifurcating channels. *AIChE J.* **2014,** *60* (7), 2692-2704.

Roberts, B. W.; Olbricht, W. L., Flow-induced particulate separations. *AIChE J.* **2003,** *49* (11), 2842-2849.

Roberts, B. W.; Olbricht, W. L., The distribution of freely suspended particles at microfluidic bifurcations. *AIChE J.* **2006,** *52* (1), 199-206.

Santiago, J. G.; Wereley, S. T.; Meinhart, C. D.; Beebe D. J.; Adrian, R. J., A particle image velocimetry system for microfluidics. *Experiments in Fluids*.**1998**, 25, 316-324.

Schmidschonbein, G. W.; Skalak, R.; Usami, S.; Chien, S., Cell distribution in capillary networks. *Microvascular Research.* **1980,** *19* (1), 18-44.

Semwogerere, D.; Morris, J. F.; Weeks, E. R.; Development of particle migration in pressure-driven flow of a Brownian suspension. *Journal of Fluid Mechanics*. **2007**, 581, 437.

Semwogerere, D; Weeks, E. R.., Shear-induced particle migration in binary colloidal suspensions. *Physics of Fluids*.**2008,** 23 (20), 043306.

Sherwood, J.M.; Kaliviotis, E.; Dusting, J.; Balabani, S., Hematocrit, viscosity and velocity distributions of aggregating and non-aggregating blood in a bifurcating microchannel. *Biomechanics and Modeling in Mechanobiology*. **2014**, 13(2), 259-273.

Siqueira, I.R.; Reboucas, R.B.; Carvalho, M.S., Particle Migration and Alignment in Slot Coating Flows of Elongated Particle Suspensions. *AIChE J.* **2017**, 63(7), 3187–3198.

Stickel, J.J.; Powel, R.L., Fluid Mechanics and Rheology of Dense Suspensions. *Annual Review of Fluid Mechanics.* **2005**, 37 (1), 129–49.

Stone, H.A.; Kim, S., Microfluidics: Basic issues, applications, and challenges. *AIChE J.* **2001**, 47:1250–54.

Thielicke, W.; Stamhuis, E.J., PIV lab - Towards User-friendly, Affordable and Accurate Digital Particle Image Velocimetry in MATLAB. *Journal of Open Research Software.* **2014**, 2(1),30.

Tropea, C.; Yarin, A.L.; Foss, J.F., Springer handbook of experimental fluid mechanics, vol 1. *Springer Science & Business Media*. **2007.**

Ushijima, S., Particle Tracking Velocimetry using Laser Beam Scanning, *Journal of Hydraulic Coastal and Environ Engineering*.**1996**, 35,99-107.

Wang, T.; Rongin, U.; Xing, Z., A micro-scale simulation of red blood cell passage through symmetric and asymmetric bifurcated vessels. *Scientific Reports*. **2016**, 6, 20262.

Warkiani, M.E.; Tay, A.K.P.; Guan, G.; Han, J., Membrane-less microfiltration using inertial microfluidics. *Scientific Reports*. **2015**, 5, 11018.

Wereley, S.; Meinhart, C.D., Recent Advances in Micro-Particle Image Velocimetry. *Annual Review of Fluid Mechanics*. **2010**, 42.

Wereley, S. T.; Gui, L., Advanced algorithms for microscale particle image velocimetry. *American Institute of Aeronautics and Astronautics Journal*.**2002**, 40, 1047-1055.

Westerweel, J., Fundamentals of Digital Particle Image Velocimetry, *Measurement Science and Technology*. **1997**, 8(12), 1379-1392.

Xi, C.; Shapley, N. C., Flows of concentrated suspensions through an asymmetric bifurcation. *Journal of Rheology.* **2008,** *52* (2), 625-647.

Yadav, S.; Reddy, M.M.; Singh, A., Shear-induced particle migration in three-dimensional bifurcation channel. *International Journal of Multiphase Flow*.**2015**, 76, 1-12.

Yadav, S.; Reddy, M.M.; Singh. Shear-induced migration of concentrated suspension through Y-shaped bifurcation channels. *Particulate* **Science** *and* **Technology**. **2016**, 34(1), 83-95.

Ye, T.; Thien, N.P.; Khoo, B.C.; Li, Y., Flow patterns and red blood cell dynamics in a U-bend.*Journal of Applied Physics*. ***2017***, 122, 084701.

Zimmerman, W. B.; Rees, J. M.; Craven, T. J., Rheometry of non-Newtonian electrokinetic flow in a microchannel T-junction, *Microfluidics and Nanofluidics.***2006**, 2,481–492.

List of publications:

Journal

- Medhi, B.J.; Agarwal, V.; Singh. A., Experimental investigation of particle migration in suspension flow through bifurcating micro-channels. AIChE J. **2018**,64(6),2293-2307.

- Siddique,A.; Medhi, B.J.; Agrawal,A.; Singh,A.; Saha, S.K., Design of a collector shape for uniform flow distribution in microchannels. Journal of Micromechanics and Microengineering. **2017**, 20, 075026-075036.

- Medhi, B.J.; Reddy, M.M.; Singh. A., Flow of concentrated suspensions in bifurcating open channels. (Under Review).

- Medhi, B.J.; Singh. A., μ-PIV/ PTV measurement of suspension flow in diverging-converging channel of varying width. (Manuscript under preparation).

Conference

- Medhi, B.J.; Agarwal, V.; Singh., A., Experimental study of suspensions flow in symmetric bifurcation Channels. CompFlu-2016, IISER Pune (India), January 2-4 (**2016**), Indian Society of Rheology.

- Medhi, B.J.; Singh., A., Flow of concentrated suspensions in bifurcating open channel. CHEMCON 2015 68th Annual Session of the Indian Institute of Chemical Engineers December 27-30 (**2015**), Indian Institute of Technology (IIT) Guwahati **.**

Appendices

Appendix A

Chapter 2

PIV & PTV software operating steps

PIVlab

First stored the images to be analyze in a separate folder (Suppose folder X)

Run Matlab

↓

Go to Folder PIVlab_1.32

Run PIVlab_GUI

In PIVlab_GUI →

↓

File → New Session

↓

Load Images from the Folder X

↓

Select sequencing style 1-2, 2-3, 3-4……

↓

Add images

↓

Import Images

Analyses Setting → Exclusion

↓

Select ROI or Draw mask for current frame (area covered under mask remain inactive during analysis)

↓

Apply Current mask to all frame

Analyses Setting → PIV setting

↓

FFT window deformation

↓

Pass 1

↓

Interrogation area (64 px) & Step (32 px) 50%

↓

Select pass 2, pass 3and pass 4 if needed

Analyze → Analyze all frames

Calibration → Select reference distance

↓

Real distance Time step

↓

Apply Calibration

Plot → Derive parameters/ modify data

↓

Velocity Magnitude

Plot → Streamlines

Extraction → Parameters from poly line

↓

Velocity

↓

Draw

↓

Plot data

↓

Save data as ASCI chart for all frame (for further analysis)

Post Processing → (if needed)

File → Save PIVlab_session

↓

Single Image or Image Sequence (AVI, JPG, BMP etc)

PTV Beta

First stored the images to be analyze in a separate folder (Suppose folder X)

Run Matlab

Go to Folder PTVlab Beta

Run PTV lab _GUI

In PTV lab _GUI →

↓

File → New Session

↓

Load Images from the Folder X

↓

Add images

↓

Import Images

Analyses Setting → Exclusion

↓

Select ROI or Draw mask for current frame (area covered under mask remain inactive during analysis)

↓

Apply Current mask to all frame

Analyses Setting → Image Pre-processing

↓

Enable subtract mean

Analyses Setting → Particle Detection

↓

Gaussian Mask

Analyses Setting → PTV setting

↓

Select Cross Correlation (In PTV algorithm,)

↓

Select by interrogation area (px) (In cross correlation parameters)

Analyze → Analyze all frames

Calibration → Select reference distance

↓

Real distance Time step

↓

Apply Calibration

Plot → Derive parameters/ modify data

↓

Velocity Magnitude

Plot → Streamlines

Extraction → Parameters from poly line

↓

Velocity

↓

Draw

↓

Plot data

↓

Save data as ASCI chart for all frame (for further analysis)

Post Processing → (if needed)

File → Save PIVlab_session

↓

Single Image or Image Sequence (AVI, JPG, BMP etc)

Appendix B

Chapter 3

Comparative chart of experimental parameter with human blood circulatory system

Table1: Comparative chart showing diameter of blood vessel and microchannel used in our experiments.

Blood Vessel	**Diameter (µm)**	**Wall Thickness (µm)**	**Micro Channel**	**Diameter (µm)**	**Wall Thickness (µm)**
Aorta	25000	2000			
Artery	4000	1000			
Vein	5000	500			
Vena cava	30000	1500	Chapter 3	500	1500
Arteriole	30	6	Chapter 4	500	1500
Terminal arteriole	10	2	Chapter 5	700,600,500, 400, 300, 200	1000
Capillary	8	0.5	Chapter 6	500	1500
Venule	20	1	Chapter 7	2000	5000

Table2: Comparative chart showing radius of blood cell components and polymer particles used in our experiments.

Blood cell	Radius(**μm**)	Volume fraction ϕ (%)	Polymer particle	Radius(**μm**)	Volume fraction ϕ (%)
RBC	6-8	40-45	PMMA	6	5
WBC	10-12	1-2	PMMA	10	5
Platelets	2-3	0.2-0.7	Polystyrene	80	30 & 40

Appendix C

Chapter 4

Comparative plot of velocity profiles for diverging and converging flow

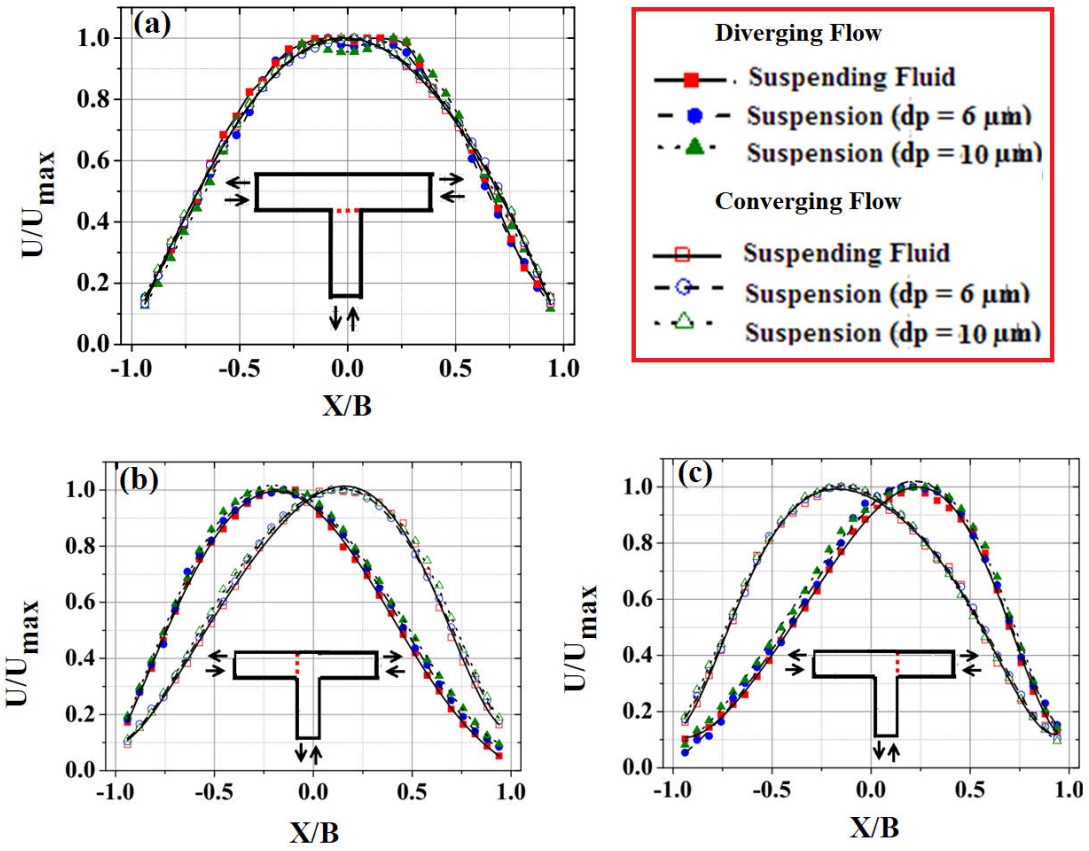

Figure1: Comparison of velocity profile for diverging and converging flow in symmetric T-bifurcation channel

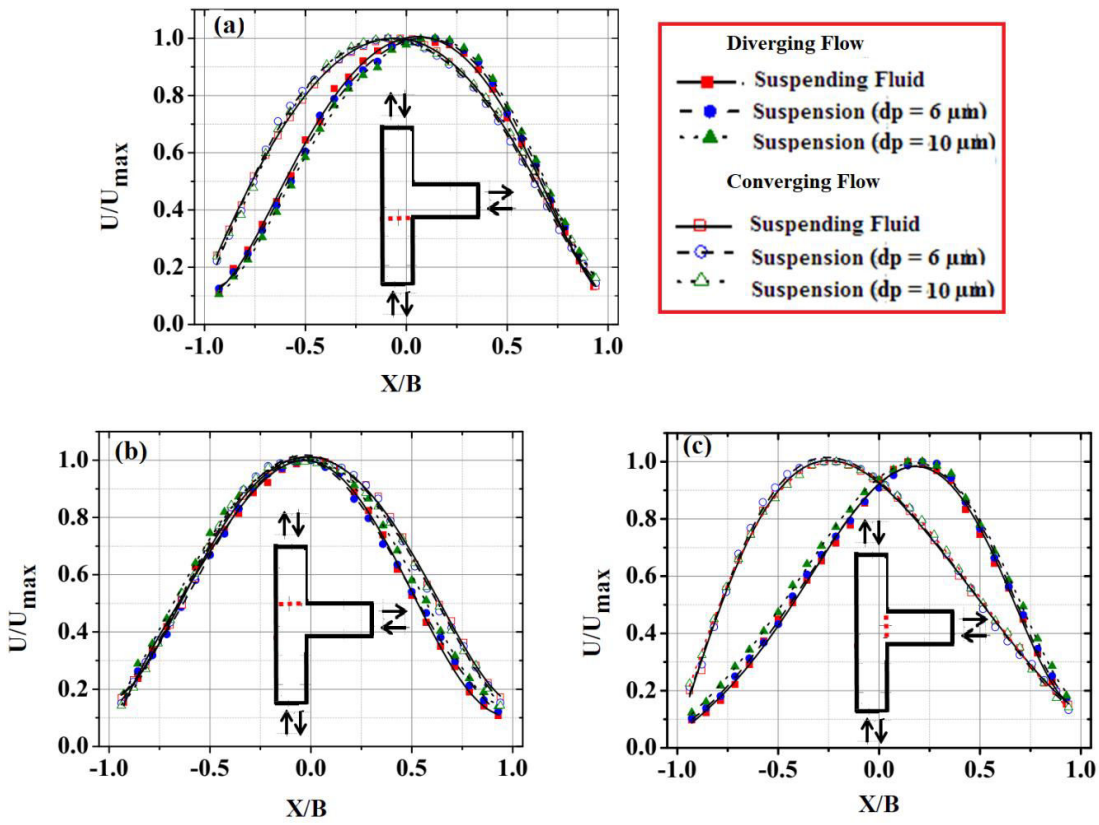

Figure2: Comparison of velocity profile for diverging and converging flow in asymmetric T-bifurcation channel.

Appendix D

Chapter 5

Comparative plot of velocity profiles with Leble et al. (2011)

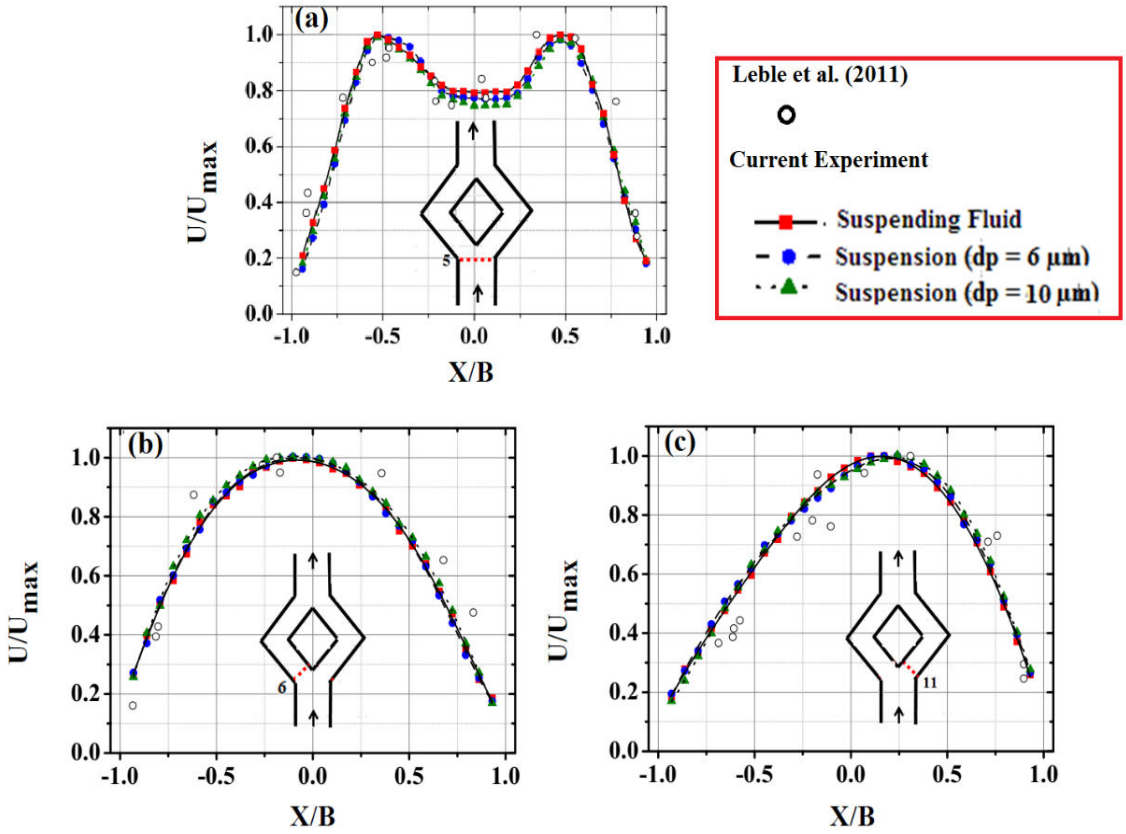

Figure 1. A comparative plot of velocity profiles from our experiment with Leble et al. (2011) for various locations in the diverging section (a) at location 5 (b) at location 6 and (d) at location 4.

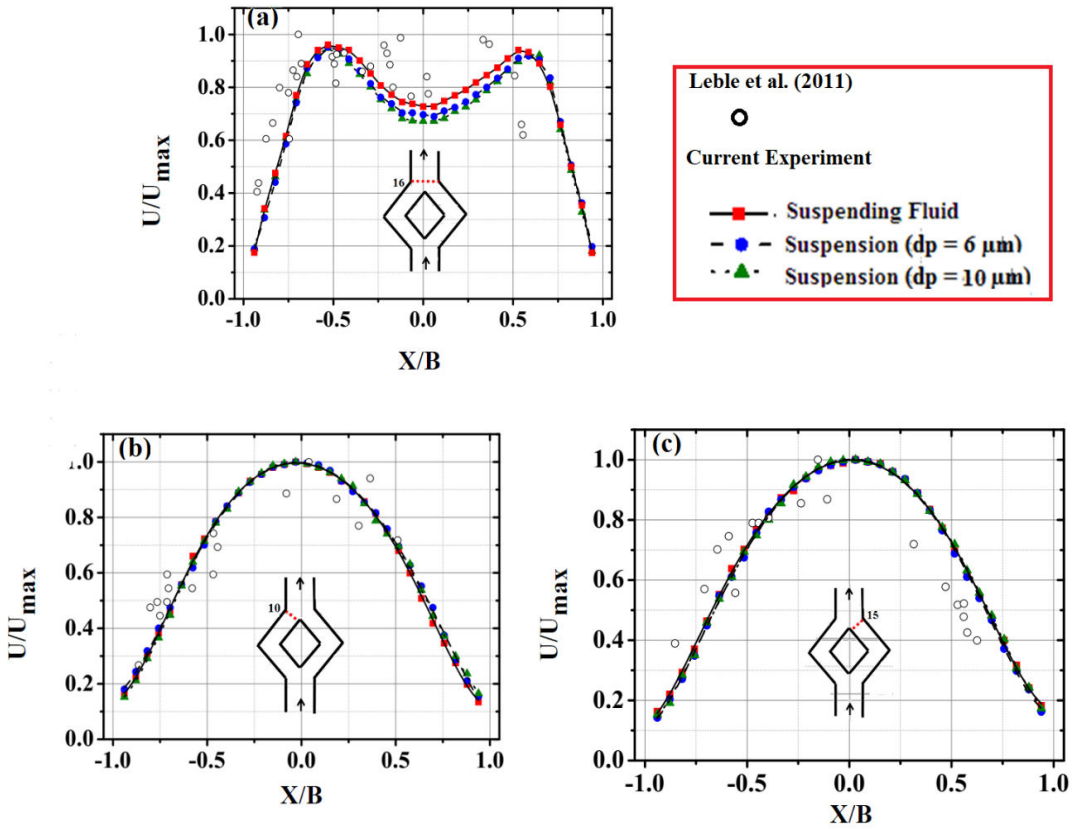

Figure 2. A comparative plot of velocity profiles from our experiment with Leble et al. (2011) for various locations in the converging section (a) at location 16 (b) at location 10 and (d) at location 15.